THE UNIVERSITY of ADELAIDE

Design and Development of a Fluidic Barrier for Solar Cavity Receivers

Elham Alipourtarzanagh

School of Mechanical Engineering

The University of Adelaide

Adelaide, Australia

A thesis submitted in fulfilment of the requirements

for the degree of Ph.D. in Mechanical Engineering

October 2020

Thesis declaration

I certify that this work contains no material which has been accepted for the award of any other degree or diploma in my name, in any university or other tertiary institution and, to the best of my knowledge and belief, contains no material previously published or written by another person, except where due reference has been made in the text. In addition, I certify that no part of this work will, in the future, be used in a submission in my name, for any other degree or diploma in any university or other tertiary institution without the prior approval of the University of Adelaide and where applicable, any partner institution responsible for the joint-award of this degree.

I acknowledge that copyright of published works contained within this thesis resides with the copyright holder(s) of those works.

I also give permission for the digital version of my thesis to be made available on the web, via the University's digital research repository, the Library Search and also through web search engines, unless permission has been granted by the University to restrict access for a period of time.

I acknowledge the support I have received for my research through the provision of an Australian Government Research Training Program Scholarship.

Elham Alipourtarzanagh

22/10/2020

Date

Acknowledgement

I would like to express my deepest gratitude and special appreciation to my supervisor, Professor Bassam Dally whose encouragement, wisdom, patience and knowledge helped me to progress toward my goals. It is impossible to show how grateful I am for his priceless mentoring not only in my academic life but also in my personal life.

I would also like to sincerely appreciate Professor Graham (‘Gus’) Nathan for his guidance during my PhD study. Special thanks for his detailed comments resulting in the improvement of my writing. My Co-supervisors; Dr Alfonso Chinnici and Dr Zhao Tian are thankfully acknowledged for their assistance throughout my research endeavours.

I have been blessed to have a loving father, Hashem, who has made numerous sacrifices for me and a wonderful mother, Kefayat, to whom I owe most of my progress in life. Words cannot express my gratitude to my siblings; Fereshteh, Baharak, Zahra, Mohammad, Leila and my lovely nephews; Alireza, Hamidreza and Amirreza. I could not make it this far without their unconditional love, constant motivation, emotional support and belief in me.

I would like to dedicate this thesis to my loving husband, Shahrooz whom we fell in love at the right time. Writing the last bit of my thesis coincided with the start of a new sensational journey with him, making the completion of my PhD an enjoyable exercise.

Finally, I would like to thank my incredible friends; Ali Tareq Sameer and Hamed Sadighi Dizaji during the new chapter of my life in Australia.

Thesis Summary

Convective heat losses from solar cavity receivers are highly non-linear and account for about 60% of total heat losses from cavity receivers. Considering the growing role of cavity receivers in concentrating solar thermal plants with a tower, minimising convective losses from these cavities enhances the thermal efficiency of the whole plant. In this project, the use of fluidic barriers to minimize convective losses for both conventional and hybrid combustion-solar receivers is assessed. Systematic experimental and numerical studies have been conducted to devise new feasible mitigation strategies while ensuring maximum solar collection efficiency.

The first phase of experiments was performed on a purpose-built, electrically heated, cavity receiver, which was placed in a large wind tunnel to directly measure the convective heat losses under a variety of operating and wind conditions. The cavity was equipped with different aerodynamic barriers to control the flow across the aperture including air blowing, air suction and a combination of air blowing and air suction curtains at variable velocity, discharge angle and position. The influence of various tilt angles (θ = 0°, 15°, 30° and 45°), wind speeds (u_w = 0, 3, 6 and 9 m/s) and wind directions (α= 0° and 45°) were examined for two fixed internal temperatures of the cavity (T_{cav} = 300℃ and 400℃). The experimental results are presented as a function of dimensionless numbers such as Richardson number, Reynolds number and relative momentum fluxes of curtain flow to wind flow wherever possible to provide a suitable comparison base. The commercial CFD package, ANSYS, was also utilized to conduct a computational study to further understand the flow features. The model was validated using available experimental data and has helped to confirm and complement knowledge generated from equivalent experimental campaigns. The results showed that directing a blown air curtain outward, toward the wind direction, offers tangible advantages over flow parallel to the aperture plane. It is also found that higher air curtain velocity, up to an optimum value, results in a higher effectiveness of the air curtains. The assessment of the effect of the orientation of the air curtain on the effectiveness demonstrated that for buoyancy dominant flow an upward blowing air curtain has a better performance than a downward blowing air curtain with a maximum difference of 47%. It is also revealed that a suction nozzle, mounted at the bottom of the aperture, is more effective than a blowing nozzle mounted at the top of the aperture, for the title angle of θ = 45°, while the measured effectiveness was 76% and 43% for wind speeds

of 0 and 9 m/s, respectively. At a yaw angle of 45°, a remarkable difference in the effectiveness was reported for various suction nozzle configurations for a wind speed of 9 m/s, highlighting the need to activate different nozzles depending on wind direction. The combination of air blowing and air suction fluidic barrier was also assessed for a tilt angle of 45° and wind speeds of 0 and 9 m/s. It is found that this approach enhances the effectiveness by 5% over the suction only approach for wind speed of 9 m/s whereas at no wind condition it reduces the effectiveness compared with suction only approach.

The second phase of the experimental study involved the use of a water tunnel and aimed at investigating the flow structure in a scaled down hybrid cavity receiver incorporating multiple internal jets, simulating fuel and air nozzles for a combustion-solar hybrid receiver. Particle Image Velocimetry, PIV, laser based technique was used to capture the instantaneous planar velocity field at multiple axial positions inside and outside the model. The effects of jet configuration, aperture size and variation of external flow velocity and direction on the internal jet decay, recirculation pattern and water ingress and egress via the aperture were recorded. The results showed high dependency of the flow structure, within the cavity, on the internal jet configuration and minor dependence on the velocity and direction of the external flow. It is also found that the mass entrainment of external flow into the cavity is significant and is strongly dependant on the aspect ratio of the aperture to the cavity, yaw angle and external flow speed. These findings helped quantify the controlling parameters and inform future strategies to mitigate the ingress of external air into the hybridised cavity receiver.

It is concluded that an adaptive air curtain system should be devised so that it could sense the wind direction and wind speed and activate one or more of the curtain nozzles, induce suction or blowing, and regulate the air speed to achieve the best performance. This work provided the foundation for utilisation of a dynamic aerodynamic active flow for real world application of solar cavity receivers to improve the thermal efficiency of concentrating solar tower plants.

Table of contents

Chapter 1- Introduction

1.1 Background

Fossil fuels, as the world's main source of energy, are formed in the Earth's crust from organic material over millions of years (Morales Pedraza, 2019). Fossil fuels are relatively inexpensive, readily available, easy to store and have high energy density (Sarkar, 2017). Hence, many technologies have been developed to utilize this energy source into a variety of sectors, commonly classified into; transport, power, industrial and domestic. Fossil fuels are projected to remain the primary source of global energy for the next few decades (EIA, 2019). On the other hand, fossil fuels' known reserves are a finite resource and are projected to last for another 100 years (Shafiee and Topal, 2009). With anticipated growth in the population of the world and the industrialisation of the major economies such as China, India and some emerging Asian economies, it is anticipated that a 45% growth, in energy demand, will occur by 2040 (IEA, 2018). This additional demand on fossil fuels and the depletion of the reserves is expected to be followed by a hike in the price of fuels (Caldara et al., 2019).

The combustion of fossil fuels has resulted in the production of greenhouse gases which is linked to irreparable harm to the environment and has resulted in well documented climate change leading to more frequent and more severe droughts, floods and storms (Dorian et al., 2006). In response, governments around the world have taken measures to prevent potential catastrophic changes in the Earth's climate by committing to a reduction in greenhouse emissions and to the use of alternative sources of energy. One of the prominent agreements is the Kyoto Protocol, which is linked to the United Nations Framework Convention on Climate Change (UNFCCC), and which commits the parties to reduce Greenhouse Gas (GHG) emissions (Mitchell, 2003). A major milestone to tackle climate change happened during the Conference of the Parties 21 at Paris (COP-21) where 195 countries resolved to keep the rise of global mean temperature to below 2°C (IPCC, 2018).

These commitments have motivated the search for promising alternative energy sources to address environmental commitments and security of supply concerns by many nations (Knox-Hayes et al., 2013, Adefarati and Bansal, 2019). Therefore, the necessary transition away from a harmful fossil fuel economy has been pursued. Electricity generation and thermal energy contribute to more than 40% of CO_2 emissions (IEA, 2020). Therefore, the improvement of energy efficiency in different sectors, especially those sectors with major carbon emissions, and the development of alternative energy sources, such as nuclear energy and sustainable and clean source of renewable energy, are the main measures taken to minimise environmental impacts and to mitigate GHG emissions.

Renewable energy resources are collected from natural sources that are constantly replenished. There are many renewable energy sources including solar, wind, biomass, geothermal and hydroelectric energy. However, there are barriers to the utilization of renewable energy sources related to the cost of production and storage, variability of supply, effective use and geographical location (Painuly, 2001, Shahnazi and Dehghan Shabani, 2020). Among the different renewable energy sources, wind and solar energy dominate the growth in renewable energy generation (EIA, 2019). Figure 1.1 illustrates the global power generation (in terawatt-hour) from low carbon sources in 2018 (IEA, 2018).

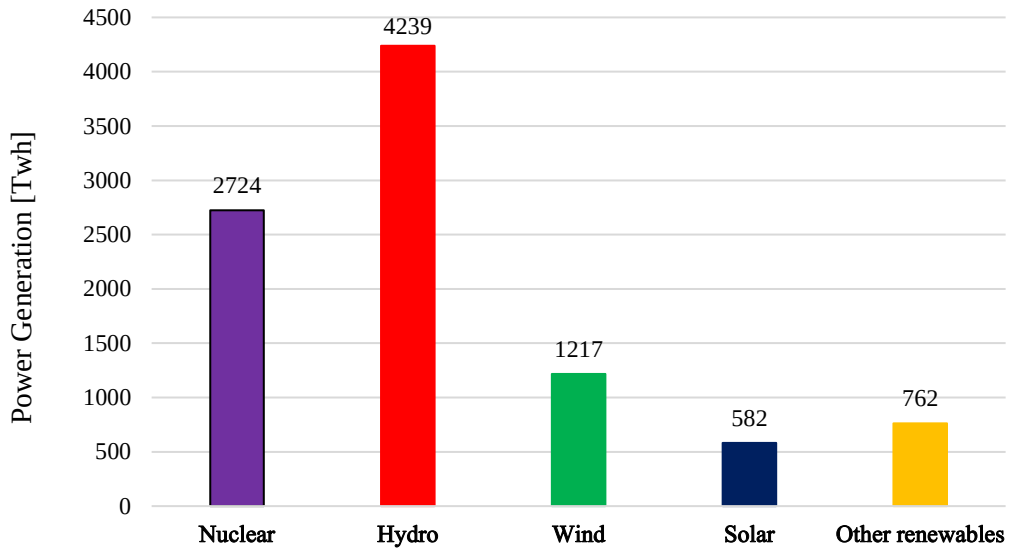

Figure 1.1- Global low-carbon power generation by source (IEA 2018).

Solar energy, as one of the most abundant renewable energy sources, can be used in either diffuse form (Photovoltaic cells) or concentrated forms such as trough, Fresnel or tower configuration. Photovoltaic (PV) panels are widely used to convert diffuse solar radiation directly into electricity using a solar PV cell composed of semiconductor cell (Parida et al., 2011). The Levelised Cost of Electricity, LCOE, using PV technology has fallen by 82% between 2010 and 2019. Such a sharp drop in the cost was driven by improving the conversion efficiency, reduction in manufacturing cost and the economy of scale (IRENA, 2020b). The global installed capacity of solar photovoltaic was about 580 GW in 2019 (IRENA, 2020a) and it is projected to grow robustly in the next five years due to cost competitiveness and support policies particularly in China, European Union, the United States, India and Japan (IEA, 2019).

In contrast, concentrating solar thermal (CST) systems use reflectors to focus the solar radiation into a target or a receiver, where higher radiation flux is achieved resulting in higher temperatures (Pitz-Paal, 2014). The targets that receive the concentrated solar radiation are usually in the form of heat exchangers that absorb solar radiation and convert it into thermal energy by transferring heat to a heat transfer fluid, HTF (Kalogirou, 2018). CST is mainly used through four different types of technologies, namely; dish, through, tower and Fresnel types.

As shown schematically in Figure 1.2, these technologies are different in terms of the designs and configuration of the receivers and mirrors (Ordorica-Garcia et al., 2011). The required thermal load and outlet temperature determine the collector type (Milani, 2019). The commercial development of concentrating solar projects had a rise between 1984 and 1995 and then no commercial project was constructed until 2005. Nonetheless, research and technology demonstration have continued during this period which have helped in the further development of the technology (Lovegrove and Stein, 2012). The experiences gained from the previous projects were useful to expedite the implementation of further projects. So that between 2010 and 2019, the cumulative CSP installed capacity rose five times globally and reached 6.3 GW while the weighted average LCOE dropped by 47%.

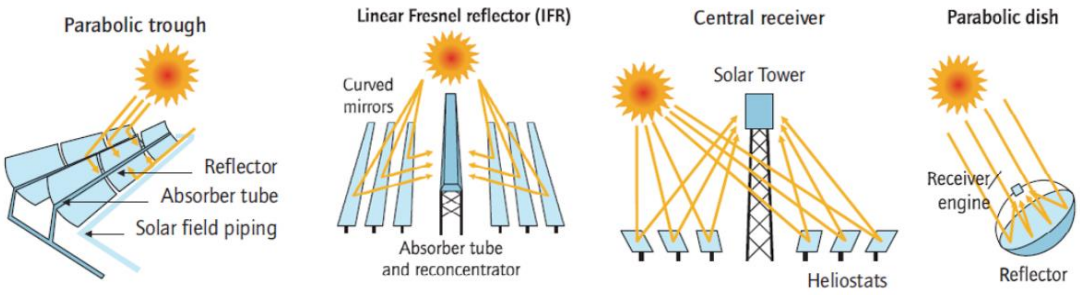

Figure 1.2- Schematics of CST technologies (Ordorica-Garcia et al., 2011).

The thermal energy generated by CST systems can be used to supply industrial heat, water desalination and steam generation to enhance oil recovery in mature and heavy oil fields or generate electricity, which is termed concentrated solar power (CSP) (Bellan et al., 2019). However, the intermittent nature of solar energy makes it necessary to develop approaches to provide a firm dispatchability of generated energy and to increase solar share. Thermal storage systems and hybridization are proposed as promising methods to enhance the application of solar energy technologies. Hybridisation of CST is applied when the solar radiation is not sufficient i.e. during the night or for cloudy weather. Hybrid solar systems can be deployed in

two forms; either stand-alone or integrated systems. Stand-alone systems utilize CST energy when available and another independent energy source, such as combustion, is used as a backup. In integrated CST, hybridised resources are integrated into solar energy and use shared infrastructure for energy convergence (Nathan et al., 2018).

A solar tower plant consists of three major subsystems, namely, the heliostat field, the tower and the solar receiver. The heat transfer fluid is heated in the receiver by the reflected and concentrated solar radiation from the reflectors, with recorded temperatures of up to 1000°C (He et al., 2019). The type of the receiver depends on the field size, working fluid, operating condition, materials and design preference. There are two main types of CST tower receivers, namely; cavity receivers and external receivers (Figure 1.3).

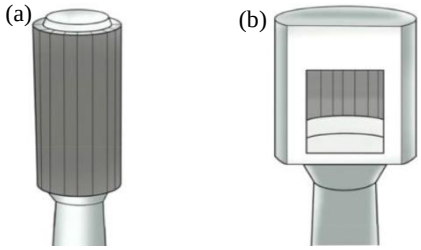

Figure 1.3- Schematics of (a) External and (b) cavity receivers (Ho and Iverson, 2014).

For the low temperature application of CST, limited to below 600℃, external receivers are used (Figure 1.4). As radiation losses scale with the temperature to the power four, limiting the temperature rise can maintain the collection efficiency at an acceptable level. A second measure is to choose materials with low emissivity. The external receivers mounted on top of the tower are surrounded by the heliostat field. Although this configuration allows the collection of solar radiation from all directions, it does suffer from radiation and convection heat losses from all sides as well (Vant-Hull, 2012, Nathan et al., 2018).

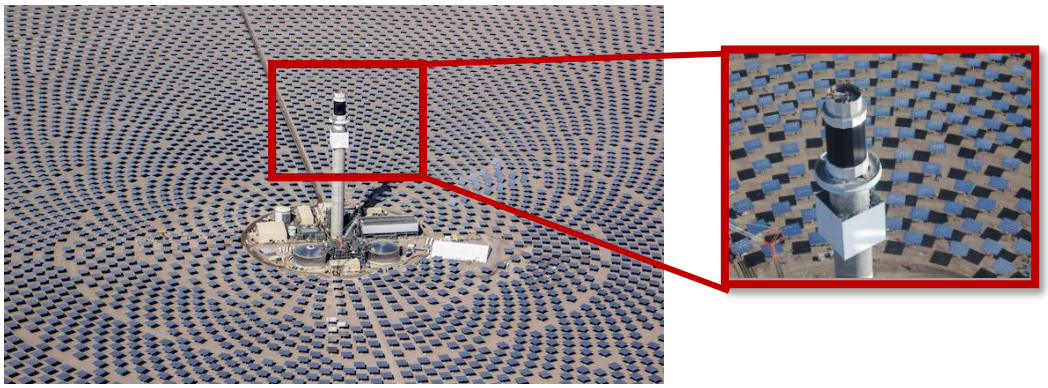

Figure 1.4- External receiver mounted on Crescent Dunes, Nevada (US Department of energy, 2020)

On the other hand, cavity receivers are known to operate at higher efficiency and be applicable for higher temperature applications (Ho and Iverson, 2014, Kim et al., 2015). Heat loss from cavity receivers is reduced because of the presence of the cavity walls and an aperture receiving the solar radiation to reduce re-radiation losses and less convective heat losses, compared with external receivers. Moreover, because they are generally faced downward, hot gases are less intended to leave the cavity through the aperture and hence the cavity receivers have the potential to maintain the high temperature within the cavity (Hinkley and Agrafiotis, 2019). Figure 1.5 presents an aerial view of Solucar Complex, solar power towers located in Spain featuring cavity-type receivers. Nonetheless, channelling radiation into a small aperture of the receiver limits the capacity of these systems and the size of the heliostat fields. Noteworthy is that solar receivers are a crucial component of a CST tower plant as they couple the heliostat field to the thermal storage and electricity generation systems and constitute about 20% of the plant investment costs (Schöttl et al., 2020). Furthermore, the size of the heliostat field, which makes up some 40-50% of the total capital of the solar plant, is directly influenced by the solar-to-thermal efficiency of the receiver (Kolb et al., 2011). Therefore, considering the importance of the role of the cavity receivers in solar tower technology, it is essential to implement strategies to increase the thermal efficiency of solar receivers.

Figure 1.5- Aerial view of Solucar Solar Platform in Spain by Abengoa, featuring tower mounted solar cavity receivers and heliostat field (Prieto et al., 2016).

Maximizing the thermal efficiency of the solar system, necessitates the minimisation of heat losses from cavity receivers that consist of convection, conduction and radiation losses. Conductive and radiative losses are relatively easy to mitigate through insulation and cavity design, respectively. Convective losses are the most complex and the hardest losses from cavity receivers to predict. It is well established that, more than 60% of the losses of the cavity, at high wind speeds, are attributed to convective heat losses, and hence it is important to apply methods in order to minimise the convective heat losses (Ma, 1993). Different methods are proposed to mitigate convective heat losses from solar cavity receivers such as varying the geometry of the cavity, covering the aperture of the cavity with transparent material, application of an aerodynamic barrier, and partially covering the aperture (McIntosh et al., 2014, Cui et al., 2013, Chang et al., 2015). The mitigation of convective losses from cavity receivers is the main interest to this thesis.

In light of the brief introduction above, it is apparent that reducing the cost and the improvement of the thermal efficiency of CST systems are essential to enhance the penetration of solar energy into the energy supply resources. Considering the significant dependence of thermal efficiency of solar cavity receivers on the mitigation of the convective heat losses, it is desirable to reduce these losses. Hence, the motivation of this thesis is to investigate advanced aerodynamic control strategies for solar cavity receivers to minimise convective heat losses.

1.2 Thesis structure

This ‘Thesis by Publication’ is in line with rules and regulations of the University of Adelaide. It is organised into seven chapters, including this introduction chapter, a literature background chapter, four published papers and a summary and conclusion chapter. The details of which are provided here below.

Chapter 1 provides a brief background containing an overview of Concentrated Solar Thermal technology and solar cavity receivers.

Chapter 2 provides background literature on the flow features of cavity receivers including both convectional cavities and cavities with internal active flows. It also provides an overview of studies that investigate convective heat losses from solar cavity receivers as well as methods to mitigate losses from cavities. Also reviewed are studies on the application of the air curtain for practical systems and the current knowledge on the design parameters of air curtains. The final section of the chapter presents the primary scientific research gaps that have been addressed in the current project.

Chapter 3 presents a published article in the ‘Solar Energy’ journal, titled “Experimental insights into the mechanism of heat losses from a cylindrical solar cavity receiver equipped with an air curtain”. This experimental work suggests that a blowing air curtain installed on a solar cavity receiver is most effective when the flow is directed at an inclination angle relative to the aperture plane of the cavity receivers. It also highlights the importance of operating conditions of the cavity receivers on the effectiveness of the air curtain and highlight the major difference with air curtain applications mounted at the entry to commercial buildings.

Chapter 4 contains an article published in ‘Applied Thermal Engineering’ journal, titled “Impact of flow blowing and suction strategies on the establishment of an aerodynamic barrier

for solar cavity receivers". This combined numerical and experimental study compares the effectiveness of two aerodynamic approaches of blowing and suction air curtains to mitigate the convective heat losses from a cylindrical cavity receiver. The results from experimental cases were used for validation of the numerical simulation to provide insights on the mechanism of the operation of an air curtain. The results highlight the need to apply adaptable strategies, based on operating conditions of the cavity, in order to achieve higher thermal efficiency through the mitigation of convective heat losses.

Chapter 5 contains an article submitted to 'Solar Energy journal, titled "An adaptive aerodynamic approach to mitigate convective losses from solar cavity receivers". The paper report results of experimental investigations at different tilt angles and the difficulties associated with high values of inverse Richardson number. It also shows that different strategies are needed for yaw/inclination angle of 45°. It highlights the need to deploy an adaptive aerodynamic strategy that can respond to the measured variation in the operating conditions.

Chapter 6 contains a published article in 'Experimental Thermal Fluids Science' journal, titled "The coupling between the internal and external flows through a hybridized solar cavity receiver under isothermal conditions". This study reports experimental insights into the flow structure within a hybridised model cavity receiver. The findings highlight the need to mitigate the ingress of external flow into the cavity through controlling the back pressure of the cavity or deployment of fluidic barriers.

Finally, chapter 7 contains a summary of the key outcomes reported in this thesis and provides a list of major conclusions. Also, the chapter contains recommendations for future work.

1.3 References

2020. CRESCENT DUNES. https://www.energy.gov/lpo/crescent-dunes.

Adefarati, T., Bansal, R.C., 2019. Reliability, economic and environmental analysis of a microgrid system in the presence of renewable energy resources. Applied Energy 236, 1089-1114.

Bellan, S., Kodama, T., Matsubara, K., Gokon, N., Cho, H.S., Inoue, K., 2019. Heat transfer and particulate flow analysis of a 30 kW directly irradiated solar fluidized bed reactor for thermochemical cycling. Chemical Engineering Science 203, 511-525.

Caldara, D., Cavallo, M., Iacoviello, M., 2019. Oil price elasticities and oil price fluctuations. Journal of Monetary Economics 103, 1-20.

Chang, H., Duan, C., Wen, K., Liu, Y., Xiang, C., Wan, Z., He, S., Jing, C., Shu, S., 2015. Modeling study on the thermal performance of a modified cavity receiver with glass window and secondary reflector. Energy Conversion and Management 106, 1362-1369.

Cui, F., He, Y., Cheng, Z., Li, Y., 2013. Study on combined heat loss of a dish receiver with quartz glass cover. Applied Energy 112, 690-696.

Dorian, J.P., Franssen, H.T., Simbeck, D.R., 2006. Global challenges in energy. Energy Policy 34(15), 1984-1991.

EIA, 2019. International Energy Outlook 2019.

He, Y.-L., Wang, K., Qiu, Y., Du, B.-C., Liang, Q., Du, S., 2019. Review of the solar flux distribution in concentrated solar power: Non-uniform features, challenges, and solutions. Applied Thermal Engineering 149, 448-474.

Hinkley, J., Agrafiotis, C., 2019. Chapter 9 - Solar Thermal Energy and Its Conversion to Solar Fuels via Thermochemical Processes, in: Polygeneration with Polystorage for Chemical and Energy Hubs. Academic Press, pp. 247-286.

Ho, C.K., Iverson, B.D., 2014. Review of high-temperature central receiver designs for concentrating solar power. Renewable and Sustainable Energy Reviews 29, 835-846.

IEA, IEA CO2 Emissions from Fuel Combustion. https://www.iea.org/subscribe-to-data-services/co2-emissions-statistics. 2020).

IEA, 2018. World Energy Outlook 2018.

IEA, 2019. Tracking Power 2019.

IPCC 2018. Global Warming of 1.5°C. An IPCC Special Report on the impacts of global warming of 1.5°C above pre-industrial levels and related global greenhouse gas emission pathways, in the context of strengthening the global response to the threat of climate change, sustainable development, and efforts to eradicate poverty. Masson-Delmotte, V., P. Zhai, H.-O. Portner, D. Roberts, J. Skwa, P.R. Shukla, A. Pirani, W. M.-O., C. Pean, R. Pidcock, S. Connors, J.B.R. Matthews, Y. Chen, X. Zhou, M.I. Gomis, E. Lonnoy, T. Maycock, & M. Tignor, A. T. W. (eds.).

IRENA,2020a.https://public.tableau.com/views/IRENARETimeSeries/Charts?:embed=y&:showVizHome=no&publish=yes&:toolbar=no.

IRENA, 2020b. Renewable Power Generation Costs in 2019. International Renewable Energy Agency, Abu Dhabi.

Kalogirou, S.A., 2018. Chapter 1 - Introduction to Renewable Energy Powered Desalination, in: Renewable Energy Powered Desalination Handbook. Butterworth-Heinemann, pp. 3-46.

Kim, J., Kim, J.-S., Stein, W., 2015. Simplified heat loss model for central tower solar receiver. Solar Energy 116, 314-322.

Knox-Hayes, J., Brown, M.A., Sovacool, B.K., Wang, Y., 2013. Understanding attitudes toward energy security: Results of a cross-national survey. Global Environmental Change 23(3), 609-622.

Kolb, G.J., Ho, C.K., MAncini, T.R., 2011. Power Tower Technology Roadmap and Cost Reduction Plan Sandia National Laboratories Albuquerque, NM.

Lovegrove, K., Stein , W., 2012. 1 - Introduction to concentrating solar power (CSP) technology, in: Concentrating Solar Power Technology. Woodhead Publishing, pp. 3-15.

Ma, R.Y., 1993. Wind Effects on Convective Heat Loss from a Cavity Receiver for a Parabolic Concentrating Solar Collector, Sandia National Laboratories.

McIntosh, A., Hughes, G., Pye, J., 2014. Use of an Air Curtain to Reduce Heat Loss from an Inclined Open-Ended Cavity, 19th Australasian Fluid Mechanics Conference. Melbourne, Australia.

Milani, D., 2019. Chapter 14 - Renewable Energy Integration in Combined Cooling, Heating, and Power (CCHP) Processes, in: Polygeneration with Polystorage for Chemical and Energy Hubs. Academic Press, pp. 459-491.

Mitchell, R.B., 2003. International environmental agreements: A survey of their features, formation, and effects, Annual Review of Environment and Resources. pp. 429-461.

Morales Pedraza, J., 2019. Chapter 1 - General Overview of the Energy Sector in the North America Region, in: Conventional Energy in North America. Elsevier, pp. 1-87.

Nathan, G.J., Jafarian, M., Dally, B.B., Saw, W.L., Ashman, P.J., Hu, E., Steinfeld, A., 2018. Solar thermal hybrids for combustion power plant: A growing opportunity. Progress in Energy and Combustion Science 64, 4-28.

Ordorica-Garcia, G., Delgado, A.V., Garcia, A.F., 2011. Novel integration options of concentrating solar thermal technology with fossil-fuelled and CO2 capture processes. Energy Procedia 4, 809-816.

Painuly, J.P., 2001. Barriers to renewable energy penetration; a framework for analysis. Renewable Energy 24(1), 73-89.

Parida, B., Iniyan, S., Goic, R., 2011. A review of solar photovoltaic technologies. Renewable and Sustainable Energy Reviews 15(3), 1625-1636.

Pitz-Paal, R., 2014. Chapter 19 - Solar Energy – Concentrating Solar Power, in: Future Energy (Second Edition). Elsevier, Boston, pp. 405-431.

Prieto, C., Osuna, R., Fernández, A.I., Cabeza, L.F., 2016. Thermal storage in a MW scale. Molten salt solar thermal pilot facility: Plant description and commissioning experiences. Renewable Energy 99, 852-866.

Sarkar, D.K., 2017. Chapter 1 - General Description of Thermal Power Plants, in: Thermal Power Plant. Elsevier, pp. 1-31.

Schöttl, P., Bern, G., van Rooyen, D.W., Fernández Pretel, J.A., Fluri, T., Nitz, P., 2020. Optimization of Solar Tower molten salt cavity receivers for maximum yield based on annual performance assessment. Solar Energy 199, 278-294.

Shafiee, S., Topal, E., 2009. When will fossil fuel reserves be diminished? Energy Policy 37(1), 181-189.

Shahnazi, R., Dehghan Shabani, Z., 2020. Do renewable energy production spillovers matter in the EU? Renewable Energy 150, 786-796.

Vant-Hull, L.L., 2012. 8 - Central tower concentrating solar power (CSP) systems, in: Concentrating Solar Power Technology. Woodhead Publishing, pp. 240-283.

Chapter 2- Background literature

Presented in this chapter are the background literature and current understanding of cavity receivers' design, both conventional and those incorporating internal jets. Also presented is a review of relevant previous studies that investigated convective heat losses from solar cavity receivers and the proposed mitigation strategies. In particular, the review focuses on studies that investigated the application of an air curtain to mitigate convection losses from cavity receivers. Finally, the research gaps addressed in the current project are presented.

2.1 Convective losses from solar cavity receivers

The quest to improve the thermal efficiency of any energy system, to reduce energy cost and to improve profitability have motivated researchers and engineers alike. Such quest is more prominent in solar thermal systems due to the high cost associated with collecting and concentrating the solar radiation, especially in a tower system. The most effective approach to maximize thermal efficiency is to mitigate heat losses from a cavity receiver. The heat losses from the cavity comprise all forms of heat transfer namely; radiation, conduction and convection. The radiation and conduction losses are relatively easy to estimate and control, whereas the convective heat loss from cavity receivers is more complex. This complexity stems from the interdependency of the design and operating conditions, for example; the geometry of the cavity receiver, its aperture and internal temperature as well as environmental conditions (Siebers and Kraabel, 1984). The majority of previous experimental and analytical studies have focused on the convective heat losses from cavity receivers as a function of the geometrical design, the inclination angle of the cavity, internal temperature distribution, wind speed and wind direction (Lee et al., 2018, Lee et al., 2019b, Lee et al., 2019a, Clausing, 1983, Clausing, 1981, Abbasi-Shavazi et al., 2020, Sinha and Gulhane, 2020, Clausing et al., 1987).

Clausing (1981) used experimental evidence to provide a correlation that estimates the convective losses from cavity receivers. This analytical and experimental study divided the interior volume of the cavity into two zones, as shown in Figure 2.1, namely; the stagnant zone and the convective zone. The stagnant zone is defined as the zone above the aperture of the cavity where hot air is stratified. In contrast, the convective zone is in the lower portion of the cavity where a large eddy occupies the zone due to the density gradient of external cold air and interior hot air. It was found that, for the particular geometry considered in this study and under normal working conditions, the wind had a minimal influence on convection losses and the orientation of the aperture had a critical influence on the buoyant flow and the height of the convective zone within the cavity.

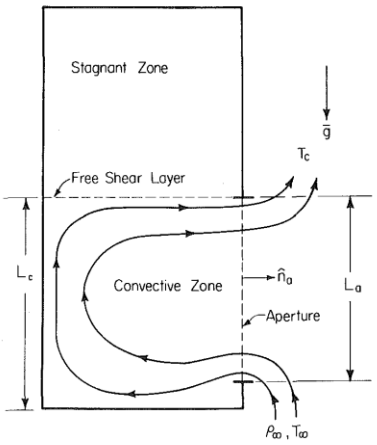

Figure 2.1- Schematics of convective and stagnant zones relevant to a cavity proposed by Clausing (1981).

Prakash *et al.* (2009) investigated the convective losses of a scaled down downward-facing cylindrical cavity receiver both experimentally and numerically. They have used dimensionless numbers relevant to convective heat losses from cavity receivers such as Nusselt number (Nu) and Grashof Number (Gr) to generalise their finding. They concluded that the convective losses for the cavity under windy conditions are generally higher than those at no wind conditions. The only exception was the side-on wind case, in which wind acted as a barrier at the aperture. It was also found that the head-on wind led to higher convective loss than the

side-on wind. It was also demonstrated that for no wind conditions, the analysis of convective heat losses at low temperatures is a reasonably accurate predictor of heat losses at high temperatures used in industrial applications up to 300℃. However, for windy conditions since the convective heat losses do not change linearly with speed, it is not feasible to extend the low-temperature analysis to high-temperature conditions. In a subsequent study, Prakash *et al.* (2010) showed that by increasing the receiver inclination, the convective losses from the aperture decrease.

Flesch *et al.* (2014) used numerical methods to investigate convection heat losses from large solar cavity receivers with fixed cavity Grashof number of $Gr = 2.9 \times 10^{10}$, and maximum wind tunnel Reynolds number of $Re = 3.4 \times 10^{5}$. They concluded that the wind parallel to the aperture could inhibit the hot air's egress from the cavity and therefore reduces convective heat losses. They also found that wind speed is a critical parameter in increasing heat losses from inclined cavities, in contrast to the horizontal cases with a tilt angle of 0°. Using a combined temperature and velocity plot, they explained the variation of the heat losses as a function of wind speed (Figure 2.2). The plot shows that the velocity vectors inside the cavity were much smaller than those outside the cavity due to the protective role of the cavity walls. They also reported that the interior part of the cavity can generally be divided into three zones known as; a) the top zone, where the temperature is equal to the wall temperature, b) the bottom zone, where the temperature is close to the ambient temperature, and c) the transitional zone between the top and bottom zones, where the temperature changed linearly from the wall temperature to the ambient temperature. The main difference of this work with the study by Clausing was the investigation of side on wind condition. Clausing model was developed for head-on wind conditions only. Their results revealed that by exposing the cavity to the wind, the upper zone shrank and the transition zone expanded. It was hypothesised that the reason

behind this is the disturbance of the thermal stratification by a slight increase of the velocity inside the cavity, induced by wind speed.

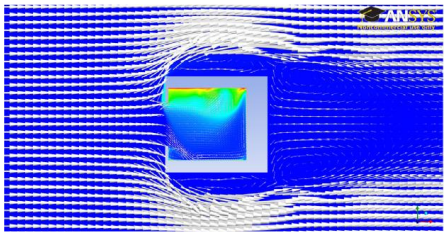

Figure 2.2- Calculated temperature contour and velocity vector plot on the central plane of a cavity receiver (Flesch et al., 2014).

Lee *et al.* (2017) used three-dimensional computational fluid dynamics (CFD) to provide insights into the impact of the cavity aspect ratio on the convective heat losses. They assessed the cavity length to diameter ratio of 0.3 to 3 for head-on wind speeds of 2, 4, 7 and 10 m/s. It was found that convective heat losses increase non-linearly with an aspect ratio (AR). The slope of the variation of natural convective heat losses with AR showed a sharp growth of 50% for the AR varying from 0.5 to 1.5 while it only increased 2.5% by variation of AR from 2 to 3. It was also found that the effect of the wind on convective heat losses is more profound for lower AR.

The effects of inhomogeneity of the cavity wall temperatures on the natural convective heat losses were investigated by Abbasi-Shavazi *et al.* (2020), in a combined analytical and experimental study. The non-uniform temperature distribution of the cavity walls reproduces more realistic operating conditions of the real-world application of the cavity receivers caused by the uneven incoming solar radiation caused by the optical arrangements and throughout the day. They found that as temperature non-uniformity of the wall increases it leads to a decrease in the convective heat losses. They proposed a new correlation based on the Nusselt number using Grashof number, characteristic length, aspect ratio and temperature non-uniformity that can be used for different geometries. In addition, they have assessed the reliability of the

developed correlations of convective heat losses in the literature and found that the Clausing correlation (Clausing et al., 1987) predicts the convective heat losses with reasonable accuracy. However, the proposed correlation in this study is more related to the practical application of cavity receivers for a wider range of operating conditions and geometry.

In a systematic experimental campaign, Lee *et al.* (2018, 2019 a,b) used a scale down model of cylindrical heated cavity (ID = 0.3m, L = 0.45m) in a large scale wind tunnel to investigate the convective heat losses. The internal surfaces of the cavity comprised 16 individually controlled heaters; on the top, bottom and back plate. This arrangement made it possible to measure the losses from different sections of the cavity and allowed the reproduction of uniform or distributed wall temperatures. They defined the Richardson number as the ratio of Grashof to the square of Reynolds number to accommodate the effect of scale, wind speed and temperature difference on the relative roles of the buoyancy and inertia forces. The investigated range of Richardson numbers covers the range of that for practical application of solar receivers with higher temperatures and size. However, careful validation should be taken for a case that has different conditions. In general, their findings demonstrated the complexity of the dependence of convective heat losses on the various parameters such as wind speed, wind direction, the tilt angle of the cavity and internal surface temperature. They found that for head-on wind conditions, as expected, the convective heat losses increase with an increase in wind speed. The dependence of the Nusselt number on the inverse Richardson number of 0 to 200, has revealed two different correlation equations, for different ranges of inverse Richardson number. For the range of inverse Richardson number less than 10, where the convective heat losses occur due to both natural and mixed convection, the governing equation was exponential. For the inverse Richardson number larger than 10 cases, where the convective losses are dominated by forced convection the Nusselt number is a function of the square root of Ri.

Noteworthy is that in the study by Lee *et al.* (2018, 2019 a,b) and for side-on wind conditions, the variation of the convective heat losses with wind speed was different from the head-on wind condition. The main discrepancy was observed at a cross wind speed of 3 m/s where the convective heat losses were less than no wind condition. This implies that low side-on wind flow can act as an aerodynamic barrier across the aperture. They also provided evidence to show that increasing the wind speed for a variety of aperture ratios, defined as the ratio of the aperture to the cavity inner diameter (D_{ap}/D_{cav}), resulted in an increase in convective heat losses. The results also showed different trends of the growth of the relative convective heat losses (defined as the convective heat losses for a given wind speed relative to that for an equivalent case at no wind condition) as a function of wind speed for different aperture ratios. So that the relative heat losses at a wind speed of 9 m/s for an aperture ratio of 0.33 were 7 times larger than that for aperture ratio of 1.0. The variation of cavity temperature at various tilt angles showed that for all cavity inclination angles, increasing the uniform temperature of the cavity increases the heat losses nonlinearly. It was also found that a beam up cavity had the lowest heat losses through the aperture compared with two cases of beam down and a tilt angle of 15°.

In summary, the finding from literature survey on convective heat losses from solar cavity receivers indicated that the geometry and shape of the cavity (Clausing, 1981, Jilte et al., 2014, Lee et al., 2017), the inclination angle of the cavity (Clausing, 1981, Hu et al., 2017, Prakash et al., 2010), wind speed and direction (Prakash et al., 2009, Flesch et al., 2014, Lee et al., 2017) and the mean temperature of the cavity and distribution of the temperature (Montiel Gonzalez et al., 2012, Abbasi-Shavazi et al., 2020, Lee et al., 2019a) are the metrics that have strong effects on the convective heat losses. It is worth noting that these studies focused on developing correlations among the parameters that influence convective heat losses and estimated losses. While very useful, nevertheless these studies did not seek to investigate

methods to mitigate convective heat losses from cavity receivers. The following sections present a background review of the studies that have implemented measures to reduce convection losses from cavity receivers.

2.2 Mitigating convective heat losses

A multitude of approaches has been proposed to decrease convective heat losses from solar cavity receivers such as varying the geometrical properties of the cavity, recovering the heat, covering the aperture with a transparent material and using an air curtain as an aerodynamic barrier across the aperture (Uhlig et al., 2014). It is worth acknowledging that the geometrical properties of the cavity are limited by other components of the whole system, such as the heliostat field design and the optical arrangements (Pujol-Nadal et al., 2015). Therefore, for a fixed geometry and inclination angle of the cavity additional strategies are needed to mitigate the losses.

The employment of a quartz window to cover the aperture of the cavity receivers has been proposed as a method to decrease the convective heat losses by permitting the solar radiation to pass through it while it covers the aperture and prevents any air exchange across the aperture and hence convective losses (Hertel et al., 2016). This approach is attributed to the transmission properties of the quartz window which is transparent to the visible solar radiation beams whereas is not transparent to the infrared wavelength of hot air within the cavity which minimizes radiation losses from the cavity (Sullivan and Kesseli, 2019). Chang *et al.* reported a 56% reduction in convective heat losses from a solar cavity receiver by the fitting of a quartz window (Chang et al., 2015). However, at elevated temperature applications, related to the practical operating conditions of solar cavity receivers, the mechanical strength of quartz window is significantly impacted by the surface defects. Also, environmental contaminants at high-temperature result in crystallization of the quarts window (Sullivan and Kesseli, 2019).

These drawbacks of a quartz window motivated further studies to find alternative solutions that do not involve the covering of the aperture with a transparent material in order to reduce convective heat losses.

Partial coverage of aperture has been proposed as an alternative method to mitigate the convective heat losses from cavity receivers by Flesch *et al.* (2016). The results showed that for a head on wind condition on a cavity with partial coverage of the aperture and a tilt angle of 60°, the natural convective heat losses reduced up to 35%, whereas for a wind speed of 5 m/s the convective heat losses increased. For a horizontal cavity, it was demonstrated that the partial coverage of the aperture reduced the convective heat losses by 20% and 22% for wind speeds of 0 and 5 m/s, respectively. However, while the coverage of the aperture reduces the convective heat losses by restricting the interaction of the flows inside and outside the cavity, it suffers from the drawbacks associated with the solid coverage that causes the restriction of the fraction of the solar radiation beams from entering the cavity. Thus this method was not deemed highly practical especially that losses increased with the increase in wind speed.

A promising strategy involved the use of an air curtain as an aerodynamic barrier for open cavities that are not sensitive to air leakage. It works by reducing the interaction between the fluids inside and outside the cavity while simultaneously permitting solar radiation into the cavity. “Aerodynamic sealing” has been extensively used in many practical applications such as industrial furnaces (Oliveira et al., 1991), open refrigerated display cabinet (Sun et al., 2017), buildings (ASHRAE 90.1; Goubran et al., 2016), refuge alternatives (Wang et al., 2017) and medical clean rooms (Knudsen et al., 2019) in order to reduce the movement of heat, moisture and mass from one space to another. Previous works on air curtain design, e.g. Oliveira *et al.* (1991), have shown that some of the parameters need to be taken into account when designing air curtains include; density gradient, momentum flux and the height of the nozzles to the

impinging surface. These parameters differ markedly from one application to another and hence different considerations need to be taken into account for each application.

2.3 Aerodynamic barriers

The principle of aerodynamic sealing is the generation of an air stream between two areas as a transparent wall to confine the target environment with specific conditions to control the heat, moisture, chemical properties, dust and mass ingress or egress (Xiao et al., 2020, Gonçalves et al., 2012). This concept has been widely used in the industry where the deployment of a solid wall is not desirable. For various applications in industry, such as industrial heat treatment that needs to prevent the mixing of the furnace gases and ambient atmosphere, contactless sealing is a promising alternative. Presented in Figure 2.3 is a schematic of the sealing device used in a furnace, with a divided slot nozzle, to prevent flow interactions between the chamber atmosphere and ambient (Oliveira et al., 1991).

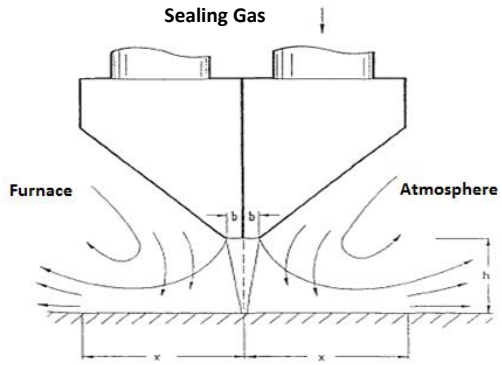

Figure 2.3- Schematic of the sealing device with divided nozzle (Oliveira et al., 1991).

A very common usage of the air curtain is to eliminate or reduce the energy and mass transfer in a doorway between two contiguous rooms in a building (Goubran et al., 2016, Costa et al., 2006, Yang et al., 2019). Air curtains have been broadly used in buildings to reduce the energy loss caused by external air infiltration through the doors. Moreover, air curtains have the potential to intercept dust and insects from entering the conditioned space. The primary

studies on air curtain date back to more than half a century ago and involved the use of mathematical models (Hayes, 1968, Hayes and Stoecker, 1969b, Hayes and Stoecker, 1969a). The developed analytical equations were used to characterize the jet flow and to quantify the heat transfer through the air curtain for building entrances. The correlations were developed based on the deflection modulus that was defined as the momentum flux of the curtain flow relative to the forces acting on either side of the air curtain. Worth mentioning is that this correlation included the transversal forces deduced by the density gradient on either side of the air curtain only while neglecting the wind deduced pressures within buildings.

In recent studies by Siren *et al.* (Sirén, 2003b, Sirén, 2003a), the design criteria of air curtains have been developed. It was found that the jet-discharging angle is a major factor for the air curtain to generate an effective aerodynamic barrier. In addition, it was found that the opening (door) height and neutral pressure level affect thermal losses indirectly through the jet momentum flux. Costa *et al.* (Costa et al., 2006) assessed the effect of the jet discharge angle on the sealing effectiveness and found that the sealing effectiveness of an air curtain increased by about 70% at the jet orientation of 15°-20° outwards, compared with that of straight discharge orientation. The effect of the velocity of the air curtain on the effectiveness of an air curtain in refrigerator rooms was assessed by Verhaeghe *et al.* (2010) and Foster *et al.* (2007). In a numerical study, Verhaeghe *et al.* (2010) observed that the losses from the cold room were higher for low jet outlet velocities. As the curtain jet velocity increased to the minimum required, as per the equation developed by Hayes (Hayes and Stoecker, 1969a), the heat transfer value reached its minimum value as well. Further increases in the jet velocity resulted in a linear increase in heat transfer. In an experimental study, Foster *et al.* (2007) discovered the effectiveness of an air curtain in a cold storage room with internal dimensions of $L \times W \times H$ = 4.8 m × 5.8 m × 3.8 m. They found that the maximum value of the air curtain effectiveness was obtained at a jet velocity of 18 m/s, while a further increase of the jet velocity

caused the effectiveness to decrease. However, due to the significant differences between the geometry and operating condition of a solar cavity receiver relative to a building, the findings of the studies on the application of air curtain in buildings needed to be assessed to investigate if they are valid for solar cavity receivers.

The primary equations used in the design of air curtain for building applications were developed by Hayes and Stoecker (1969 a,b) by using the deflection modulus method. The deflection modulus was defined as the ratio between the momentum flux of the air curtain at the outlet and the transversal forces acting on it. The transversal forces were induced by the temperature difference on both sides of the air curtain, such that

$$D_m = \frac{\rho_{ac} b_{ac} u_{ac}^2}{gH(\rho_c - \rho_h)} \qquad (1)$$

where ρ_{ac} is the density of the air flow of air curtain, b_{ac} is the width of the air curtain, u_{ac} is the velocity of air curtain flow, g is the gravitational acceleration, H is the height of the opening, ρ_c is the density of the air on the cold side and ρ_h is the density of the air on the hot side.

The minimum value of D_m was estimated with an empirical constant based on the ratio of the width of the nozzle to the height of the opening (see Figure 2.4 for an example of these correlations).

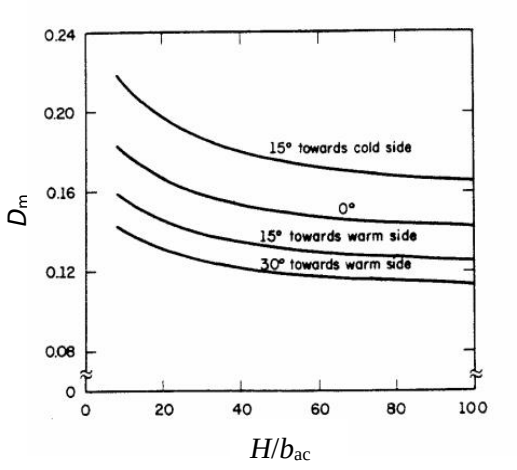

Figure 2.4- Minimum deflection module required to maintain an unbroken curtain (Hayes and Stoecker, 1969b).

Zhang *et al.* (2018) modified the deflection modulus method to correlate the effect of wind flow on the air curtain performance when designing a road tunnel. The study investigated the effect of an air curtain in a road tunnel to prevent the flue gases ingress from spreading into the tunnel in case of the fire at the entrance of the tunnel. However, the "piston effect" created by the movement of the vehicles in a tunnel, which spreads the fire, was not negligible. Thus, Zhang et al. added wind pressure term (Equation 4) to the equation of the deflection modulus (Hayes and Stoecker, 1969b). The total pressure difference in both sides of the air curtain ΔP_{ac} includes the pressure gradient induced by buoyance forces, ΔP_1, and the pressure gradient induced by the wind, ΔP_2.

$$\Delta P_{ac} = \Delta P_1 + \Delta P_2 \quad (2)$$

$$\Delta P_1 = gH(\rho_h - \rho_c) \quad (3)$$

$$\Delta P_2 = 0.5\rho_w u_w^2 \quad (4)$$

where g is the gravitational acceleration (m/s^2), H is the height of the air curtain (the height of the opening), ρ_h, ρ_c and ρ_w are the density of the air from the hot side, cold side and wind flow, respectively and u_w is the wind speed. Using the deflection modulus (D_m), they proposed a correlation (Equation 5) to calculate the momentum of the air curtain to form a stable aerodynamic barrier.

$$(\rho_{ac} b_{ac} u_{ac}^2)_{min} = D_{m,min}[(gH(\rho_c - p_h) + 0.5 p_w u_w^2]H \quad (5)$$

where ρ_c is the density of the air from the air curtain and b is the width of the air curtain outlet.

The minimum value of D_m is estimated with the same empirical constant developed by Hayes and Stoecker (1969 a,b). The minimum velocity of the air curtain can be obtained from Equation (6) and is defined as the velocity sufficient to generate a jet intensity in the entrance of the tunnel to resist the transversal interferences and block the fire.

$$u_{ac\,min} = \sqrt{\frac{D_{m,min}[gH(\rho_c - \rho_h) + 0.5\rho_w u_w^2]H}{\rho_{ac} b_{ac}}} \quad (6)$$

While these correlations are important for the applications they have been developed for, it is clear that there are substantial differences between the geometrical (shape, aperture, inclination, etc.) and operation aspects (inside temperature, density gradients, wind speeds, wind direction, etc.) of a tunnel and that of a solar cavity receiver. Therefore, characterising air curtain design to be employed for tower type solar cavity receivers needs to be examined.

2.4 Air curtain application for solar cavity receivers

The initial analytical studies on the application of the air curtain as an aerodynamic barrier to minimize convective heat losses from solar cavity receivers showed the economic and technical viability of this method (Taussig, 1984). The main goal of employing externally controlled air streams across the cavity aperture is to constrain air infiltration through the aperture. Thus, it inhibits the hot air inside from leaving the cavity and stops the cold outside air from entering the cavity (Ho et al. 2014, Zhang et al., 2015). Noticeable is that the majority of early research into the use of an air curtain for solar receivers are limited to numerical and analytical methods due to the complexity of conducting such experiments at realistic conditions (Qaisrani et al., 2019, Fang et al., 2019, Yang et al., 2018).

One of the very few qualitative experimental studies to examine the effect of applying a fluidic curtain in the vicinity of the aperture were those of McIntosh et al. and Hughes et al. (McIntosh et al., 2014, Hughes et al., 2015). A transparent model cavity immersed in water was used to emulate an air curtain using water as a working fluid. Salinity water and freshwater with an equivalent density ratio of hot air within a cavity at 500 ℃ to the surrounding air were utilised. The planar jet of the ambient water was used to simulate an “air curtain” across the aperture. Qualitative investigations using visual observations (Figure 2.5) showed that by using an aero-window the stagnation zone inside the cavity expands and therefore, the simulated convective heat losses from the cavity decreases. Although these studies provided useful

perspectives into the application of a fluidic barrier across the aperture, they suffered from some serious limitations regarding the dynamic effects of inertia balance relative to the remarkable temperature differences in the flow.

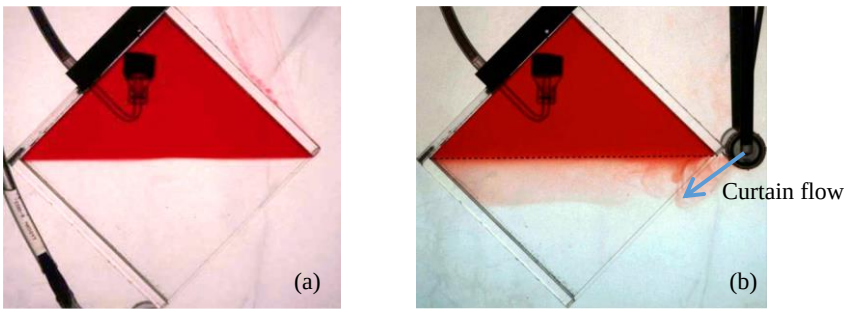

Figure 2.5- Qualitative demonstration of stagnation zone within a cavity for the cases (a) without an air curtain and (b) with an air curtain injecting fluid in the vicinity of the aperture.

In the same study, Hughes *et al.* (2015) also conducted a numerical study that investigated the effect of the air curtain speed and inclination angle on the natural convective losses from an inclined cylindrical cavity. The findings showed that the air curtain has the potential to reduce convective heat losses. However, they found that in cases where the jet was "too strong" or misdirected, the losses are likely to increase. They asserted that a 50% reduction in natural convective heat losses is achievable by using an air curtain with a suitable inclination angle and jet velocity. They presented the plots showing the calculated temperature fields in the longitudinal center plane of the cylindrical cavity for the case without an air curtain, and for two cases with air curtain and different sealing modes, namely "partially-sealed" and "fully-sealed". The results provided new insights into the interaction of the air curtain flow and the hot air inside the cavity. They showed that in the "fully sealed" case, the air curtain builds a virtual wall across the aperture plane. The buoyancy force of the hot air was not large enough to cause the hot flow to entrain the air curtain. Hence, the stagnation zone inside the cavity expands. While in the "partially sealed" case the hot air escapes upward from the aperture and counteracts the momentum of the air curtain. This study presented useful information on the

effect of the curtain jet speed and direction, on the convective heat losses in solar cavity receivers. However, the investigation was limited to natural convection mitigation and the effects of external wind flow were not explored.

In a computational study, Zhang *et al.* (2015a) investigated the influence of air curtain speed and discharge angle on the convective heat losses under various tilt angles of the cavity. Their data showed that an optimum jet speed should be found and applied for each operating condition including the jet discharge angle and inclination angle of the cavity to achieve the desired convective heat loss mitigation. The effectiveness was defined by using the convective heat losses of equivalent cases with an air curtain (Q_{ac}) and without an air curtain (Q_0) as the ratio of as the difference of Q_o and Q_{ac} to Q_0. It was also found that when the jet speed was increased to a value more than the optimum value, referred to as "super stable", the effectiveness decreased. The main heat losses in a "super stable" case were due to mixing of the turbulent jets at high speed with hot air inside the cavity. These studies provided important insights into the heat transfer mechanism when applying an air curtain across the aperture of a solar cavity receiver. It is noteworthy that the numerical models used in this study were only validated using cases without an air curtain. This limits their usefulness especially that there is sufficient evidence to show that air curtains can act to increase heat losses at particular designs and operating conditions. Furthermore, this study was limited to no wind conditions and therefore, the impact of external wind on the performance of the air curtain was not investigated.

In a numerical study, Yong *et al.* (2018) used a solar dish receiver at 723K and an air fan to generate two modes of forced air across the aperture of a cavity with various inclination angles. In the first mode, the pressure of the fan was set to values less than zero generating air jet injecting upward from the lower part of the opening. While in the second type, setting the fan pressure to values larger than zero Pa, the air was injected downward from the upper side

of the opening. The results were obtained at the pressure level of -30 Pa to $+40$ Pa to adjust the speed of the forced air flow across the aperture. It was concluded that by applying an air curtain, the convective heat losses could be reduced up to 58%. The results showed that the upward air curtain had performed better than a downward blowing air curtain. It was also pointed out that the airflow from the air curtain should not exceed a certain velocity threshold, since by increasing the forced airflow as it is depicted in Figure 2.6, the large eddy inside the cavity, induced by the curtain flow, in the proximity of the aperture expanded. This increased the calculated turbulence intensity inside the cavity and it was followed by an increase in the convective heat losses in the vicinity of the aperture. This pronounced the need to find the optimal airflow of the aero-window for the air curtain design. However, this study was limited to the buoyancy dominated flows and further work needs to be done to explore the effect of wind speed on the performance of the air curtain for different configurations of upward or downward blowing.

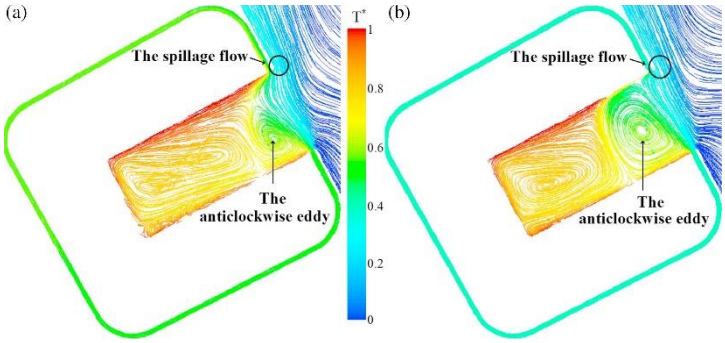

Figure 2.6- The calculated pathlines of the normalised temperature for upward blowing air curtain in the central cross section of the cavity for the inclination angle of $\theta = -30°$ and fan pressure of (a) -20 Pa, (b) -30 Pa. Note: Normalised temperature has been defined as the difference of the temperature at each point with the minimum temperature of the cavity related to the temperature difference of the point with the maximum temperature and the minimum temperature. ($T^* = \frac{T - T_{min}}{T_{max} - T_{min}}$). (Yang et al., 2018)

Fang *et al.* (2019) investigated the influence of the curtain outlet velocity and temperature, and the inclination and width of the air curtain flow on heat losses, through a

computational study. Their results showed that the application of an air curtain enlarges the stagnation zone inside the cavity and the downward-facing air nozzle causes the largest boost in loss mitigation. The variation of convective heat losses as a function of the velocity of the air curtain confirmed that for all cases, including for different outlet widths and flow temperature of the air curtain, at an optimum outlet velocity the heat losses reached their minimum value. However, the presented numerical results are relevant to no wind condition and the effect of the characteristics of the air curtain for windy conditions is yet to be assessed experimentally.

In the literature, very few studies have investigated the impact of wind speed on the air curtain in solar cavity receivers. In a numerical study, Flesch *et al.* (2016) analysed the application of the air curtain for solar cavity receivers under windy conditions. They developed a numerical model of the cavity and validated the case for no modification with available experimental data. They used this model to calculate the convective heat losses for wind speeds varying between 0 to 5 m/s for tilt angles of 0° and 60° with air curtain velocity of 0 to 5 m/s. Utilising the temperature contours and velocity vectors, the impact of head-on wind on the stagnation zone, for both cases of no wind and wind speed of 5 m/s, was demonstrated. It was found that for the horizontal cavity, the convective losses decrease by increasing the curtain speed up to an intermediate value, and then further increase of the jet speed led to an increase in the losses. For the larger inclination angle of the cavity, the optimum curtain speed in which the convective heat losses were minimum was markedly less than that of the horizontal cavity. However, the study did not provide dimensionless numbers relative to the investigated cases to generalise the findings. Thus, a detailed investigation of the wind speed effects on the air curtain performance is yet to be conducted.

2.5 Hybrid Solar Combustion Receiver

The hybridisation of Concentrated Solar Thermal (CST) with other energy sources is being developed to supply firm power, guarantee dispatchability and achieve cost-effective power generation for the times when solar flux is not sufficient. Among the variety of energy sources, combustion is believed to be compatible with CST technology considering the potential of both technologies to be applied for high-temperature applications (Nathan et al., 2018, Corona and San Miguel, 2015, Zhou, 2014). The hybridisation of solar and combustion can be implemented in two arrangements of stand-alone and integrated form (Figure 2.7). In stand-alone systems, combustion is provided as a backup power source for solar technology whereas in an integrated system a solar receiver and a combustor are combined into a single device. The integrated systems have the advantage of sharing the same infrastructure and hence potential reduced capital costs. The integrated systems also reduce operation and maintenance costs because the integration of both energy sources eliminates start-up and shout down and the need for ramp up during intermittent periods (clouds) and the risk of thermal shocks (Nathan et al., 2014). The Hybrid Solar Receiver Combustor (HSRC) is a recently developed hybrid system that uses a single chamber as both the combustion chamber and the solar cavity receiver (Nathan et al., 2013). The cavity incorporates multiple jets providing air and fuel for the combustion process to occur. The HSRC has the potential to be operated in three modes namely; “combustion only”, “solar only” and “hybrid solar and combustion”. This technology has the potential to be compatible with thermal storage systems which enhances the efficiency of the system compared with stand-alone combustion hybridisation (Nathan et al., 2018). The techno-economic assessments revealed that the application of the HSRC system in a power plant has the potential to reduce both the capital and levelised cost of electricity (LCOE) for a power plant up to 51% and 24%, respectively, compared with the solar only system (Nathan et al., 2014). It was also found that relative to an equivalent stand-alone solar and boiler hybrid

system, the HSRC has the potential to reduce the LCOE and fuel consumption up to 17% and 31%, respectively.

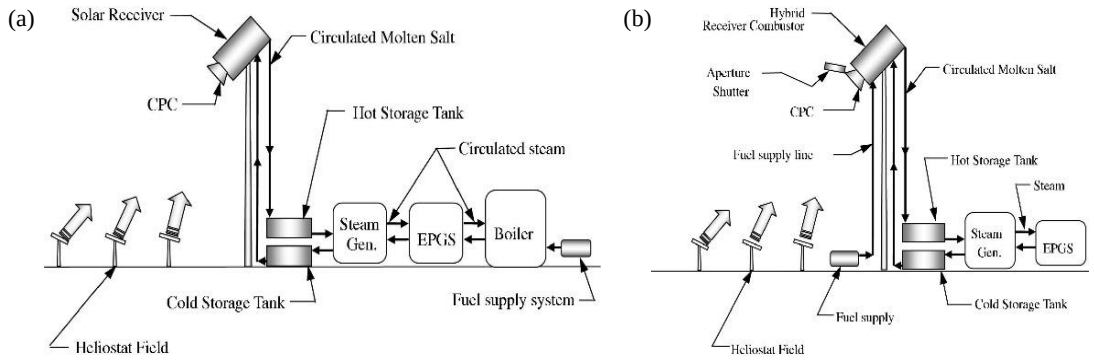

Figure 2.7- Schematic diagram of the hybrid solar power tower configured as (a) stand-alone and (b) integrated system (Nathan et al., 2014).

The experimental demonstration of a 20-kWh$_{th}$ HSRC technology (Chinnici et al., 2018) was successfully conducted by designing and building a laboratory scale device as shown in Figure 2.8. The device features an insulated cavity with an aperture fitted on the front plane to receive solar radiation. A coiled heat exchanger was used in the internal surface of the cavity using air as the heat transfer fluid. Using N-type thermocouples the temperature of the fluid at the inlet and outlet of the heat exchanger and in different sections along the internal surface of the cavity was measured. The annular jet arrangements were featured to provide air and fuel into the cavity with an intense recirculation of hot products to effectively establish the Moderate or Intense Low oxygen Dilution (MILD) combustion regime. MILD combustion regime is characterised by a high recirculated volumetric reaction to offer low pollutants such as NOx emissions, good heat transfer and relatively uniform temperature distribution. A 5-kW xenon-arc solar simulator was used to simulate the solar radiation for solar only and mixed mode of operations. A wide range of fuels was used for the combustion process and the thermal characteristics and pollutant emissions of fuels were measured and recorded. The results showed that MILD combustion regime was successfully established within the chamber. It was also found that the three modes of operation yield similar thermal efficiency. For the operation

of the device in mixed mode, it was found that the interaction of the fluids in the surrounding ambient with the gases inside the cavity did not significantly affect the stability and heat flux profile of the MILD combustion. While the convective heat losses in solar only mode constitute 60% of the total losses, for the mixed mode of operation the sum of radiative and convective losses accounts for 6% of the losses only. However, the study reported the results of the aperture to cavity diameter ratio of 0.2 and the effects of larger aperture ratios have not been reported. Moreover, the effect of external wind on the combustion and convective heat losses from the chamber was not considered in this study.

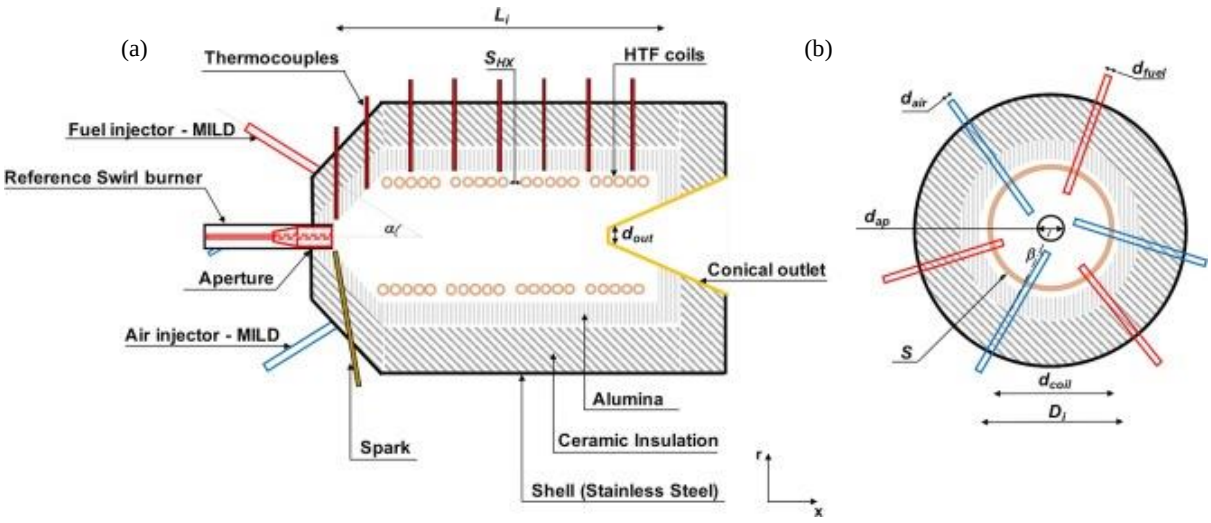

Figure 2.8- Schematics diagram of the HSRC device a) the side view presenting the position of the thermocouples b) the end view (Chinnici et al., 2018).

In a subsequent study, Chinnici *et al.* (2020) measured the effect of solar to combustion ratio on the performance of an HSRC. This study showed how changing the solar intensity and variation of solar to combustion ratio changes the performance of the HSRC. It was found that for a large range of solar to combustion ratios the stability of MILD combustion occurs. This indicates that the MILD combustion can be used to compensate for variability in the solar resource. However, the neglected in this study was the effect of variation of the external flow on the stability of the combustion process.

Flow behaviours within the HSRC can be categorised into three main features depending on the operation mode. In the solar only mode, where no jet is used and the aperture is open to receive the solar radiation, the cavity can be considered as a conventional cavity receiver. In the combustion only mode, where fuel and air are provided through multiple impinging jets into the cavity to establish a combustion regime and where the aperture is closed, the flow behaviour is similar to that for a combustion chamber and features jets in a confined cylinder. In the mixed mode of operation, the air and fuel are provided into the cavity through multiple jets and the aperture is opened to receive the solar radiation. While there is an immense body of literature on the flow behaviour within the combustion chambers and conventional cavity receivers, there is a lack of knowledge on the flow features relevant to the latter category of HSRC flow i.e. in the mixed mode of operation. It is important to investigate the interaction of flows inside and outside the hybrid cavity, as the entertainment of the external flow has the potential to change the flow features within the cavity. It can affect the combustion process and the stability of the combustion by changing the air to fuel ratio. Moreover, the entrainment of the cold external air into the cavity has the potential to increase the convective heat losses through the aperture.

2.6 Flow features induced by multiple jets in confined flow

A great deal of attention has been devoted to studies of both reacting and non-reacting flows induced by jets within a chamber (Zhu and Shih, 1994, Dahm and Dimotakis, 1987, Fitzgerald and Garimella, 1998, Boushaki et al., 2008). From these studies, it was found that flow features within an enclosure are primarily affected by the inclination angle of jets to the chamber axis. In an experimental study, Gao *et al.* (2013) used the Particle Image Velocimetry (PIV) technique to investigate the flow characteristics generated by two opposed round jets inside Confined Impinging Jet Reactors (CIJRs) under isothermal condition. They found that for a jet Reynolds number range of 10620 to 21210, the effect of the jet Reynolds number on

the velocity distribution in the cavity was negligible. They also observed that the stagnation point, where the jets emerged and the flow velocity was zero, substantially depended on the jet velocity ratio of two jets. The results showed that for the geometry they used, and to keep the stagnation point at the centre of the chamber, hence to have a symmetric flow pattern within the chamber, an equal flow rate through the jets is essential. It was also found that as the distance between the jets axis to the end of the cavity increased, the zone with high turbulence kinetic energy decreases. Worth noting is that these experiments were conducted in a cavity without an aperture, therefore, the effect of external flow on the flow behaviour within the chamber has not been investigated.

Chammem *et al.* (2013) used a combination of experimental and numerical techniques to investigate the flow field of inclined jets in a large longitudinal enclosure. They characterised the flow dynamics resulting from the impingement of two inclined jets with different jets pitch angles and Reynolds numbers. It was found that each jet in the confined space, behaves like a single jet initially. As the jets evolve further, the outer edges of the jets started to interact with each other to form one combined jet. The position of the "resulting jet" formation, depended on the pitch angle of the jets so that for larger pitch angles, the resulting jet developed further downstream. It was also found that the turbulence intensity, the velocity decay rate and the jet spreading rate depend on the jet Reynolds number.

In a series of studies Long *et al*. (2017, 2018a,b, 2019) investigated the flow features of isothermal multiple jets in a confined chamber under a variety of conditions relevant to practical applications such as solar receiver reactor, gas turbine engines and multiple burner combustors. In a combined experimental and numerical study (Long et al., 2017), the isothermal flow within a scaled down cylindrical cavity equipped with planar symmetric jets was characterised. They utilised the PIV technique as the experimental method to investigate flow behaviour using water as the working fluid. For the numerical modelling, they used the

Reynolds-Averaged Navier-Stokes (RANS) method to develop a 3 dimensional (3-D) computational fluid dynamic (CFD) model. They investigated the influence of the number of the jets and inclination angle on the flow dynamics under isothermal conditions by using 2 and 4 jets configured as inclined jets with inclination angles to the chamber axis (α_j) of 25° and 50° whereas the Reynold number of the jet flow was fixed at 10,500. The results showed that (see Figure 2.9) four major flow regimes were observed within the cavity with a significant dependence on the inclination angle and number of the jets. The flow regimes included a central recirculation regime for $0° \leq \alpha_j < 10°$, an external recirculation zone with a jet impingement point for $10° \leq \alpha_j < 35°$, reverse flow for $35° \leq \alpha_j < 60°$ and a secondary dominant external recirculation zone for $60° \leq \alpha_j < 90°$. It was found that the flow stability, dominant flow recirculation zone and turbulent intensity were mainly controlled by the inclination angle while the number of jets had a secondary impact on the flow stability, the turbulence intensity and the transition of the recirculation regime.

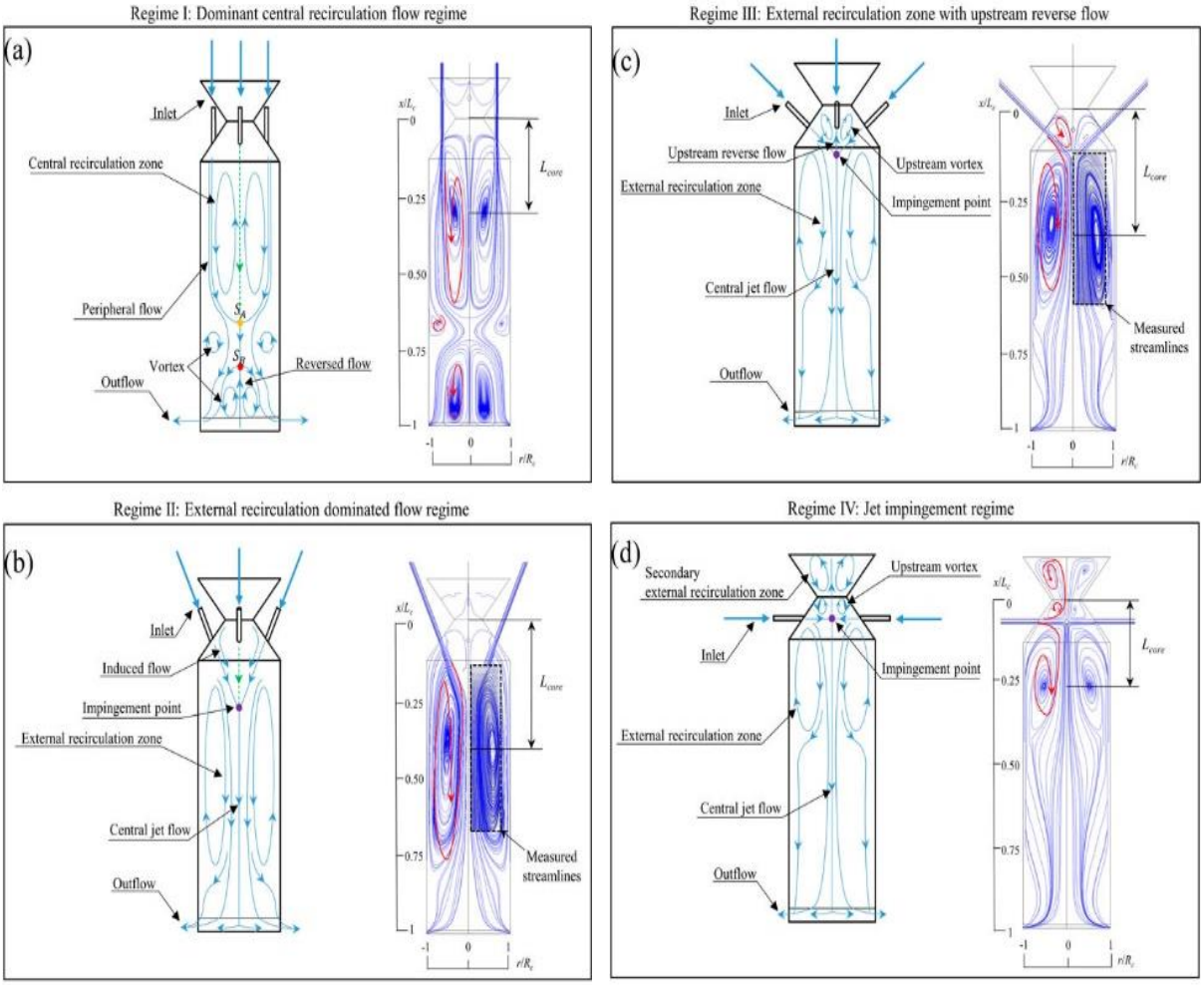

Figure 2.9- Diagrams showing the flow fields induces by multiple impinging jets in a cylindrical chamber for four jets with inclination angles of (a) 0°, dominant central recirculation flow regime, (b) 25°, external recirculation dominated flow regime, (c) 50°, external recirculation zone with upstream reverse flow, (d) 90°, jet impingement regime (Long et al., 2017).

In a subsequent experimental study, Long *et al.* (2018b) investigated the flow behaviour within cylindrical cavity equipped with four rotationally symmetric jets with inclination angle (α_j) varying over 25° to 45° and a tangential component to the chamber axis (θ_j) termed as azimuth angle varying from 0° to 15°. It was found that the jet azimuthal angles have a first-order influence on flow behavior within the cavity so that the strength of the resulting jet flow changed reversely with the value of azimuthal angle whereas the strength of reverse flow increased as the azimuthal angle increases. The extent of turbulence and flow unsteadiness were also significantly influenced by the jet azimuthal angle.

In a following study, Long *et al.* (2018) investigated the effect of the aspect ratio of a cavity with four swirling jets on the flow field within a cylindrical cavity. It was revealed that for jets with an inclination angle of 25° and azimuthal angle over the range of 5° to 15°, the flow features within the cavity strongly depended on the aspect ratio of the cavity. As depicted in Figure 2.10, three different flow patterns namely; external and central recirculation zones, external recirculation zone with a resulting flow and external recirculation zone with no resulting flow regimes, were observed over the aspect ratio of 1 to 3. The effect of aspect ratio and back pressure variation was significant over the aspect ratio of 1 to 1.5, whereas their effect was weak for larger aspect ratios.

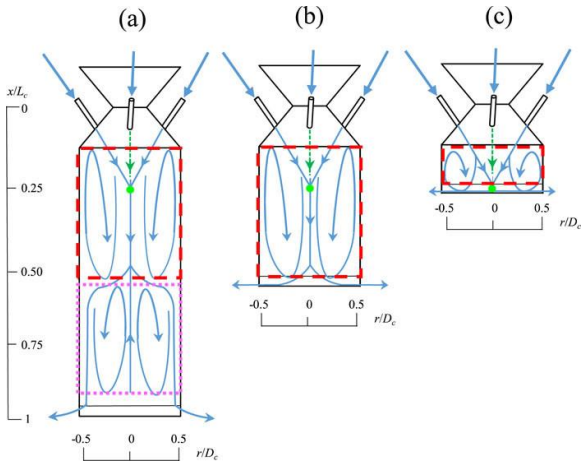

Figure 2.10- Schematic diagrams of the flow features within a cylindrical cavity induced by multiple impinging jets for aspect ratios (L_c/D_c) of 1-3. (a) External and central recirculation zones, (b) External recirculation zone with a resulting flow, (c) External recirculation zone with no resulting flow (Long et al., 2018).

A wide range of studies has been devoted to investigating the precessing vortex core (PVC), defined as the precession of the vortex-core relative to the axis of an axisymmetric device, for single jet application (Syred, 2006). These studies showed that flow features, combustion efficiency and mixing performances of vortex devices are significantly influenced by PVC. An experimental study by Long *et al.* (2019) provided both qualitative and quantitative information on the interaction of the isothermal flows from multiple confined jets within a cylindrical cavity. The jets were configured with swirl angles (θ_j) of 5° and 15° and

inclination angles (α_j) of 25° and 45° at a fixed jet Reynolds number of $Re = 10500$. As presented in Figure 2.11, for the jet configurations they used, three distinctive flow regimes were identified based on the extent of the central recirculation zone (CRZ) and the external recirculation zone (ERZ). While a PVC occurred for all three flow regimes, the following main flow characteristics were observed for each regime. For the jet configuration of α_j = 45° and θ_j = 15°, magnitude of the tangential velocity was the strongest along the chamber central line within CRZ and the cavity was dominantly covered by CRZ. For jet configuration of α_j = 25° and θ_j = 5°, ERZ was the dominant flow feature within the cavity and the value of the tangential velocity was weak. For the jet configuration of α_j = 25° and θ_j = 15°, the extents of CRZ and ERZ were relatively similar and the flow was characterised by a medium swirl.

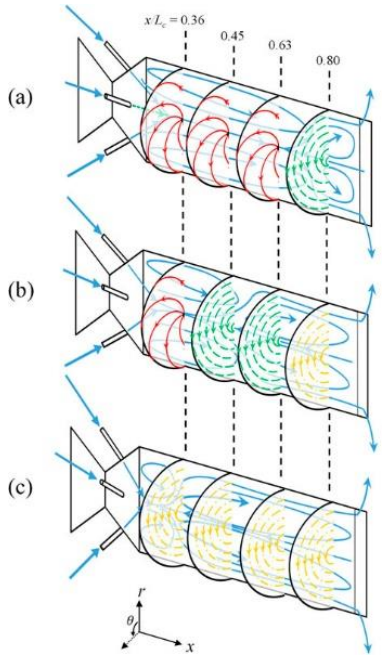

Figure 2.11 - Schematic diagram of three dominant flow features within a confined cylindrical cavity incorporating multiple impinging jets with the configuration of (a) $\alpha_j = 25°$ and $\theta_j = 5°$, (b) $\alpha_j = 25°$ and $\theta_j = 15°$ and (c) $\alpha_j = 45°$ and $\theta_j = 15°$ (Long et al., 2019).

While the discussion above concerning the flow behaviour of jets in a confined flow provides an understanding of the flow features within a cavity, the flow features within a cavity incorporating multiple jets and an open aperture with an external flow are yet to be fully

explored. Therefore, it is essential to better understand the interaction of external and internal flow behaviours of such cavities and to develop strategies to mitigate the convective heat losses from hybrid solar cavities.

2.7 Scalability and dimensional analysis

In the engineering and physical sciences, dimensional analysis is a well-developed method to reduce the number of experimental variables. Dimensional analysis is also associated with two main advantages of gaining analytical insights into a given phenomenon and the scalability of results. The scalability of results makes it possible to generalise results to similar systems of differing scales (Albrecht et al., 2013, Shen et al., 2014). Many engineering fluid mechanics problems are solved by testing the smaller-scale models. To apply scaling principles, one should consider similarity requirements between a prototype and a model. The similarity requirements include geometric, dynamics and kinematic similarities. Geometric similarity requires that all linear dimensions have the same scale ratio. Strictly speaking, satisfying geometric similarity is essential for any meaningful model test. To apply kinematic similarity, velocity and acceleration ratios at similar points of the model and the prototype should be the same. Dynamic similarity involves the equality of the ratios of different forces at similar points of the model and the prototype (Gerhart et al., 1992). In order to achieve the complete dynamic similarity between geometrically similar flows, the dimensionless groups must be reproduced in the same values. For instance, same Reynolds number between a model and prototype is ensured for dynamically similar flows (Zohuri, 2015).

In the literature, the experimental studies on the convective heat losses from solar cavity receivers and the studies investigating the effectiveness of air curtain utilised the dimensional analysis to express the system with independent variables and dimensionless parameters. These dimensionless numbers can be divided into three main categories of the geometry of cavity,

the operation of a cavity and the application of an air curtain. The first group includes the aperture to cavity diameter (D_{ap}/D_{cav}) and length to the diameter of the cavity (L_{cav}/D_{cav}) (Lee et al. 2017; Kasaeian et al., 2021). The second group includes Reynolds number, Grashof number, Nusselt number and Richardson number of the cavity (Clausing, 1981; Siebers & Kraabel, 1984; He et al, 2019; Kim et al, 2015; Lee et al, 2019a; b; Lipiński et al, 2021). The last group includes deflection modulus, the relative velocity of air curtain flow to wind flow, the momentum ratio of the air curtain to wind flow and effectiveness (Fang et al., 2019, Hayes and Stoecker, 1969 a,b, Khayrullina et al., 2020). For instance, the wind speed for tower mounted cavity receivers is in the range of 15 to 20 m/s. This corresponds to a Reynolds number in the order of 10^6 (Clausing, 1981). The Grashof number is estimated to be in order of 10^{12} for practical cavity receivers (Le Quere, 1981). The Richardson number also is used to characterise the heat transfer regime within cavity receivers. For head-on wind directions, natural and mixed convection control convective heat losses below an inverse Richardson number of 10, while forced convection dominates above this threshold (Ma, 1993).

2.8 Research gaps

The above background literature has provided valuable insights into the importance of mitigating convective heat losses from standard and hybrid solar cavity receivers and how a fluidic barrier across the aperture can assist in mitigating these losses. Despite the many studies, some research gaps remain in the literature which requires further research. Some of these gaps are:

- The interaction of the flows across the aperture of a hybrid cavity receiver, with induced flows inside the cavity, is not yet understood;
- The effects of the flow pattern induced by multiple impinging jets on flow through a cavity aperture have not been ascertained;

- The effects of wind speed and direction on air ingress and its impact on the combustion process inside a hybrid cavity receiver have not been well-understood;
- Systematic assessment of the key controlling parameters influencing the performance of a fluidic barrier system for a solar receiver under windy condition has not been established;
- The influences of operating conditions of a cavity on the performance of the air curtain for windy conditions have not been investigated experimentally;
- The feasible approaches to design air curtain with regards to either the active flow type (injection or suction) or curtain configuration in the vicinity of the aperture have received limited attention.

2.9 Project aim and objectives

To address the above-identified gaps in the literature, the current study aims to develop an aerodynamic based approach for convective heat loss mitigation from tower-mounted solar cavity receivers (including hybrid solar-combustion systems). That is, this aerodynamic barrier will minimize fluid ingress/egress into and from the solar receiver as well as prevent hot gases from leaving the cavity through the aperture, for a standard cavity receiver and the hybrid solar receiver combustor operating in the mixed-mode. Hence, in a systematic combined numerical and experimental campaign, the application of an air curtain to minimize convective heat losses from a heated cavity receiver for a series of wind speeds and air curtain operating conditions was examined. The main aim of this study is to deduce the mechanism of the convective heat losses from solar cavity receivers and to provide a basis for understanding the parameters associated with loss mitigation approaches.

The specific objectives of the present project, to address the aim and gaps, are to:

1. Design and assess fluidic barrier concepts for a scaled model of the cavity receiver;
2. Examine the configurations of air curtain for different convective heat transfer regimes;
3. Develop and validate 3-D CFD model and use to provide additional understanding of the flow behaviour within the cavity and the interaction of the external flows of wind and aerodynamic barriers;
4. Evaluate the relationship between the internal flow patterns and flow characteristics in the vicinity of the aperture of a hybrid cavity affected by the external wind.

2.10 References

ASHRAE 90.1, 2010. Energy standard for buildings except low-rise residential buildings. American Society of Heating, Refrigerating and Air-Conditioning Engineers Inc, I-P Edition, Atlanta, GA.

Abbasi-Shavazi, E., Torres, J.F., Hughes, G., Pye, J., 2020. Experimental correlation of natural convection losses from a scale-model solar cavity receiver with non-isothermal surface temperature distribution. Solar Energy 198, 355-375.

Adefarati, T., Bansal, R.C., 2019. Reliability, economic and environmental analysis of a microgrid system in the presence of renewable energy resources. Applied Energy 236, 1089-1114.

Albrecht, M. C., Nachtsheim, C. J., Albrecht, T. A., Cook, R. D. 2013. Experimental Design for Engineering Dimensional Analysis. Technometrics, 55, 257-270.

Bellan, S., Kodama, T., Matsubara, K., Gokon, N., Cho, H.S., Inoue, K., 2019. Heat transfer and particulate flow analysis of a 30 kW directly irradiated solar fluidized bed reactor for thermochemical cycling. Chemical Engineering Science 203, 511-525.

Boushaki, T., Mergheni, M.A., Sautet, J.C., Labegorre, B., 2008. Effects of inclined jets on turbulent oxy-flame characteristics in a triple jet burner. Experimental Thermal and Fluid Science 32(7), 1363-1370.

Caldara, D., Cavallo, M., Iacoviello, M., 2019. Oil price elasticities and oil price fluctuations. Journal of Monetary Economics 103, 1-20.

Chammem, T., Mhiri, H., Vauquelin, O., 2013. Experimental and computational investigation of Reynolds number effect on the longitudinal ventilation in large enclosure of twin inclined jets. Building and Environment 67, 87-96.

Chang, H., Duan, C., Wen, K., Liu, Y., Xiang, C., Wan, Z., He, S., Jing, C., Shu, S., 2015. Modeling study on the thermal performance of a modified cavity receiver with glass window and secondary reflector. Energy Conversion and Management 106, 1362-1369.

Chinnici, A., Nathan, G.J., Dally, B.B., 2018. Experimental demonstration of the hybrid solar receiver combustor. Applied Energy 224, 426-437.

Chinnici, A., Nathan, G.J., Dally, B.B., 2020. Experimental investigation of the influence of solar-to-fuel ratio on performance and stability characteristics of hybrid solar-MILD hydrogen processes. Proceedings of the Combustion Institute.

Clausing, A.M., 1981. An analysis of convective losses from cavity solar central receivers. Solar Energy 27(4), 295-300.

Clausing, A.M., 1983. Convective Losses From Cavity Solar Receivers—Comparisons Between Analytical Predictions and Experimental Results. Journal of Solar Energy Engineering 105(1), 29-33.

Clausing, A.M., Waldvogel, J.M., Lister, L.D., 1987. Natural Convection From Isothermal Cubical Cavities With a Variety of Side-Facing Apertures. Journal of Heat Transfer 109(2), 407-412.

Corona, B., San Miguel, G., 2015. Environmental analysis of a Concentrated Solar Power (CSP) plant hybridised with different fossil and renewable fuels. Fuel 145, 63-69.

Costa, J.J., Oliveira, L.A., Silva, M.C.G., 2006. Energy savings by aerodynamic sealing with a downward-blowing plane air curtain—A numerical approach. Energy and Buildings 38(10), 1182-1193.

Cui, F., He, Y., Cheng, Z., Li, Y., 2013. Study on combined heat loss of a dish receiver with quartz glass cover. Applied Energy 112, 690-696.

Dahm, W.J.A., Dimotakis, P.E., 1987. Measurements of entrainment and mixing in turbulent jets. AIAA Journal 25(9), 1216-1223.

Dorian, J.P., Franssen, H.T., Simbeck, D.R., 2006. Global challenges in energy. Energy Policy 34(15), 1984-1991.

EIA, 2019. International Energy Outlook 2019. EIA.

Fang, J., Tu, N., Torres, J.F., Wei, J., Pye, J.D., 2019. Numerical investigation of the natural convective heat loss of a solar central cavity receiver with air curtain. Applied Thermal Engineering 152, 147-159.

Fitzgerald, J.A., Garimella, S.V., 1998. A study of the flow field of a confined and submerged impinging jet. International Journal of Heat and Mass Transfer 41(8), 1025-1034.

Flesch, R., Grobbel, J., Stadler, H., Uhlig, R., Hoffschmidt, B., 2016. Reducing the convective losses of cavity receivers. 1734, 030014.

Flesch, R., Stadler, H., Uhlig, R., Pitz-Paal, R., 2014. Numerical analysis of the influence of inclination angle and wind on the heat losses of cavity receivers for solar thermal power towers. Solar Energy 110, 427-437.

Foster, A.M., Swain, M.J., Barrett, R., D'Agaro, P., Ketteringham, L.P., James, S.J., 2007. Three-dimensional effects of an air curtain used to restrict cold room infiltration. Applied Mathematical Modelling 31(6), 1109-1123.

Gao, Z., Han, J., Xu, Y., Bao, Y., Li, Z., 2013. Particle Image Velocimetry (PIV) Investigation of Flow Characteristics in Confined Impinging Jet Reactors. Industrial & Engineering Chemistry Research 52(33), 11779-11786.

Gerhart, P. M., Gross, R. J. & Hochstein, J. I. 1992. Fundamentals of Fluid Mechanics: Solutions Manual, Addison-Wesley Publishing Company.

Gonçalves, J.C., Costa, J.J., Figueiredo, A.R., Lopes, A.M.G., 2012. CFD modelling of aerodynamic sealing by vertical and horizontal air curtains. Energy and Buildings 52, 153-160.

Goubran, S., Qi, D., Saleh, W.F., Wang, L., Zmeureanu, R., 2016. Experimental study on the flow characteristics of air curtains at building entrances. Building and Environment 105, 225-235.

Hayes, F., 1968. Heat transfer characteristics of the air curtain- A plane jet subjected to transverse pressure and temperature gradients(Heat transfer characteristics of plane jet air curtain subject to transverse pressure and temperature gradients).

Hayes, F.C., Stoecker, W.F., 1969a. Design data for air curtains. ASHRAE Trans.

Hayes, F.C., Stoecker, W.F., 1969b. Heat transfer characteristics of the air curtain. ASHRAE Trans.

He, Y.-L., Wang, K., Qiu, Y., Du, B.-C., Liang, Q., Du, S., 2019. Review of the solar flux distribution in concentrated solar power: Non-uniform features, challenges, and solutions. Applied Thermal Engineering 149, 448-474.

Hertel, J., Uhlig, R., Söhn, M., Schenk, C., Helsch, G., Bornhöft, H., 2016. Fused silica windows for solar receiver applications. AIP Conference Proceedings 1734(1), 030020.

Hinkley, J., Agrafiotis, C., 2019. Chapter 9 - Solar Thermal Energy and Its Conversion to Solar Fuels via Thermochemical Processes, in: Polygeneration with Polystorage for Chemical and Energy Hubs. Academic Press, pp. 247-286.

Ho, C.K., Iverson, B.D., 2014. Review of high-temperature central receiver designs for concentrating solar power. Renewable and Sustainable Energy Reviews 29, 835-846.

Ho, C.K., J.M. Christian, A.C. Moya, J. Taylor, D. Ray, and J. Kelton, 2014, Experimental and Numerical Studies of Air Curtains for Falling Particle Receivers, in Proceedings of ASME 2014 8th International Conference on Energy Sustainability, ES-FuelCell2014-6632, Minneapolis, MN, June 29 - July 2, 2014.

Hu, T., Jia, P., Wang, Y., Hao, Y., 2017. Numerical simulation on convective thermal loss of a cavity receiver in a solar tower power plant. Solar Energy 150, 202-211.

Hughes, G., Pye, J., Kaufer, M., Abbasi- Shavazi, E., Zhang, J., McIntosh, A., Lindley, T., 2015. Reduction of convective losses in solar cavity receivers, SolarPACES 2015. Cape Town, South Africa.

IEA, IEA CO2 Emissions from Fuel Combustion. https://www.iea.org/subscribe-to-data-services/co2-emissions-statistics. 2020).

IEA, 2018. World Energy Outlook 2018.

IEA, 2019. Tracking Power 2019.

IRENA,2020a.https://public.tableau.com/views/IRENARETimeSeries/Charts?:embed=y&:showVizHome=no&publish=yes&:toolbar=no.

IRENA, 2020b. Renewable Power Generation Costs in 2019. International Renewable Energy Agency, Abu Dhabi.

Jilte, R.D., Kedare, S.B., Nayak, J.K., 2014. Investigation on Convective Heat Losses from Solar Cavities under Wind Conditions. Energy Procedia 57, 437-446.

Kalogirou, S.A., 2018. Chapter 1 - Introduction to Renewable Energy Powered Desalination, in: Renewable Energy Powered Desalination Handbook. Butterworth-Heinemann, pp. 3-46.

KASAEIAN, A., KOURAVAND, A., VAZIRI RAD, M. A., MANIEE, S. & POURFAYAZ, F. 2021. Cavity receivers in solar dish collectors: A geometric overview. Renewable Energy, 169**,** 53-79.

KHAYRULLINA, A., VAN HOOFF, T., ALANIS RUIZ, C., BLOCKEN, B. & VAN HEIJST, G. 2020. Minimum momentum flux ratio required to prevent air curtain breakthrough in case of cross-curtain pressure gradients: CFD versus analytical equation. Building Simulation, 13, 943-960.

Kim, J., Kim, J.-S., Stein, W., 2015. Simplified heat loss model for central tower solar receiver. Solar Energy 116, 314-322.

Knox-Hayes, J., Brown, M.A., Sovacool, B.K., Wang, Y., 2013. Understanding attitudes toward energy security: Results of a cross-national survey. Global Environmental Change 23(3), 609-622.

Knudsen, L.L., Naydenov, K.G., Rasmussen, C., Melikov, A.K., Fang, L., 2019. Risk for contamination in a cleanroom with weakened aerodynamic barrier, IOP Conference Series: Materials Science and Engineering.

Kolb, G.J., Ho, C.K., MAncini, T.R., 2011. Power Tower Technology Roadmap and Cost Reduction Plan Sandia National Laboratories Albuquerque, NM.

Le Quere P, Penot F, Mirenayat M., 1981. Experimental study of heat loss through natural convection from an isothermal cubic open cavity, Sandia National Laboratories, SAND81-8014.

Lee, K.L., Chinnici, A., Jafarian, M., Arjomandi, M., Dally, B., Nathan, G., 2018. Experimental investigation of the effects of wind speed and yaw angle on heat losses from a heated cavity. Solar Energy 165, 178-188.

Lee, K.L., Chinnici, A., Jafarian, M., Arjomandi, M., Dally, B., Nathan, G., 2019a. The influence of wall temperature distribution on the mixed convective losses from a heated cavity. Applied Thermal Engineering 155, 157-165.

Lee, K.L., Chinnici, A., Jafarian, M., Arjomandi, M., Dally, B., Nathan, G., 2019b. The influence of wind speed, aperture ratio and tilt angle on the heat losses from a finely controlled heated cavity for a solar receiver. Renewable Energy 143, 1544-1553.

Lee, K.L., Jafarian, M., Ghanadi, F., Arjomandi, M., Nathan, G.J., 2017. An investigation into the effect of aspect ratio on the heat loss from a solar cavity receiver. Solar Energy 149, 20-31.

Long, S., Lau, T.C.W., Chinnici, A., Tian, Z.F., Dally, B.B., Nathan, G.J., 2017. Experimental and numerical investigation of the iso-thermal flow characteristics within a cylindrical chamber with multiple planar-symmetric impinging jets. Physics of Fluids 29(10), 105111.

Long, S., Lau, T.C.W., Chinnici, A., Tian, Z.F., Dally, B.B., Nathan, G.J., 2018a. The influence of aspect ratio on the iso-thermal flow characteristics of multiple confined jets. Physics of Fluids 30(12), 125108.

Long, S., Lau, T.C.W., Chinnici, A., Tian, Z.F., Dally, B.B., Nathan, G.J., 2018b. Iso-thermal flow characteristics of rotationally symmetric jets generating a swirl within a cylindrical chamber. Physics of Fluids 30.

Long, S., Lau, T.C.W., Chinnici, A., Tian, Z.F., Dally, B.B., Nathan, G.J., 2019. Characteristics of swirling and precessing flows generated by multiple confined jets. Physics of Fluids 31(5), 055102.

Lovegrove, K., Stein , W., 2012. 1 - Introduction to concentrating solar power (CSP) technology, in: Concentrating Solar Power Technology. Woodhead Publishing, pp. 3-15.

Ma, R.Y., 1993. Wind Effects on Convective Heat Loss from a Cavity Receiver for a Parabolic Concentrating Solar Collector, Sandia National Laboratories.

McIntosh, A., Hughes, G., Pye, J., 2014. Use of an Air Curtain to Reduce Heat Loss from an Inclined Open-Ended Cavity, 19th Australasian Fluid Mechanics Conference. Melbourne, Australia.

Milani, D., 2019. Chapter 14 - Renewable Energy Integration in Combined Cooling, Heating, and Power (CCHP) Processes, in: Khalilpour, K.R. (Ed.) Polygeneration with Polystorage for Chemical and Energy Hubs. Academic Press, pp. 459-491.

Mitchell, R.B., 2003. International environmental agreements: A survey of their features, formation, and effects, Annual Review of Environment and Resources. pp. 429-461.

Montiel Gonzalez, M., Hinojosa Palafox, J., Estrada, C.A., 2012. Numerical study of heat transfer by natural convection and surface thermal radiation in an open cavity receiver. Solar Energy 86(4), 1118-1128.

Morales Pedraza, J., 2019. Chapter 1 - General Overview of the Energy Sector in the North America Region, in: Morales Pedraza, J. (Ed.) Conventional Energy in North America. Elsevier, pp. 1-87.

Nathan, G.J., Battye, D.L., Ashman, P.J., 2014. Economic evaluation of a novel fuel-saver hybrid combining a solar receiver with a combustor for a solar power tower. Applied Energy 113, 1235-1243.

Nathan, G.J., Dally, B., Ashman, P.J., Steinfeld, A., 2013. A hybrid receiver- combustor.

Nathan, G.J., Jafarian, M., Dally, B.B., Saw, W.L., Ashman, P.J., Hu, E., Steinfeld, A., 2018. Solar thermal hybrids for combustion power plant: A growing opportunity. Progress in Energy and Combustion Science 64, 4-28.

Oliveira, L.A., Costa, J.J., Carvalho, M.G., Gerhardt, H.J., Kramer, C., 1991. On aerodynamic sealing for industrial applications. Journal of Wind Engineering and Industrial Aerodynamics 37(3), 255-268.

Ordorica-Garcia, G., Delgado, A.V., Garcia, A.F., 2011. Novel integration options of concentrating solar thermal technology with fossil-fuelled and CO2 capture processes. Energy Procedia 4, 809-816.

Painuly, J.P., 2001. Barriers to renewable energy penetration; a framework for analysis. Renewable Energy 24(1), 73-89.

Parida, B., Iniyan, S., Goic, R., 2011. A review of solar photovoltaic technologies. Renewable and Sustainable Energy Reviews 15(3), 1625-1636.

Pitz-Paal, R., 2014. Chapter 19 - Solar Energy – Concentrating Solar Power, in: Future Energy (Second Edition). Elsevier, Boston, pp. 405-431.

Prakash, M., Kedare, S.B., Nayak, J.K., 2009. Investigations on heat losses from a solar cavity receiver. Solar Energy 83(2), 157-170.

Prakash, M., Kedare, S.B., Nayak, J.K., 2010. Determination of stagnation and convective zones in a solar cavity receiver. International Journal of Thermal Sciences 49(4), 680-691.

Prieto, C., Osuna, R., Fernández, A.I., Cabeza, L.F., 2016. Thermal storage in a MW scale. Molten salt solar thermal pilot facility: Plant description and commissioning experiences. Renewable Energy 99, 852-866.

Pujol-Nadal, R., Martínez-Moll, V., Sallaberry, F., Moià-Pol, A., 2015. Optical and thermal characterization of a variable geometry concentrator using ray-tracing tools and experimental data. Applied Energy 155, 110-119.

Qaisrani, M.A., Fang, J., Jin, Y., Wan, Z., Tu, N., Khalid, M., Rahman, M.U., Wei, J., 2019. Thermal losses evaluation of an external rectangular receiver in a windy environment. Solar Energy 184, 281-291.

Sarkar, D.K., 2017. Chapter 1 - General Description of Thermal Power Plants, in: Thermal Power Plant. Elsevier, pp. 1-31.

Schöttl, P., Bern, G., van Rooyen, D.W., Fernández Pretel, J.A., Fluri, T., Nitz, P., 2020. Optimization of Solar Tower molten salt cavity receivers for maximum yield based on annual performance assessment. Solar Energy 199, 278-294.

Shafiee, S., Topal, E., 2009. When will fossil fuel reserves be diminished? Energy Policy 37(1), 181-189.

Shahnazi, R., Dehghan Shabani, Z., 2020. Do renewable energy production spillovers matter in the EU? Renewable Energy 150, 786-796.

Shen, W., Davis, T., Lin, D. K. J., Nachtsheim, C. J. 2014. Dimensional Analysis and Its Applications in Statistics. Journal of Quality Technology, 46, 185-198.

Siebers, D.L., Kraabel, J.S., 1984. Estimating convective energy losses from solar central receivers. Sandia National Labs., Livermore, CA (USA), United States.

Sinha, R., Gulhane, N.P., 2020. Mathematical Modeling of Heat Losses from Cylindrical Cavity Receiver in Solar Parabolic Dish. Springer Singapore, Singapore, pp. 1-11.

Sirén, K., 2003a. Technical dimensioning of a vertically upwards-blowing air curtain - Part II. Energy and Buildings 35(7), 697-705.

Sirén, K., 2003b. Technical dimensioning of a vertically upwards blowing air curtain - Part I. Energy and Buildings 35(7), 681-695.

Sullivan, S.D., Kesseli, J.B., 2019. Design and test validation of a novel low-cost quartz window for reducing heat losses in concentrating solar power applications. AIP Conference Proceedings 2126(1), 030058.

Sun, J., Tsamos, K.M., Tassou, S.A., 2017. CFD comparisons of open-type refrigerated display cabinets with/without air guiding strips. Energy Procedia 123, 54-61.

Syred, N., 2006. A review of oscillation mechanisms and the role of the precessing vortex core (PVC) in swirl combustion systems. Progress in Energy and Combustion Science 32(2), 93-161.

Taussig, R.T., 1984. Aerowindows for central solar receivers. American Society of Mechanical Engineers, Winter Annual Meeting, New Orleans, LA, 12.

Uhlig, R., Flesch, R., Gobereit, B., Giuliano, S., Liedke, P., 2014. Strategies Enhancing Efficiency of Cavity Receivers. Energy Procedia 49, 538-550.

Vant-Hull, L.L., 2012. 8 - Central tower concentrating solar power (CSP) systems, in: Concentrating Solar Power Technology. Woodhead Publishing, pp. 240-283.

Verhaeghe, G., Van Belleghem, M., Willockx, A., Verhaert, I., De Paepe, M., 2010. Study of air curtains used to restrict infiltration into refrigerated rooms.

Wang, S., Jin, L., Ou, S., Li, Y., 2017. Experimental air curtain solution for refuge alternatives in underground mines. Tunnelling and Underground Space Technology 68, 74-81.

Xiao, D., Li, X., Fang, Z., Yan, W., Jiang, Y., Zhao, X., 2020. Investigation of the dust control performance of a new transverse-flow air curtain soft-sealing system. Powder Technology 362, 238-245.

Yang, S., Alrawashdeh, H., Zhang, C., Qi, D., Wang, L., Stathopoulos, T., 2019. Wind effects on air curtain performance at building entrances. Building and Environment 151, 75-87.

Yang, S., Wang, J., Lund, P.D., Wang, S., Jiang, C., 2018. Reducing convective heat losses in solar dish cavity receivers through a modified air-curtain system. Solar Energy 166, 50-58.

Zhang, J.J., Pye, J.D., Hughes, G.O., 2015a. Active Air Flow Control to Reduce Cavity Receiver Heat Loss, 9th International Conference on Energy Sustainability collocated with the ASME 2015 Power Conference. San Diego, California, USA, p. V001T005A023.

Zhang, J.J., Pye, J.D., Hughes, G.O., 2015b. Active Air Flow Control to Reduce Cavity Receiver Heat Loss. (56840), V001T005A023.

Zhang, L., Yan, Z.-z., Li, Z.-h., Wang, X.-m., Han, X.-f., Jiang, J.-c., 2018. Study on the Effect of the Jet Speed of Air Curtain on Smoke Control in Tunnel. Procedia Engineering 211, 1026-1033.

Zhou, C., 2014. Hybridisation of solar and geothermal energy in both subcritical and supercritical Organic Rankine Cycles. Energy Conversion and Management 81, 72-82.

Zhu, J., Shih, T.H., 1994. A Numerical Study of Confined Turbulent Jets. Journal of Fluids Engineering 116(4), 702-706.

Zohuri, B. 2015. Dimensional Analysis and Self-Similarity Methods for Engineers and Scientists, Switzerland, Springer, Cham.

Chapter 3-
Experimental insights into the mechanism of heat losses from a cylindrical solar cavity receiver equipped with an air curtain

Statement of Authorship

Title of Paper	Experimental insights into the mechanism of heat losses from a cylindrical solar cavity receiver equipped with an air curtain
Publication Status	☑ Published ☐ Accepted for Publication ☐ Submitted for Publication ☐ Unpublished and Unsubmitted work written in manuscript style
Publication Details	Solar Energy Volume 201, 1 May 2020, Pages 314-322

Principal Author

Name of Principal Author (Candidate)	Elham Alipourtarzanagh		
Contribution to the Paper	Performed experiments, acquisition of data, interpret data, writing of the manuscript and acted as the corresponding author.		
Overall percentage (%)	70%		
Certification:	This paper reports on original research I conducted during the period of my Higher Degree by Research candidature and is not subject to any obligations or contractual agreements with a third party that would constrain its inclusion in this thesis. I am the primary author of this paper.		
Signature		Date	06/10/2020

Co-Author Contributions

By signing the Statement of Authorship, each author certifies that:

i. the candidate's stated contribution to the publication is accurate (as detailed above);

ii. permission is granted for the candidate in include the publication in the thesis; and

iii. the sum of all co-author contributions is equal to 100% less the candidate's stated contribution.

Name of Co-Author	Alfonso Chinnici		
Contribution to the Paper	Conceptualization, supervised the research and contributed in academic discussion		
Signature		Date	7/10/2020

Name of Co-Author	Graham J Nathan		
Contribution to the Paper	Conceptualization, methodology development, review and editing manuscript, supervision, project administration and funding acquisition		
Signature		Date	8/10/2020

Name of Co-Author	Bassam Dally			
Contribution to the Paper	Conceptualization, methodology development, review and editing manuscript, supervision, project administration and funding acquisition			
Signature			Date	6-10-2020

Solar Energy 201 (2020) 314–322

Contents lists available at ScienceDirect

Solar Energy

journal homepage: www.elsevier.com/locate/solener

Experimental insights into the mechanism of heat losses from a cylindrical solar cavity receiver equipped with an air curtain

Elham Alipourtarzanagh*, Alfonso Chinnici, Graham J. Nathan, Bassam B. Dally

Centre for Energy Technology, School of Mechanical Engineering, the University of Adelaide, Adelaide, South Australia 5005, Australia

ARTICLE INFO

Keywords:
Solar cavity receiver
Concentrated solar thermal
Air curtain
Convective heat losses
Control strategy

ABSTRACT

We report on the effectiveness of an air curtain to mitigate convective heat losses from a heated cylindrical cavity receiver operated at fixed tilt (15°) and yaw angles (0°). The cavity was heated electrically with a controller to maintain a constant inside temperature of 300 °C, varying wind speed, air curtain velocity and discharge angle. It was found that the greatest convective heat losses occur over the lower internal surfaces of the cavity for all cases, spanning both natural and forced convection regimes, while a discharge angle of 30° relative to the face of the cavity is more effective than a parallel curtain, which was found to increase heat losses. It was also found that, for a discharge angle of 0°, increasing the velocity of the air curtain leads to higher convective heat losses. However, for a curtain discharge angle of 30°, increasing the air curtain velocity can reduce heat losses by up to 60%. The measured distribution of air temperature across the aperture plane and convective heat losses through the surface were used to provide insight into the causes of these observations. These results suggest that, for tilted, tower-mounted cavity receivers, the orientation of an air curtain should be directed with a component towards the wind, rather than parallel to the aperture plane.

1. Introduction

Tower-mounted cavity receivers are under development for Concentrating Solar Thermal energy (CST) technology owing to their potential to lower radiation losses, which is particularly important for high temperature applications (Vant-Hull, 2012). Solar receivers have the crucial role in CST systems of absorbing the concentrated solar radiation and transferring it to a heat transfer fluid (Romero et al., 2002). Hence, a key research driver is the need to minimize heat losses from a cavity receiver in order to enhance thermal efficiency and reduce solar thermal energy costs (Clausing, 1981, 1983; Lee et al., 2018; Lee et al., 2019a, b; Siebers and Kraabel, 1984; Taussig, 1984; Uhlig et al., 2014). However, while the radiation losses have received much attention, the convective heat losses are both more complex and more poorly understood. This complexity stems from the interdependency of the operating conditions, the geometry of the cavity receiver and environmental conditions (Siebers and Kraabel, 1984). Therefore, the overall objective of the present investigation is to advance understanding of potential approaches to mitigate convective heat losses from cavity receivers.

The majority of the previous investigations of the convective heat losses from cavity receivers have considered the geometrical shape, the inclination angle of the cavity, internal temperature distribution, wind speed and wind direction (Clausing, 1981, 1983; Lee et al., 2018; Lee et al., 2019a, b). However, little attention has been given to the potential for active flow control devices, such as air curtains, to mitigate convective losses. This previous work has identified that the internal flow is typically divided into two zones, namely the upper stagnant zone, where hot air is stratified, and the low convective zone, driven by buoyancy and/or wind (Clausing, 1981). Lee (Lee et al. (2018, 2019b) found, through measurements in a wind tunnel, two regimes in the dependence of the Nusselt number on the inverse Richardson number. For head-on wind directions, natural and mixed convection control convective heat losses below an inverse Richardson number of 10, while forced convection dominated above this threshold (Lee et al., 2018). However, the relationship depends both on wind direction and cavity dimensions. Interestingly, they also found that, for some wind speeds and a side-on wind direction, the convective heat losses are even lower than for the case with no wind at all. This is significant, because it suggests that an air curtain may be able to generate a barrier to convective losses across the aperture. However, no measurements of the effect of an air curtain on convective losses have been reported to date.

The use of an air curtain as an aerodynamic barrier to convective heat losses from solar cavity receivers has been proposed previously (Uhlig et al., 2014). Furthermore, a preliminary estimate suggests that this could be economically and technically viable (Taussig, 1984).

* Corresponding author.
E-mail address: elham.alipour@adelaide.edu.au (E. Alipourtarzanagh).

https://doi.org/10.1016/j.solener.2020.03.004
Received 11 December 2019; Received in revised form 7 February 2020; Accepted 2 March 2020
Available online 12 March 2020

Nomenclature

A	area (m^2)
b	width of the air curtain (m)
D	diameter (m)
g	gravity (m/s^2)
H	height (m)
K	thermal conductivity (W/m K)
L	length (m)
P	pressure (Pa)
Q	heat transferred (W)
T	temperature (°C)
u	velocity (m/s)
W	width (m)

Greek Letters

α	yaw angle of the cavity (°)
β	thermal expansion coefficient (1/K)
ε	effectiveness
θ	tilt angle of the cavity (°)
μ	Viscosity (kg/m. s)
ρ	density (kg/m^3)
ϕ	discharge angle of the air curtain (°)

Non-Dimensional Numbers

D_m	deflection modulus
Gr	Grashof number, $Gr = \frac{\rho^2 g\beta(T_{wall}-T_a)D_{cav}^3}{\mu^2}$
Nu	Nusselt number, $Nu = \frac{Q_{conv}D_{cav}}{A_{total,cav}(T_{wall}-T_a)k_{ref}}$
Re	Reynolds number, $Re = \frac{\rho u_w D_{cav}}{\mu}$
Ri	Richardson number, $Ri = \frac{Gr}{Re^2} = \frac{g\beta(T_{wall}-T_a)D_{cav}}{u_w^2}$

Subscripts or Superscripts

a	ambient
ac	air curtain
ap	aperture
c	cold side
cav	cavity
h	hot side
l	losses
n-ac	no air curtain
ref	reference
w	wind

Abbreviations

ac	Air Curtain
CST	Concentrating Solar Thermal
conv	convection
rad	radiation
cond	conduction
SLPM	standard litter per minute

However, it should be noted that the air curtain is acting as an aerodynamic barrier and do not seal the cavity receivers completely in a way that the transparent windows do. Therefore, while the air curtain can be applied for cavities with chemical reactions which are not sensitive to the air leakage (Jafarian et al., 2017), for cavities with sensitive reactions to air leakage (Romero and Steinfeld, 2012) further considerations and improvements of the aerodynamic barrier are required. Aerodynamic barriers have been extensively used in many practical applications, such as industrial furnaces (Oliveira et al., 1991), open refrigerated display cabinets (Sun et al., 2017), buildings (Goubran et al., 2016) and refuges (Wang et al., 2017) to reduce the penetration of heat, moisture and mass from one space to another. Previous work (Oliveira et al., 1991) has shown that some of the parameters need to be taken into account when designing air curtains, including the density gradient, momentum flux and the height of the nozzles above the impinging surface relative to the nozzle width. However, the relative significance of these parameters differs markedly from one application to another, so that work from one investigation cannot be directly translated to another. Hence, the present paper seeks to identify those parameters of an air curtain which affect the applications of solar cavity receivers.

A number of mathematical models have also been used to estimate the heat transfer through an air curtain and to characterise its flow (Hayes, 1968; Hayes and Stoecker, 1969a, b). Hayes and Stoecker (1969a, b) developed analytical equations to design air curtains for building applications. They based their correlations on the ratio of air curtain momentum flux to the traverse forces on the height of the air curtain, deduced by the density gradient on either side of the air curtain. Worthy of note is that they did not consider the effect of wind load on the air curtain in their equation because it is negligible within a building. More recently, Siren (Sirén (2003a, b), developed equations to design the dimensions of air curtains, but also for building applications. They found that the jet-discharge angle is an important parameter for air curtain stability. Other important parameters are the ratio of the door height to the width of the air curtain and the jet momentum flux. Costa (Costa et al. (2006) assessed the effect of the jet discharge angle on the effectiveness of the air curtain and found it to increase by about 70% for an outward orientation of 15°–20°, compared with that of a vertical discharge. It is also known (Fang et al., 2019; Hayes and Stoecker, 1969a; Hughes et al., 2015; Verhaeghe et al., 2010; Zhang et al., 2015) that there is an optimal discharge velocity, with heat losses increasing as the jet velocity exceeds the optimal value. However, due to the significant differences between the geometry and operating conditions, such as the temperature and wind speed of a solar cavity receiver relative to a building, it can be expected that these previous correlations will have poor validity for solar cavity receivers under windy conditions.

Perhaps the equations of greatest relevance were developed by Zhang (Zhang et al. (2018), as an extension from previous studies for buildings (Hayes and Stoecker, 1969a, b). The total pressure difference across the two sides of the air curtain ΔP_{ac} is the sum of the pressure gradient induced by the temperature difference per meter of the width of the air curtain, ΔP_1, and that induced by the wind, ΔP_2.

$$\Delta P_{ac} = \Delta P_1 + \Delta P_2 \tag{1}$$

$$\Delta P_1 = gH(\rho_h - \rho_c) \tag{2}$$

$$\Delta P_2 = 0.5\rho_w u_w^2 \tag{3}$$

where g is the gravity, H is the height of the air curtain (the height of the opening), ρ_h is the density of the air on the hot side, ρ_c is the density of the flow in the cold side, ρ_w is the density of the blowing air induced by the wind, which is equal to the air density at the cold side, and u_w is the wind speed. The Deflection Modulus (D_m) is defined by Hayes (Hayes and Stoecker, 1969b) as the ratio between the momentum flux of the air curtain at the outlet and the force exerted by the height of the air curtain, driven by the total pressure gradient on either side of the jet flow. By applying the total pressure gradient from Eq. (1), the deflection modulus is:

$$D_m = \frac{(\rho_{ac} b_{ac} u_{ac}^2)}{[(gH(\rho_c - p_h) + 0.5\rho_w u_w^2]H}. \quad (4)$$

The proposed minimum deflection modulus ($D_{m,\min}$) to generate sufficient jet intensity at the entrance of a road tunnel to resist any traverse interference and inhibit flow through the opening, can be estimated with an empirical constant based on the ratio of the width of the nozzle to the height of the opening (b_{ac}/H) (Hayes and Stoecker, 1969a). By rearranging Eq. (4) the minimum velocity required to achieve $D_{m,\min}$ and form a stable aerodynamic barrier can be found using Eq. (5) as follows:

$$u_{ac,min} = \sqrt{\frac{D_{m,min}[gH(\rho_c - \rho_h) + 0.5\rho_w u_w^2]H}{\rho_{ac} b_{ac}}}. \quad (5)$$

Given the differences between conditions in a building and solar receiver, noted above, one aim of the present investigation is to assess the extent to which these correlations apply and to assess the effective parameters on the performance of the air curtain to minimise the convective heat losses from solar cavity receivers.

To address the above-identified gaps in the literature, the aim of the current study is to advance understanding both of the effectiveness of air curtains for solar cavity receivers and the relevance of previous equations in describing them. This is to be undertaken through systematic experimental investigation, using a series of air curtains for a heated cylindrical cavity receiver for a series of wind speeds, discharge angles and velocities.

2. Methodology

An experimental campaign was conducted with an electrically-heated cavity receiver placed in the open section of a large wind tunnel with a cross-section of 2.75 m × 2.19 m, at the University of Adelaide. The average wind speeds used in this study were u_w = 0, 3, 6 and 9 m/s.

The experimental details of the heated cavity used in the current study have been published previously by Lee et al. (2018), so only a brief description is provided here. The cavity has a length of 0.45 m, an internal diameter of 0.30 m and is fitted with an aperture on the front face of 0.10 m in diameter. The blockage ratio of the cavity to the open test section of the wind tunnel is 4.1%, which is sufficiently low for any confinement effects to be negligible. The tilt angle of the cavity is set to 15° below the horizontal, while the yaw angle relative to the wind is set to 0°. The inside surface of the cavity is lined with 16 heating elements, with 12 mounted annularly, each covering a 180° arc in both the upper and lower half, as well as another four circumferential rings mounted on the back wall, as described by Lee et al. (2018). These surface-mounted heaters are made of copper, due to its high thermal conductivity. The external surface of the heaters is covered by 40 mm of fiber insulation, made from mineral wool covered by an aluminum foil to reduce conductive heat loss. Mica insulators are used between the heaters as thermal insulators to minimise the conductive heat transfer between heaters. The heaters are individually controlled by a feedback controller that can be set to the desired temperature. The temperature of the heaters is recorded using K– type thermocouples with washers attached to the respective copper surface. It is assumed that the temperature of the whole copper surface is uniform due to the high thermal conductivity of the copper. Datataker DT85, Matlab and Simulink programs, and an Arduino and DMX lighting system are used for the power controllers. The power required to keep the temperature of each heater at a set point is also recorded for 300 s after steady-state conditions have been reached. The steady-state condition is defined as being reached when both the variation of temperature of each heater is below ± 0.5 °C and the variation of the total heat is less than ± 5% of the total power for cases where the total power is above 2 kW and ± 100 W for the cases where the total power is below 2 kW for 300 s. The temperature across the aperture was measured by using a K-type thermocouple. The mean temperature was deduced from measurements over 300 s at different points across the aperture. This allowed the estimation of the average air temperature at the aperture plane.

A purpose-designed air curtain nozzle is mounted above the aperture, blowing downward across the aperture. The air curtain consists of three different sections: an air supply, distribution plenum and nozzle. The compressed air is provided by a Kaeser rotary screw compressor SM9 through a ½" size pipe to the air supply section of the air curtain. The distribution section has a 25° angle of expansion from the air supply to the nozzle. The compressed air passes through the distribution plates inside the body and exits via the nozzle. The air curtain has an outlet gap of 2 mm width and a length of 165 mm. The resulting airflow is uniform to within ± 2%, with an outlet velocity of 20 ± 0.4 m/s across the exit plane. Fig. 1 presents a schematic diagram of the cavity and air curtain used in the current study. The relative inclination angle of the curtain to the cavity surface, ϕ, was varied over the range 0° to 30° by rotating the air nozzle around the pivot point.

The modified deflection modulus equation developed by Zhang et al. (2018) (Eq. (5)) was used to find the minimum velocity of the air curtain. For the present condition, the height of the aperture (H) was 0.10 m, the temperature of the internal surface was 300 °C, at which temperature the density of the air is $\rho_h = 0.84\ \frac{kg}{m^3}$, the air curtain and the wind were both at 25 °C, at which temperature the density of the air is $\rho_{ac} = \rho_w = 1.18\ \frac{kg}{m^3}$, respectively. Therefore, the minimum outlet velocity of the air curtain (u_{ac}) is 16 m/s to achieve $D_{m,\min}$ of 0.17 to establish an optimal shielding at u_w = 9 m/s. Hence we used a safety

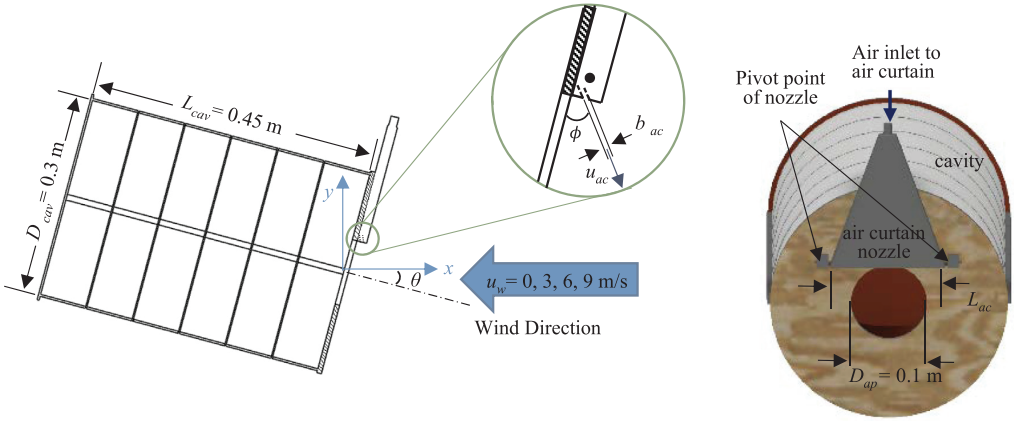

Fig. 1. A schematic diagram of the cavity and air curtain (ac) used in the current study. Here, θ is the cavity tilt angle and ϕ is the air curtain discharge angle.

factor of 0.15 and set the target air curtain velocity to 18 m/s, although we also assessed velocities of 4.5 and 9.0 m/s. The volumetric air flow rates were controlled by using Alicat Scientific MCR-1000 SLPM to 80 SLPM, 160 SLPM and 320 SLPM.

The total heat losses (Q_{total}) from the cavity comprise the sum of the conduction (Q_{cond}), convection (Q_{conv})and radiation (Q_{rad}) heat losses. These can each be determined from a sequential process following our earlier work (Lee et al., 2018). The heat losses through the walls via conduction can be measured by repeating the experiment with identical experimental conditions, except that the aperture is closed. The radiation heat losses are measured from a fourth-order dependence on temperature. The convection heat losses then are determined by subtraction of the conduction and radiation heat losses.

$$Q_{conv} = Q_{total} - (Q_{cond} + Q_{rad}) \tag{6}$$

The Richardson number (Eq. (7)) was used to generalize the results and to reduce the data from related assessments reported previously for other temperatures and receiver sizes.

$$Ri = \frac{Gr}{Re^2} = \frac{g\beta(T_{wall} - T_a)D_{cav}}{u_w^2} \tag{7}$$

Furthermore, the mean Nusselt number was calculated as follows:

$$Nu = \frac{total\ \ convective\ \ heat\ \ transfer}{conductive\ \ heat\ \ transfer} = \frac{Q_{conv}D_{cav}}{A_{total,cav}(T_{wall} - T_a)k_{ref}} \tag{8}$$

where the total inner area of the cavity is 0.495 m^2. A reference temperature for the properties of the air was defined as follows:

$$T_{ref} = \frac{T_{wall}}{2} + \frac{T_a}{2}, \tag{9}$$

k_{ref} is the thermal conductivity of the air at T_{ref}.

The effectiveness of the air curtain (ε) is defined as:

$$\varepsilon = \frac{Q_{conv,n-ac} - Q_{conv,ac}}{Q_{conv,n-ac}}, \tag{10}$$

where $Q_{conv,ac}$ is the measured convective heat losses for each experimental case with an air curtain and $Q_{conv,n-ac}$ is the convective heat losses for the same conditions but without an air curtain.

The convective heat losses are reported for a fixed cavity temperature of 300 °C only. However, the Richardson number can be used to estimate findings to other cavity temperatures and larger diameters following previous work (Lee et al., 2018; Lee et al., 2019a). In addition, Eq. (4) shows that the effect of the temperature of the cavity on the deflection modulus and the stability of the air curtain become negligible for sufficiently windy conditions. For instance, with a wind speed of 9 m/s and an air curtain velocity of 18 m/s, a change to the temperature of the cavity from 300° C to 1000 °C changes the deflection modulus by only 0.6%.

Table 1 presents the experimental conditions assessed for the 32 cases. Of these, 4 were performed with a closed aperture to measure the conductive heat losses, 4 with different wind speeds to measure the convective heat losses without an air curtain and 24 were performed with a series of velocities and discharge angles of the air curtain.

The estimated uncertainty of the velocity of the air curtain derived from the flow meter is ± 0.4%. The maximum uncertainty of the heat losses contributed from each heater including that of the thermocouples and control devices is 3.1% of the total measured heat losses. The uncertainty of the measured wind speed of the wind tunnel is ± 0.1 m/s.

3. Results and discussion

3.1. Effectiveness as a function of discharge angle

Fig. 2 (a) presents the values of the effectiveness of the air curtain (Eq. (10)), ε (%) as a function of the velocity of the air curtain for different wind speeds of u_w = 0, 3, 6 and 9 m/s and for two different air curtain discharge angles of ϕ = 0° and 30° but for constant values of yaw angle (α = 0°), tilt angle (θ = 15°) and cavity surface temperature (300 °C). The results show that the air curtain typically has a better performance for a discharge angle of 30° than for a discharge angle of 0°. For instance, for u_w = 0 m/s and u_{ac} = 18 m/s, the effectiveness of the air curtain is 60% for ϕ = 30° but −43% for ϕ = 0°. Overall, the impact of the discharge angle on the effectiveness is more significant with the higher velocities of the air curtain. For example, with a wind speed of 3 m/s, the effectiveness of the air curtain for two different discharge angles of 0° and 30° increases by a factor of 4.8 (from 4% to 19%) and then by a factor of 2.4 (from 19% to 46%), as u_{ac} is increased by factors of two from 4.5 to 9 m/s and then to 18 m/s.

The effectiveness of the 0° curtain angle exhibits a maximum for a particular value of air-speed. This suggests that there are two competing effects. On the one hand, increasing the jet speed increases the resistance of the jet to the wind, reducing its penetration into the cavity, while on the other hand it also induces its own circulation of fluid within the chamber, the strength of which increases with the jet speed. This optimal jet velocity is 4.5 m/s for the low wind speed case, but increases with the wind speed. However, the functions of optimal jet velocity are complex and non-linear, with the relationship between the different data sets i.e. for different speeds being variable.

Fig. 2 (b) presents the measured effectiveness of those cases with a discharge angle of ϕ = 30°. It can be seen that the greatest effectiveness of 60% is achieved for the no-wind condition and the highest value of u_{ac} = 18 m/s. However, the greatest effectiveness for the case of a windy condition is only 33%, which is achieved for the case of u_w = 6 m/s and u_{ac} = 18 m/s. It can also be seen that increasing the velocity of the air curtain reduces natural and forced convective heat losses from the cavity for this head-on wind condition with the 30° outward jet configuration.

The effect of wind speed on the effectiveness of the air curtain can also be seen in Fig. 2 (b). It is clear that the air curtain achieves better performance at lower wind speeds for different air curtain velocities. By increasing the wind speed for most cases, the effectiveness of the air curtain decreases. For instance, the value of ε drops from 47% to 11% by increasing the wind speed from 0 m/s to 9 m/s at u_{ac} = 4.5. This is mainly due to the penetration of more lateral flow through the air curtain and then into the cavity with an increase in the wind speed, which in turn increases the convective heat losses.

3.2. Convection heat losses distribution inside the cavity

Fig. 3 presents an image of the distributions over the surface of the measured heat losses from each segment of the cavity and of the distribution of air temperature in the aperture plane for a series of air

Table 1
List of experimental conditions for thirty two cases. Note: N/A = not applicable.

Wind speed u_w [m/s]	Yaw angle α [°]	Tilt angle θ[°]	Temperature of the wall [°C]	Length to diameter ratio	Aperture ratio [–]	The velocity of the air curtain u_{ac} [m/s]	The discharge angle of the air curtain ϕ [°]
0, 3, 6, 9	0°	15°	300	1.5	0.33	N/A	N/A
						4.5, 9, 18	0°, 30°
0, 3, 6, 9	0°	15°	300	1.5	0.0	N/A	N/A

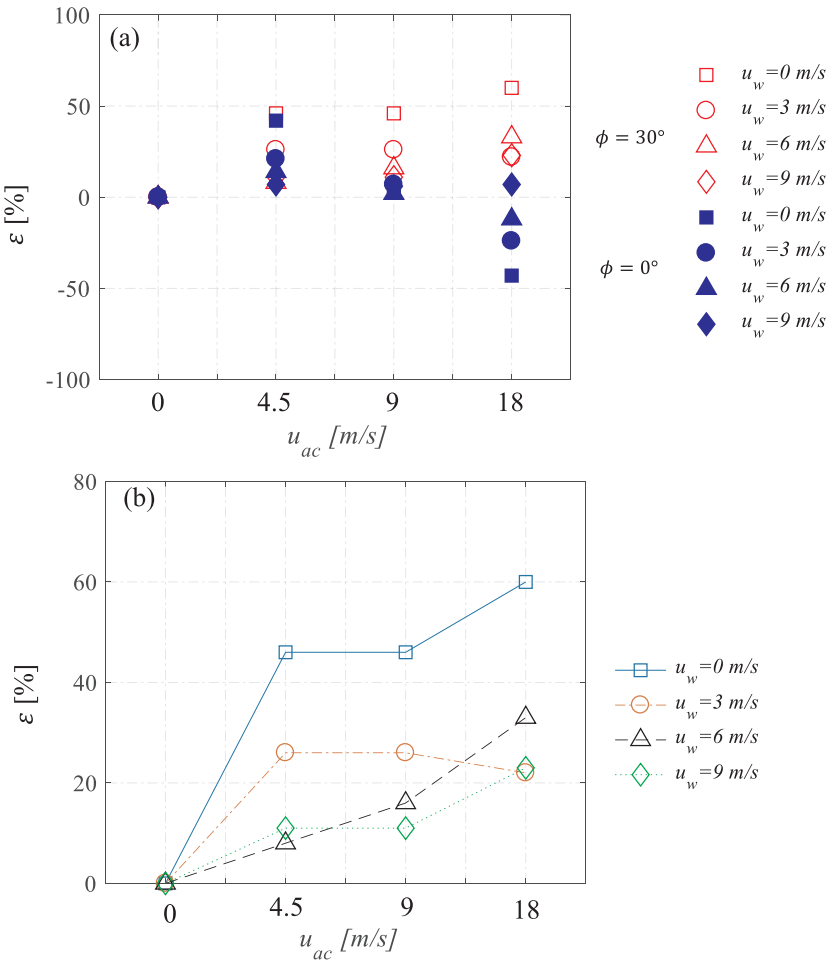

Fig. 2. Values of the effectiveness percentage, ε [%], as a function of velocity of the air curtain u_{ac} = 0, 4.5, 9 and 18 m/s, for wind speeds of u_w = 0, 3, 6 and 9 m/s, (a) for an air curtain angle of ϕ = 0° and 30° and (b) for an air curtain angle of ϕ = 30°. Test conditions: α = 0°, T = 300 °C, θ = 15°.

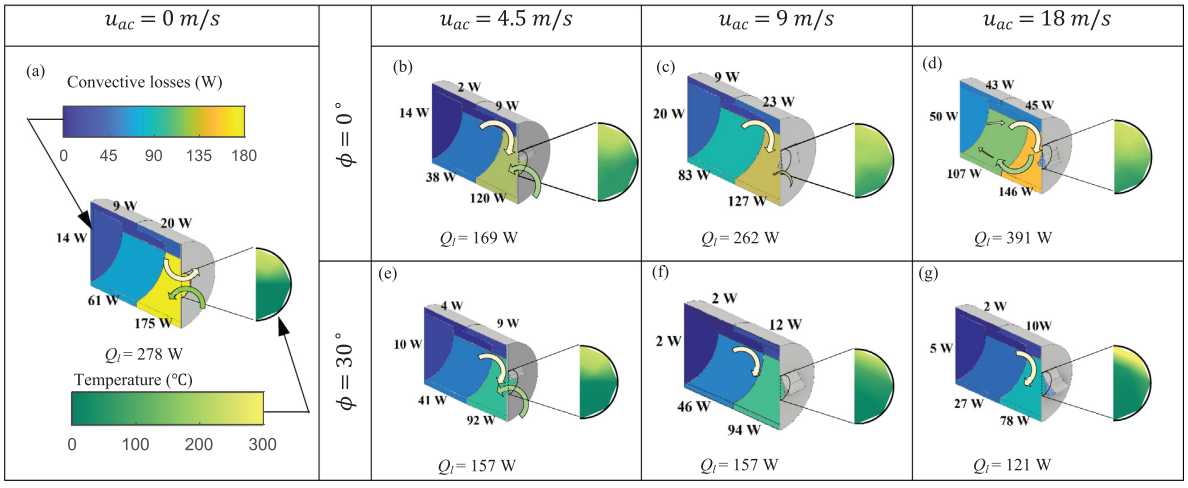

Fig. 3. Colour maps of the distribution over the surface of the measured convective heat losses (W) and of the temperature of the air in the aperture plane for a series of conditions as shown, spanning a series of two different curtain discharge angles (0° and 30°) and four different velocities of the air curtain (0, 4.5, 9 and 18 m/s). The test conditions: T = 300° C, θ = 15°, α = 0° and no wind.

curtain speeds and orientations but for a single value of wind speed, $u_w = 0$ m/s, i.e. $1/Ri = 0$. The temperature distribution across the aperture for the case without any air curtain, corresponding to natural convection (Fig. 3a), shows that buoyancy causes the hot gases to leave the cavity from the upper side of the aperture whilst cold air enters the cavity from the lower part of the aperture. This buoyancy-driven behaviour is consistent with that which has been observed previously e.g. (Wu et al., 2010). The temperature distribution at the aperture plane shows that the air flowing through the upper part of the aperture is at 260 °C and the lower part is at 25 °C. The figure also shows the convective heat losses drop in all sections of the cavity by using the air curtain at a velocity of 4.5 m/s, for both a discharge angle of 0° and 30°. This implies that the air curtain counters the flow pattern generated by natural convection to inhibit the transversal hot flow through the aperture, resulting in approximately 40% less convective heat losses from the cavity. For a discharge angle of 0°, increasing the velocity of the air curtain to 9 m/s causes the convective heat losses to increase relative to the case with $u_{ac} = 4.5$ m/s. This gives further evidence that increasing the velocity of the air curtain above the local optimal value acts to increase the mixing between the cold air curtain and hot air inside the cavity to increase the convective heat losses. Consistent with this, a further increase in the velocity of the air curtain to 18 m/s acts to further increase the convective heat losses from all sections of the cavity, so that the total heat losses are higher than that for no air curtain. The finding of an optimal velocity of the air curtain is consistent with previous numerical work which confirms that convective losses can be increased by using an air curtain with too high a speed or a misdirected jet (Hughes et al., 2015).

Fig. 3 (e-g), presents the equivalent results for the cases with an air curtain at $\phi = 30°$. It can be seen that, in contrast with the case for $\phi = 0°$, the heat losses continue to decrease with an increase of the velocity of the air curtain over the same range. This suggests that the discharge angle of 30° reduces the mixing of the jet flow with the hot fluid in the cavity, although it still inhibits the natural convection flow pattern. While not necessarily an optimal angle, the 30° case is clearly better than the reference of $\phi = 0°$.

Fig. 3 also shows that the front lower part of the cavity contributes the most to the total convective heat losses for all of these experimental cases. For example, for $u_{ac} = 18$ m/s, where the air curtain has the best performance, the convective heat losses from the lower front part of the cavity contribute more than 60% to the total convective heat losses.

Fig. 4 presents the corresponding distributions of convective heat losses and temperature distributions across the aperture for a wind speed of 6 m/s ($1/Ri = 19.3$). The case with no air curtain (Fig. 4a) shows a uniform distribution of relatively cold air through the aperture plane, which is in a good agreement with the previous findings (Prakash et al., 2010). The total convective heat losses for this case are 811 W, which is 2.9 times higher than the 287 W lost for the equivalent no wind condition (Fig. 3a). This highlights the importance of wind in inducing heat losses through an aperture, as found previously (Prakash et al., 2010). The use of an air curtain with $\phi = 0°$, causes a 14% reduction in convective losses for $u_{ac} = 4.5$ m/s to 697 W. However, further increases in u_{ac} lead to progressively greater losses, so that the convective losses are 11% greater than the case without a curtain for $u_{ac} = 18$ m/s. The measured temperature distributions at the aperture plane show that the whole aperture plane is at almost the same temperature as the surroundings for zero and low curtain speeds, but increase at the top of the aperture for higher wind speeds. This is consistent with the curtain generating a stronger recirculation within the cavity that entrains cavity fluid toward the curtain along the top of the cavity, which increases convective heat losses through the top of the cavity.

Fig. 4 (e–g) presents the effect of the air curtain at a discharge angle of 30°. It can be seen that, in contrast with the case for $\phi = 0°$, but consistent with the trends with $u_w = 0$ m/s, the convective losses progressively decrease with an increase in u_{ac} to result in a 32% reduction of losses for $u_{ac} = 18$ m/s relative to the case for no curtain. Nevertheless, the convective losses are still a factor of two greater than that for the natural convection case, showing that further optimisation is still needed.

Consistent with the no wind condition, the greatest convective heat losses occur at the front lower part of the cavity. However, the distribution of heat losses for a wind speed of 6 m/s is more uniform than that for the no wind condition. For example, the lower front and lower rear section of the cavity for the 6 m/s case contributes to 29% and 30% of total convective heat losses, respectively for $u_{ac} = 9$ m/s and $\phi = 30°$, while for the equivalent no wind cases 64% and 22% of the total heat losses occur at the lower front and lower rear sections, respectively. This significant difference in heat flux distribution (Alipourtarzanagh et al., 2019) highlights the importance of understanding the convective flow patterns before seeking to develop a strategy to mitigate the heat losses from the cavity. The previous suggestion of applying an active air flow over the lower part of the cavity (Yang et al., 2018) is another option to decrease the convective heat

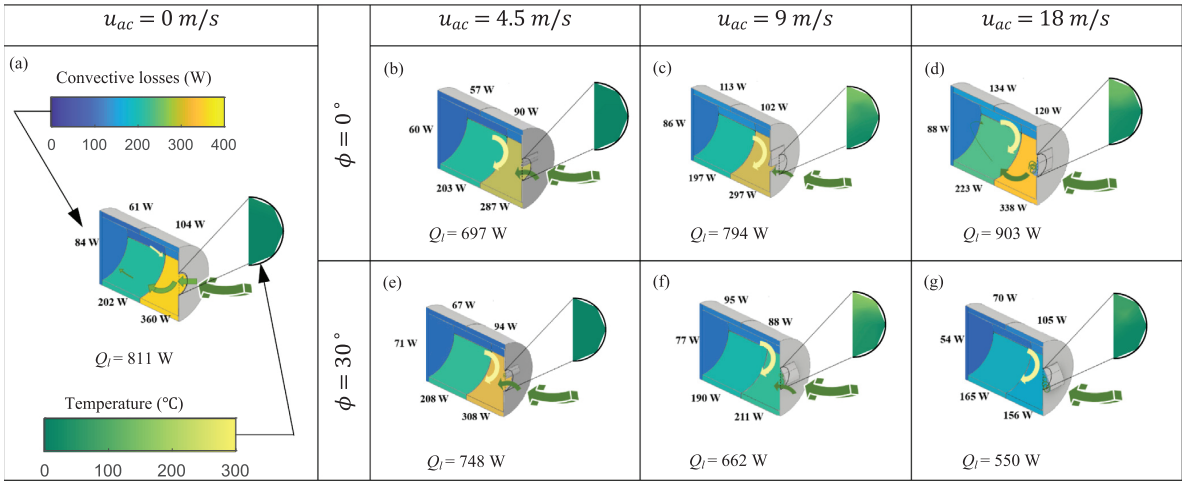

Fig. 4. Colour maps of the distribution over the surface of the measured convective heat losses (W) and of the temperature of the air in the aperture plane for a series of conditions as shown, spanning a series of two different curtain discharge angles (0° and 30°) and four different velocities of the air curtain (0, 4.5, 9 and 18 m/s). The test conditions: $u_w = 6$ m/s, T = 300° C, $\theta = 15°$ and $\alpha = 0°$.

losses from the lower part of the cavity.

3.3. Effect of the air curtain velocity relative to the wind speed

Fig. 5 presents the effectiveness as a function of the ratio of curtain speed to the wind speed for a combination of u_w = 3, 6 and 9 m/s and u_{ac} = 4.5, 9 and 18 m/s for two different ranges of inverse Richardson number and for $\phi = 30^{\circ}$. The results for $\phi = 0^{\circ}$, are not presented here as the employment of the air curtain parallel to the aperture plane increases the convective heat losses and, therefore, is potentially not a case to be applied to cavity receivers. It can be seen that, for all of the operating conditions analysed here, the results collapse onto two straight lines. For $1/Ri < 10$, the effectiveness is almost independent of the curtain speed but decreases slightly (by 5%) with an increase in u_{ac}/u_w from 1.5 to 6. Hence a low velocity air curtain is effective at reducing losses and the effectiveness is not very sensitive to the curtain speed. On the other hand, for $1/Ri > 10$ the effectiveness increases linearly with u_{ac}/u_w to a maximum for $u_{ac}/u_w = 3$. This indicates that, despite the complexity of the heat transfer between the cavity and the ambient surrounds, it can be described by a relatively simple linear relationship.

3.4. Non-dimensional heat transfer

Fig. 6 presents the variation of the Nusselt number (Eq. (8)) as a function of the inverse Richardson number for all of the experimental cases with an air curtain. It can be seen that *Nu* increases approximately linearly with *1/Ri* for all cases, consistent with previous understanding that wind increases convective losses. It can also be seen that the trend in the influence of curtain speed is opposite for the two cases. That is, *Nu* increases with u_{ac} for $\phi = 0^{\circ}$ but decreases with an increase in u_{ac} for $\phi = 30^{\circ}$. This is consistent with the results presented above. Furthermore, *Nu* becomes independent from u_{ac} for high values of *1/Ri* (forced-convection dominant) for $\phi = 0^{\circ}$, while the opposite is true for $\phi = 30^{\circ}$, where *Nu* becomes independent from u_{ac} at low values of 1/Ri (natural-convection dominant). These results are significant in showing that the performance of the air curtain is relatively robust for $\phi = 30^{\circ}$. In contrast with $\phi = 0^{\circ}$, a higher velocity of the air curtain does not adversely affect the performance of the air curtain.

3.5. Relationship between effectiveness and the deflection modulus

Fig. 7 displays the dependence of the effectiveness on the deflection modulus for the experimental cases with a discharge angle of 30° and at a yaw angle of $\alpha = 0^{\circ}$. As defined in Eq. (4), the deflection modulus is the ratio between the momentum flux of the air curtain at the outlet and the transversal forces acting on the height of the air curtain due to the density difference and the wind momentum. The figure reveals that in the range $0.01 < D_m < 0.5$, a slight increase in D_m results in a sharp increase in the effectiveness. However, for $D_m > 0.9$, an increase of D_m leads to a minor change in the effectiveness values.

Since D_m, scales approximately with ${u_{ac}}^2$ it is likely to be desirable to select D_m values near to the elbow point. This is because further increases in D_m above the elbow point will result in a relatively small increase in ε for a large increase in u_{ac}. Furthermore, fan power scales with ${u_{ac}}^3$ and is likely also to increase the noise from the air curtain. A cost-benefit analysis would be required on a case-by-case basis to evaluate the optimal design point.

Fig. 8 compares the effectiveness as a function of D_m, for the current study, with that from a previous numerical study of air curtains designed for doorways of buildings (Costa et al., 2006). It can be seen that the effectiveness of the air curtain is higher for buildings than for the present cavity receiver, with a maximum value of ~0.90, while for the same range of D_m, the effectiveness in the current cavity receiver is half that at a maximum value of ~0.46. On the one hand, there are some plausible reasons for these differences, while on the other, these differences suggest that there is a lot of scope for further improvements in effectiveness for the curtain with further optimisation of the design. One key difference between the operating conditions in solar cavity receivers and buildings is that the temperature difference across the air curtain is many times higher. Secondly, the external wind speed acting on the air curtain in the solar receiver is a crucial parameter that can be disregarded in buildings. Finally, the shape of the two is different. It is also worth noting that fixed values of both H/b_{ac} and air temperature were used for the present air curtain. Therefore, further work is needed to generalise the relationship between the effectiveness and deflection modulus for independent variations of each controlling parameter. Hence there are good reasons to expect that there is potential to increase the effectiveness with further assessment of the controlling parameters.

4. Conclusions

We have experimentally demonstrated, for the first time, that an air curtain can be used to significantly reduce convective losses from a cylindrical solar cavity receiver, albeit for only one configuration of tilt angle relative to the horizontal and yaw angle relative to the wind. The key findings are as follows:

1) That there is a trade-off between the potential of the curtain to inhibit convective losses by inhibiting the internal flows that tend to drive hot fluid out from the cavity, and for its potential to increase convective losses by augmenting mixing between the curtain and the internal cavity flows. Therefore, it is necessary for the curtain to be directed with a component flowing into the wind if heat losses are to be mitigated, especially for the higher values of discharge velocity of the air curtain.
2) Increasing the velocity of the air curtain from values below the threshold increases the aerodynamic barrier across the aperture, thereby decreasing the convection losses.
3) An increase in wind speed reduces the effectiveness of the air curtain. The most effective case of reducing convection heat losses was for the case with $\phi = 30^{\circ}$ and u_{ac} = 18 m/s, corresponding to a deflection modulus of 13 at the no wind condition ($1/Ri = 0$), for which the effectiveness is found to be 60%. However for the higher wind speeds where the forced convection losses are dominant, the highest effectiveness of 0.33 was achieved at u_{ac} = 18 m/s ($D_m = 0.35$), $\phi = 30^{\circ}$ at u_w = 6 m/s ($1/Ri = 19.37$).

Notwithstanding the potential benefits of a wind curtain, the extent

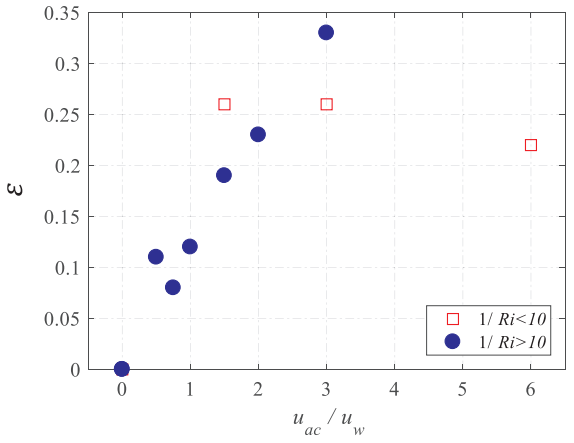

Fig. 5. Effect of the ratio of the air curtain to wind speed on the effectiveness of the air curtain for two different ranges of reverse Richardson number. Test conditions: $\alpha = 0^{\circ}$, $\phi = 30^{\circ}$, T = 300 °C.

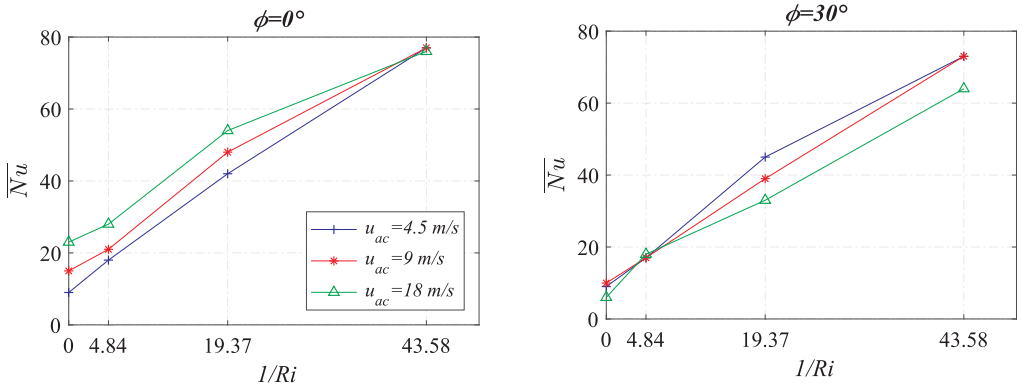

Fig. 6. The variation of the Nusselt number with the inverse Richardson number for three velocities of air curtain u_{ac} = 4.5, 9 and 18 m/s. Test conditions: θ = 15°, T = 300 °C, α = 0°.

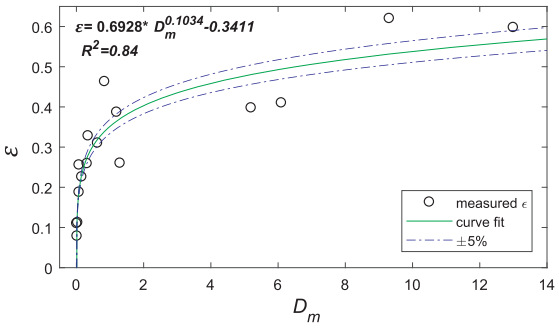

Fig. 7. Effectiveness of the air curtain as a function of deflection modulus for α = 0° and ϕ = 30°.

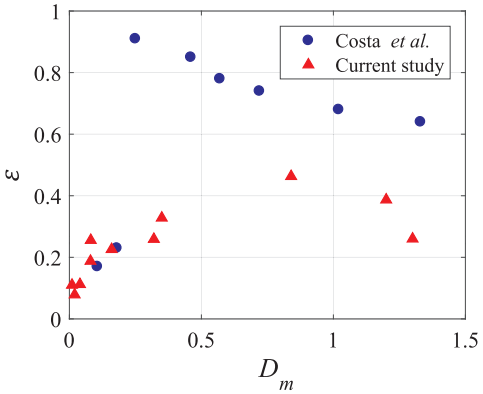

Fig. 8. Comparison of the effectiveness of the air curtain as a function of the deflection modulus for two different applications of solar receivers (current study) and buildings (Costa et al., 2006).

to which a global optimisation can be achieved is at present limited by the relatively poor level of understanding both of the internal flow-field under relevant conditions and of the interaction between the curtain and the wind across the wide range of possible orientations. Hence more detailed understanding of these complex interactions is needed to devise solutions that can significantly mitigate convective losses in practical devices.

Declaration of Competing Interest

The authors declare that they have no known competing financial interests or personal relationships that could have appeared to influence the work reported in this paper.

Acknowledgment

The authors would like to acknowledge the financial support of ARENA from grant 2015/RND054, from the Australian Research Council under grant LP110200060 and for the Premier's Science and Research Fund under grant 2007/1436. Ms Elham Alipour would like to thank Dr Ka Lok 'Leok' Lee for his training on the experimental setup and Mr Marc Simpson, Thebarton laboratory coordinator, for all his assistance with the experiments most sincerely.

References

Alipourtarzanagh, E., Chinnici, A., Nathan, G.J., Dally, B.B., 2019. Experimental Investigation on the Influence of an Air Curtain on the Convective Heat Losses from Solar Cavity Receivers under Windy Condition, SolarPaces 2019. Daegu, South Korea.
Clausing, A.M., 1981. An analysis of convective losses from cavity solar central receivers. Sol. Energy 27 (4), 295–300.
Clausing, A.M., 1983. Convective losses from cavity solar receivers—comparisons between analytical predictions and experimental results. J. Sol. Energy Eng. 105 (1), 29–33.
Costa, J.J., Oliveira, L.A., Silva, M.C.G., 2006. Energy savings by aerodynamic sealing with a downward-blowing plane air curtain—A numerical approach. Energy Build. 38 (10), 1182–1193.
Fang, J., Tu, N., Torres, J.F., Wei, J., Pye, J.D., 2019. Numerical investigation of the natural convective heat loss of a solar central cavity receiver with air curtain. Appl. Therm. Eng. 152, 147–159.
Goubran, S., Qi, D., Saleh, W.F., Wang, L., Zmeureanu, R., 2016. Experimental study on the flow characteristics of air curtains at building entrances. Build. Environ. 105, 225–235.
Hayes, F., 1968. Heat transfer characteristics of the air curtain- A plane jet subjected to transverse pressure and temperature gradients(Heat transfer characteristics of plane jet air curtain subject to transverse pressure and temperature gradients).
Hayes, F.C., Stoecker, W.F., 1969a. Design data for air curtains. ASHRAE Trans.
Hayes, F.C., Stoecker, W.F., 1969b. Heat transfer characteristics of the air curtain. ASHRAE Trans.
Hughes, G., Pye, J., Kaufer, M., Abbasi- Shavazi, E., Zhang, J., McIntosh, A., Lindley, T., 2015. Reduction of convective losses in solar cavity receivers, SolarPACES 2015. Cape Town, South Africa.
Jafarian, M., Arjomandi, M., Nathan, G.J., 2017. Thermodynamic potential of molten copper oxide for high temperature solar energy storage and oxygen production. Appl. Energy 201, 69–83.
Lee, K.L., Chinnici, A., Jafarian, M., Arjomandi, M., Dally, B., Nathan, G., 2018. Experimental investigation of the effects of wind speed and yaw angle on heat losses from a heated cavity. Sol. Energy 165, 178–188.
Lee, K.L., Chinnici, A., Jafarian, M., Arjomandi, M., Dally, B., Nathan, G., 2019a. The influence of wall temperature distribution on the mixed convective losses from a heated cavity. Appl. Therm. Eng. 155, 157–165.
Lee, K.L., Chinnici, A., Jafarian, M., Arjomandi, M., Dally, B., Nathan, G., 2019b. The influence of wind speed, aperture ratio and tilt angle on the heat losses from a finely

controlled heated cavity for a solar receiver. Renew. Energy 143, 1544–1553.
Oliveira, L.A., Costa, J.J., Carvalho, M.G., Gerhardt, H.J., Kramer, C., 1991. On aerodynamic sealing for industrial applications. J. Wind Eng. Ind. Aerodyn. 37 (3), 255–268.
Prakash, M., Kedare, S.B., Nayak, J.K., 2010. Determination of stagnation and convective zones in a solar cavity receiver. Int. J. Therm. Sci. 49 (4), 680–691.
Romero, M., Buck, R., Pacheco, J.E., 2002. An update on solar central receiver systems, projects, and technologies. J. Sol. Energy Eng. 124 (2), 98.
Romero, M., Steinfeld, A., 2012. Concentrating solar thermal power and thermochemical fuels. Energy Environ. Sci. 5 (11).
Siebers, D.L., Kraabel, J.S., 1984. Estimating convective energy losses from solar central receivers. Sandia National Labs., Livermore, CA (USA), United States.
Sirén, K., 2003a. Technical dimensioning of a vertically upwards-blowing air curtain - Part II. Energy Build. 35 (7), 697–705.
Sirén, K., 2003b. Technical dimensioning of a vertically upwards blowing air curtain - Part I. Energy Build. 35 (7), 681–695.
Sun, J., Tsamos, K.M., Tassou, S.A., 2017. CFD comparisons of open-type refrigerated display cabinets with/without air guiding strips. Energy Procedia 123, 54–61.
Taussig, R.T., 1984. Aerowindows for central solar receivers. American Society of Mechanical Engineers, Winter Annual Meeting, New Orleans, LA, 12.
Uhlig, R., Flesch, R., Gobereit, B., Giuliano, S., Liedke, P., 2014. Strategies enhancing efficiency of cavity receivers. Energy Procedia 49, 538–550.
Vant-Hull, L.L., 2012. 8 - Central tower concentrating solar power (CSP) systems, Concentrating Solar Power Technology. Woodhead Publishing, pp. 240–283.
Verhaeghe, G., Van Belleghem, M., Willockx, A., Verhaert, I., De Paepe, M., 2010. Study of air curtains used to restrict infiltration into refrigerated rooms.
Wang, S., Jin, L., Ou, S., Li, Y., 2017. Experimental air curtain solution for refuge alternatives in underground mines. Tunn. Undergr. Space Technol. 68, 74–81.
Wu, S.Y., Xiao, L., Cao, Y., Li, Y.R., 2010. Convection heat loss from cavity receiver in parabolic dish solar thermal power system: A review. Sol. Energy 84 (8), 1342–1355.
Yang, S., Wang, J., Lund, P.D., Wang, S., Jiang, C., 2018. Reducing convective heat losses in solar dish cavity receivers through a modified air-curtain system. Sol. Energy 166, 50–58.
Zhang, J.J., Pye, J.D., Hughes, G.O., 2015. Active Air Flow Control to Reduce Cavity Receiver Heat Loss. V001T005A023.
Zhang, L., Yan, Z.-Z., Li, Z.-H., Wang, X.-M., Han, X.-F., Jiang, J.-C., 2018. Study on the effect of the jet speed of air curtain on smoke control in tunnel. Procedia Eng. 211, 1026–1033.

Chapter 4-

Impact of flow blowing and suction strategies on the establishment of an aerodynamic barrier for solar cavity receivers

Statement of Authorship

Title of Paper	Impact of Flow Blowing and Suction strategies on the establishment of an aerodynamic barrier for solar cavity receivers
Publication Status	☑ Published ☐ Accepted for Publication ☐ Submitted for Publication ☐ Unpublished and Unsubmitted work written in manuscript style
Publication Details	Applied Thermal Engineering Volume 180, 5 November 2020, 115841

Principal Author

Name of Principal Author (Candidate)	Elham Alipourtarzanagh		
Contribution to the Paper	Performed experiments, performed numerical modelling, acquisition of data, interpret data, writing of the manuscript and acted as the corresponding author.		
Overall percentage (%)	70%		
Certification:	This paper reports on original research I conducted during the period of my Higher Degree by Research candidature and is not subject to any obligations or contractual agreements with a third party that would constrain its inclusion in this thesis. I am the primary author of this paper.		
Signature		Date	06/10/2020

Co-Author Contributions

By signing the Statement of Authorship, each author certifies that:

i. the candidate's stated contribution to the publication is accurate (as detailed above);

ii. permission is granted for the candidate in include the publication in the thesis; and

iii. the sum of all co-author contributions is equal to 100% less the candidate's stated contribution.

Name of Co-Author	Alfonso Chinnici		
Contribution to the Paper	Assisted with the numerical modelling, supervised the research and contributed in academic discussion		
Signature		Date	7/10/2020

Name of Co-Author	Graham J Nathan		
Contribution to the Paper	Conceptualization, methodology development, review and editing manuscript, supervision, project administration and funding acquisition		
Signature		Date	8/10/2020

Name of Co-Author	Bassam Dally		
Contribution to the Paper	Conceptualization, methodology development, review and editing manuscript, supervision, project administration and funding acquisition		
Signature		Date	6-10-2020

Applied Thermal Engineering 180 (2020) 115841

Contents lists available at ScienceDirect

Applied Thermal Engineering

journal homepage: www.elsevier.com/locate/apthermeng

Impact of Flow Blowing and Suction strategies on the establishment of an aerodynamic barrier for solar cavity receivers

Elham Alipourtarzanagh*, Alfonso Chinnici, Graham J. Nathan, Bassam B. Dally

Centre for Energy Technology, School of Mechanical Engineering, the University of Adelaide, Adelaide, South Australia 5005, Australia

HIGHLIGHTS

- Effectiveness of using air curtains for cavity receivers investigated both numerically and experimentally.
- Effects of wind speed, extraction angle and suction velocity on effectiveness quantified.
- Upward blowing curtain is more efficient than downward type for low wind speeds.
- Suction performs better than blowing at high wind speed.
- For tilted cavity receivers blowing air curtain increases the convective heat losses.

ARTICLE INFO

Keywords:
Solar cavity receiver
Air curtain
Air suction
Effectiveness
Convective heat losses
Control strategy

ABSTRACT

This study compares two aerodynamic approaches to minimize convective losses from cavity receivers, namely blowing and suction. A laboratory-scale cavity receiver was operated in a large wind tunnel at varying wind speed and tilt angle. The inner surface of the cavity was heated to a constant temperature of 300 °C by finely controlled electrical heaters. The measured electric energy required to maintain the heaters at the same temperature was used to provide a direct measure of losses from the receiver. An air curtain was engineered to provide curtain of air blown either downward or upwards across the aperture. Suction was alternatively applied through a nozzle positioned below the aperture for a series of suction flowrates. A numerical study was also conducted using a commercial CFD package and validated with available data. It was found that the upward blowing air curtain performs better than the downward curtain for the buoyancy dominant conditions. Moreover, the measured effectiveness of the downward blowing air curtain at tilt angle of the cavity of 45° showed that the application of air curtain with higher velocities increases the convective heat losses over the case with no air curtain. When comparing the performance of air curtain with air suction, it was found that for the low range of relative momentum ratio of curtain to wind flow, suction performs better than blown air. Finally, this study highlights the need for adaptable strategies, based on operating condition, to minimize heat losses and improve the thermal efficiency of cavity receivers.

1. Introduction

Concentrated solar thermal (CST) technology is increasingly pursued owing to its potential capability of cost-competitive power and cater for high-temperature applications including industrial heat and power generation [1,2]. Though the heliostats constitute some 40–50% of the total capital cost of a power tower plant [3], the tower-type cavity receiver have a major effect on the performance of CST systems by absorbing the reflected sunlight and transforming light into heat with high efficiency [4]. The lower heat losses of cavity receivers compared with the external receiver [5], together with its higher operating temperatures are key motivations for the development of cavity receivers [6]. The overall efficiency of a CST system depends on the radiation absorption efficiency, the conversion of solar radiation into useful thermal energy and the transformation of the thermal energy into work [7]. The conversion efficiency depends upon the design parameters, the scale of the cavity receiver and the heat losses, namely convective, conductive and radiative losses. While analytical methods can be used to estimate conduction and radiation terms reasonably well, convective heat losses are the most difficult to predict owing to their complex dependence on multiple parameters including geometry (e.g. size, aperture ratio and inclination angle) and operating conditions

* Corresponding author.
E-mail address: elham.alipour@adelaide.edu.au (E. Alipourtarzanagh).

https://doi.org/10.1016/j.applthermaleng.2020.115841
Received 5 June 2020; Received in revised form 29 July 2020; Accepted 31 July 2020
Available online 05 August 2020
1359-4311/

Nomenclature

A	area (m^2)
b	air curtain width (m)
D	diameter (m)
g	gravitational acceleration (m/s^2)
K	heat transfer coefficient (W/m^2 K)
L	length (m)
$M^{''}$	momentum flux (kg/ms^2)
$\dot{M}$	momentum ($kg\ m/s^2$)
P	power (W)
Q	heat losses (W)
T	temperature (°C)
U	velocity (m/s)

Subscripts

∞	ambient
B	blowing
0	control flow
Ap	aperture
cav	cavity
H	hydraulic
S	suction
W	wind

Greek letters

A	cavity yaw angle (°)
β	thermal expansion coefficient (1/k)
ε	effectiveness
θ	cavity tilt angle (°)
μ	viscosity (kg/(m. s))
ρ	density (kg/m^3)
ϕ	inclination angle of the aerodynamic barrier (°)

Non-dimensional numbers

Gr	Grashof number,$Gr = \frac{\rho^2 g\beta(T_{wall}-T_\infty)D_{cav}^3}{\mu^2}$
Re	Reynolds number,$Re = \frac{\rho uD}{\mu}$
Ri	Richardson number,$Ri = \frac{Gr}{Re^2} = \frac{g\beta(T_{wall}-T_\infty)D}{u_w^2}$

Abbreviations

CST	Concentrating Solar Thermal
Conv	convection
LES	Large Eddy Simulation
Rad	radiation
RANS	Reynolds-Averaged Navier-Stokes
Cond	conduction

(e.g. temperature, wind speed and wind direction) [8]. Notwithstanding their complexity, convective losses can be important, particularly at high wind speeds. For some conditions, convective heat losses can contribute to > 60% of heat losses from a cavity [9]. Hence, it is desirable to provide understanding as to how convective losses can be reduced cost-effectively to enhance the thermal efficiency of a CST system. Thus, this study aims to identify effective strategies to reduce convective heat losses from central tower solar cavity receivers.

Among the recommended methods under development to reduce the convective heat losses from cavity receivers include the following: varying the geometry, heat recovery, the use of a window and air curtains [10], the latter method has received most attention recently [11–13]. Air curtains have been widely deployed to reduce not only the convective heat losses but also the exchange of mass and moisture in other applications such as industrial furnaces, buildings, food industry and mining industry [14–19]. The application of air curtain to solar cavity receivers has been proposed a few decades ago [20] as a potential method to minimise the influences both of an external wind and of buoyancy without interfering with the incoming radiation. Since then, several numerical studies have investigated the influence of an air curtain speed and inclination angle on heat losses from solar cavities [12,13,21]. They found that an optimum jet-speed (air curtain speed) exists for each value of the jet discharge angle and inclination angle of the cavity and provided useful insights into the likely heat transfer mechanisms. However, the absence of experimental data on the efficiency of an air curtain on a solar cavity receiver has limited the capacity to validate these models, and hence the confidence in their findings. Indeed, this lack of experimental data may be a contributing cause for the majority of previous numerical studies being undertaken for the case of no wind [12,13]. Furthermore, recent experimental evidence [22] have shown that air curtains can increase heat losses from some configurations under particular operating conditions. Therefore, there is a need for experimental assessment of the influence of the key operating conditions on the effectiveness of an air curtain, especially under windy conditions, and for a series of tilt angles of the cavity.

There are many ways with which an air curtain could be configured at the front of a cavity aperture. However, little is known of their relative effectiveness and operating cost across the range of possible wind speed and wind direction conditions. The majority of previous studies have assessed the case in which air is blown downward from the upper side of the aperture [12,13,21]. However, in an isolated numerical study, Yang et al. [23] assessed a case in which both blowing and suction were employed simultaneously from diametrically opposite directions across the cavity in either the upward or downward directions. They found that, although both directions can reduce convective heat losses, the *upward blowing* case yields better performance than the *downward blowing* air curtain case under similar operating conditions. However, there are only limited data available to date for the upward blowing case, so that further investigations are needed both to confirm this finding and to deepen understanding it. Furthermore, no experimental comparison of relative effectiveness of upward and downward blowing air curtains without a suction mechanism on the opposite side of the aperture, or of the suction only strategy, has yet been reported.

Given the aforementioned gaps, we aim in this study to assess, experimentally, the effectiveness of alternative configurations of air curtain induced by either blowing or suction in reducing convective heat losses from solar cavity receivers. This has been carried out through a systematic experimental investigation of the influence of the parameters of wind speed, discharge angle and momentum flux of the aerodynamic barrier and cavity tilt angle, using a heated cavity receiver mounted in an open jet wind tunnel. Findings from a numerical investigation also have been used to provide a better understanding of the flow behaviour within the cavity for a variety of operating conditions.

2. Methodology

2.1. Experimental approach

2.1.1. Experimental test rig

A systematic experimental investigation was carried out with an electrically heated cylindrical cavity receiver in a large wind tunnel. Detailed experimental descriptions of the heated cavity were provided previously by Lee *et al.* [24], so that only an overview is presented here. The cavity had a length and internal diameter of 0.45 m and 0.3 m, respectively and an aperture of 0.10 m in diameter on the front face.

The ratio of the projected area of the cavity to the 2.75 m × 2.19 m test section of the wind tunnel is adequately low (4.1%) to disregard any blockage effect. The cavity yaw angle relative to the wind was set to 0°. The cavity tilt angle which is defined as the angle of the normal direction of the aperture plane to the horizontal plane was systematically varied between 0°, 30° and 45°. Four values of the average air speeds of wind tunnel were assessed, namely u_w = 0, 3, 6 and 9 m/s.

The internal surfaces of the cavity consisted of 16 copper plates, each attached to a heating element. Both upper and lower half of the cavity were covered with 6 annular heaters, each covering a 180° arc. The back plate of the cavity was also covered with 4 circumferential ring heaters. The external surfaces of the heaters were covered with an insulation mineral wool of 40 mm thickness. To avoid significant heat transfer between heaters, mica insulators were used between each plate. The system was also controlled to maintain the identical internal surface temperature of 300 °C by separately controlling the power supplied to each heater. The temperature of each copper plate, measured using K– type thermocouples, was assumed to be uniform considering the high thermal conductivity of the copper. The power controller system employed Datataker DT85 to read the measured temperatures and transfer them to MATLAB and Simulink programs to transfer an output power signal using an Arduino to DMX (lighting) controller. The controlled power supplied to the heaters via the DMX controller was recorded at steady state conditions defined as being

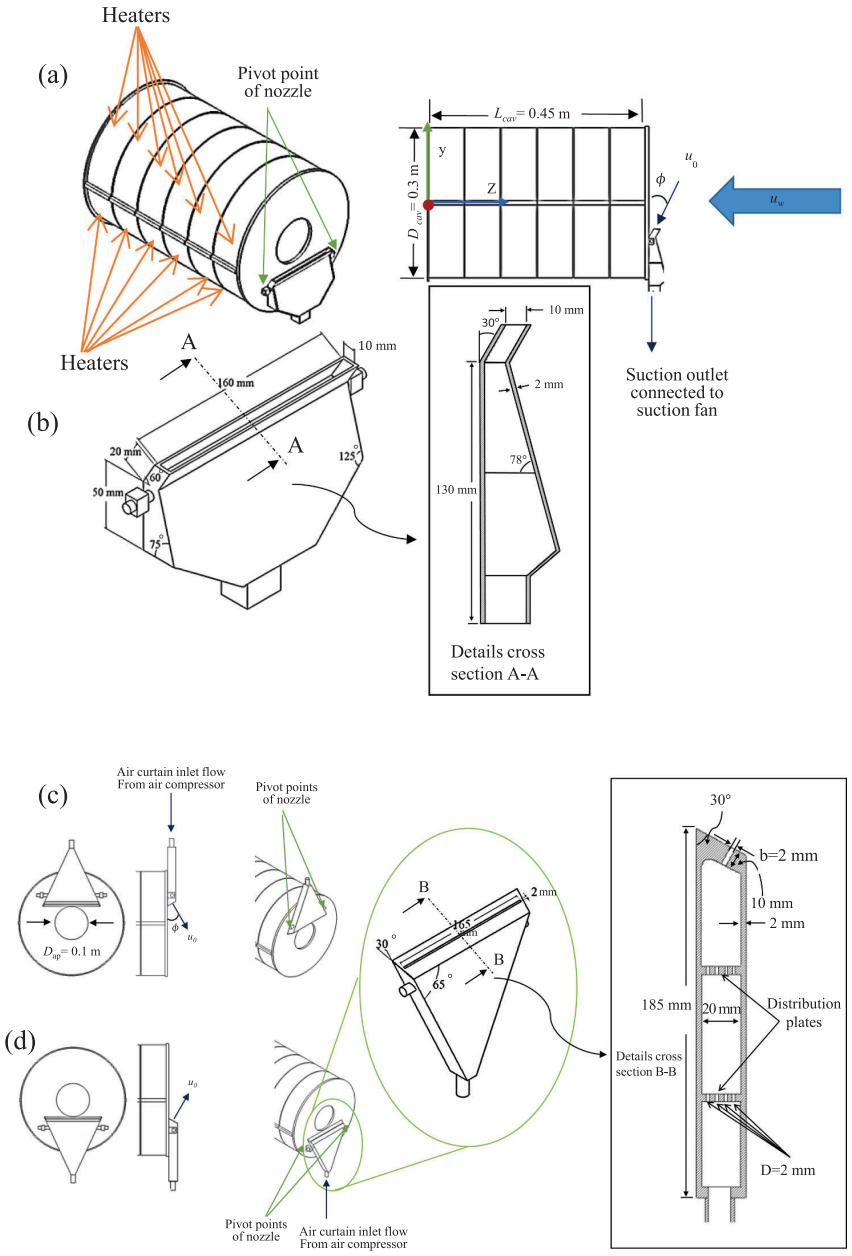

Fig. 1. A schematic diagram of (a) cavity with air suction nozzle (b) air suction nozzle (c) cavity and downward blowing air curtain and (d) cavity and upward blowing air curtain.

reached when both the variation of temperature of each heater is less than ± 0.5 °C in a 300 s period and that of the total heat supplied is less than ± 5% for cases where the total power is above 2 kW and ± 100 W for the cases where the total power is below 2 kW.

2.1.2. Air injection system

A purpose-designed air curtain was used to provide air flow from a rectangular slit of 2 mm width and 165 mm length as shown in Fig. 1 following our previous work [22]. A compressor (Kaeser rotary screw SM9) was used to supply compressed air through a ½" size pipe to the air curtain inlet. The air curtain was attached to either the upper or lower sides of the aperture to provide either the downward or upward blowing air curtain configurations, respectively. The relative discharge angle of the curtain to the aperture plane was fixed at $\phi = 30^{\circ}$. The bulk mean exit velocity of air curtain of u_b = 4.5, 9, and 18 m/s were assessed, consistent with our previous study, together with a greater outlet velocity of 36 m/s to expand the range of air curtain velocities. These velocities were controlled using an Alicat Scientific mass flow controller, MCR-1000 SLPM.

2.1.3. Air suction system

The suction nozzle, which was alternatively used to withdraw air from one side of the aperture, had a width of 10 mm and a length of 160 mm (Fig. 1). The mounting arrangement allowed the extraction angle to be varied between 0° to 30°. A vacuum cleaner (Vax Pet Pro Barrel Vacuum) with a power rating of 2400 W was adapted in this study to draw air through the nozzle. The velocity on in the axis of the suction line was measured with a heavy-duty Pitot tube anemometer (Extech HD350) assuming the flow is fully developed to find the flow rate.

The performance of the control devices were compared both at the same value of nozzle power (supplied by the fan) and at the same value of momentum flux. The momentum flux compares the aerodynamic influence, while the nozzle power characterises the parasitic energy penalty of the control device. The power consumption of the air curtain at the nozzle was calculated using Eq. (1):

$$P_0 = \frac{1}{2}\rho_0 A_0 u_0^3, \tag{1}$$

where P is the power, ρ_0 is the density of the air curtain flow, A_0 is the area of the nozzle and u_0 is the bulk-mean exit velocity of the air curtain. To have equal power for the blown air curtain P_b and the suction case, P_s. Hence, for an outlet injection velocity of u_b = 4.5, 9 and 18 m/s and $A_b = 0.002 \times 0.165\text{m}^2$, the suction velocity for the area of $A_s = 0.01 \times 0.16\text{m}^2$ is 2.63, 5.26 and 10.52 m/s, respectively. The maximum power required corresponds to the vacuum velocity of 14.79 m/s. Fig. 1 illustrates a schematic diagram of the cavity where 1(a) shows the suction configuration, 1(c) shows the upward blowing, and (d) shows the downward blowing air curtain used in the current study.

2.1.4. Effectiveness and momentum rate calculation

The total heat losses from each experimental case comprise the sum of the power to the 16 electric heaters. For the cases with an open aperture, this includes the total power required to compensate for the sum of the conduction (Q_{cond}), convection (Q_{conv})and radiation (Q_{rad}) losses from the cavity, while, for the cases that aperture is closed, the total losses only include the conduction losses. The radiation losses that occur through the aperture of the cavity have a fourth-order dependence on temperature. Thus, the convection heat losses were obtained by subtraction of conduction and radiation heat losses from total heat losses following earlier work [24].

$$Q_{conv} = Q_{total} - (Q_{cond} + Q_{rad}) \tag{2}$$

The effectiveness (ε) of the aerodynamic barrier was derived from the measurements taken, at each condition, defined as:

$$\varepsilon = \frac{Q_{conv,n-0} - Q_{conv,0}}{Q_{conv,n-0}}, \tag{3}$$

where $Q_{conv,0}$ is the measured convection losses for the case with control flow and $Q_{conv,n-0}$ is the convective heat losses for the equivalent conditions but without a control flow Effectiveness of 1.0 means that convective heat losses are perfectly eliminated, the effectiveness of 0.0 means that there is no change of the convective heat losses, while a negative value indicates that the convective heat losses have increased when compared with the reference case without an aerodynamic barrier.

The momentum of the wind flow at the aperture plane is calculated from Eq. (4):

$$\dot{M}_w = \rho A_{ap} u_w^2 \tag{4}$$

where ρ is the density of the air, A_{ap} is the aperture area.

The momentum of the curtain flow is calculated similarly from Eq. (5):

$$\dot{M}_0 = \rho A_0 u_0^2 \tag{5}$$

where A_0 is the nozzle inlet/outlet area.

The momentum flux of wind flow ($M^{"}_w$) and the curtain flow ($M^{"}_0$) are obtained from dividing the momentum ratio by A_{ap} and A_0, respectively.

2.1.5. Main dimensionless numbers

The following dimensionless numbers were used to provide insight and broaden the relevance to other conditions:

(a) The Reynolds number of the air curtain at the exit plane, is the ratio of inertial forces to viscous forces, as follows.

$$Re_0 = \frac{\rho u_0 b}{\mu}, \tag{6}$$

where b is $_{\text{the}}$ width of the outlet gap of the air curtain (Fig. 2).

(b) The Richardson number defined by Eq. (9), is the ratio of the Grashof number to the square of cavity Reynolds number [24–27]. It presents the flow shear term to the buoyancy terms within the cavity [28].

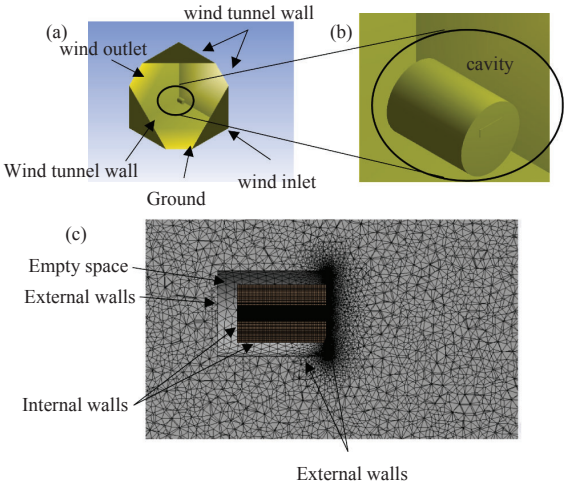

Fig. 2. (a) Geometry of the cavity and domain, (b) Geometry of the cavity and the downward blowing air curtain (c) mesh structure of the domain and internal volume of the cavity.

$$Gr = \frac{g\beta(T_w - T_\infty)D_{cav}^3}{\nu^2}[24, 28], \quad (7)$$

$$Re = \frac{u_w \times D_{cav}}{\nu}[24, 27], \quad (8)$$

$$Ri = \frac{Gr}{Re^2} = \frac{g\beta(T_{wall} - T_\infty)D_{cav}}{u_w^2}, \quad (9)$$

where g is the gravitational acceleration and β is the thermal expansion coefficient.

The inverse Richardson number is being used to characterise the convective heat losses regime within the cavity. At no wind speed, where $1/Ri = 0$, buoyancy forces play a key role in convective heat transfer. Hence, natural convection is dominant at no wind or low wind conditions. As the wind speed increases the inverse Richardson number increases, and the flow regime within the cavity transitions from buoyancy dominated ($1/Ri < 0.1$) to a mixed regime ($0.1 < 1/Ri < 10$) and a momentum dominated regime ($1/Ri > 10$) [9,24].

2.1.6. Experimental cases

Table 1 presents the key experimental conditions investigated in the presented study, including the cavity orientation, the wind speed, aerodynamic barrier speed and the inclination angle. It is worth noting that the following parameters were fixed for all experimental cases: the wall temperature ($T_{cav} = 300$ °C), the yaw angle ($\alpha = 0°$), the length-to-diameter cavity ratio ($L_{cav}/D_{cav} = 1.5$), and the aperture-to-cavity diameter ratio of ($D_{ap}/D_{cav} = 0.33$), for the open aperture cases.

2.1.7. Uncertainty

The estimated uncertainty of the velocity of the blown air of the air curtain driven from the accuracy of the flowmeter is ± 0.4% while the standard deviation of the velocity across the air curtain gap is 2%. The uncertainty of the air suction velocity driven from the accuracy of the flowmeter is ± 0.6%. The variation of the measured velocity on the axis of suction airway contributes to 1.83% uncertainty of the velocity measurements. Therefore, the uncertainty in bulk mean exit velocity of the air curtain is ± 3.66%. The average wind speed was measured by point measurements of wind speed at the test section with a standard deviation of 0.11 m/s. It should be noted that the wind speed measurements were performed at the beginning of each experiment with a certain wind speed. Therefore, the variation of wind speed during the test due to the variation of the air temperature (± 2 °C) of the wind tunnel has not been considered. Hence, the uncertainty in the calculation of inverse Richardson number is 1.02%. The maximum uncertainty of the heat losses contributed from each heater, including that of the thermocouples and control devices, is 3.1% (±25 W) of the maximum power.

2.2. Numerical approach

A 3-D computational fluid dynamics (CFD) model was developed using the commercial software ANSYS CFX 2020 R1 to provide additional understanding of the flow behaviour within the cavity and the interaction of the external flows of wind and aerodynamic barriers, utilising the Reynolds-Averaged Navier-Stokes (RANS) method. The modeled geometry was simplified relative to the experimental receiver as illustrated in Fig. 2(a). The cavity was positioned in the middle of the computational domain with a length of 20 times the diameter of the cavity to match the unconfined flow condition of the tunnel, following previous studies [29]. ANSYS/Meshing 2020 R1 was used to generate a non-uniform unstructured grid using the sweep method and a first layer thickness inflation over the walls (with an inflation factor of 1.2) to generate a higher mesh density inside the cavity compared to the enclosure domain (Fig. 2c). A mesh of approximately 5×10^6 elements was used for all the cases tested. The suitability of the mesh was checked by mesh independence and mesh quality test. The quality of the mesh was checked for skewness, aspect ratio orthogonality and expansion factor, according to Tian et al. [30]. Mesh independence was checked on a coarser mesh (2.5×10^6) and a denser mesh (9×10^6). Air was chosen as the working fluid (ideal gas, with the full "Buoyant" model). Radiation was not included in the model because the experimental data highlighted that, for the operating conditions chosen, it only accounts for < 5% of the total heat losses. Both Large Eddy Simulation (LES) and Reynolds Averaged Navier Stokes (RANS) models have been used in previous studies to predict flow features from air curtains [12,16,31,32]. In a study by Moureh and Yataghene [31] it is concluded that LES performs better than RANS models to predict the flow behavior. However, considering the high computational cost associated with LES and the 'sufficient accuracy' of k-ε turbulence closure model for the purposes of this work, it was selected for our study. This follows many successful previous studies using k-ε for similar flows. All the equations were discretised using a high resolution method. The convergence criterion for all cases was set to be 1×10^{-5} (r.m.s), also employing the total heat flux from the walls as monitoring point for convergence. A computer with Intel Core i7-6700 processor and an available RAM of 16.0 GB was used for all the calculations for an average of 20 h CPU-time to achieve the desired convergence.

The convective heat losses from the cavity were calculated from the experimental data by subtracting the measured heat conduction through the walls and radiation through the aperture from the total measured heat losses. The deduced convective heat losses were then used for model validation. Therefore, the thermal radiation from walls and conduction between internal and external walls were not included in our model. Hence, the external walls of the cavity were set as adiabatic walls. Based on this, the heat flux from the internal cavity walls, at a fixed temperature, would correspond to the convective heat losses from inside the cavity. Table 2 presents the boundary conditions used for the numerical simulation.

2.2.1. Model validation

The CFD model was compared with the available experimental results to provide confidence in the predicted trends and insights into the likely mechanisms. Comparisons of the measured and predicted values of heat transfer coefficient were made at sixteen positions of the cavity. Fig. 3 illustrates schematically the different sections of the cavity. The total convective heat losses and the distribution of losses from the different sections of the cavity were used to assess the validity of the numerical modeling, for all the cases. Table 3 presents the measured absolute values of convective heat losses from the different sections and corresponding calculated losses from the CFD modelling for each

Table 1
List of experimental conditions.

Wind speed u_w [m/s]	Cavity Tilt angle θ [°]	Type and orientation of the aerodynamic barrier	Aerodynamic barrier velocity, (u_o) [m/s]	Discharge/drawing angle of aerodynamic barrier ϕ [°]
0, 3, 6, 9	0	Blowing, upward	0, 4.5, 9, 18, 36	30°
0, 3, 6, 9	0	Blowing, downward	4.5, 9, 18, 36	30°
0, 3, 6, 9	0	Suction	2.63, 5.26, 10.52, 14.79	0°, 15°, 30°
0, 3, 6, 9	30	Blowing, downward	0, 4.5, 9, 18, 36	30°
0, 3, 6, 9	45	Blowing, downward	0, 4.5, 9, 18, 36	30°

Table 2
Boundary conditions used for the numerical modelling.

Boundary	Condition
Cavity external walls	Adiabatic wall at initial temperature of 25 °C
Domain walls	Wind inlet – Normal direction and uniform speed
	Wind outlet – Opening with relative pressure of 0 Pa
	Ground – No-slip wall
	Sidewalls – Opening with relative pressure of 0 Pa
Cavity internal walls	No-slip wall – fixed temperature at 300 °C
Air curtain- blowing	Inlet uniform velocity
Air suction	Outlet uniform velocity

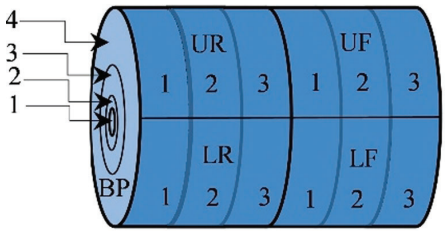

Fig. 3. Sketch of the terminology used to label the 16 measurements of heat transfer in the cavity. UF: Upper front, UR: Upper rear, LR: Lower rear, LF: Lower rear, BP: Back plate.

section, for the case featuring wind speed 0 m/s, tilt 0° with no air curtain case. The table also reports the percentage of the losses obtained from experimental and numerical methods, for the same case. Similarly, Fig. 4 presents the comparison of the measured relative convective heat loss distribution from the different sections of the cavity with those calculated from CFD, for the same case. It can be seen that the CFD predictions agree with the measured heat losses to within 0.3% for the total values and to within 7.6% maximum difference in some individual sections. The availability of convection heat transfer coefficient at 16 points inside the cavity also enabled heat flux profile to be compared. Worth noting is that Nusselt number is directly correlated with the flow velocity and its interaction with inner surface of the cavity. The agreement shows in the figures below, both globally and locally, are deemed to be sufficient to utilize the CFD results to provide insight into the effect of controlling parameters on mechanisms driving the heat transfer within the device.

3. Results and discussion

3.1. Effectiveness of air suction system

Fig. 5 presents the measured values of the effectiveness of the aerodynamic barrier (Eq. (3)), ε (%) for a series of the velocity of the air suction (u_0 = 2.63, 5.26, 10.52, 14.79 m/s) for u_w = 0, 3, 6 and 9 m/s and three extraction angles of ϕ = 0°, 15°, and 30° at cavity tilt angle of 0°. The results show that the application of suction at the vicinity of the aperture, especially for lower wind speeds, leads to a significant reduction in convective heat losses achieving effectiveness of 83%. From the literature [33] it is known that, for the buoyancy-driven case with a wind speed of 0 m/s, the hot gases exits the cavity through the upper side of the aperture while the cold air flows into the cavity from the lower part of the aperture. This interaction of the fluids inside and outside the cavity causes recirculation of the air in the lower part of the cavity (the convective zone) while the hot gases are stranded in the upper part of the cavity in the stagnation zone. Fig. 6 presents the measured convective heat losses from different sections of the cavity for the cases with air suction ($Q_{conv,0}$) relative to that of the no air suction case ($Q_{conv,n\text{-}0}$) for u_w = 0 m/s. It is clear from the figure that heat losses in the lower front section (LF), which contribute the most to the total heat losses, decrease significantly for the cases with a suction flow across the aperture. Table 4 presents the heat loss reduction from each section of the cavity related to a total reduction in each case. The table shows that 52% of the reduction in convective heat losses occurs in the lower front section (LF) of the cavity at u_0 = 14.79 m/s. This implies that air suction from the lower side of the aperture inhibits the cold air from entering the cavity. As a consequence, the losses from the cavity decrease not only in the lower part, but also in all other sections due to the inhibiting of the large eddy within the cavity. As depicted in Fig. 5, for the wind speeds of 0 and 3 m/s, at a tilt angle of θ=0°, increasing the velocity of the extracted flow through the suction nozzle increases the effectiveness significantly. In particular, increasing the suction velocity from 2.63 to 14.79 m/s causes a 77% increase in the effectiveness for no wind condition and suction angle of ϕ = 0°. However, for higher wind speeds of u_w = 9 m/s, increasing the drawing velocity from 2.63 m/s to 14.79 m/s, slightly changes the effectiveness by around 4%. Fig. 5 also illustrates the effect of the suction angle on the effectiveness. As it can be seen, for conditions of both higher suction power and lower wind speeds, the suction angle has a slight influence on the effectiveness. However, for the higher wind speeds, the air suction flow parallel to the aperture plane has a better performance.

Fig. 7 presents the calculated temperature contours and velocity vectors at the center plane of the cavity (X = 0), for suction velocities cases of 0.0, 2.63, 5.26 and 10.52 m/s, at wind speed of 3 m/s. It can be seen that, for the case without an aerodynamic barrier, cold air enters the cavity from the lower side of the aperture while hot gasses leave from the upper side of the aperture. The use of the air suction with a low drawing speed partially inhibits cold air from entering the cavity. As the suction drawing velocity increases, penetration of cold air into the cavity decreases and, as a result, the low temperature zone within the cavity shrinks. To compare the effectiveness of the aerodynamic barrier, the stagnation zone inside the cavity is defined as the integrated internal volume of the cavity featuring air temperature higher than 227 °C. It can be seen that the calculated volume of the stagnation zone volume inside the cavity indicates an increase from 3.1×10^{-3}m^3 for no suction case to 9.9×10^{-3}, 17.7×10^{-3} and 18.2×10^{-3}m^3 for u_0 = 2.63, 5.26 and 10.52 m/s, respectively.

The velocity vectors in the mid-plane of the cavity illustrate the interactions between the flows inside and outside the cavity. The

Table 3
Absolute and relative heat losses from different sections of the cavity under no wind condition obtained from experimental measurements and calculation of numerical modelling for no air curtain case at a tilt angle of 0°.

		Cavity sections																
		UR			*UF*			*LR*			*LF*			*BP*				*Total*
		1	*2*	*3*	*1*	*2*	*3*	*1*	*2*	*3*	*1*	*2*	*3*	*1*	*2*	*3*	*4*	
Experiment	*Absolute (W)*	2.9	4.1	3.4	3	4.6	1	16.4	24.1	24.1	30.2	60	47.9	0.5	5.1	4	2.9	234.2
	Relative (%)	1.2	1.7	1.5	1.3	2	0.4	7	10.2	10.3	12.8	25.8	20.4	0.2	2.2	1.7	1.2	100
CFD	*Absolute (W)*	7.3	8.5	9	5	6.1	3.1	16	20	20	27	40	36	1.9	5.4	8.5	5.5	219.2
	Relative (%)	3.3	3.9	4.1	2.3	2.8	1.4	7.3	9.1	9.1	12.3	18.2	16.4	0.9	2.5	3.9	2.5	100

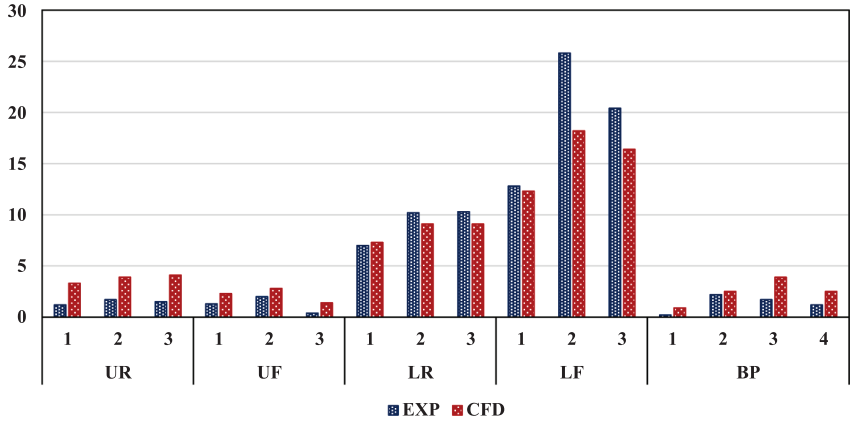

Fig. 4. Comparison of modelled and measured convective heat loss from different sections of the cavity relative to the total convective heat losses from cavity at $u_w = 0$ m/s, no air curtain and $\theta = 0^\circ$ (UF: Upper front, UR: Upper rear, LR: Lower rear, LF: Lower front, BP: Back plate).

application of the suction results in a lower velocity of the flow through the aperture plane, and causes a reduction in the external cold air flow velocity into the cavity. Accordingly, the hot air zone inside the cavity expands and this results in less convective heat losses, hence the effectiveness of the aerodynamic barrier increases. It should be noted that a further increase in the extraction velocity has the potential to draw air from inside the cavity into the suction nozzle and therefore increase rather than decrease the convective heat losses.

3.2. Effect of blowing versus suction

Fig. 8 presents the measured values ε (%) as a function of nozzle power for blowing and suction and for various wind speeds at a cavity tilt angle of 0°. The results show that for an equal fan power consumption at lower wind speeds ($u_w = 0$ and 3 m/s), where $1/Ri < 10$, the air blowing curtain yields better performance for the lower fan power consumption. For high power cases, the results shows that sucking air yields higher effectiveness than blown air with an exception of the wind speed of 6 m/s. The discrepancy in the effectiveness at $u_w = 6$ m/s is not well understood and is likely to be related to uncertainty in the experimental data. The results for higher wind speeds ($u_w = 6$ and 9 m/s) where $1/Ri > 10$ show that overall the suction flow has a better performance than the blowing type. This implies that for the same operating condition of the cavity at a tilt angle of 0°, higher thermal efficiency can be achieved through lower fan power for an air suction system rather than air blowing curtain.

Fig. 9 presents the computed temperature contours and velocity vectors at the mid-plane of the cavity for the same conditions of the aerodynamic barrier of suction and downward blowing air curtain for wind speed of $u_w = 3$ m/s and power consumption of 139×10^{-3}W. The results show that the volume of the stagnation zone for the suction case is 17.7×10^{-3}m^3 while for downward blowing air curtain with the same power consumption, the volume is 11.7×10^{-3}m^3 (a reduction of 34%). Therefore, the larger zone with higher air temperature within the cavity shows that the convective heat losses in the suction case are less than those for the downward blowing air curtain. The main difference between the two cases can be understood by observing the calculated flow behaviour at the aperture plane. For the suction case, air extraction inhibits the cold air from entering the cavity while blowing, through the air curtain inhibits hot air from escaping through the upper side of the aperture. However, the air curtain also generates flow recirculation in the lower region of the cavity which induces external cold air to enter the cavity. This can be seen in Fig. 9d, as a high velocity zone in the lower part of the cavity at the vicinity of the aperture. The ingress of cold air flow, with high velocity, induced by the air curtain leads to a different type of convective heat losses. That is, it generates these two competing effects which make control challenging.

Fig. 10 presents the measured values of ε for two cases of downward

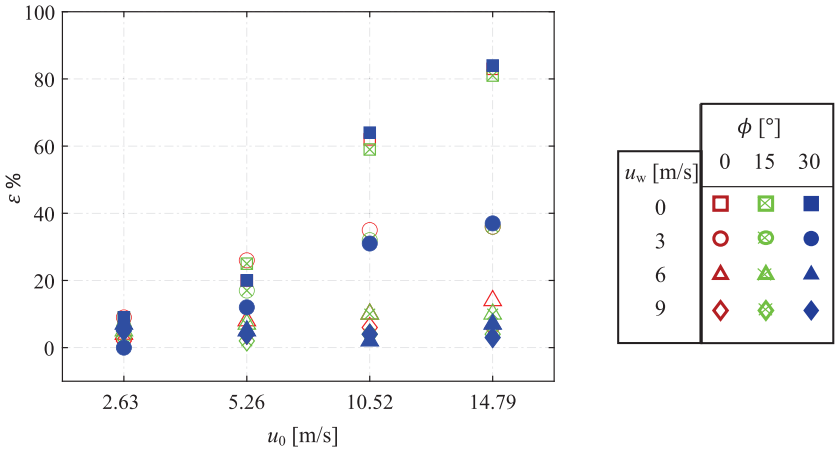

Fig. 5. Measured values of effectiveness (Eq. (3)), ε %, as a function of velocity of the air suction $u_0 = 2.63$, 5.26, 10.52 and 14.79 m/s, for $u_w = 0$, 3, 6 and 9 m/s, and a suction angle of $\phi = 0^\circ$, 15° and 30°. Test conditions: $\alpha = 0^\circ$, T = 300 °C, $\theta = 0^\circ$.

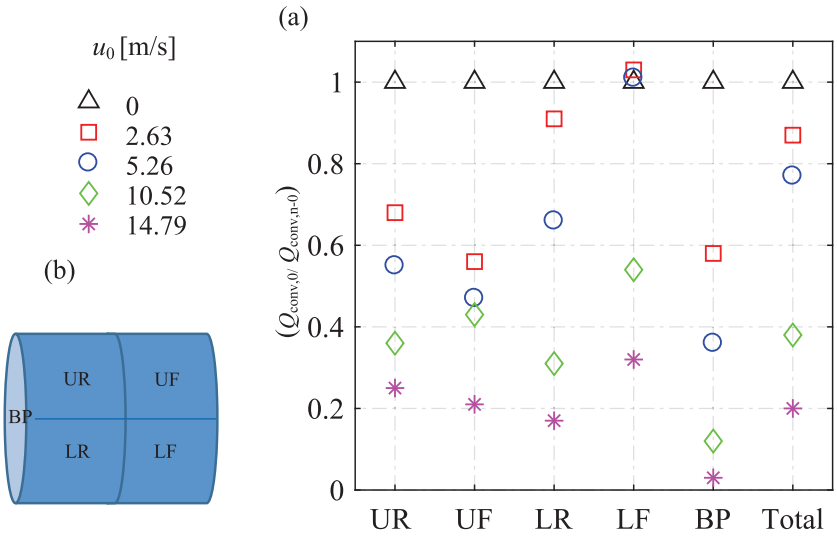

Fig. 6. (a) Measured relative convective heat losses ($Q_{conv,0}/Q_{conv,n-0}$) from different sections of the cavity for u_0 = of 0, 2.63, 5.26, 10.52 and 14.79 m/s, to the similar cases with no suction case at a wind speed of 0 m/s. Test conditions: α = 0°, T = 300 °C, θ = 0°. (b) Different section of the cavity (UR: Upper rear, UF: Upper front, LR: Lower rear, LF: Lower front, BP: Back plate).

Table 4
Measured percentage of the reduction of convective heat losses from each section of the cavity relative to the total reduction compared with the equivalent case with no suction.

u_0 [m/s]	Upper Rear	Upper Front	Lower Rear	Lower Front	Back Plate
2.63	19	26	27	−24	52
5.26	12	14	44	−4	35
10.52	5	5	28	46	16
14.79	5	5	26	52	13

blown air curtain and air suction as a function of the momentum ratio of the curtain flow relative to that of the wind ($\dot{M}_0/\dot{M}_w$) using a logarithmic scale for two ranges of $1/Ri < 10$ and $1/Ri > 10$, at θ=0°, $\alpha = 0°$ and $T_{cav} = 300$ °C. It is clear from the figure that ε increases logarithmically with $\dot{M}_0/\dot{M}_w$ for both cases of air suction and blowing. This first order collapse of the data shows that the momentum ratio has a first order influence on effectiveness. It can also be seen that it is possible to reach an effectiveness of order of 50%, but only for regime in which buoyancy is significant, $1/Ri < 10$.

The figure also shows that, for an equivalent value of the momentum ratio, a suction flow typically has a higher effectiveness than a blown flow for $1/Ri > 10$ but has a lower effectiveness for $1/Ri < 10$. In contrast to the air suction cases, some conditions of blowing at relatively low momentum ratio result in a negative effectiveness, for which the convective heat losses are increased relative to the case with no control. Under these conditions, the flow from the curtain augments the circulation of external flow into the cavity. Nevertheless, since these conditions occur in the regime where effectiveness is relatively low anyway, it should be possible to avoid this regime.

From the figure, it also is apparent that, for both blowing and sucking, inverse Richardson number has a significant influence on the effectiveness. That is, a useful value of effectiveness is only achieved in regime where buoyancy is significant ($1/Ri < 10$). In contrast, the maximum effectiveness achieved in the momentum dominated regime ($1/Ri > 10$), of the order 10%. This suggests that it may be difficult for air curtains to be effective in windy environments.

3.3. Effect of blowing air orientation

The variation of air curtain effectiveness with the inverse

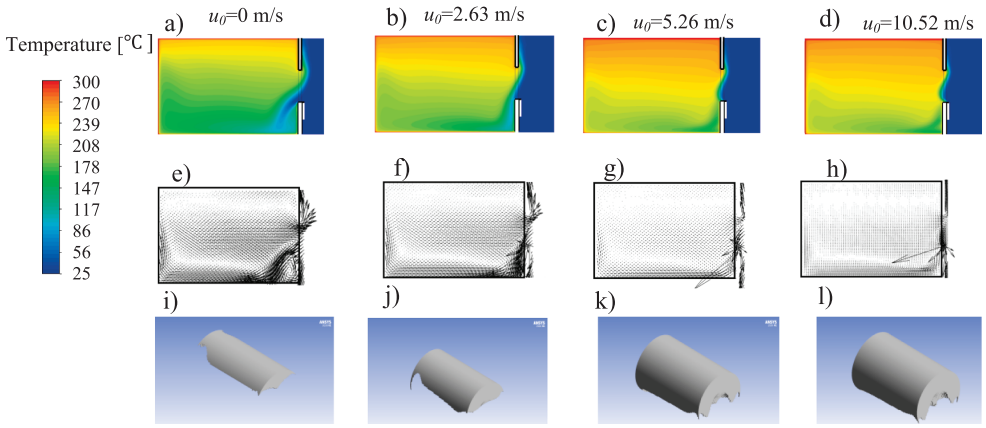

Fig. 7. (a–d) Temperature contours (e–h) velocity vectors and (i–l) iso-volume of the cavity with temperature higher than 227 °C in the mid-plane of the cavity obtained by numerical calculation for the conditions of no suction, u_0 = 2.63, 5.26 and 10.52 m/s in the first to fourth columns from left to right. Test conditions: α = 0°, T = 300 °C, θ = 0°.

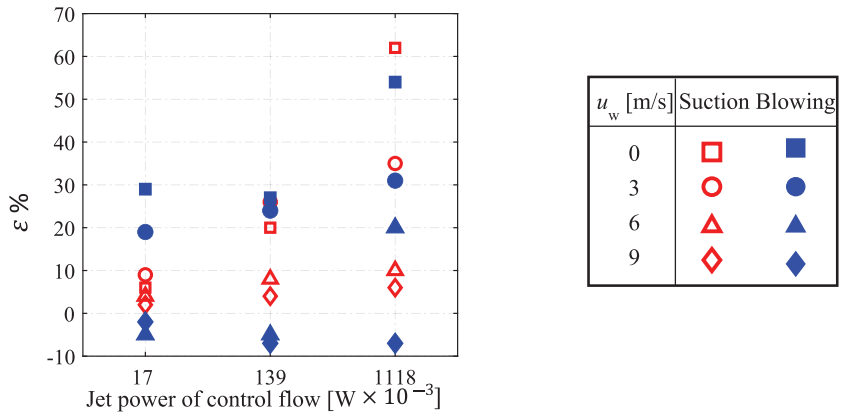

Fig. 8. Values of measured effectiveness, ε (%), as a function of power required to be supplied by a fan for two different aerodynamic barrier mechanisms of blowing and suction, for wind speeds of u_w = 0, 3, 6 and 9 m/s. Test conditions: α = 0°, T = 300 °C, θ = 0°, ϕ = 30°.

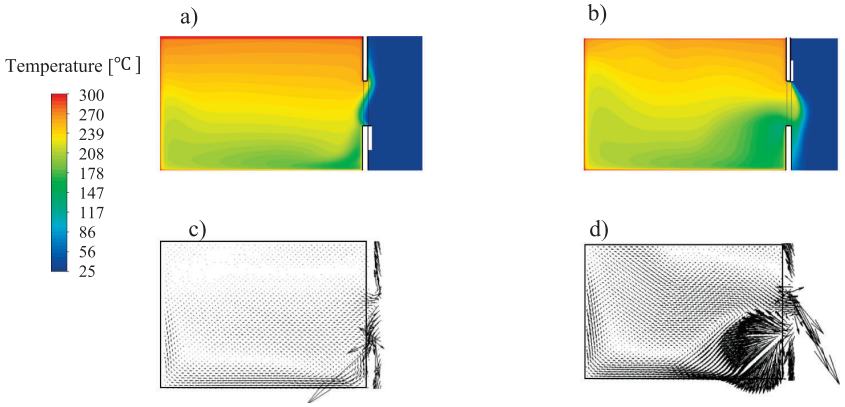

Fig. 9. Computed temperature contours (a–b) and velocity vectors (c–d) in the mid-plane of the cavity for the conditions of suction velocity of u_0 = 5.26 m/s (a, c) and downward air curtain velocity of u_0 = 9 m/s (b, d), corresponding to a fan power of 139 × 10^{-3} W, at wind speed of 3 m/s. Test conditions: α = 0°, T = 300 °C, θ = 0°.

Richardson number ($1/Ri$ = 0, 4.8, 19.37 and 43 corresponding to u_w = 0, 3, 6 and 9 m/s) for two orientation of upward and downward blowing curtain, u_0 = 4.5, 9, 18 and 36 m/s and a tilt angle of θ = 0° is presented at Fig. 11. The figure shows that for the low values of $1/Ri$, an upward blowing air curtain has a better performance than a downward blowing type for the equivalent experimental condition. However, the difference becomes negligible for the highest inverse Richardson number. This is consistent with the curtain direction being important in the buoyancy-dominated regime but not in the inertia-dominated regime.

It can also be seen that the difference between the effectiveness of two orientations is more significant for lower wind speeds. For example, the upward blowing is more effective than the downward blowing by 47% for $1/Ri$ = 0 and a curtain velocity of 9 m/s. However, the upward orientation is 4% worse for $1/Ri$ = 43 with a curtain velocity of up to 36 m/s. This provides additional evidence that the

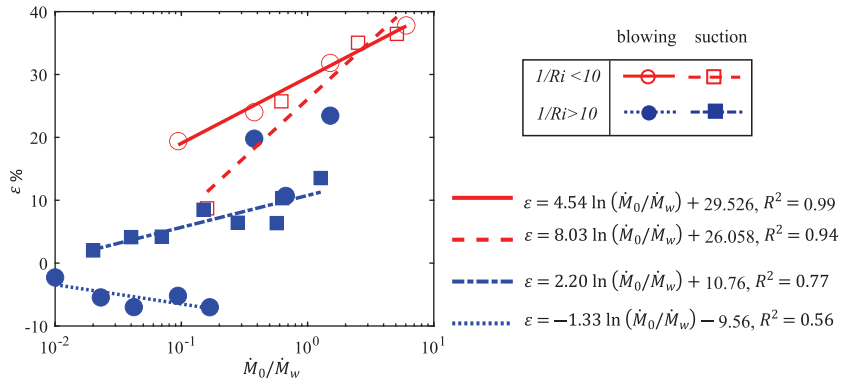

Fig. 10. Measured values of effectiveness, ε (%), as a function of momentum ratio of control flow (suction and blowing) relative to the momentum ratio of wind flow for 1/Ri < 10 and 1/Ri > 10. Test conditions: ϕ = 30°, α = 0°, T = 300 °C, θ = 0°. (Note that the horizontal axis is plotted on a logarithmic scale.)

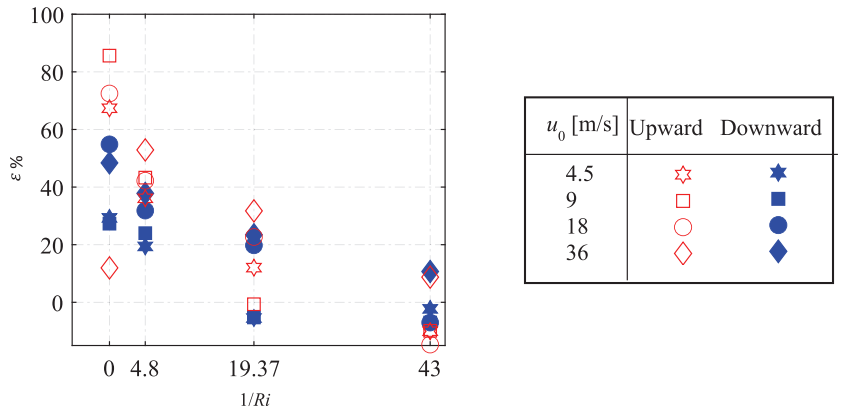

Fig. 11. Variation of measured values of effectiveness, ε (%), with inverse Richardson number (1/Ri = 0, 4.8, 19.37 and 43) for the velocity of the air curtain of u_0 = 4.5, 9, 18 and 36 m/s, for two upward and downward blowing air curtains. Test conditions: ϕ = 30°, α = 0°, T = 300 °C, θ = 0°.

orientation of the air curtain is only important for the buoyancy dominated regime ($1/Ri < 10$). This is also consistent with the previous work of [22], which shows that the most losses occur from the front lower part of the cavity for no air curtain cases. Hence, the upward blowing air curtain is more effective in inhibiting the heat losses from the lower part of the aperture. As $1/Ri$ is increased, the forced convective heat losses dominate and this results in the independence of the effectiveness of air curtain from its orientation. Hence, overall it is more effective to apply an upward blowing air curtain than a downward directed one, but only when buoyancy is significant.

Fig. 11 also shows that, for a no wind condition, as the velocity of the air curtain increases from 18 to 36 m/s in either direction the effectiveness of the curtain reduces. That is, increasing the velocity of the air curtain above its optimum value can reduce the performance of convective losses and increase the mixing of the curtain flow with the hot air in the cavity. Therefore, to maximise the effectiveness of the air curtain it is desirable to control the speed of air curtain relative to the wind.

Further insight into the causes of the differences between the two orientations of the air curtain can be obtained from the CFD results. Fig. 12 presents the computed temperature contours and velocity vectors at the mid-plane of the cavity for upward blowing and downward blowing air curtain with curtain velocity of 9 m/s and a wind speed of 3 m/s where $1/Ri$ = 4.8 and both buoyancy and inertia forces are significant. It can be seen that the upward blowing curtain inhibits the cold air from entering the cavity. However, the curtain deflection downstream from the exit results in the mixing of the blown flow with hot air within the upper region of the cavity, seen in Fig. 12.c as high velocity region at the upper side of the cavity in the proximity of the aperture. For the downward blown air curtain, despite some inhibiting of the hot air from leaving the cavity through the upper side of the aperture, the deflection augments the mixing of the curtain with cold air through the lower side of the aperture. As can be seen in Fig. 12d, this augments the extent of air recirculation in the lower zone of the cavity. The comparison of the temperature contours in the mid-plane of the cavity suggests that the lower part of the cavity is at a higher temperature for the upward blown air curtain than the downward blown one. The size of the stagnation zone is 48% of the internal volume of the cavity for upward blown case and only 36% for the downward blown case.

3.4. Effect of cavity tilt angle

Fig. 13 presents measured values of the effectiveness (Eq. (3)) of the downward blown air curtain with a discharge angle of ϕ = 30°, and for four values of cavity Reynolds number and $1/Ri$ as a function of tilt angle. It should be noted that Richardson number here changes by variation of the wind speed only which results in changing of the Reynolds number of the cavity as well. It can be seen that, for all values of $1/Ri$ (Re_{cav}), εdecreases as the tilt angle is increased from 0° to 45°, especially for higher values of u_o. For cases with $1/Ri > 10$, where the forced convection dominates heat losses, application of the air curtain increases the convective heat losses to 1.83 times of that for no air curtain cases. This suggests that for the cavities with a tilt angle of 45°, the application of blown air curtain is not beneficial in reducing convective heat losses. As the tilt angle of the cavity is increased to θ = 45°,

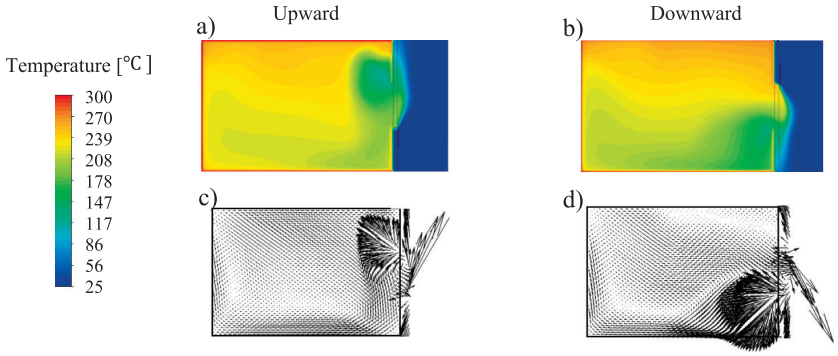

Fig. 12. Computed temperature contours (a–b) and velocity vectors (c–d) in the mid-plane of the cavity for the conditions of downward and upward blowing for u_0 = 9 m/s and at wind speed of 3 m/s (1/Ri = 4.8). Test conditions: α = 0°, T = 300 °C, θ = 0°.

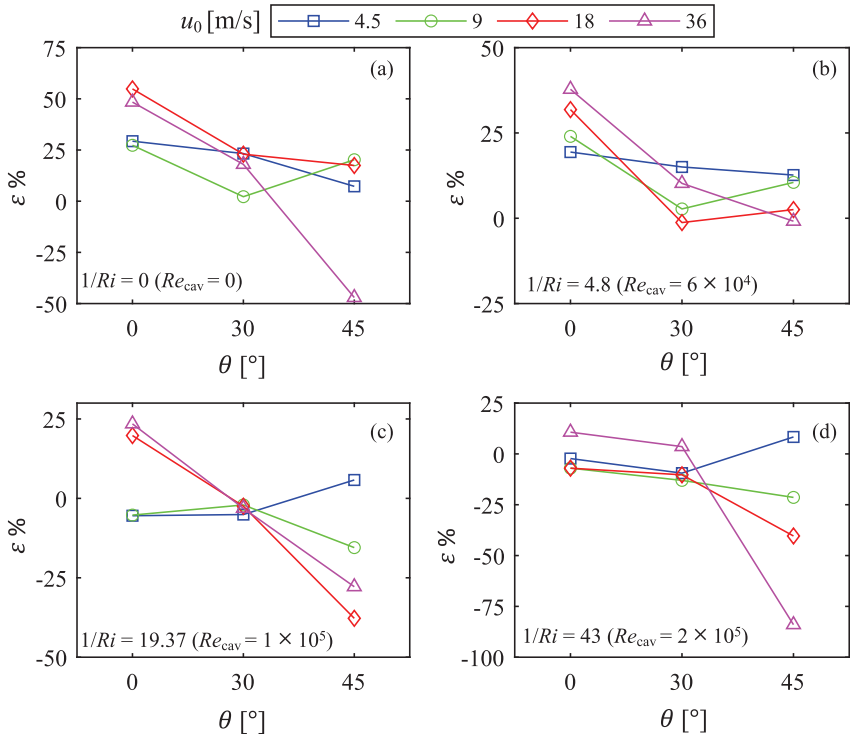

Fig. 13. Measured values of effectiveness (Eq. (3)), ε %, as a function inverse Richardson number for u_0 = 4.5, 9, 18 and 36 m/s and for tilt angles of 0°, 30° and 45°. Test conditions: ϕ = 30°, α = 0°, T = 300 °C.

for the buoyancy dominated regimes, the size of the stagnation zone increases [34]. This has two consequences, first is that the convective heat losses reduce and second is that the stagnation zone becomes more sensitive to any disturbances in the vicinity of the aperture. This is because the size of the stagnation zone depends on the tilt angle of the cavity. The variation of εwith the tilt angle of the cavity indicates that both the relative angle of the air curtain to the aperture plane (ϕ) and that of the curtain flow to the wind are important.

The figure also shows that for the turbulent regime of the cavity flow (Re_{cav} > 4000), as can be seen in Fig. 13(b)–(d), and for the variety of tilt angles the variation of ε is more dependent on convection flow regime than turbulent flow regime. So that for the transition convection regime (Fig. 13b), where the flow is turbulent, the effectiveness of order 25–50% is achievable for the horizontal cavity, while for the same turbulent flow regime illustrated in Fig. 13(c) and (d) lower values of effectiveness is measured. This highlights the importance of convective flow regimes on the effectiveness of air curtain so that the highest values of effectiveness is achieved for the buoyancy dominant flow.

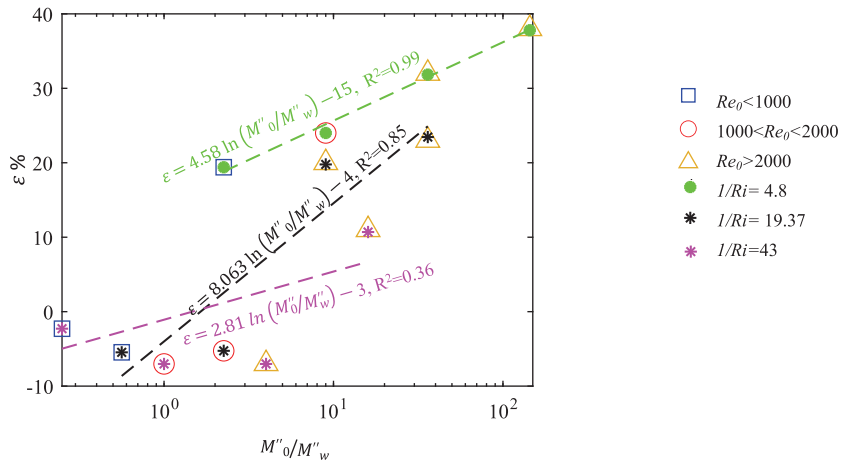

Fig. 14. Measured values of effectiveness, ε (%), as a function of momentum flux ratio of downward blowing air curtain to the wind flow for different ranges of Reynolds number Re_0 < 1000, 1000 < Re_0 < 2000 and Re_0 > 2000. Test conditions: ϕ = 30°, α = 0°, T = 300 °C, θ = 0°.

3.5. Effect of curtain flow regime

Fig. 14 displays the measured effectiveness ε (%) of the downward blown air curtain with a discharge angle of $\phi = 30^{\circ}$, as a function of the momentum flux ratio for different ranges of the Reynolds number of the air curtain (These momentum fluxes have been only changed through the velocity of the air curtain and wind speed, noting that the jet momentum also depends on density of the air curtain (i.e. the air curtain temperature) and the width of the curtain nozzle). The discharged airflow from the air curtain nozzle is not confined for a distance of 50 times that of the jet width from nozzle exit, and hence can be considered as a free jet [35,36]. It should be acknowledged that the lateral external wind flow and the buoyancy forces induced by the hot gases within the cavity affect the nozzle flow. The effect of external wind flow was investigated previously by changing the wind speed for the same operating condition of the air curtain including the velocity, discharge angle and nozzle exit area. This section aims to evaluate the effect of both the initial condition of the jet, at the nozzle exit, and the resulting Richardson number in the cavity. It can be seen that ε mostly increases with the momentum flux ratio and that its function depends on curtain flow regimes. For air curtain velocities in the $Re_0 < 1000$, the variation of ε exhibits a downward trend with the increase in momentum flux ratio corresponding to $M_0^{"}/M_w^{"} < 0.5$. While for higher $M_0^{"}/M_w^{"}$ the effectiveness increases with the momentum ratio. An air curtain in the range of $Re_0 < 1000$ in the vicinity of the aperture appears to partially inhibit the interaction of the flows inside and outside the cavity. However, the momentum of the air curtain is not adequate to establish a significant fluidic barrier across the aperture so that the maximum effectiveness is limited to 20%. It also can be seen that for higher values of curtain Reynolds number, ε increases as the relative momentum flux increases. This can be interpreted as that the increase in the curtain momentum flux results in the augmentation of the curtain flow ability to inhibit the interaction of flows inside and outside the cavity while the wind flow cannot penetrate the curtain flow.

The figure also presents the same data categorised by inverse Richardson number. The results show that although the Reynolds number of the air curtain impacts the effectiveness, the impact of the $1/Ri$ is more significant. So that at $1/Ri = 43$, the effectiveness for all three ranges of Re_0 is low. Although the data does not suggest an equation with high R-square value, it generally suggests that the maximum effectiveness is achieved for the low $1/Ri$ and high Re_0.

4. Conclusions

The effectiveness of two different strategies of reducing the convective heat losses by means of air curtain (*air blown* and *suction*) across the aperture of a cylindrical solar cavity receiver have been assessed experimentally and numerically. The key findings are as follows:

(1) The application of the blown air curtain for a downward tilted cavity ($\theta = 45^{\circ}$), was shown to be ineffective in mitigating heat losses, and it even increased the convective heat losses, relative to the no air curtain case, for higher velocity of the air curtain;
(2) The effectiveness of both blowing and sucking, for horizontal cavity, decreases with the inverse Richardson number, so that either can be reasonably effective in the buoyancy dominated regime, but neither is very effective in the momentum dominant regime.
(3) For the cases assessed here, the effectiveness of applying a low amount of momentum at the aperture plane, for the momentum dominated regime, via suction is typically more effective at reducing convective heat losses than by blowing;
(4) For the same nozzle power required to be supplied by fan, the downward blown air curtain featured a better performance than air suction at lower wind speeds and low fan power consumption. However, at higher power consumption suction has a better performance;
(5) The upward blowing curtain was found to provide better performance than the downward blowing air curtain in the buoyancy dominated regime. Hence, for zero wind speed, the upward blowing air curtain was found to perform 47% better than the downward blowing one. However, the difference is negligible in the momentum-dominate regime;

Declaration of Competing Interest

The authors declare that they have no known competing financial interests or personal relationships that could have appeared to influence the work reported in this paper.

Acknowledgments

This research has been financed by ARENA (grant 2015/RND054), the Australian Research Council (grant LP110200060) and the Premier's Science and Research Fund (grant 2007/1436).

References

[1] P. Haseli, M. Jafarian, G.J. Nathan, High temperature solar thermochemical process for production of stored energy and oxygen based on CuO/Cu2O redox reactions, Sol. Energy 153 (2017) 1–10.
[2] G.J. Nathan, M. Jafarian, B.B. Dally, W.L. Saw, P.J. Ashman, E. Hu, et al., Solar thermal hybrids for combustion power plant: a growing opportunity, Prog. Energy Combust. Sci. 64 (2018) 4–28.
[3] A. Pfahl, J. Coventry, M. Röger, F. Wolfertstetter, J.F. Vásquez-Arango, F. Gross, et al., Progress in heliostat development, Sol. Energy 152 (2017) 3–37.
[4] J.B. Fang, J.J. Wei, X.W. Dong, Y.S. Wang, Thermal performance simulation of a solar cavity receiver under windy conditions, Sol. Energy 85 (2011) 126–138.
[5] Y. Tian, C.Y. Zhao, A review of solar collectors and thermal energy storage in solar thermal applications, Appl. Energy 104 (2013) 538–553.
[6] R. Pitz-Paal, Chapter 19 – Solar Energy – Concentrating Solar Power, in: T.M. Letcher (Ed.), Future Energy, second ed., Elsevier, Boston, 2014, pp. 405–431.
[7] M. Jafarian, M. Arjomandi, G.J. Nathan, The energetic performance of a novel hybrid solar thermal & chemical looping combustion plant, Appl. Energy 132 (2014) 74–85.
[8] J.A. Harris, T.G. Lenz, Thermal performance of solar concentrator/cavity receiver systems, Sol. Energy 34 (1985) 135–142.
[9] R.Y. Ma, Wind Effects on Convective Heat Loss from a Cavity Receiver for a Parabolic Concentrating Solar Collector, Sandia National Laboratories, 1993.
[10] R. Uhlig, R. Flesch, B. Gobereit, S. Giuliano, P. Liedke, Strategies enhancing efficiency of cavity receivers, Energy Procedia 49 (2014) 538–550.
[11] A. McIntash, G. Hughes, J. Pye, Use of an air curtain to reduce heat loss from an inclined open-ended cavity, 19th Australasian Fluid Mechanics Conference. Melbourne, Australia, (2014).
[12] J. Fang, N. Tu, J.F. Torres, J. Wei, J.D. Pye, Numerical investigation of the natural convective heat loss of a solar central cavity receiver with air curtain, Appl. Therm. Eng. 152 (2019) 147–159.
[13] J.J. Zhang, J.D. Pye, G.O. Hughes, Active Air Flow Control to Reduce Cavity Receiver Heat Loss. 2015. V001T05A23.
[14] L.A. Oliveira, J.J. Costa, M.G. Carvalho, H.J. Gerhardt, C. Kramer, On aerodynamic sealing for industrial applications, J. Wind Eng. Ind. Aerodyn. 37 (1991) 255–268.
[15] J.J. Costa, L.A. Oliveira, M.C.G. Silva, Energy savings by aerodynamic sealing with a downward-blowing plane air curtain—a numerical approach, Energy Build. 38 (2006) 1182–1193.
[16] S. Wang, L. Jin, S. Ou, Y. Li, Experimental air curtain solution for refuge alternatives in underground mines, Tunn. Undergr. Space Technol. 68 (2017) 74–81.
[17] J.C. Viegas, F. Oliveira, D. Aelenei, Experimental study on the aerodynamic sealing of air curtains, Fluids 3 (2018) 49.
[18] F.C. Hayes, W.F. Stoecker, Heat transfer characteristics of the air curtain, ASHRAE Trans. (1969).
[19] K. Sirén, Technical dimensioning of a vertically upwards blowing air curtain – Part I, Energy Build. 35 (2003) 681–695.
[20] R.T. Taussig, Aerowindows for Central Solar Receivers. American Society of Mechanical Engineers, Winter Annual Meeting, New Orleans, LA, 1984, pp. 12.
[21] G. Hughes, J. Pye, M. Kaufer, E. Abbasi- Shavazi, J. Zhang, A. McIntosh, et al. Reduction of convective losses in solar cavity receivers. SolarPACES 2015. Cape Town, South Africa, 2015.
[22] E. Alipourtarzanagh, A. Chinnici, G.J. Nathan, B.B. Dally, Experimental insights into the mechanism of heat losses from a cylindrical solar cavity receiver equipped with an air curtain, Sol. Energy 201 (2020) 314–322.
[23] S. Yang, J. Wang, P.D. Lund, S. Wang, C. Jiang, Reducing convective heat losses in solar dish cavity receivers through a modified air-curtain system, Sol. Energy 166 (2018) 50–58.
[24] K.L. Lee, A. Chinnici, M. Jafarian, M. Arjomandi, B. Dally, G. Nathan, Experimental investigation of the effects of wind speed and yaw angle on heat losses from a heated cavity, Sol. Energy 165 (2018) 178–188.

[25] K.L. Lee, A. Chinnici, M. Jafarian, M. Arjomandi, B. Dally, G. Nathan, The influence of wall temperature distribution on the mixed convective losses from a heated cavity, Appl. Therm. Eng. 155 (2019) 157–165.
[26] K.L. Lee, A. Chinnici, M. Jafarian, M. Arjomandi, B. Dally, G. Nathan, The influence of wind speed, aperture ratio and tilt angle on the heat losses from a finely controlled heated cavity for a solar receiver, Renew. Energy 143 (2019) 1544–1553.
[27] R. Huhn, Beitrag zur thermodynamischen Analyse und Bewertung von Wasserwärmespeichern in Energieumwandlungsketten, Technical University of Dresden, 2006.
[28] P.L. Quere, J.A.C. Humphrey, F.S. Sherman, Numerical calculation of thermally driven two-dimensional unsteady laminar flow in cavities of rectangular cross section, Numer. Heat Transf. 4 (1981) 249–283.
[29] K.L. Lee, M. Jafarian, F. Ghanadi, M. Arjomandi, G.J. Nathan, An investigation into the effect of aspect ratio on the heat loss from a solar cavity receiver, Sol. Energy 149 (2017) 20–31.
[30] Z.F. Tian, G.J. Nathan, Y. Cao, Numerical modelling of flows in a solar-enhanced vortex gasifier: Part 1, comparison of turbulence models, Prog. Comput. Fluid Dyn. Int. J. 15 (2015).
[31] J. Moureh, M. Yataghene, Large-eddy simulation of an air curtain confining a cavity and subjected to an external lateral flow, Comput. Fluids 152 (2017) 134–156.
[32] Y.T. Ge, S.A. Tassou, A. Hadawey, Simulation of multi-deck medium temperature display cabinets with the integration of CFD and cooling coil models, Appl. Energy 87 (2010) 3178–3188.
[33] T. Taumoefolau, S. Paitoonsurikarn, G. Hughes, K. Lovegrove, Experimental investigation of natural convection heat loss from a model solar concentrator cavity receiver, J. Solar Energy Eng. 126 (2004) 801,7.
[34] R.D. Jilte, S.B. Kedare, J.K. Nayak, Investigation on convective heat losses from solar cavities under wind conditions, Energy Procedia 57 (2014) 437–446.
[35] J. Moureh, M. Yataghene, Numerical and experimental investigations on jet characteristics and airflow patterns related to an air curtain subjected to external lateral flow, Int. J. Refrig. 67 (2016) 355–372.
[36] R.C. Deo, J. Mi, G.J. Nathan, The influence of Reynolds number on a plane jet, Phys. Fluids 20 (2008) 075108.

Chapter 5-

An adaptive aerodynamic approach to mitigate convective losses from solar cavity receivers

Statement of Authorship

Title of Paper	An adaptive aerodynamic approach to mitigate convective losses from solar cavity receivers
Publication Status	☐ Published ☐ Accepted for Publication ☑ Submitted for Publication ☐ Unpublished and Unsubmitted work written in manuscript style
Publication Details	Solar Energy

Principal Author

Name of Principal Author (Candidate)	Elham Alipourtarzanagh
Contribution to the Paper	Performed experiments, acquisition of data, interpret data, writing of the manuscript and acted as the corresponding author.
Overall percentage (%)	70%
Certification:	This paper reports on original research I conducted during the period of my Higher Degree by Research candidature and is not subject to any obligations or contractual agreements with a third party that would constrain its inclusion in this thesis. I am the primary author of this paper.
Signature	Date: 06/10/2020

Co-Author Contributions

By signing the Statement of Authorship, each author certifies that:

i. the candidate's stated contribution to the publication is accurate (as detailed above);
ii. permission is granted for the candidate in include the publication in the thesis; and
iii. the sum of all co-author contributions is equal to 100% less the candidate's stated contribution.

Name of Co-Author	Alfonso Chinnici
Contribution to the Paper	Conceptualization, supervised the research and contributed in academic discussion
Signature	Date: 7/10/2020

Name of Co-Author	Graham J Nathan
Contribution to the Paper	Conceptualization, methodology development, review and editing manuscript, supervision, project administration and funding acquisition
Signature	Date: 8/10/2020

Name of Co-Author	Bassam Dally			
Contribution to the Paper	Conceptualization, methodology development, review and editing manuscript, supervision, project administration and funding acquisition			
Signature			Date	6-10-2020

An adaptive aerodynamic approach to mitigate convective losses from solar cavity receivers

Elham Alipourtarzanagh[1], Alfonso Chinnici, Graham J. Nathan and Bassam B. Dally

Centre for Energy Technology, School of Mechanical Engineering, the University of Adelaide, Adelaide, South Australia 5005, Australia

Abstract

We explore the potential for adaptive air barriers to mitigate convective heat losses from cavity receivers, especially at large tilt angles, using both suction and blowing nozzles. A heated scaled-down cylindrical cavity receiver was fitted with nozzles on four sides of the aperture, at 30° to the aperture plane. The tilted cavity receiver is mounted in a large wind tunnel to allow systematic variation of wind speed and direction. The effectiveness of different nozzle arrangements was calculated from the measured convective heat losses for a series of different mitigation strategies. The results reveal that a suction nozzle mounted at the bottom of the aperture is more effective than a blowing nozzle mounted at the top of aperture, for tilt angles of $\theta = 45°$, and under different wind speeds. The effectiveness ranged from 0 at low suction flow rate to ~80% at high suction flow rate. With the use of three suction nozzles, at the bottom and both sides of aperture, the effectiveness decreased markedly for both tilt angles and all wind speeds. For more challenging conditions of a 45° tilt angle and 45° yaw angle, the most effective approach is the use of suction through nozzles aligned diametrically opposite to the wind, while other nozzle combinations were ineffective in mitigating losses. Finally, the results highlight the need to apply an adaptive aerodynamic strategy that can respond to measured changes in the environmental conditions to achieve the highest thermal efficiency.

Nomenclature:

A	area (m^2)		α	yaw angle of the cavity (°)
D	diameter (m)		β	thermal expansion coefficient (1/K)
g	gravitational acceleration (m/s^2)		ε	effectiveness
L	length (m)		θ	tilt angle of the cavity (°)
$\dot{M}$	momentum ($kg\ m/s^2$)		μ	viscosity (kg/(m. s))
M''	momentum flux (kg/ms^2)		ρ	density (kg/m^3)
Q	heat losses (W)		ϕ	inclination angle of the aerodynamic barrier (°)
T	temperature (℃)			
u	velocity (m/s)			
$\dot{V}$	flow rate (m^3/s)			

Greek Letters

Non-Dimensional Numbers

Gr Grashof number, $Gr = \frac{\rho^2 g\beta(T_{wall}-T_\infty)D_{cav}^3}{\mu^2}$

[1] Corresponding Author: Elham.alipour@adelaide.edu.au

Re Reynolds number, $Re = \frac{\rho u_w D_{cav}}{\mu}$

Ri Richardson number, $Ri = \frac{Gr}{Re^2} = \frac{g\beta(T_{wall}-T_\infty)D_{cav}}{u_w^2}$

Subscripts

∞ ambient

ap aperture

b blown air curtain

c control flow

cav cavity

ref reference

s suction air curtain

w wind

Abbreviations

cond conduction

conv convection

CSP Concentrating Solar Power

CST Concentrating Solar Thermal

rad radiation

1. Introduction

Concentrated Solar Thermal (CST) technologies use reflectors to concentrate sunlight into receivers to absorb solar energy and convert it to thermal energy. This thermal energy can be used for a variety of engineering processes such as power generation, termed Concentrated Solar Power (CSP), or for direct uses such as direct use of the steam for enhanced oil recovery (Bellan et al., 2019; Pitz-Paal, 2014). There is growing interest in tower-mounted receivers , which now comprise 10% of the CSP market and have reached 30% of the plants under construction (Okoroigwe and Madhlopa, 2016). The main advantages of solar tower systems are their high thermal efficiency (more than 60%) and high operating temperatures, which are not dissimilar to conventional power plants (Hoffschmidt et al., 2012). The efficiency of the total power plant is predominantly correlated with the performance of the central receiver (Breeze, 2016), making it crucially important to maximize its thermal efficiency by minimising the heat losses from the receiver. There are two main types of solar tower receivers, i.e. cavity receivers and external receivers. The external receivers are used with surrounding heliostat fields and can therefore collect more energy per unit of distance from the tower, which enables greater thermal input and economies of scale (Hassan, 2016; Rodriguez-Sanchez et al., 2015). Cavity receivers for solar towers have a complementary advantage over external receivers in their capacity to achieve higher temperatures due to reduced radiative losses (Vant-Hull, 2012), although they result in lower optical efficiency of the field and lower thermal input per tower. Furthermore, whilst radiative losses tend to dominate at high temperatures, nevertheless, convective heat losses can still contribute up to 60% of the total losses from a cavity receiver, particularly in windy environments (Ma, 1993). Hence, significant effort has been invested to begin to quantify these losses and develop methods to minimise such convective heat losses (Clausing, 1981, 1983; Hu et al., 2017; Jilte et al., 2014; Lee et al., 2018; Lee et al., 2019a, b; Lee et al., 2017; Leporini et al., 2018; Lipiński et al., 2020; Prakash et al., 2010; Siebers and Kraabel, 1984; Wu et al., 2015).

Parameters that affect the convective heat losses from cavity receivers include: the cavity shape, aspect ratio, aperture ratio, inclination and yaw angles, internal temperature and wind speed (Clausing, 1981, 1983; Hu et al., 2017; Jilte et al., 2014; Lee et al., 2018; Lee et

al., 2019a, b; Lee et al., 2017; Prakash et al., 2010; Siebers and Kraabel, 1984; Wu et al., 2015). The majority of previous investigations into convective losses have been restricted to quantifying these losses, with relatively few reporting on the effectiveness of potential mitigation strategies. Worth noting is that the heliostat field design and optical efficiency influence the geometry of the cavity and also limit the type of mitigation strategies that could potentially be applied (Pujol-Nadal et al., 2015). Those strategies that have been proposed include an aerodynamic barrier (Alipourtarzanagh et al., 2019; Alipourtarzanagh et al., 2020; Fang et al., 2019; McIntash et al., 2014; Taussig, 1984; Yang et al., 2018; Zhang et al., 2015a, b), quartz window (Chang et al., 2015; Cui et al., 2013) and partial coverage of the aperture (Flesch et al., 2016). Here we choose to assess the application of aerodynamic barriers, which typically consist of an airstream directed across the aperture to minimise both the egress of hot air from the cavity and the ingress of cold air from the surrounding atmosphere.

In our previous experimental studies (Alipourtarzanagh et al., 2019; Alipourtarzanagh et al., 2020), we investigated the effectiveness, with regard to lowering convective heat losses, of an external air curtain, blowing air in the proximity of the aperture, using a heated cylindrical cavity. The cavity was placed at a tilt angle of 15° in a large wind tunnel with a varying mean air velocity of 0, 3, 6 and 9 m/s. Such conditions provide a range of inverse Richardson numbers from 0 to 43 for the fixed internal temperature and geometry of the cavity. The inverse Richardson number is proportional to the wind speed and characterises the convective heat losses within the cavity. The convective heat transfer regime within the cavity transitions from buoyancy dominated ($1/Ri < 0.1$) to a mixed regime ($0.1 < 1/Ri < 10$) and a momentum dominated regime ($1/Ri > 10$) by increasing the external wind speed (Huhn, 2006). For the buoyancy dominated flow regime (low $1/Ri$), hot air leaves the cavity from the upper side of the aperture, while for a momentum dominated regime (high $1/Ri$) the whole aperture is within the convection zone. By direct measurement of the convective heat losses from a cylindrical cavity for the cases with an air curtain and the equivalent cases without an air curtain, the effectiveness of each air curtain configuration was determined. This effectiveness has been quantified as a function of external wind speed, air curtain velocity and discharge angle. The results highlighted that, for head on wind conditions, the velocity and discharge angle of the air curtain play a significant role in reducing convective losses from cavity receivers. Considering the expansion of the curtain flow, it is highly beneficial for the air curtain flow to be discharged at an angle of 30° relative to the aperture plane to prevent the curtain flow entraining into the cavity. It is also found that for the 30° discharge angle, increasing the curtain velocity increases the effectiveness of the air curtain by establishing an aerodynamic barrier that partially inhibits the interaction of flows inside and outside the cavity. Nonetheless, even with a favourable discharge angle, the effectiveness of the blowing air curtain was found to decrease from 60% effectiveness for the no wind condition to 20% for the momentum dominated heat transfer regime. The findings of these studies provided insights into the trends and impact of controlling parameters, as well as the mechanism for convective heat loss mitigation by using an air curtain. However, they did not include the effects of the Grashof number and wind direction. Therefore, in this paper, we aim to investigate the influence of the Grashof number and yaw angle of the cavity on the effectiveness of the air curtain.

Previous investigations by the authors using experiments (Alipourtarzanagh et al., 2019; Alipourtarzanagh et al., 2020) and a combined experimental and numerical study (Alipourtarzanagh et al., 2020) have shown that the effectiveness of applying a low amount of curtain momentum flow at the aperture plane for a momentum dominated regime via suction is typically more effective at suppressing convective heat losses than blowing. Those results also highlighted that an upward blowing air curtain performed better than a downward blowing orientation for buoyancy dominated flows in a horizontal cavity, recording a maximum effectiveness improvement of 58%. This is because an upward blowing air curtain inhibits the external cold air stream from being induced into the cavity from the lower side of the aperture. It was also found that for a cavity at a tilt angle of 45°, downward blown air curtains are very ineffective, with the convective heat losses increasing by 80%. However, the cavity receiver is usually directed downward to achieve the most efficient design of the tower (Vant-Hull, 2012). The need to find a better approach that allows suppression of convection losses for all relevant conditions, including higher tilt angles and high inverse Richardson number, remains unaddressed. This need has, in part, motivated the current work.

Considering the above findings (Alipourtarzanagh et al., 2019; Alipourtarzanaghet al., 2020; Alipourtarzanagh et al., 2020), it is hypothesised that the controlled use of four aerodynamic barriers (directed upward, downward and in each lateral direction) coupled with a wind direction sensor, will be more effective in reducing convective losses than a single nozzle. We also aim to determine the combinations of suction and blowing as a function of wind direction and speed that have the potential to be the most effective. We aim to achieve this through a systematic experimental investigation, with a view to advancing understanding of the most efficient loss mitigation approaches informed control strategies.

2. Methodology

2.1 Experimental apparatus

A small scale model of a cylindrical cavity receiver (0.3 m ID, 0.45 m length and 0.1 m aperture) was designed and built for use in a large wind tunnel (Figure 1). The open jet test section of th ewind tunnel was used (2.75 m × 2.19 m × 5.5 m) with a moderate level of turbulenceintensity (0.15%~6%). Only a brief description of the essential components is provided here because a more complete description is presented by Lee at *al.* (Lee et al., 2018). The wind direction relative to the aperture plane, which changes with the weather conditions in real operation conditions, was systematically varied for yaw angles (defined as the lateral angle of the normal direction of the aperture relative to the wind direction) between $\alpha = 0°$ and 45° (Figure 2.b). Similarly, the tilt angle of the cavity, defined as the inclination angle of the cavity was systematically varied between $\theta = 0°$ and 45° in 15° increments (Figure 2.a) to cover the range of the common tilt angles of solar cavity receivers in real world applications. The average air speeds of the wind tunnel assessed were varied between u_w = 0, 3, 6 and 9 m/s, corresponding to inverse Richardson numbers of 0, 4.8, 19.4 and 43.6, to achieve the buoyancy dominated, mixed and momentum convection regimes.

The interior surface of the prototype receiver consists of 16 copper plates attached to electrical heaters. The required power to maintain the temperature of each heater at a given value was measured and controlled with a power control system. The temperature of the heaters

(T_{cav} = 300℃ or 400℃) was measured using K-Type thermocouples and then transferred to the Simulink application of the MATLAB program on a computer using a Datataker. The output power signal from the computer was transferred to a DMX (lighting) controller with an Arduino. The controlled power supplied to the heaters via the DMX controller was recorded at steady state conditions, defined as being reached when the variation in the temperature of each heater was less than ±0.5 °C in a 300 s period for cases where the total power was above 2 kW, and the variation of total power supplied to all heaters was less than ±100 W for cases where the total power was below 2 kW.

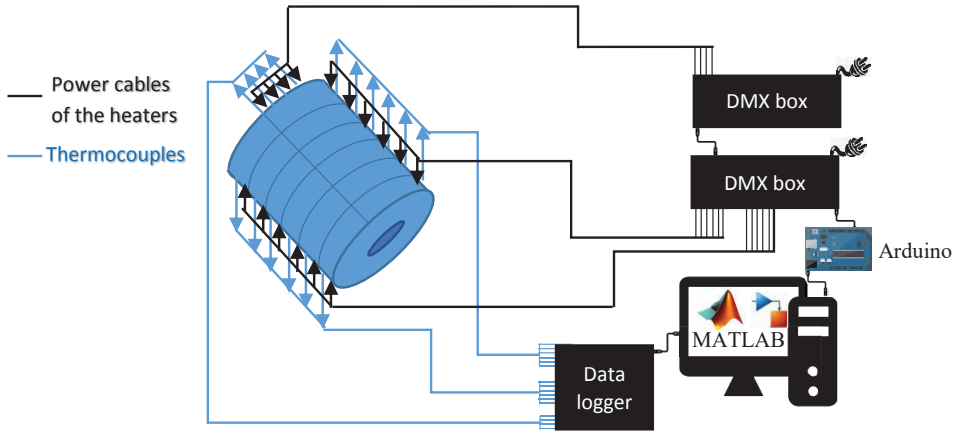

Figure 1- A schematic diagram of the power control system and temperature measurements.

2.2 Aerodynamic barrier

Purpose-designed air blown and air suction nozzles were used to provide aerodynamic flow across the aperture of the cavity following our previous work (Alipourtarzanagh et al., 2020). The same air blown system was used to provide airflow from a 2 mm wide and a 165 mm long rectangular slit, as shown in Figure 2.e, at a discharge angle of ϕ = 30° relative to aperture plane. The air flow was provided to the air curtain nozzle using a rotary screw compressor (Kaeser -SM9) through a ½" pipe to the air supply section of the air curtain at a variety of volumetric airflow rates, using a flowmeter (Alicat Scientific MCR-1000 SLPM). Three specially designed suction nozzles were used to withdraw air across the aperture of the cavity from the lower and the two lateral sides of the aperture. The nozzles' inlets had a width of 10 mm and a length of 100 mm (Figure 2.d) and were fixed at an extraction angle of 30° relative to the aperture plane. The inlet of a blower (Leister ® G90L2) was connected to a settling chamber, drawing air from three air lines connected to the suction nozzles. The suction flow rate of each nozzle was driven from the measured air velocity at the axis of each pipe using a heavy-duty Pitot tube anemometer (Extech HD350) and assuming there was fully developed airflow in the pipes. Each air line was equipped with a globe valve to adjust the airflow rate of each nozzle to ensure equal flows through each. Worth noting is that the difference in the cross sectional area of the exit and inlet of the air blown and air suction nozzles, respectively, is due to hardware limitations and pressure drop. The operating conditions of each method have been adjusted to take account of such differences.

2.3 Convective heat losses and effectiveness calculation

The total heat losses (Q_{total}) from a cavity receiver are comprised of convection (Q_{conv}) and conduction losses (Q_{cond}) through the walls and radiation losses (Q_{rad}) through the aperture. For the cases where the aperture is closed, the total losses equal the conduction losses, while the radiation losses depend on the fourth power of the absolute temperature and hence can be calculated from the known wall temperature. Therefore, the convective heat losses are defined by Equation (1):

$$Q_{conv} = Q_{total} - (Q_{cond} + Q_{rad}). \quad (1)$$

The effectiveness (ε) of the aerodynamic barrier is defined as the difference between the measured convective heat losses for the cases with an aerodynamic barrier relative to those of the cases without an aerodynamic barrier (reference cases) for the equivalent conditions:

$$\varepsilon = \frac{Q_{conv,ref} - Q_{conv,c}}{Q_{conv,ref}}, \quad (2)$$

where $Q_{conv,c}$ and $Q_{conv,ref}$ are the measured convective heat losses for each case with and without an aerodynamic barrier, respectively.

2.4 Richardson number calculation

The Richardson number, defined by Equation 3, is the ratio of the Grashof number to the square of the Reynolds number.

$$Ri = \frac{Gr}{Re^2} = \frac{\frac{\rho^2 g\beta(T_{wall} - T_\infty)D_{cav}^3}{\mu^2}}{\left(\frac{\rho u_w D_{cav}}{\mu}\right)^2} = \frac{g\beta(T_{wall} - T_\infty)D_{cav}}{u_w^2}, \quad (3)$$

where g and β are the gravitational acceleration and thermal expansion coefficient, respectively. The Grashof number is a dimensionless number that scales the buoyancy forces relative to the viscous forces and can therefore be used to characterize the heat transfer mode in a fluid (Shah et al., 2018). The Reynolds number is defined as the ratio of inertial forces to the viscous forces within a fluid, which indicates whether the flow is steady, transitional or turbulent (LaNasa and Upp, 2014). The Richardson number defines the relative significance of the buoyancy forces driving natural convection within the chamber, to inertia forces driven by the wind. It is worth noting that D_{ap} could be used as charachtristics length for calculation of the Richardson number. This will introduce fixed valus of inverse Richardson numers. However, the value of inverse Richardson number for highest wind speed examined in the paper will be in the range of momentum dominated regim.

2.5 Momentum, Momentum flux and flow rate calculation

The momentum of the suction curtain flow is calculated using Equation 4:

$$\dot{M}_s = \rho A_s u_s^2 \quad (4)$$

where A_s is the nozzle outlet area.

The momentum of the wind flow through the aperture is similarly calculated using Equation 5:

$$\dot{M}_w = \rho A_{ap} u_w^2 \quad (5)$$

where A_{ap} is the aperture area.

The momentum flux of the curtain flow (M_c'') are obtained from dividing the momentum ratio by A_c (the outlet/inlet area of the suction/blown curtain).

The curtain volumetric flow rate is calculated using Equation (6):

$$\dot{V} = A_s \times u_s. \quad (6)$$

1

2

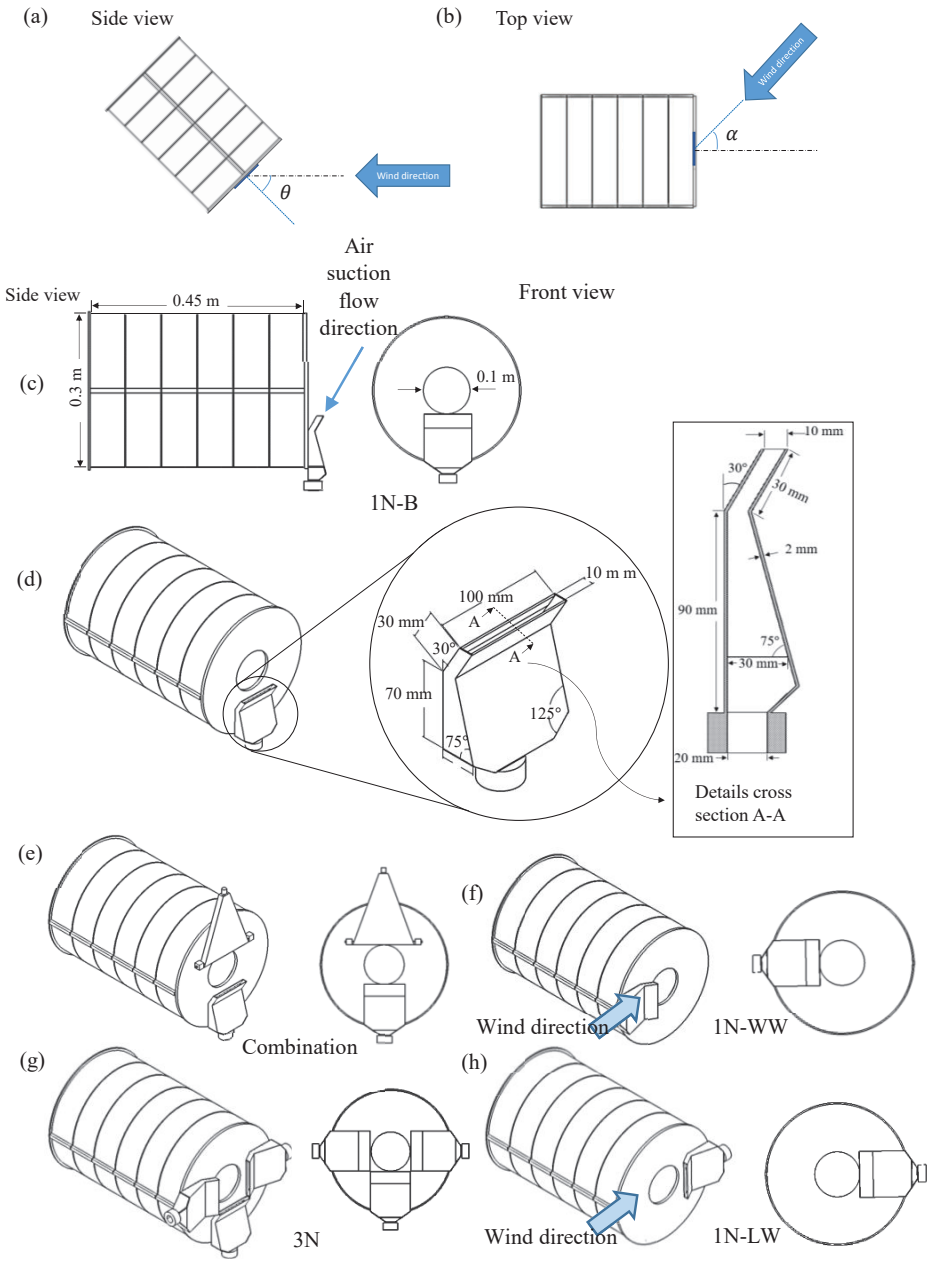

Figure 2- Definition of a) tilt angle (θ) of the cavity relative to the horizontal axis and b) yaw angles (α) relative to the wind, c) schematic diagram of the cavity and suction nozzle configurations at the base of the aperture (1N-B), d) details of the suction nozzle, e) combination of blown and suction air curtain, (f-h) suction nozzle configurations: one nozzle (1N-WW), 3 nozzles (3N) and 1 nozzle (1N-LW).

2.6 Experimental cases

Presented in Table 1 are the experimental conditions assessed in the paper. It can be seen that the cavity tilt (θ) is varied over the range 0° to 45° with a 15° increment and two yaw (α) angles of 0° and 45°, the wind speed (u_w) and aerodynamic barrier speed (u_b, u_s), for the different configurations of the aerodynamic barriers. It is worth noting that the aperture-to-cavity diameter ratio ($D_{ap}/D_{cav} = 0.33$) and the cavity length-to-diameter ratio ($L_{cav}/D_{cav} = 1.5$) were fixed.

Table 1- List of experimental conditions.

Aerodynamic configuration	Wind speed, u_w [m/s]	Cavity tilt angle θ [°]	Cavity Yaw angle α [°]	Velocity of air curtain flow u_c [m/s]	Cavity temperature T_{cav} [°C]	Aperture ratio [-]
Suction-1N-B	0, 3, 6, 9	0, 45	0	3.06, 6.17, 12.37	300	0.33
Suction- 3-N						
Suction- 1N-B	9	15,30	0	3.06, 6.17, 12.37	300	
Suction- 1N-B	3,6,9	45	45	3.06, 6.17, 12.37	300	
Suction- 1N-ww	9	45	45	3.06, 6.17, 12.37	300	
Suction- 1N-lw						
Suction- 3N						
Suction- 1N-B	9	45	0	3.06, 6.17, 12.37	400	
Combination of suction and air curtain	9	45	0	u_b: 4.5, 6.75, 9 u_s: 1, 2, 2.5, 3.06, 6.17, 8, 12, 12.37	300	
	0			u_b: 4.5, 6.75, 9 u_s: 1, 2, 2.5, 3.06, 3.5, 4, 4.5, 5, 5.5, 6.17, 8, 12.37, 18.5		
Closed aperture cases						
Not applicable	0, 3, 6, 9	0, 45	0	Not applicable	300	0
	9	15, 30	0		300	
	3, 6, 9	45	45		300	

2.7 Uncertainty

The uncertainty of the mean wind speed, Richardson number, heat loss measurements and velocity of blown air curtain are as reported in our previous work (Alipourtarzanagh et al., 2020), which used the same apparatus. The estimated uncertainty of the air suction system, deduced from the accuracy of the Pitot tube, is ±0.6%. The variation of the measured velocity on the axis of the suction airway contributes to a 2.1% uncertainty of the velocity measurements. Therefore, the uncertainty in the bulk mean exit velocity of the air curtain is ± 2.3%.

3. Results

3.1 Air Suction only from one nozzle at different tilt angles and zero yaw angle

Figure 3 presents the measured effectiveness of the air suction configuration 1N-B, for three values of suction flowrate ($\dot{V}_s = 3 \times 10^{-3}, 6 \times 10^{-3}$ and $12\times 10^{-3}\ m^3/s$), an inverse Richardson number of 0, 4.8, 19.4 and 43.6 and two tilt angles of (a) $\theta = 0°$ and (b) $\theta = 45°$. It is clear from Figure 3.a, which corresponds to cases with a tilt angle of $\theta = 0°$, that ε increases with the suction flowrate for the majority of cases. For instance, ε was found to

increase by 41%, 19% and 6% with an increase in $\dot{V}_s$ from 3×10^{-3} to $12\times 10^{-3}\ m^3/s$ for $1/Ri$ = 4.8, 19.4 and 43.6, respectively. However, for $1/Ri$ =0, where the convective heat transfer regime is buoyancy dominated, although increasing $\dot{V}_s$ from 3×10^{-3} to $6 \times 10^{-3}\ m^3/s$ results in a 33% increase in ε, a further increase of $\dot{V}_s$ to $12\times 10^{-3}\ m^3/s$ reduces the effectiveness by 9%. When comparing Q_{conv} from the internal surfaces of the cavity, for these two specific cases, namely $\dot{V}_s$= 6×10^{-3} and $12\times 10^{-3}\ m^3/s$, it is clear that increasing the suction flow rate increases the losses from all sections by up to 60%, mostly in the lower front part of the cavity. This implies that, for no wind conditions, extracting air from the suction nozzle at rates higher than an optimum value will increase the cooling from the lower front zone of the cavity in the proximity of the suction nozzle. Since the optimal degree of such rate varies with the wind speed, dynamic control of the mitigation strategies to account for this is desirable. From the figure, it is also apparent that the effectiveness drops as the inverse Richardson number increases. For example, for a suction flow rate of $12\times 10^{-3}\ m^3/s$, an effectiveness of the order of 60% is achieved for $1/Ri$ = 0, while this drops to 6% for the higher inverse Richardson number of 43.6.

Figure 3.b presents the variation of the effectiveness with suction flow rate for a variety of inverse Richardson numbers for the cavity tilt angle $\theta = 45°$. It is apparent that the relationship between effectiveness and the suction flowrate is complex for different inverse Richardson numbers. At $1/Ri$ = 0, the effectiveness reaches a maximum value of 76% at $\dot{V}_s = 6 \times 10^{-3} m^3/s$ and then decreases to 42% by increasing the suction flowrate to $12\times 10^{-3} m^3/s$. A comparison of the distribution of the losses from different sections in the cavity between these two cases shows that 80% of differences in the convective heat losses occur at the lower front section of the cavity. This implies that, as for the case with a tilt angle of $\theta = 0°$, too much suction results in the extraction of the air from inside the cavity and this leads to higher convective heat losses compared with the case with a lower suction flowrate. However, unlike the tilt angle of 0°, the effectiveness does not increase monotonically with the suction flowrate. For example for $1/Ri$ = 4.8 and 19.4 as the suction flow rate increases: the effectiveness drops and increases again. However, the variation of effectiveness for $1/Ri$ = 4.8 is less than that for $1/Ri$= 19.4, so that the variation in suction flowrate from 3×10^{-3} to $12\times 10^{-3}\ m^3/s$ results in a 17% improvement in effectiveness; while for $1/Ri$= 19.4 the value of ε only increases by 6% for the same variation in suction flow rate. In addition, for $1/Ri$= 43.6, there is an upward trend of effectiveness as a function of $\dot{V}_s$, so that effectiveness reaches a maximum value of 42% for $\dot{V}_s = 12 \times 10^{-3} m^3/s$.

A comparison between the results presented in Figures 3.a and 3.b shows that the effectiveness of suction is higher at $1/Ri$ =43.6, and is higher than that for $1/Ri$ = 19.4 and 4.8 and for a tilted cavity at θ = 45°. This contrasts with the results for a horizontal cavity, where increasing the inverse Richardson numbers results in lower effectiveness. This suggests that it is possible to address the challenges associated with reducing the convective heat losses for a tilt angle of $\theta = 45°$ identified previously (Alipourtarzanagh et al., 2020). At this angle, the external aerodynamics, coupled with internal buoyancy forces, were previously found to pose a major challenge to the use of a blowing air curtain as a mitigation strategy for all values of $1/Ri$.

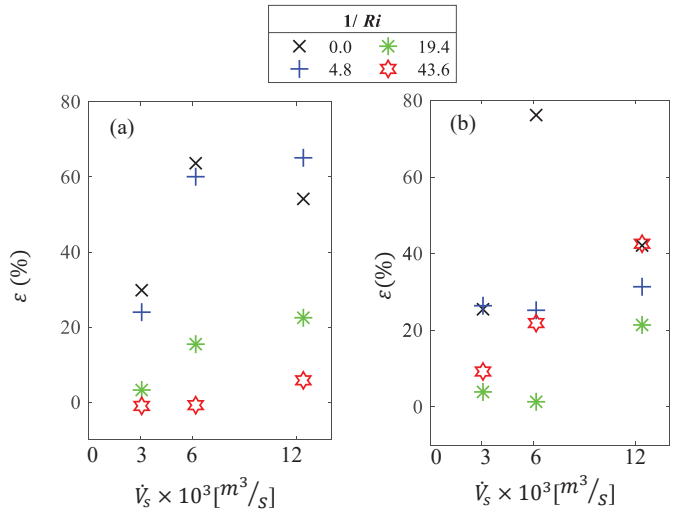

Figure 3- The variation of effectiveness ε (%) with the suction flowrate ($\dot{V}_s = 3 \times 10^{-3}, 6 \times 10^{-3}$ and $12 \times 10^{-3}\ m^3/s$) for inverse Richardson numbers of 0, 4.8, 19.4 and 43.6. Data are presented for the tilt angles of (a) $\theta = 0°$ and (b) $\theta = 45°$. Test conditions: $\alpha = 0°$, T_{cav}= 300℃, nozzle configuration: 1N-B.

Figure 4 presents the absolute values of convective heat losses from the cavity for a tilt angle of 45°, for $1/Ri$ = 0, 4.8, 19.4 and 43.6 and for a suction flow rate of $\dot{V}_s = 0$ and $12 \times 10^{-3} m^3/s$. The results show that increasing the suction flowrate to $\dot{V}_s = 12 \times 10^{-3} m^3/s$ is most effective for $1/Ri$ =43.6, where the heat losses are almost halved from 292 W to 168 W. The effect of suction is not as prominent for the other three cases of $1/Ri$= 0, 4.8 and 19.44 (93 to 54 W, 105 to 72 W, 162 to 127 W). This implies that, despite the air suction, the penetration of external air into the cavity increases with the wind speed. These results confirm the deduction that the effectiveness increases as the air suction flowrate increases towards an optimum value. It can therefore be suggested that the application of air suction from other sides of the aperture (right and left), especially for higher wind speeds where the losses are dominated by forced convection, is likely to improve the isolation of the internal zone of the cavity from the surroundings and hence reduce losses.

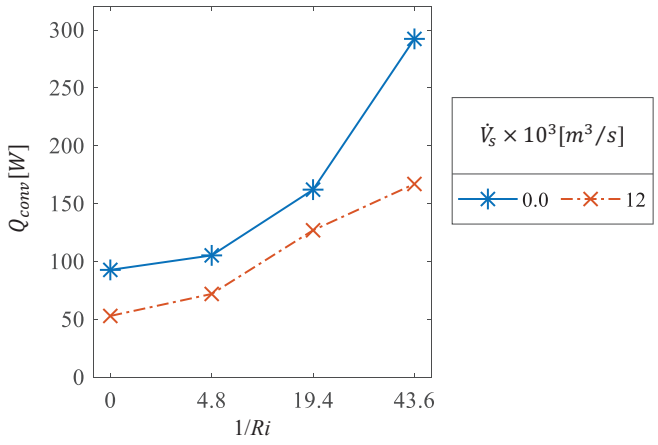

Figure 4- Absolute convective heat losses Q_{conv} [W] as a function of inverse Richardson number for $\dot{V}_s = 0$ and $12\times 10^{-3} m^3/s$. Test conditions: $\theta = 45°, \alpha = 0°$, T_{cav}= 300℃, nozzle configuration: 1N-B.

Figure 5 displays the effectiveness of one air suction nozzle configured as 1N-B as a function of the momentum of the suction flow (Equation 4) relative to that of wind flow (Equation 5) through the aperture ($\dot{M}_s/\dot{M}_w$). The test conditions include $1/Ri = 43$ for the head on wind direction ($\alpha = 0°$) and cavity tilt angles of $\theta = 0°$, 15°, 30° and 45°. These variations of momentum ratios have been implemented here by changing the velocity of the air curtain at a wind speed of 9 m/s, although the momentum also depends on the density of the air curtain and the inlet area of the suction nozzle. It is apparent from the figure that the effectiveness increases with the momentum ratio, for all tilt angles. One possible explanation for this is that a higher momentum of suction relative to that of wind flow strengthens the aerodynamic barrier across the aperture, which inhibits the interaction of flows inside and outside the cavity. As the suction momentum increases, more external air is drawn into the suction nozzle. This guides the external wind flow into the suction nozzle rather than blowing it into the cavity and, as a result, the convective heat losses are reduced.

The figure also shows that the effectiveness of the suction increases with the tilt angle of the cavity, so that a maximum effectiveness of 42% is achieved for a tilt angle of 45°. The trend contrasts the trend of the effectiveness of the blown air curtain with the tilt angle of the cavity (Alipourtarzanagh et al., 2020), which showed that the effectiveness of a blown air curtain decreases with an increase in the tilt angle of the cavity. This also suggests that the potential benefits of air suction are more favorable than blowing for tilted cavity receivers.

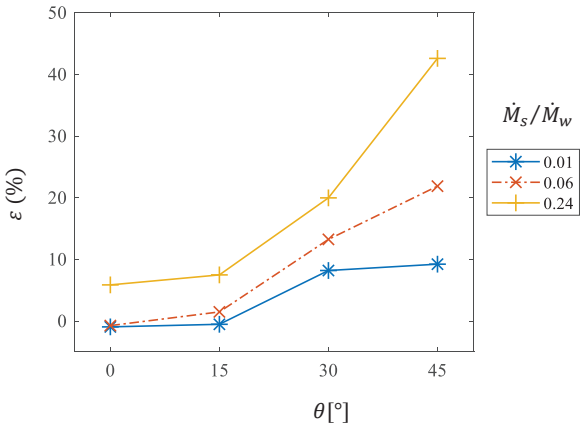

Figure 5- The effectiveness ε (%) of air suction, as a function of the momentum ratio of the suction flow to wind flow through the aperture for $1/Ri$ = 43 and $\theta = 0°$, 15°, 30° and 45°. Test conditions: $\alpha = 0°$, T_{cav}=300℃, nozzle configuration: 1N-B.

3.2 Air Suction only from three nozzles at different tilt angles and zero yaw angle

Figure 6 presents the effectiveness of the three nozzle configurations of the air suction system (Figure 2.g) as a function of the suction flowrate, which was held equal from each nozzle ($\dot{V}_s = 3 \times 10^{-3}, 6 \times 10^{-3}$ and $12\times 10^{-3}\ m^3/s$) for a variety of inverse Richardson numbers and for a head-on wind direction (α = 0°), with a cavity wall temperature of 300℃ and two different tilt angles of (a) $\theta = 0°$ and (b) $\theta = 45°$. Comparing these results (Figure 6.a) with those in Figure 3.a, it can be seen that even the highest value of the effectiveness achieved with the three nozzles is significantly less than was achieved with only one suction nozzle on the lower side of the aperture. At the same time, the power to activate three nozzles is increased three times. Hence this configuration is undesirable. Figure 6.a also shows that the highest effectiveness for wind speeds assessed here is achieved for $\dot{V}_s = 6 \times 10^{-3} m^3/s$, with a value of 33% for $1/Ri$= 4.8. However, a further increase in the suction flow rate to $12\times 10^{-3}\ m^3/s$ results in a dramatic drop in effectiveness.

Comparing the results presented in Figure 6.b with those presented in Figure 3.b, it can be seen that the use of three nozzles instead of one also has an adverse impact on performance for a tilt angle of $\theta = 45°$. The sharp decrease in the effectiveness to -76%, -234% and -65% for $1/Ri$= 0, 4.8 and 19.4 is likely due to the induction of additional cold air into the cavity through the use of the three air suction nozzles. The only sight exception is the case of the highest inverse Richardson number, $1/Ri$= 43.6, where an increase in the suction flowrate increases the effectiveness. However, the value of the highest achieved effectiveness for simultaneous application of three nozzles is 39%, which is 3% less than that for applying one suction nozzle alone. Returning to the hypothesis posed in the previous section, it is now possible to conclude that the simultaneous application of suction through three nozzles does not improve performance over the use of only one nozzle that is optimally oriented relative to the wind.

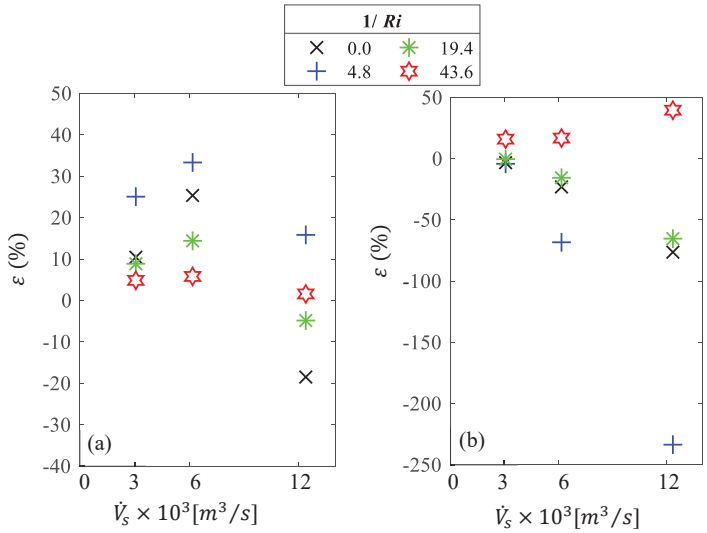

Figure 6- The effectiveness ε (%) of the cases with three nozzles, all applying the same amount of air suction (Figure 2.g), as a function of the suction flowrate from each nozzle ($\dot{V}_s = 3 \times 10^{-3}, 6 \times 10^{-3}$ and $12\times 10^{-3}\ m^3/s$) at different inverse Richardson numbers of 0, 4.8, 19.4 and 43.6 for (a) $\theta = 0°$ and (b) $\theta = 45°$. Test conditions: $\alpha = 0°$, T_{cav}=300℃.

3.3 Air Suction configuration at both yaw and tilt angles of 45°

Figure 7 presents the effectiveness of various configurations of air suction nozzles as a function of wind speed for the case where both the yaw and tilt angles are 45°, $1/Ri = 43.6$ and T_{cav}=300℃. The figure shows that the use of only one suction nozzle below the aperture increases the convective heat losses over the no suction case by approximately 2.4 times for a suction flow rate of $12\times 10^{-3}\ m^3/s$. That is, this configuration increases the ingress of external air into the cavity. It further suggests that the transverse orientation of the angle of the suction nozzle to wind flow is undesirable. The figure also reveals the same trend observed in Figure 6, that the use of three nozzles for suction (below and on both lateral sides) also increases the convective heat losses. The use of a single nozzle on the wind-ward side of the aperture also increases the convective heat losses by up to 3.5 times for the suction flow rates assessed here. However, by activating suction on the lee-ward side nozzle, i.e. with the wind directed toward the active suction nozzle inlet, a 61% reduction in the convective heat losses was achieved for the case $\dot{V}_s = 6 \times 10^{-3}10^{-3}\ m^3/s$. This highlights the importance of nozzle orientation relative to the wind direction to reduce the convective heat losses.

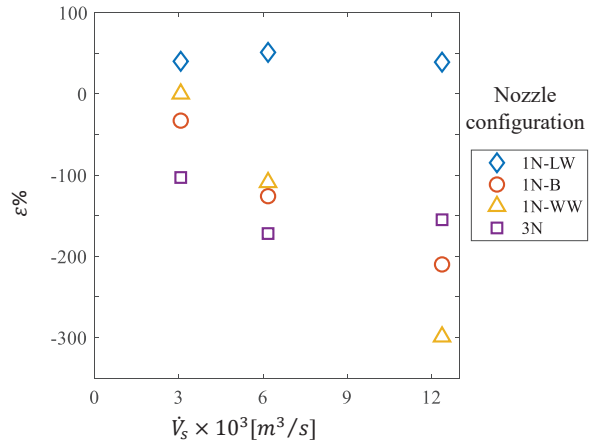

Figure 7- The effectiveness (ε%) of different air suction configurations as a function of the suction flowrate from each nozzle ($\dot{V}_s = 3 \times 10^{-3}, 6 \times 10^{-3}$ and $12\times 10^{-3}\ m^3/s$) at $1/Ri = 43.6$, for $\theta = 45°$, $\alpha = 45°$, T_{cav}=300℃.

Figure 8 presents the effectiveness of a single air suction nozzle configured as 1N-LW, for a cavity at tilt and yaw angles of 45° for 1/Ri = 4.8, 19.4 and 43.6 and T_{cav} = 300℃. It is apparent from the figure that this configuration is effective for the high inverse Richardson number regime in which the convective heat losses are dominated by momentum. However, in the low inverse Richardson number regime, $1/Ri = 4.8$, the effectiveness becomes negative, indicating an increase in the convective heat losses compared with the no air suction case. That is, the use of side nozzles for suction has an adverse impact where buoyancy forces dominate and result in increased egress of hot gases from the cavity to exit the cavity. That is, leeward suction is only effective in the momentum dominated regime.

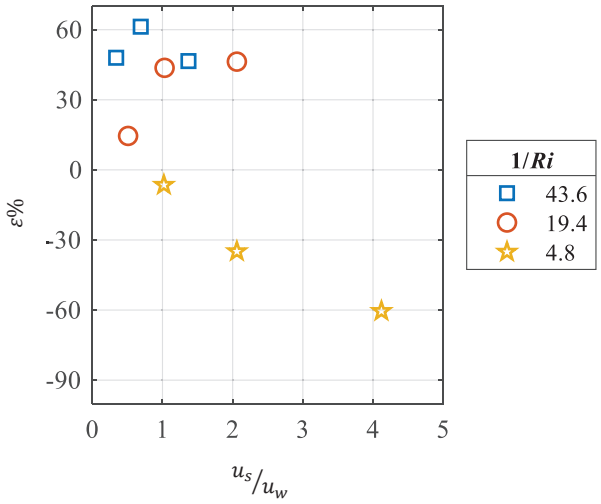

Figure 8- The effectiveness ε (%) of air suction configurations of 1N-LW, as a function of the relative velocity of suction to wind at $1/Ri = 4.8$, 19.4 and 43.6 for $\theta = 45°$, $\alpha = 45°$, T_{cav}=300℃.

3.4 Effect of the Grashof number

Figure 9 presents the effectiveness of one suction nozzle configured as 1N-B, as a function of the momentum flux of suction to wind flow (M_s''/M_w'') for two values of cavity Grashof numbers (Equation 3), for a cavity with $\theta = 45°$ and a head on wind condition. Worth noting is that the Grashof number was changed via the wall temperature of the cavity (from 300℃ to 400℃) only. It can be seen that the effectiveness increases with M_s''/M_w'' for both Grashof numbers. However, the effectiveness of the air suction is lower for the higher Grashof number. For example, suction is only half as effective for 7.06×10^8, compared with 9.62×10^8 for a momentum flux ratio of 1.89. This suggests that more suction is needed with higher temperatures.

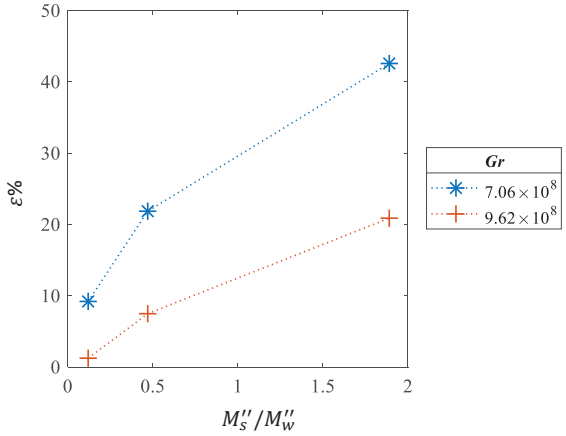

Figure 9- The effectiveness ε (%) of air suction configurations of 1N-B, as a function of the momentum flux of the suction flow to wind flow through the aperture for Gr = 7.06× 10^8 and 9.62 ×10^8 for $\theta = 45°$, $\alpha = 0°$.

3.5 Combination of air suction and air blowing

Figure 10 presents the effectiveness of aerodynamic barriers that comprise a combination of diametrically opposed nozzles to provide both air blowing and air suction (Figure 2.e), as a function of the fractional momentum of suction. Data are presented for θ = 45° and a) $1/Ri$ = 43.6 and b) $1/Ri$ = 0. The figure shows that for the momentum dominated heat transfer regime, $1/Ri$ = 43.6, the average effectiveness increases in proportion to the relative momentum flux of suction to the total momentum flux for all cases. That is, in general, suction is more effective than blowing, although the details are nuanced since the relationships are not exactly linear for each individual data set. This trend is consistent with the results from Figure 3.b. The results also show that a 16% improvement, from 22% to 38%, in the effectiveness of the combined aerodynamic barrier over the suction only was achieved at M_s''= 146 kg/ms^2. However, the combined blowing and suction approach had an improvement of only 5% in maximum effectiveness over the suction only case, from 43% to 48%.

Comparison between the results presented in Figures 3.a and 10.a, shows that the combination of an air suction and air blown curtain does not always lead to higher effectiveness compared with application of air suction only. For instance, the effectiveness of the combined case of $\frac{M_s''}{M_s''+M_b''}$ = 0.65, where M_s''= 181 kg/ms^2 (corresponding to $\dot{V}_s = 12\times10^{-3}$) and M_b''= 96 kg/ms^2, is 16% lower compared with the suction only case of $\dot{V}_s = 12\times10^{-3}$. This suggests

that a combination of air suction and air blowing should be applied for cases with low blown curtain momentum flux to achieve higher effectiveness when compared with cases with suction alone.

The results obtained for the effectiveness of a combination of both air blowing and air suction for the case of no wind, i.e. $1/Ri = 0$, are presented in Figure 10.b. It can be seen that the general trend is opposite from that for $1/Ri = 43.6$. That is, there is a general trend that effectiveness decreases as $\frac{M_s''}{M_s''+M_b''}$ increases. However, a closer examination reveals that each data set has a maximum or particular value of $\frac{M_s''}{M_s''+M_b''}$. For example, the maximum value of ε occurs at $\frac{M_s''}{M_s''+M_b''} = 0.3$ for $M_b''/M_{s-max}'' = 0.13$. Notwithstanding this point, the general collapse of the data shows that the momentum of a blown air curtain has a primary influence on the effectiveness, so that the maximum value occurs with more momentum from the blown than from the suction nozzles. For instance, the effectiveness is 33% for $\frac{M_s''}{M_s''+M_b''} \cong 0.70$ and 5% for $M_b''/M_{s-max}'' = 0.13$ and 0.30, respectively. It is worth noting that the maximum effectiveness of the suction only aerodynamic barrier is 76% (Figure 3.b), which is 15% higher than that of the combined approach of the aerodynamic barrier.

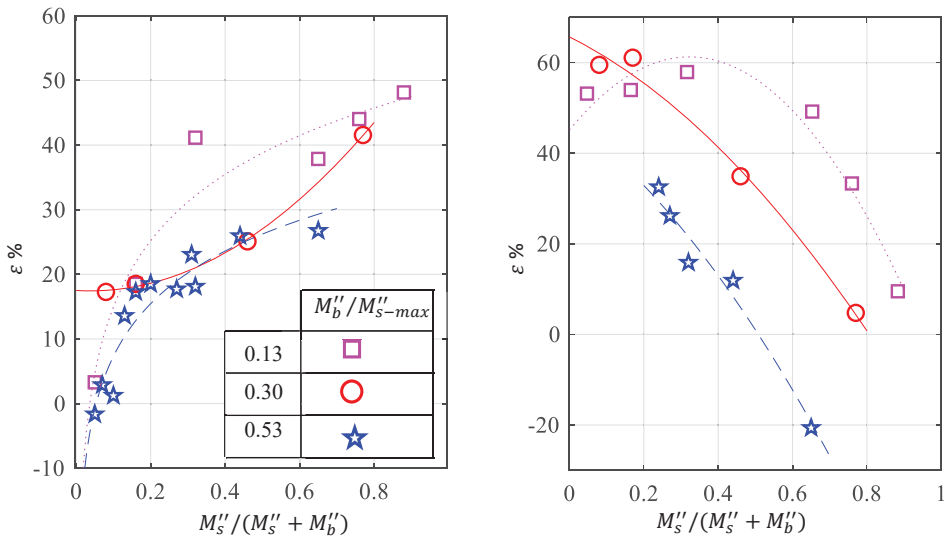

Figure 10- The effectiveness ε (%) of a combination of air suction and air curtain (Figure 2.a), as a function of momentum flux of suction to that of total suction and blowing for different relative blown air curtain momentum fluxes for a) $1/Ri = 43.6$ and b) $1/Ri = 0$. Test conditions: T_{cav}= 300°C, $\theta = 45°$ and $\alpha = 0°$. Note: $M_{s-max}'' =$ 180.56 kg/ms^2

4. Discussion

The results have shown that air suction results in major improvement in effectiveness over those found previously for cases where the cavity tilt angle is 45°, especially at higher inverse Richardson numbers, corresponding to high wind speeds. An effectiveness of 43% was achieved for $\theta = 45°$, $\alpha = 0°$ and $1/Ri = 43.6$, which constitutes an 84% improvement over those

identified in our previous work (Alipourtarzanagh et al., 2020). Nevertheless, for equal fan power consumption with the horizontal cavity orientation at higher wind speeds, air suction performed worse than the air blowing options (Alipourtarzanagh et al., 2020), and even resulted in a negative effectiveness for some cases. The reason for the improved performance of the air suction nozzle for a tilted cavity over the horizontal case is deduced to be due to the influence of buoyancy in generating a 'stagnation zone' in the upper part of the cavity for the tilted case, even in the presence of some wind, which is not the case for the horizontal configuration. Suction helps to maintain this dead zone better than blowing. This was supported by the analysis of the heat losses from the various sections of the cavity interior surface. The importance of maximising the size of the stagnation zone is also consistent with the observation that an optimum flow rate for suction momentum can typically be found, above which effectiveness is reduced. Extracting too much air is deduced to decrease the size of this stagnation zone.

The present work has also reinforced the hypothesis that different nozzle configurations are needed for different wind directions, relative to the cavity. For example, the use of three suction nozzles positioned to the windward, leeward and under-sides of the aperture did not offer any improvement over the use of a single suction nozzle positioned below the aperture for the case of head-on wind and a tilted cavity. However, all three nozzles are important for winds with a sideward component for which the suction nozzle on the opposite side from the wind direction yields the best performance. The need to optimise the use of the nozzles for each wind condition can also be seen from the finding that the activation of the side nozzle increases the convective heat losses by 50% for the sideward wind conditions in the buoyancy dominant regime. Similarly, for the natural convection regime where $1/Ri = 0$, the combination of air suction and blown air curtain reduced the effectiveness compared with the suction only cases, although the combination is beneficial for other cases. Together these observations show the nozzles will need to be controlled dynamically relative to the wind speed and direction, although the development of such a control system is beyond the scope of the present investigation.

The combined effects of blown and suction air for a head-on wind with a high inverse Richardson number and cavity tilt angle of 45° was found to be more effective than sucking alone. It is hypothesised that the downward blown air curtain acts to inhibit hot air from leaving the upper side of the aperture, while the suction nozzles on the bottom side will help redirect external air, to inhibit the induction of cold air from entering the aperture from below. For the preset cases, this additional benefit was modest, with the combined approach increasing the effectiveness of the air curtain by around 5%. Nevertheless, further investigations may identify greater benefits.

5. Conclusions

The effectiveness of configurable aerodynamic barriers to offer potential for adaptive control to reduce convective heat losses from a cylindrical solar cavity receiver has been measured experimentally. The measurements show that it is necessary to switch between nozzles oriented in different directions to accommodate the different wind directions, which implies that an adaptive aerodynamic strategy will be needed to achieve the highest thermal efficiency.

The following specific conclusions can be drawn:

- **For a head-on wind:**
  - For a cavity receiver tilted downward at 45°, the most effective nozzle configuration identified for either a head-on wind or no wind is one suction nozzle positioned below the aperture. This yielded an effectiveness of 83% and 43% for the buoyancy and momentum dominated regimes, respectively. The application of air suction from three sides of the aperture (both lateral and one lower sides) significantly increases the convective heat losses.
  - For a horizontal cavity receiver, the trends of variation of effectiveness with nozzle configuration are similar to 45°, although the details are different.
  - For a cavity receiver tilted downward at 45°, the combination of a blowing and suction air curtain with a variety of the fractional momentum flux of suction for $1/Ri$ = 43.6 showed a 5% improvement in effectiveness compared with a suction only approach. However, for a no wind condition, suction only was found to have higher effectiveness over the combined approach.
  - For a cavity receiver tilted downward at 45°, the effectiveness improves with the inverse Richardson number, either by increasing the wind speed or decreasing the temperature of the cavity, so that for $1/Ri$ = 43.6 a maximum effectiveness of 43% is achieved.

  - For a horizontal cavity receiver and tilted downward at 15°, 30° and 45°, the effectiveness for a momentum dominated heat transfer regime increases with the suction flowrate. However, for a no wind condition, lower extraction is needed to prevent suction of cavity air.

- **For a cross wind:**
  - For a cavity receiver tilted downward at 45°, the most effective nozzle configuration identified for high inverse Richardson numbers is one suction nozzle in the leeward position (i.e. directed across the aperture toward the wind). An effectiveness of 60% has been measured for this case.
  - For a low inverse Richardson number, the side nozzle configuration increases the convective heat losses by more than 50%.
  - The available evidence suggests that these trends will apply for other inclination angles; however, more work is needed to confirm and optimise these cases.

Acknowledgments

The authors would like to acknowledge the financial support of ARENA (grant 2015/RND054), the Australian Research Council (grant LP110200060) and the SA Premier's Science and Research Fund (grant **2007/1436)**. Miss Elham Alipour would like to sincerely thank Mr Darren Faulkner, Thebarton laboratory technician, for his assistance during the experimental campaign.

References:

Direct absorption receivers. https://www.dlr.de/sf/en/desktopdefault.aspx/tabid-10695/18601_read-43763/.

Power Tower Projects-NREL. https://solarpaces.nrel.gov/by-technology/power-tower. 2020).

Alipourtarzanagh, E., Chinnici, A., Nathan, G.J., Dally, B.B., 2019. Experimental Investigation on the Influence of an Air Curtain on the Convective Heat Losses from Solar Cavity Receivers under Windy Condition. SolarPaces 2019.

Alipourtarzanagh, E., Chinnici, A., Nathan, G.J., Dally, B.B., 2020. Experimental insights into the mechanism of heat losses from a cylindrical solar cavity receiver equipped with an air curtain. Solar Energy 201, 314-322.

Alipourtarzanagh, E., Chinnici, A., Nathan, G.J., Dally, B.B., 2020. Impact of Flow Blowing and Suction strategies on the establishment of an aerodynamic barrier for solar cavity receivers. Applied Thermal Engineering, 115841.

Bellan, S., Kodama, T., Matsubara, K., Gokon, N., Cho, H.S., Inoue, K., 2019. Heat transfer and particulate flow analysis of a 30 kW directly irradiated solar fluidized bed reactor for thermochemical cycling. Chemical Engineering Science 203, 511-525.

Breeze, P., 2016. Chapter 5 - Solar Towers, in: Breeze, P. (Ed.) Solar Power Generation. Academic Press, pp. 35-40.

Chang, H., Duan, C., Wen, K., Liu, Y., Xiang, C., Wan, Z., He, S., Jing, C., Shu, S., 2015. Modeling study on the thermal performance of a modified cavity receiver with glass window and secondary reflector. Energy Conversion and Management 106, 1362-1369.

Clausing, A.M., 1981. An analysis of convective losses from cavity solar central receivers. Solar Energy 27(4), 295-300.

Clausing, A.M., 1983. Convective Losses From Cavity Solar Receivers—Comparisons Between Analytical Predictions and Experimental Results. Journal of Solar Energy Engineering 105(1), 29-33.

Cui, F., He, Y., Cheng, Z., Li, Y., 2013. Study on combined heat loss of a dish receiver with quartz glass cover. Applied Energy 112, 690-696.

Fang, J., Tu, N., Torres, J.F., Wei, J., Pye, J.D., 2019. Numerical investigation of the natural convective heat loss of a solar central cavity receiver with air curtain. Applied Thermal Engineering 152, 147-159.

Flesch, R., Grobbel, J., Stadler, H., Uhlig, R., Hoffschmidt, B., 2016. Reducing the convective losses of cavity receivers. 1734, 030014.

Hassan, A.H.A., 2016. Solar tower power plant optimization: a review.

Hoffschmidt, B., Alexopoulos, S., Rau, C., Sattler, J., Anthrakidis, A., Boura, C., O'Connor, B., Hilger, P., 2012. 3.18 - Concentrating Solar Power, in: Sayigh, A. (Ed.) Comprehensive Renewable Energy. Elsevier, Oxford, pp. 595-636.

Hu, T., Jia, P., Wang, Y., Hao, Y., 2017. Numerical simulation on convective thermal loss of a cavity receiver in a solar tower power plant. Solar Energy 150, 202-211.

Huhn, R., 2006. Beitrag zur thermodynamischen Analyse und Bewertung von Wasserwärmespeichern in Energieumwandlungsketten, Faculty of Mechanical Engineering. Technical University of Dresden.

Jilte, R.D., Kedare, S.B., Nayak, J.K., 2014. Investigation on Convective Heat Losses from Solar Cavities under Wind Conditions. Energy Procedia 57, 437-446.

LaNasa, P.J., Upp, E.L., 2014. 2 - Basic Flow Measurement Laws, in: LaNasa, P.J., Upp, E.L. (Eds.), Fluid Flow Measurement (Third Edition). Butterworth-Heinemann, Oxford, pp. 19-29.

Lee, K.L., Chinnici, A., Jafarian, M., Arjomandi, M., Dally, B., Nathan, G., 2018. Experimental investigation of the effects of wind speed and yaw angle on heat losses from a heated cavity. Solar Energy 165, 178-188.

Lee, K.L., Chinnici, A., Jafarian, M., Arjomandi, M., Dally, B., Nathan, G., 2019a. The influence of wall temperature distribution on the mixed convective losses from a heated cavity. Applied Thermal Engineering 155, 157-165.

Lee, K.L., Chinnici, A., Jafarian, M., Arjomandi, M., Dally, B., Nathan, G., 2019b. The influence of wind speed, aperture ratio and tilt angle on the heat losses from a finely controlled heated cavity for a solar receiver. Renewable Energy 143, 1544-1553.

Lee, K.L., Jafarian, M., Ghanadi, F., Arjomandi, M., Nathan, G.J., 2017. An investigation into the effect of aspect ratio on the heat loss from a solar cavity receiver. Solar Energy 149, 20-31.

Leporini, M., Corvaro, F., Marchetti, B., Polonara, F., Benucci, M., 2018. Experimental and numerical investigation of natural convection in tilted square cavity filled with air. Experimental Thermal and Fluid Science 99, 572-583.

Lipiński, W., Abbasi-Shavazi, E., Chen, J., Coventry, J., Hangi, M., Iyer, S., Kumar, A., Li, L., Li, S., Pye, J., Torres, J.F., Wang, B., Wang, Y., Wheeler, V.M., 2020. Progress in heat transfer research for high-temperature solar thermal applications. Applied Thermal Engineering, 116137.

Ma, R.Y., 1993. Wind Effects on Convective Heat Loss from a Cavity Receiver for a Parabolic Concentrating Solar Collector, Sandia National Laboratories.

McIntash, A., Hughes, G., Pye, J., 2014. Use of an Air Curtain to Reduce Heat Loss from an Inclined Open-Ended Cavity, 19th Australasian Fluid Mechanics Conference. Melbourne, Australia.

Okoroigwe, E., Madhlopa, A., 2016. An integrated combined cycle system driven by a solar tower: A review. Renewable and Sustainable Energy Reviews 57, 337-350.

Pitz-Paal, R., 2014. Chapter 19 - Solar Energy – Concentrating Solar Power, in: Letcher, T.M. (Ed.) Future Energy (Second Edition). Elsevier, Boston, pp. 405-431.

Prakash, M., Kedare, S.B., Nayak, J.K., 2010. Determination of stagnation and convective zones in a solar cavity receiver. International Journal of Thermal Sciences 49(4), 680-691.

Pujol-Nadal, R., Martínez-Moll, V., Sallaberry, F., Moià-Pol, A., 2015. Optical and thermal characterization of a variable geometry concentrator using ray-tracing tools and experimental data. Applied Energy 155, 110-119.

Rodriguez-Sanchez, M.R., Sanchez-Gonzalez, A., Marugan-Cruz, C., Santana, D., 2015. Flow patterns of external solar receivers. Solar Energy 122, 940-953.

Shah, N.A., Animasaun, I.L., Ibraheem, R.O., Babatunde, H.A., Sandeep, N., Pop, I., 2018. Scrutinization of the effects of Grashof number on the flow of different fluids driven by convection over various surfaces. Journal of Molecular Liquids 249, 980-990.

Siebers, D.L., Kraabel, J.S., 1984. Estimating convective energy losses from solar central receivers. Sandia National Labs., Livermore, CA (USA), United States.

Taussig, R.T., 1984. Aerowindows for central solar receivers. American Society of Mechanical Engineers, Winter Annual Meeting, New Orleans, LA, , 12.

Vant-Hull, L.L., 2012. 8 - Central tower concentrating solar power (CSP) systems, Concentrating Solar Power Technology. Woodhead Publishing, pp. 240-283.

Wu, S.-Y., Shen, Z.-G., Xiao, L., Li, D.-L., 2015. Experimental study on combined convective heat loss of a fully open cylindrical cavity under wind conditions. International Journal of Heat and Mass Transfer 83, 509-521.

Yang, S., Wang, J., Lund, P.D., Wang, S., Jiang, C., 2018. Reducing convective heat losses in solar dish cavity receivers through a modified air-curtain system. Solar Energy 166, 50-58.

Zhang, J.J., Pye, J.D., Hughes, G.O., 2015a. Active Air Flow Control to Reduce Cavity Receiver Heat Loss. (56840), V001T005A023.

Zhang, J.J., Pye, J.D., Hughes, G.O., 2015b. Active Air Flow Control to Reduce Cavity Receiver Heat Loss, 9th International Conference on Energy Sustainability collocated with the ASME 2015 Power Conference. San Diego, California, USA, p. V001T005A023.

Chapter 6-

The coupling between the internal and external flows through a hybridized solar cavity receiver under isothermal conditions

Statement of Authorship

Title of Paper	The coupling between the internal and external flows through a hybridized solar cavity receiver under isothermal conditions
Publication Status	☑ Published ☐ Accepted for Publication ☐ Submitted for Publication ☐ Unpublished and Unsubmitted work written in manuscript style
Publication Details	Experimental Thermal and Fluid Science Volume 113, 1 May 2020, 110028

Principal Author

Name of Principal Author (Candidate)	Elham Alipourtarzanagh		
Contribution to the Paper	Performed experiments, acquisition of data, interpret data, writing of the manuscript and acted as the corresponding author.		
Overall percentage (%)	65%		
Certification:	This paper reports on original research I conducted during the period of my Higher Degree by Research candidature and is not subject to any obligations or contractual agreements with a third party that would constrain its inclusion in this thesis. I am the primary author of this paper.		
Signature		Date	06/10/2020

Co-Author Contributions

By signing the Statement of Authorship, each author certifies that:

i. the candidate's stated contribution to the publication is accurate (as detailed above);

ii. permission is granted for the candidate in include the publication in the thesis; and

iii. the sum of all co-author contributions is equal to 100% less the candidate's stated contribution.

Name of Co-Author	Alfonso Chinnici		
Contribution to the Paper	Conceptualization, supervised the research and contributed in academic discussion		
Signature		Date	7/10/2020

Name of Co-Author	Zhao Feng Tian		
Contribution to the Paper	Conceptualization, supervised the research and contributed in academic discussion		
Signature		Date	08/10/2020

Name of Co-Author	Graham J Nathan		
Contribution to the Paper	Conceptualization, methodology development, review and editing manuscript, supervision, project administration and funding acquisition		
Signature		Date	8/10/2020

Name of Co-Author	Bassam Dally		
Contribution to the Paper	Conceptualization, methodology development, review and editing manuscript, supervision, project administration and funding acquisition		
Signature		Date	6-10-2020

Experimental Thermal and Fluid Science 113 (2020) 110028

Contents lists available at ScienceDirect

Experimental Thermal and Fluid Science

journal homepage: www.elsevier.com/locate/etfs

The coupling between the internal and external flows through a hybridized solar cavity receiver under isothermal conditions

Elham Alipourtarzanagh*, Alfonso Chinnici, Zhao Feng Tian, Graham J. Nathan, Bassam B. Dally

Centre for Energy Technology, School of Mechanical Engineering, the University of Adelaide, Adelaide, South Australia 5005, Australia

A B S T R A C T

An experimental investigation of the interaction between the internal and external flows through a simplified laboratory-scale hybrid solar cavity receiver is presented. The experiments were conducted under isothermal conditions using the Particle Image Velocimetry (PIV) technique. The device comprises a cylindrical chamber (70 mm inner diameter and 225 mm long) fitted with four jets (3.35 mm inner diameter) simulating fuel and air supply and an aperture. Four different configurations have been tested, with two different jet inclination angles (25° and 50°) and with two different jet azimuthal angles (0° and 5°). Water was used as the working fluid and the models were placed in a water channel with variable speed to allow the influence of an external flow to be simulated. The results show that the flow behaviour within the cavity is strongly dependent on the jets' configuration, the aperture ratio and tilt angle. A significant flow of external fluid was entrained through the aperture for all of configurations, with an additional 22% and 42% to the internal flow for the ($\alpha_j = 25°$, $\gamma_j = 0°$) case with zero and 0.24 m/s exteral velocity, respectively. The effect of openning the apreture on jet decay, turbulence intensity and recirculation pattern was also recorded. It is found that while opening the aperture and introducing an external flow have little qualitative influence on the flow pattern and jet decay, the turbulence intensity in the proximity of the aperture changes considerably. The need to manage the complex interactions between the external and internal flows through the cavity receiver is defined.

1. Introduction

Solar energy is playing a growing role in displacing the fossil-based energy systems that have powered human society historically. A major obstacle for wider implementation of all solar energy technologies is the intermittent nature of the resource, resulting in the need for energy storage. The development of photovoltaic cells for electricity generation and their successful commercialisation have resulted in a large number of installations, in more than 30 countries, exceeding 500 GW [1]. The cumulative installation of Concentrating Solar Thermal energy (CST), on the other hand, is presently slightly above 5 GW [2]. CST installations, however, are expected to increase rapidly, in the near future, due to the relatively low cost of storing thermal energy at a relatively large scale, to that of storing electricity [3]. Furthermore, in generating heat directly, CST has potential application in a wide range of industrial processes that require mostly thermal energy, which contribute more than a third of the CO_2 emissions worldwide [4]. There is therefore a need to support the further development of CST technology.

A concerted effort is being spent to increase the viability of Concentrating Solar Thermal, CST, technology as a replacement of fossil fuel powered combustion systems and to increase its share of renewable energy generation. These efforts are mostly directed towards reducing the cost associated with solar radiation concentration [5] and ensuring dispatchable and firm supply. The two major approaches to increase dispatchability are thermal energy storage systems and hybridisation of solar systems with other renewable resources or conventional combustion [6]. The novel hybrid solar receiver and combustor (HSRC) technology combines a solar cavity receiver with a combustor in a single device [7–9]. As with other combustion hybrids, the HSRC guarantees firm supply, but it also brings other advantages of reduced infrastructure cost, reduced start-up losses and the potential to reduce thermal cycling of the receiver due to short-term fluctuations of the solar resource [10]. The HSRC can be operated under any of three different modes: solar only, combustion only and mixed mode [10]. Fig. 1 presents the main features of the HSRC, schematically. When the HSRC is operated in the mixed-mode, energy is introduced into the chamber both through the open aperture, via the concentrated solar radiation, and through the burners via the fuel and air combustion. This mode is used when the solar resource is relatively low, for example due to the passage of cloud [10]. The momentum of the reactants' jets within the chamber control the flow patterns and resulting pressure gradients within the cavity, which are modified further by the combustion process. These pressure gradients have the potential to increase either the egress of hot gaseous products from the cavity, through the aperture, or the induction of cold air through the aperture. Both of these scenarios are undesirable because they will reduce the thermal efficiency of the device. Furthermore, since the cavity is installed on top of a tower, where wind speeds are greater than at ground level, convective

* Corresponding author.
E-mail address: elham.alipour@adelaide.edu.au (E. Alipourtarzanagh).

https://doi.org/10.1016/j.expthermflusci.2019.110028
Received 7 June 2019; Received in revised form 22 November 2019; Accepted 19 December 2019
Available online 30 December 2019
0894-1777/

Nomenclature

A_{ap}	aperture area [m^2]
D_{ap}	diameter of the aperture [m]
D_c	diameter of the cavity [m]
D_j	jet diameter [m]
H	height of the region of interest [m]
L_c	length of the cavity [m]
L_j	length of the jet supply pipe [m]
$\dot{m}_{ap}$	mass flow rate through the aperture [$kg{\cdot}s^{-1}$]
$\dot{m}_{red}$	reduction in mass flow rate through the aperture [$kg{\cdot}s^{-1}$]
P_{ap}	changes in the pressure at the aperture [Pa]
P_i	jet impingement point [m]
P_{min}	point of minimum axial velocity along the centre line of the cavity [m]
P_{outlet}	fluid pressure at the cavity outlet [Pa]
P_s	stagnation point [m]
r	radial distance from centre of the cavity [m]
R_p	pressure ratio
Re	Reynolds Number based on jet diameter
V_{ap}	The velocity of the flow through the aperture [$m{\cdot}s^{-1}$]
V_j	the nozzle bulk mean exit velocity [$m{\cdot}s^{-1}$]
V_s	velocity of free stream [$m{\cdot}s^{-1}$]
V_x	axial velocity [$m{\cdot}s^{-1}$]
V_y	radial velocity [$m{\cdot}s^{-1}$]
W	width of the region of interest [m]
W_{out}	width of outlet gap [m]
x	axial distance from the aperture [m]

Greek symbols

α_j	Inclination angle of the jet [degrees]
γ_j	Azimuth angle of the jet [degrees]
θ	Tilt angle of the cavity [degrees]
μ	Dynamic viscosity [$N{\cdot}s{\cdot}m^{-2}$]
ρ	density [$kg{\cdot}m^{-3}$]

Abbreviation

AR	Aperture Ratio (ratio of the diameter of the aperture to the diameter of the cavity)
CIJR	Confined Impinging Jet Reactor
CRZ	Central Recirculation Zone
CST	Concentrated Solar Thermal
ERZ	External Recirculation Zone
FFT	Fast Fourier Transform
HSRC	Hybrid Solar Receiver and Combustor
MILD	Moderate or Intense Low-oxygen Dilution
sCMOS	scientific Complementary Metal-Oxide Semiconductor

losses from the ingress of cold air to the cavity cannot be neglected. The interaction of the flow dynamics inside the cavity with those induced by wind outside it is essential to design receivers that are more efficient. The way to control this interaction will depend on the back pressure from the exhaust outlet, the reactants and products from combustion and wind speed and direction. As a result, more understanding is needed of the flow characteristics within the hybrid cavity for the case of an open aperture, particularly in the vicinity of the aperture plane in order to minimize the convection losses.

Only a few studies have reported on the flow-field associated with a HSRC. In an experimental study, Chinnici *et al.* demonstrated the successful operation of a laboratory-scale HSRC at ~20 kW capacity. Their configuration used nozzles with an inclination angle of 30° and an azimuth angle of 5°. This configuration provided effective circulation needed to establish the Moderate or Intense Low-oxygen Dilution, MILD, combustion regime within the cavity. It also provided sufficient convective heat transfer to the heat exchangers in the cavity. Their investigation estimated an air entrainment of 12%, from the ambient surrounds, in the mixed mode of operation for an aperture ratio of 0.33, using this jets' configuration [12]. However, no previous investigation has measured the air entrainment for larger aperture ratios, providing a need to also investigate such configurations. Also neglected, was the influence of the speed and direction of external wind, noting that the direction has two components owing to the tilt of a solar cavity receiver relative to the horizontal direction. Hence, there is also a need to investigate these influences.

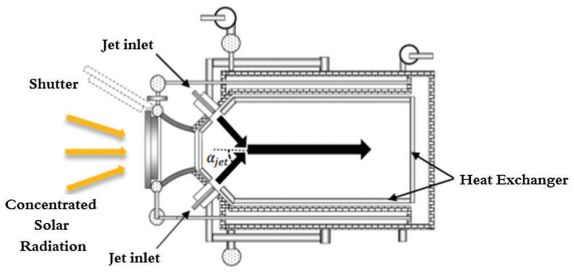

Fig. 1. Schematic diagram of the Hybrid Solar Receiver Combustor [11].

The inclination angle of jets to the chamber axis has been found to have a first order influence on the behaviour of both reacting and non-reacting flows within an enclosed volume [13–16]. It is found that jet deflection enhances the mixing, improves heat transfer and reduces pollutant emissions. More pertinent to the present study, Long *et al.* [17] also found that the flow pattern can also affect the pressure gradient across the aperture plane of a solar cavity receiver. The same authors conducted a series of experimental and numerical studies, and investigated the flow within a cylindrical cavity, similar to the HSRC configuration, equipped with four jets and using water as the working fluid [17–21]. These studies investigated the influence of the number of the jets, their inclination angle (α_j) and their azimuthal angles on the flow pattern inside the cavity. All studies where carried out with a throat but a closed aperture. Their numerical study identified four flow regimes within the cavity, namely: a strong inward annular recirculation regime for $0° \leq \alpha_j < 10°$, an outward recirculation dominant flow regime for $10° \leq \alpha_j < 40°$, an outward recirculation with backflow regime for $40° \leq \alpha_j < 60°$ and a jet impinging flow regime for $60° \leq \alpha_j < 90°$. It revealed that the mean flow field within a cavity depends strongly on the inclination angle and the number of jets [17]. In addition, the extent of the backflow inside the cavity and through the throat also depends on the inclination angle of the jets [19]. In another study, Long *et al.* considered rotationally symmetric jets within a cylindrical chamber. They showed that the jet azimuthal angle also has a significant influence on the flow pattern inside the cavity [20]. They also investigated the effect of the aspect ratio of the cavity (L_c/D_c) on the flow regimes within the chamber. They found that by changing the back pressure through the variation of the aspect ratio, three different regimes are observed in the cavity chamber [21]. These studies are important as they discovered the physics of fluid such as velocity decay, turbulence intensity and recirculation zone related to the stability and control of the combustion process. However, no previous work has investigated the effect of the external flow conditions of the flow characteristics inside a cavity when the aperture is opened, a condition of direct relevance to the mixed mode of operation.

The interaction between external and internal flows in a solar

receiver will generate convective heat losses, which are undesirable. Considerable experimental and numerical studies have been conducted to investigate the main parameters affecting the convective heat losses from standard cavity receivers, which do not incorporate any internal jets [22–24]. These parameters include the geometric characteristics of the cavity [25] and external flow conditions including wind speed and wind direction [26,27]. In the studies devoted to the investigation of the interaction of the flows inside and outside the solar cavity receivers, the effect of buoyancy and temperature distribution is a critical factor. However, buoyancy is only of second order importance in HSRCs, where confined reacting flows driven by jet mixing and where inertia typically dominates over buoyancy [28]. For such flows, the interaction between the internal and external flows in a confined cavity can be reliably investigated and implied using isothermal studies.

As described above, although some studies have been conducted to investigate flow behaviour in either conventional cavities under windy condition, or a hybrid solar-combustion cavity with closed aperture, no studies are found which examine the flow behaviour of a hybrid solar receiver with both internal jets and open aperture. Hence, the present experimental study is focussed on both the flow behaviour within and the interaction between internal and external flows, in a simplified laboratory-scale hybrid solar cavity receiver under different operation conditions. The main aim is to investigate the effect of an external flow on the resulting flow pattern of multiple jets inside a confined cylindrical cavity of relevance to HSRC. In particular, the study aims to better understand the influence on size and location of recirculation zones, velocity decay, mass exchange and turbulence intensity as they all have influence on the established combustion regimes inside and convective cooling from the cavity. Therefore, in this study the effects of jet configuration, aperture ratio, external flow velocity and cavity yaw angle are reported and analysed.

2. Methodology

An experimental campaign was conducted to measure the flow field within a jet-driven cavity receiver, and in the near external field using particle imaging velocimetry (PIV) technique. The investigation is similar to that of Long *et al.* except that the aperture is open to the external environment, while their model was sealed [17–21]. The reference configuration for the present investigation, notably the choice of inclination and azimuth angles of the jets, was selected to match the case for which good performance was measured in a laboratory-scale prototype [12]. The range of variables in the inclination and azimuthal angles was chosen to represent the key regimes identified from previous studies. The devices were built from acrylic, which has a similar refractive index to water resulting in low optical distortion for measurements of the internal flows.

2.1. Experimental setup

The key geometric features and a photograph of the experimental configuration are presented in Fig. 2 and reported in Table 1. The device was made of inter-changeable components to allow all key parameters to be varied systematically. The cylindrical model was 74 mm in internal diameter and 225 mm in length, with an annular gap of 3 mm as the outlet for the 'exhaust'. The back pressure to the flows within the

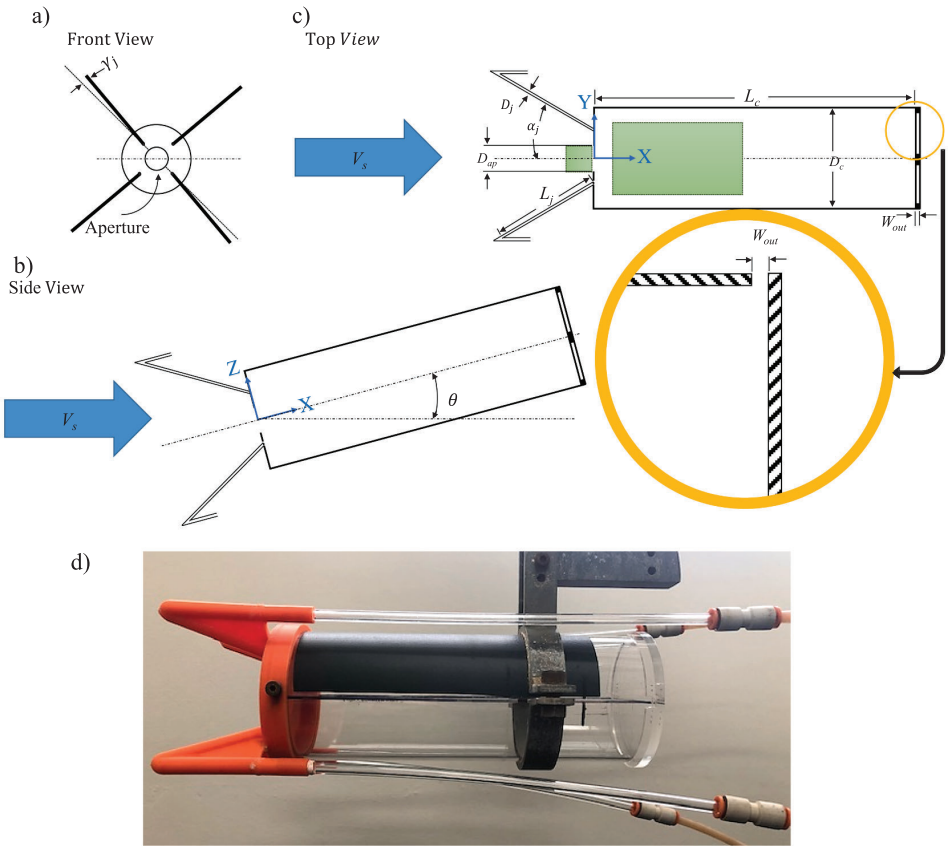

Fig. 2. A schematic diagram and photograph of the device being measured, showing key geometric features and notation. Here the camera field of view is highlighted with green. (For interpretation of the references to color in this figure legend, the reader is referred to the web version of this article.)

Table 1
Values of the geometric parameters of the experimental configurations.

Geometric Parameter	Value
L_c	225 mm
D_c	74 mm
L_j	150 mm
W_{out}	3 mm
θ	0°, 10°, 30°, 45°
D_j	3.35 mm
D_{ap}	18.5 mm, 24.6 mm, 37 mm
α_j	25°,50°
γ_j	0°, 5°

cavity could be changed by either changing the length of the cavity or the outlet gap. However, these dimensions were fixed for the present study. The aperture face consists of a disk with an interchangeable aperture of different diameters of 18.5 mm to 24.6 mm and 37 mm resulting in a D_{ap}/D_c ratio of 0.25, 0.33 and 0.50. In addition, four equi-spaced nozzles, each of 3.35 mm inner diameter were chosen to simulate the reactantas flow into the chamber. The diameter of the aperture was varied for the case with an inclination angle of $\alpha_j = 25^\circ$ and an azimuth angle of $\gamma_j = 0^\circ$. This allowed the investigation of aperture size ratio on the flow behaviour, while keeping all other parameters the same (see Table 2).

Two jet inclination angles (α_j) 25° and 50°, were selected based on previous work [12,19]. In addition, two azimuth nozzle angles were selected, $\gamma_j = 0^\circ$ and 5° to investigate in the effect of a swirling flow within the cavity [29].

To investigate the effect of the cavity tilt angle relative to the cross-flow direction on the mass flow rate through the aperture, the cavity was held at different tilt angles, as shown in part (b) of Fig. 2. Tests were conducted for the case with an inclination angle of $\alpha_j = 25^\circ$ and an azimuthal angle of $\gamma_j = 0^\circ$, while the tilt angles of the cavity were changed from $\theta = 0^\circ$, to 10°, 30° and 45°. Noteworthy, due to the non-buoyancy condition of the experiment, only the angle relative to the flow matters. Hence, this angle could be both yaw angle and tilt angle of the cavity.

The tests were conducted in a recirculating water channel at the University of Adelaide, which can generate free stream velocity of up to 0.3 m/s. The water tunnel test section is made of acrylic, with a length of 2.0 m and a cross-section of 0.5 m × 0.5 m. The experimental device is submerged in water and is supported using a low blockage frame.

The experimental models were scaled-down from a full-scale concept design using well-established similarity principles [30]. In this case, it was based on constant velocity ratio between the jet and external fluids, together with maintaining a turbulent Reynolds number in the internal jets. A common range of the jet velocity exit for different fuels including methane, propane and ethylene is 100 m/s [31]. Therefore, to satisfy the kinematic similarity in the jet exit and the aperture, the velocity ratio of the flow in the nozzle exit and aperture must be the same in the model and the prototype. Further, to mimic wind speeds of 9, 6, 3 and 0 m/s, for the jet exit velocity of 2.8 m/s in experiments corresponding to a jet Reynolds number of 10500, the velocity of the water channel was set to 0.24, 0.16, 0.08 and 0.0 m/s, respectively.

The blockage ratio of the test rig to the test section of the water channel was 7.2%, which is small enough to prevent any significant influence from the walls of the water channels. The water supplied to the jets was pumped from the reservoir of the water channel with a horizontal multi-stage pump (Calpeda MXHM 202E) close coupled to two glass tube flowmeters (ABB ¾'-21-G-10/83) with a float (3/4 GUSVT-511). The outlet of each flow meter was connected to a distribution manifold system that divided the flow equally into two flows. The flow was provided to the jets via four flexible tubes of equal length. The volume flow rate to all four jets was set to 1.4 Lt/min and, as noted above, resulting in a jet inlet velocity of 2.8 m/s and a Reynolds number $\left(Re = \frac{\rho V_j D_j}{\mu}\right)$ of 10,500. The flow rate to each jet was measured to ensure that the flow rate through each jet was equal to within ± 1%. The length of perfectly straight pipes was set to 150 mm (> 40 diameters) and each was connected to a gently curved flexible hose more than 100 diameter, which is sufficient to closely approach a fully developed pipe flow [32].

2.2. PIV system and image processing

The main components of the PIV system are a laser source, a camera and a pulse generator, as illustrated schematically in Fig. 3. A laser sheet of ~2 mm thickness generated from the second harmonic of a double-pulsed Nd: YAG laser source at 532 nm wavelength was aligned horizontally with the mid-plane of the cylinder. The camera field of view, as highlighted with green color in Fig. 2, was 50 mm × 80 mm (inside the cavity) and 30 mm × 30 mm (outside the cavity) to provide a spatial resolution of 0.05 mm × 0.05 mm for each pixel. For the experimental case of $\alpha_j = 25^\circ$, $\gamma_j = 5^\circ$ the measured area was reduced to 40 mm × 80 mm due to the restricted view caused by the supply pipes. Due to the restrictions caused by the material used in the aperture face, no visualisation of the internal flow was possible in the region closer than 15 mm from the aperture plane. However, the mass flow rate through the aperture was determined by measurements immediately upstream from the aperture (0.05 mm).

The flow was seeded with Dantec polyamide seeding particles, having a mean diameter of 50 μm, the density of which corresponded to 1.03 g/cm^3. The seeding particles were added to the water in the reservoir of the water channel at the start of the test campaign. This was sufficient to provide good seeding for the region of interest, given that detailed measurement of the jet exit plane could be avoided by selection of a fully developed pipe flow as the inlet condition.

The movement of the tracer particles was captured and recorded using a scientific Complementary Metal-Oxide Semiconductor (sCMOS) camera (Andor Zyla 5.5) with 5.5-megapixel resolution. The camera was positioned right the side of the water channel and captured the Mie scattering from the particles in the flow via a reflection on a mirror underneath the water channel oriented at a 45-degree angle to the viewing plane (as shown in Fig. 3, below). The images were acquired at a rate of 15 Hz for all measurements with a separation time between laser pulses of 4 ms and 0.15 ms for the measurements outside and inside the chamber, respectively. The Andor SOLIS image capturing software was used for image recording through a computer using a pulse generator (Berkeley Nucleonics, Model 565) to synchronize the laser and the camera. For each measurement case, 600 and 250 successive image pairs were captured for internal and external measurements, respectively. The images were processed using PIVlab [33] and a

Table 2
Details of the experimental conditions. Apertures with a diameter of 18.5 mm, 24.6 mm and 37 mm are referred to by the letters, S (for small), M (for medium) and L (for large), in their respective Case Reference names.

Case Ref.	α_j [°]	γ_j [°]	D_{ap} [mm]	θ [°]	Velocity of the water channel, V_s [m.s^{-1}]
C25-0-M-0	25	0	24.6	0	Blocked aperture (B), 0.0, 0.08, 0.16, 0.24
C25-5-M-0	25	5			
C50-0-M-0	50	0			
C50-5-M-0	50	5			
C25-0-S-0	25	0	18.5	0	0.0, 0.08, 0.16, 0.24
C25-0-L-0			37		
C25-0-M-10			24.6	10	
C25-0-M-30				30	
C25-0-M-45				45	

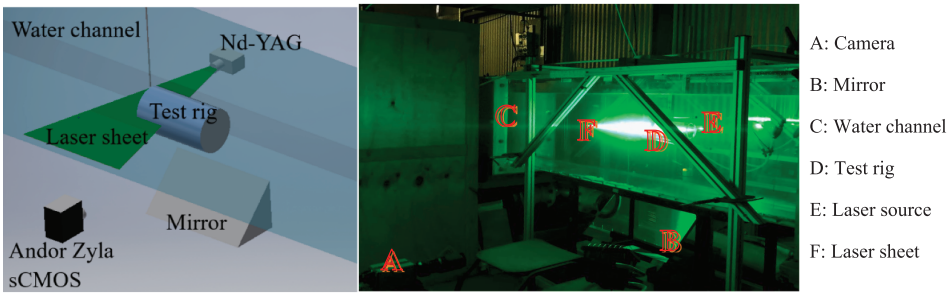

Fig. 3. Schematic diagram and photograph of the PIV setup.

Fast Fourier Transform (FFT) cross-correlation algorithm applied to a 32 × 32 pixel interrogation window with 50% overlap.

The mass flow rate through the aperture was quantified by an integral of the velocity profiles as shown in Eq. (1) [34].

$$\dot{m}_{ap} = \int_{A_{ap}} \rho V_{ap} dA \tag{1}$$

2.3. Uncertainty

The uncertainties of the measurements were estimated from the precision of the instruments and measuring techniques, as well as from the uncertainty in the dimensions of the experimental models. The experimental models were manufactured with a tolerance of ± 0.1 mm linear and ± 0.5° angular. The measurement uncertainty arising from the flowmeters was estimated to be ~1%. The measurement error of the stream velocity of the water channel was found to be 0.8%. The overall uncertainty associated with the PIV measurements were assessed through a systematic study. To find out a sufficient number of image-pairs, in order to achieve a statics independency, a sensitivity study was carried out. A set of 1200 image-pairs of successive images was taken for both internal and external measurements. The results from the internal measurements showed less than 1% difference in central velocity decay when the number of image pairs exceeded 600 pairs. While for the external flow measurements the difference in the velocity profile in the proximity of the aperture was less than 1% for more than 250 image-pairs. Therefore, 600 and 250 successive image pairs were used for internal and external measurements, respectively. The error caused by the inaccuracy of the spatial resolution was determined to be less than 1.25% as a result of using a grid plate with 1 mm × 1 mm for calibration. The spatial particle image processing error was estimated to be around 1/10 of the seed particle diameter [35]. Therefore, the experimental error in velocity measurements caused by the particle size, which is 50 μm, is 5 μm in every laser pulse. The average particle displacement based on the delay time between successive image pairs within the central region of the cavity, where the highest velocity of the flow occurs, is 1.12 mm. Hence, the experimental error in velocity measurements caused by the particle size is 0.4%. The mean particle displacement in each laser pulse is approximately 11–13 pixels which is 0.375 of the interrogation length. The overall uncertainty associated with the spatial correlations and time-averaged measurements is less than 4% [36]. The overall uncertainty of the measured mean velocities for the present study was therefore estimated to be less than ± 5% based on the method of Cox and Baybutt [37].

3. Results and discussion

3.1. Mean flow fields

1. Radial profiles of the normalized mean axial and radial velocity

Figs. 4–7 present the averaged radial profiles of the mean axial (V_x) and radial (V_y) velocities, normalized by the nozzle bulk exit velocity (V_j), at four cross-sections along the centreline of a cylindrical cavity for C25-0-M-0, C25-5-M-0, C50-0-M-0 and C50-5-M-0, respectively. Data are presented at four locations judged to concisely represent the flow, although data for other locations are also available. Each figure presents the two velocity components for the three cases, one for blocked aperture and two for an opened aperture with V_s = 0.0 m/s and V_s = 0.24 m/s. Results from V_s = 0.08 m/s and 0.16 m/s test cases are not shown for brevity. The cross sections are at four axial distances along the cavity in the plane (x, y) as labelled in Fig. 2.

Fig. 4(a) reveals that the axial velocity profile for the blocked aperture case has two peaks at three sections upstream from the jet's impingement point at x/L_c = 0.17, 0.22 and 0.29. Downstream from the point where the jets interact and merge, the axial velocity profile exhibits only one peak at the centreline (r/D_c = 0). This corresponds to x/L_c = 0.39. This feature of a combined jet on the centreline is well known from previous work [18]. From Fig. 4(b) it can be seen that the direction of the radial velocity, V_y, on two sides of the centreline, is reversed, while the magnitudes of the radial velocities at two sides are similar in different sections. Since the values of the axial velocities on two sides of the centreline are the same, this implies the presence of a symmetrical mean flow within the cavity.

From Fig. 4(c) it is clear that the shape of the axial velocity profile for the blocked aperture is similar to that for the opened aperture and V_s = 0.0 m/s. However, at section x/L_c = 0.17 it is clear that the normalized axial velocity, for the case with the external velocity of 0.24 m/s, is 5 times larger than that of the blocked aperture case. By comparing Fig. 4(b) and (d), it is concluded that the external flow has a major effect on the radial velocity profile in the different sections. For instance, at section x/L_c = 0.22, the maximum radial velocity occurs at r/D_c = 0.1, while by opening the aperture, the peak velocity occurs at r/D_c = 0.02. However, the magnitude of the radial profile is small compared with the axial velocity. Hence, the flow patterns, as is shown in more detail below (Fig. 9), do not change significantly with the change of the radial velocity profile.

From Fig. 5(a), corresponding to the non-swirling jet with an inclination angle of 50°, it is clear that the axial velocity profiles feature one peak in the centreline at x/L_c = 0.15. This implies that these measurement planes are downstream from the impingement point. Further downstream from the aperture, at x/L_c = 0.22 and x/L_c = 0.30, the axial velocity profile exhibits one peak with lower velocity magnitude indicating the velocity decay along the centreline of the cavity. While the shape of the profiles are not influenced significantly by the opening or closing of the aperture, or increasing the external velocity, nevertheless the influence on the magnitude of the normalized axial velocity is significant. The magnitude of the axial velocity in the centreline of the cavity, at the point where the combined jet is formed, increases. This indicates that the external 'wind' directed into the cavity strengthens the resulting jet flow in the centre of the cavity.

Fig. 5(b), (d) and (f) indicate that the radial velocity profile changes

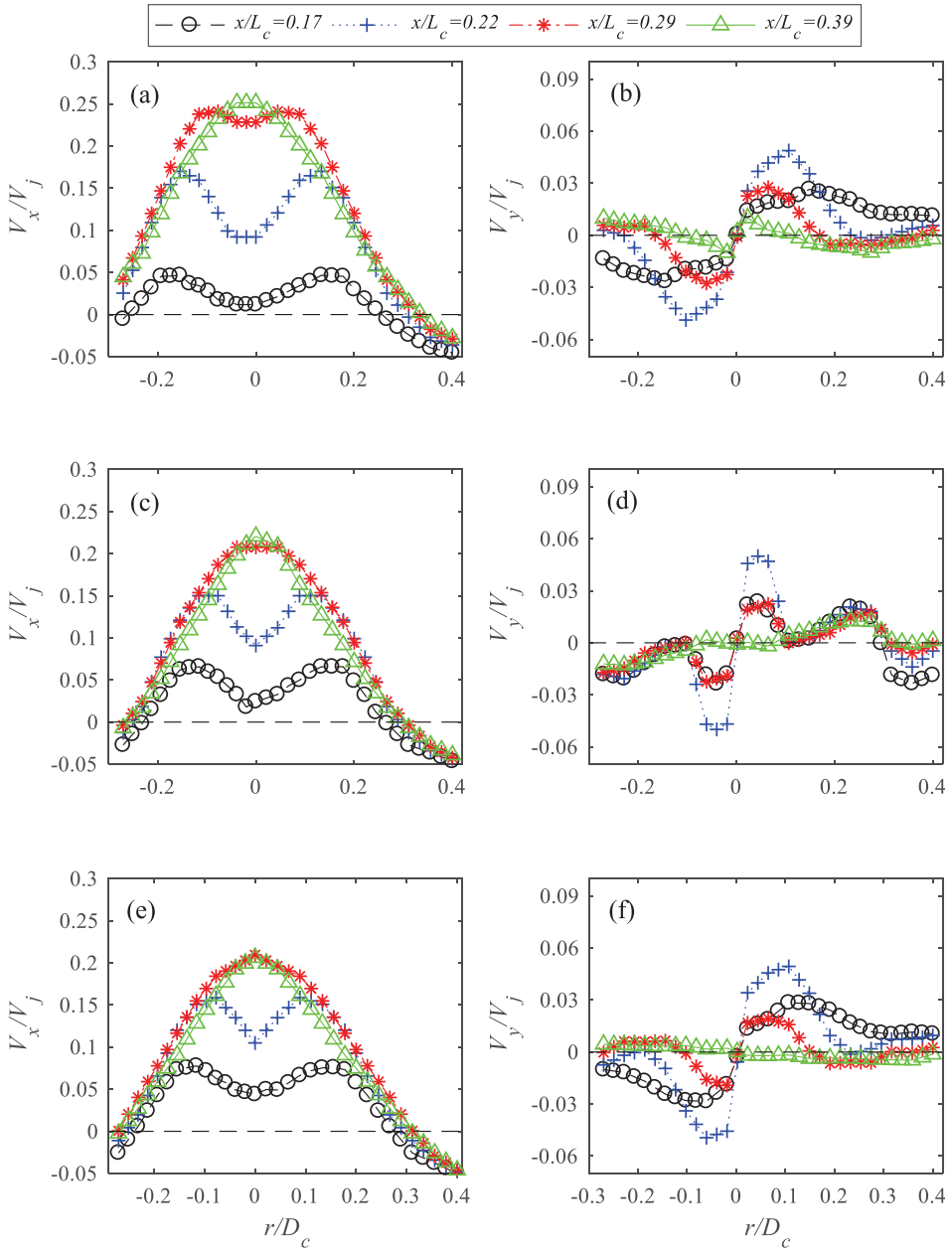

Fig. 4. Radial profiles of the normalized mean axial velocity, V_x/V_j, and normalized mean radial velocity V_y/V_j, at four cross-sections along the centreline of a cylindrical cavity, where $\alpha_j = 25^\circ$ and $\gamma_j = 0^\circ$, for the cases of (a) V_x/V_j, blocked aperture, (b) V_y/V_j blocked aperture, (c) V_x/V_j, opened aperture $V_s = 0.0$ m/s (d) V_y/V_j, opened aperture $V_s = 0.0$ m/s (e) V_x/V_j, opened aperture $V_s = 0.24$ m/s, (f) V_y/V_j, opened aperture $V_s = 0.24$ m/s.

significantly in $|r/D_c| = 0.2$ to 0.3 at $x/L_c = 0.11$ from negative values to positive values as a result of opening the aperture and the introduction of the external velocity. This also implies that the location of the recirculation zones changes by opening the aperture and increasing the external velocity.

Fig. 6(a) presents the case for blocked aperture and swirling case with an inclination angle of 25°. It can be observed that the axial velocity is negative at the axial position of $x/L_c = 0.39$. The negative axial velocity indicates that a large scale vortex with inward rotation termed Central Recirculation Zone (CRZ) is formed in this section. By opening the aperture, as shown in Fig. 6(c) and (e), the axial velocity at $x/L_c = 0.39$ is no longer negative. This implies that a large-scale vortex with outward rotation, termed the External Recirculation Zone (ERZ) expands streamwise and the CRZ moves further downstream. Fig. 6(b), (d) and (f) show, for closed aperture and opened aperture cases, that the magnitude of the radial velocity profiles, at different sections, in two sides of the centreline are similar with reversed direction.

Fig. 7 presents the case for the swirling nozzle, $\alpha_j = 50^\circ$ and an azimuth angle of 5°. The figure shows that the axial velocity profile exhibits a double peak, consistent with the swirling case for $\alpha_j = 25^\circ$.

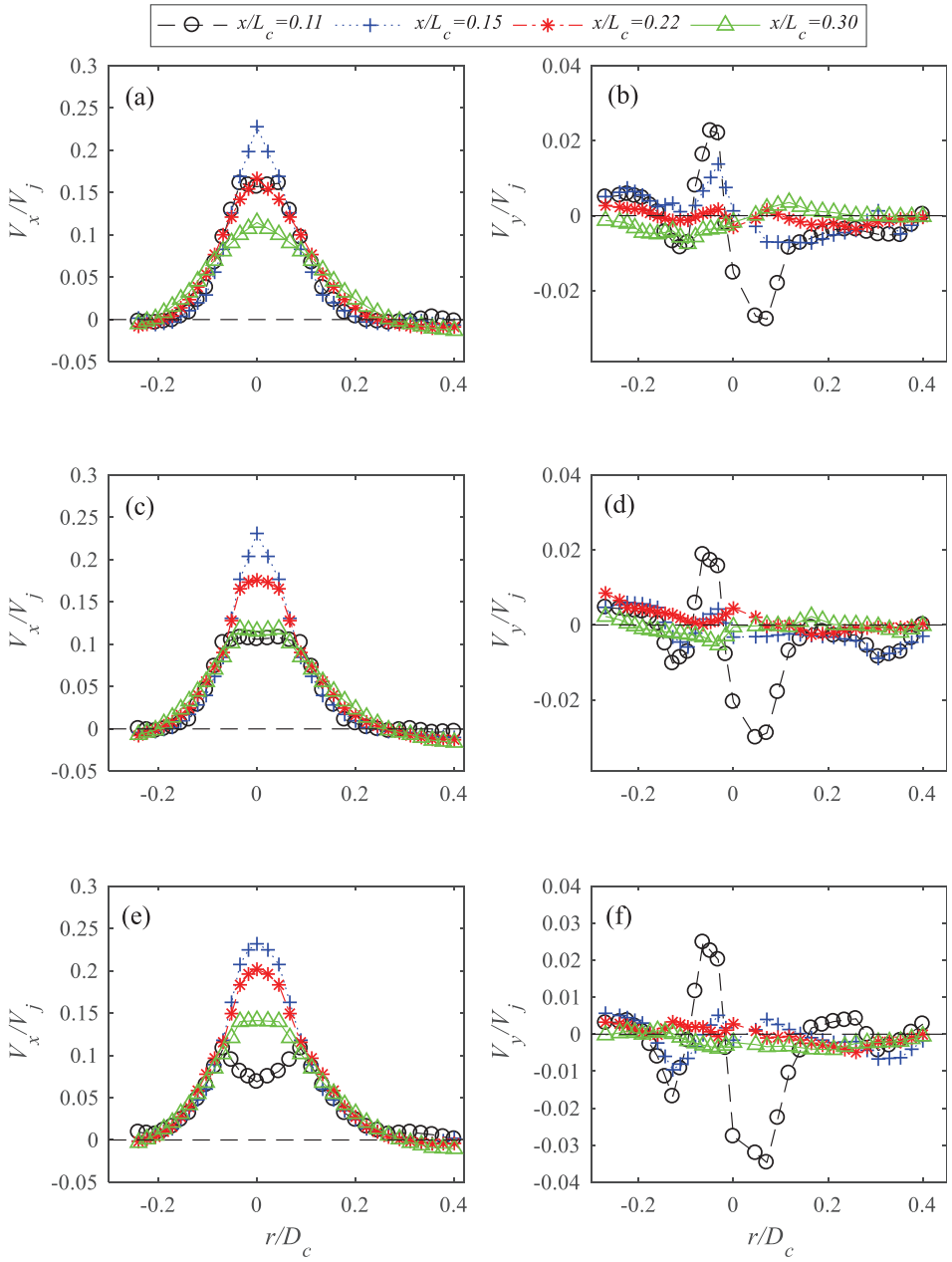

Fig. 5. Radial profiles of the normalized mean axial velocity, V_x/V_j, and normalized mean radial velocity V_y/V_j, at four cross-sections along the centreline of a cylindrical cavity, where $\alpha_j = 50^\circ$ and $\gamma_j = 0^\circ$, for the cases of (a) V_x/V_j, blocked aperture, (b) V_y/V_j blocked aperture, (c) V_x/V_j, opened aperture $V_s = 0.0$ m/s (d) V_y/V_j, opened aperture $V_s = 0.0$ m/s (e) V_x/V_j, opened aperture $V_s = 0.24$ m/s, (f) V_y/V_j, opened aperture $V_s = 0.24$ m/s.

Negative values of the axial velocity can also be seen at $x/L_c = 0.30$ indicating the presence of a CRZ. The axial velocity profile for the blocked case has two peaks at the distance where the jets interact. Consistent with the finding of Long et al. [20], the combined jet is divergent for cases with jets oriented with an azimuth angle and is not formed on the centreline of the cavity.

The velocity profiles in Figs. 4–7, show that the changes to flow structure within a cavity are influenced by changes to the inclination and azimuth angles of the jets rather than by the magnitude of the external flow over the ranges of conditions assessed here. By comparing the mean axial velocities presented in the right-hand columns of Fig. 4 with those in Fig. 6, and similarly Fig. 5 with Fig. 7, it can be seen that, for the fixed inclination angle, increasing the azimuth angle of the jet from 0° to 5°, changes the general flow structure. These changes are related to the position of ERZ and CRZ and the strength of the resulting jet. As for the swirling cases with an azimuth angle of 5°, for both inclination angles of 25° and 50°, the velocity profiles reveal the presence of a CRZ. This is consistent with the finding from a previous study of the rotational jets within a cylindrical chamber [20]. The generation of a CRZ is typically desirable in many combustion processes because it is

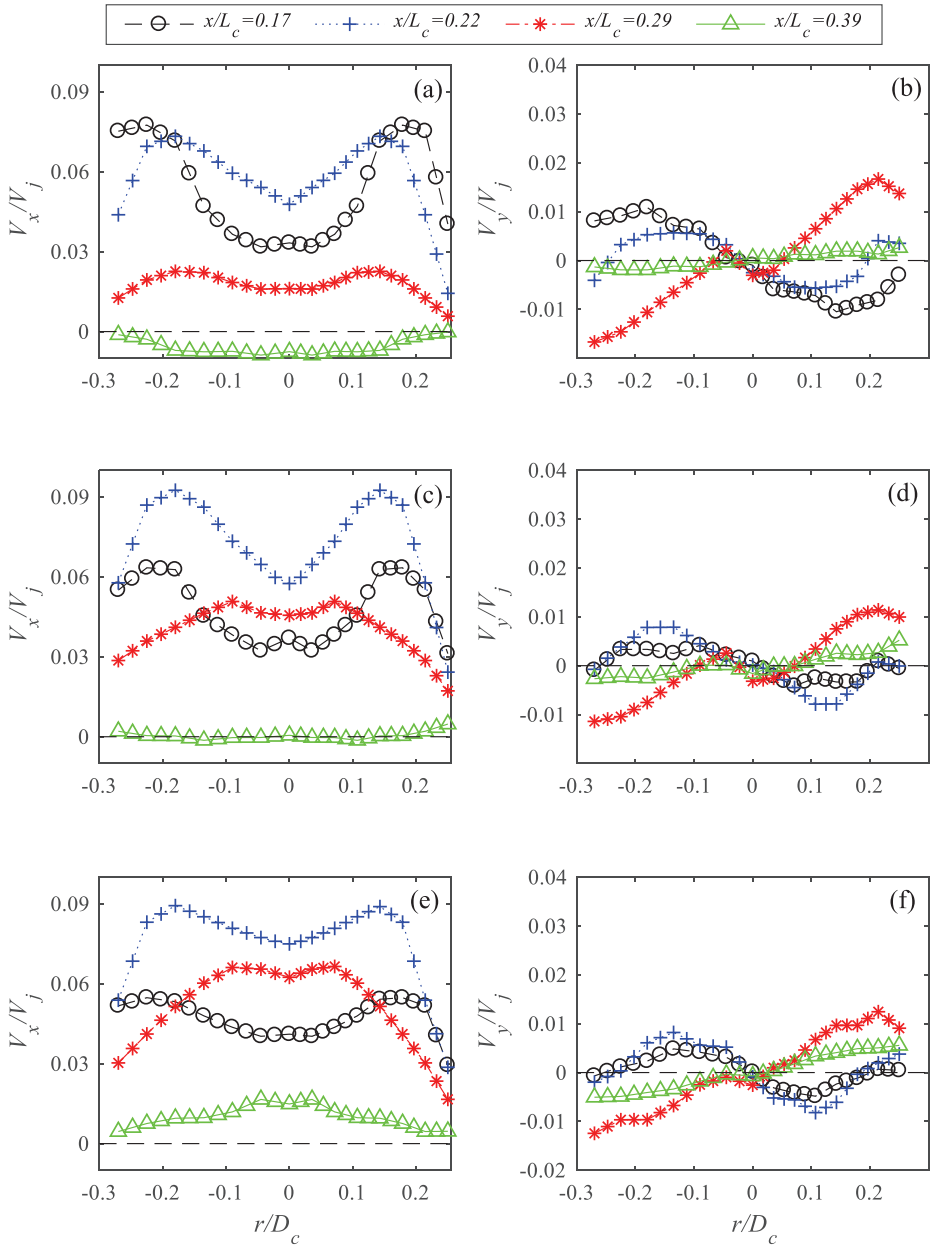

Fig. 6. Radial profiles of the normalized mean axial velocity, V_x/V_j, and normalized mean radial velocity V_y/V_j, at four cross-sections along the centreline of a cylindrical cavity, where $\alpha_j = 25^\circ$ and $\gamma_j = 5^\circ$, for the cases of (a) V_x/V_j, blocked aperture, (b) V_y/V_j blocked aperture, (c) V_x/V_j, opened aperture $V_s = 0.0$ m/s (d) V_y/V_j, opened aperture $V_s = 0.0$ m/s (e) V_x/V_j, opened aperture $V_s = 0.24$ m/s, (f) V_y/V_j, opened aperture $V_s = 0.24$ m/s.

typically associated with a high rate of heat release and a stable and compact flame [38], while the location of the CRZ has an impact on the interaction with the external flow.

2. Measured contours, vectors and streamlines within the cavity

Fig. 8 presents the contours of the ensemble averaged axial velocity (V_x) normalized by the nozzle exit velocity (V_j) for different experimental conditions and for C25-0-M-0 configuration. The operating conditions presented include: (a) blocked aperture and open aperture with different stream velocities of (b) $V_s = 0.0$ m/s, (c) $V_s = 0.08$ m/s, (d) $V_s = 0.16$ m/s and (e) $V_s = 0.24$ m/s in the midplane (Z = 0) of the cavity. Fig. 9 presents the measured ensemble averaged streamline topology for the same experimental cases as presented in Fig. 8 and in the same plane. The streamlines are labelled with arrows showing the flow direction. It is worth noting that the measuring plane is in between the two jet planes (Fig. 2). Here, the jet impingement point (P_i) is defined as the location of the maximum mean axial velocity along the centerline of the cavity. The stagnation point (P_s) is defined as the location of zero velocity point along the centreline of the chamber. The point of minimum axial velocity (P_{min}) is the location of the minimum mean axial velocity along the centreline.

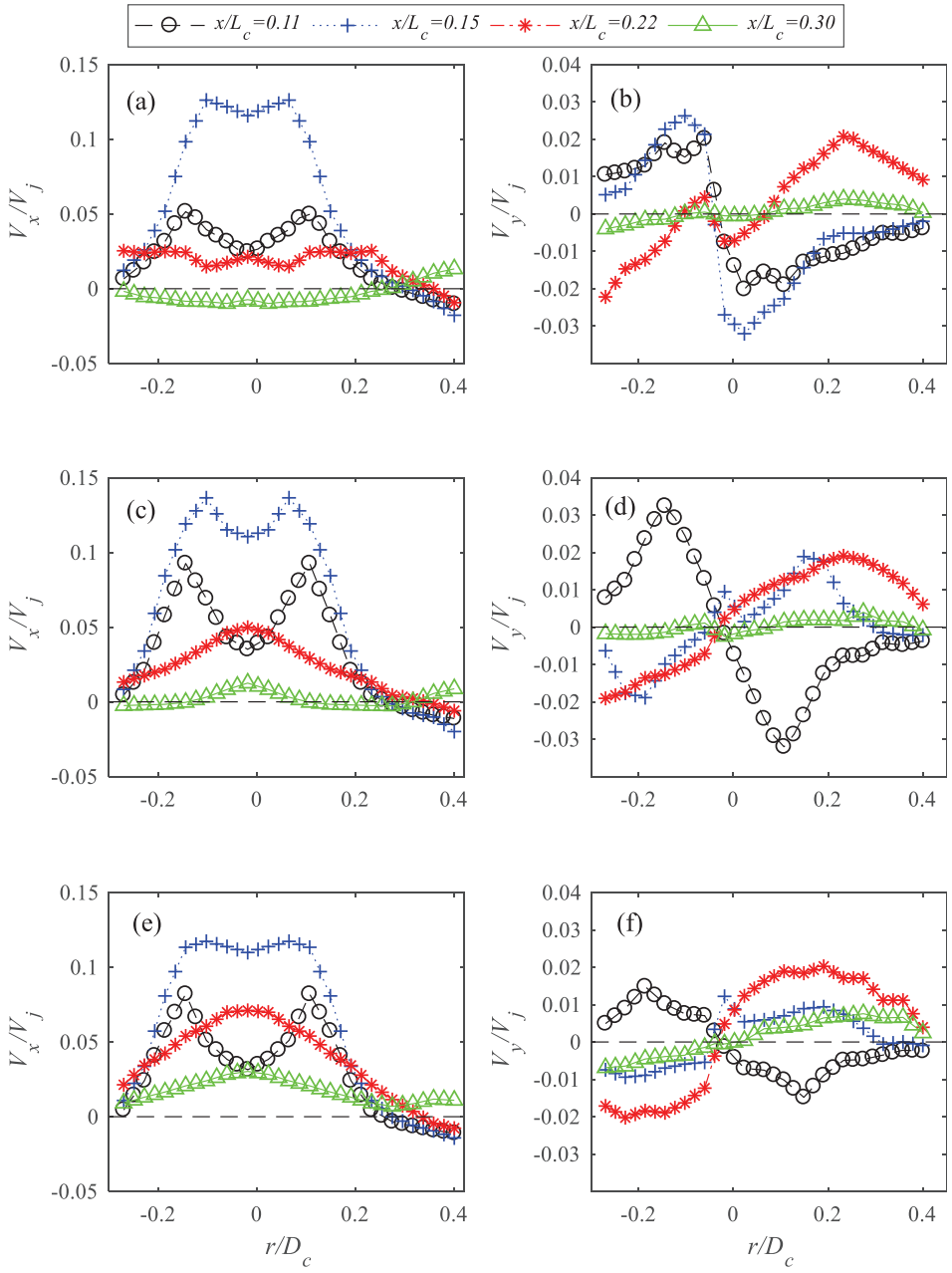

Fig. 7. Radial profiles of the normalized mean axial velocity, V_x/V_j, and normalized mean radial velocity V_y/V_j, at four cross-sections along the centreline of a cylindrical cavity, where $\alpha_j = 50^\circ$ and $\gamma_j = 5^\circ$, for the cases of (a) V_x/V_j, blocked aperture, (b) V_y/V_j blocked aperture, (c) V_x/V_j, opened aperture $V_s = 0.0$ m/s (d) V_y/V_j, opened aperture $V_s = 0.0$ m/s (e) V_x/V_j, opened aperture $V_s = 0.24$ m/s, (f) V_y/V_j, opened aperture $V_s = 0.24$ m/s.

From Fig. 8, it can be seen that mean flow fields for all cases are symmetrical. For the blocked aperture case presented in Fig. 8(a), it can be seen that jets interact at point $x/L_c \cong 0.24$ to form a combined jet. The resulting jet spreads along the centerline. This is consistent with the results presented in previous studies [19,39] for inclined jets in a confined flow. As can be seen from Fig. 8(b), opening the aperture has little influence on the flow structure within the cavity. However, it generates a zone of positive velocity fluid immediately downstream from the aperture, which is associated with the induction of ambient fluid into the cavity, even for $V_s = 0.0$ m/s. This implies that the pressure in the cavity is lower than that of the ambient fluid. The velocity contours in the vicinity of the aperture in Fig. 8(b)–(e) exhibit higher velocities in this region compared with the blocked aperture. This shows that increasing the external velocity augments the induction of external fluid into the cavity, consistent with the direction of the wind being the same as that of the axial component of the jets.

From Fig. 9, it is clear that opening the aperture leads to a qualitative change to the topology of the streamlines near to the aperture plane and in the centre of the cavity. The direction of the streamlines reverses from being directed upstream with aperture closed, to

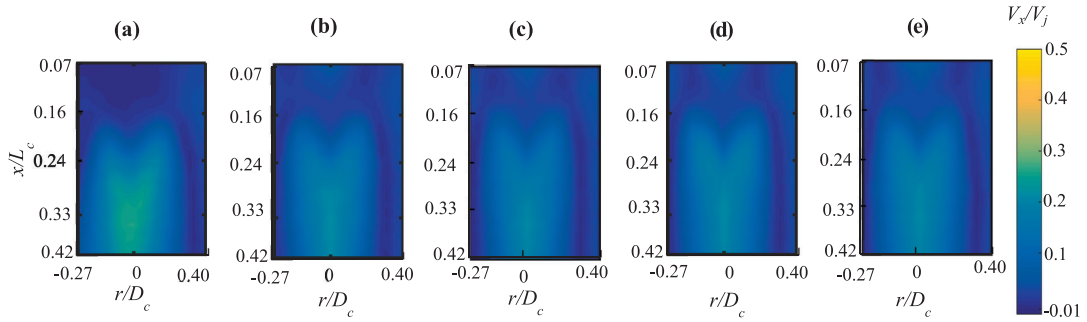

Fig. 8. Contours of the measured normalized mean axial velocity (V_x/V_j) for the case with $\alpha_j = 25^\circ$ and $\gamma_j = 0^\circ$ for the conditions of: (a) blocked aperture, (b) opened aperture, $V_s = 0.0$ m/s, (c) opened aperture, $V_s = 0.08$ m/s, (d) opened aperture, $V_s = 0.16$ m/s and (e) opened aperture, $V_s = 0.24$ m/s.

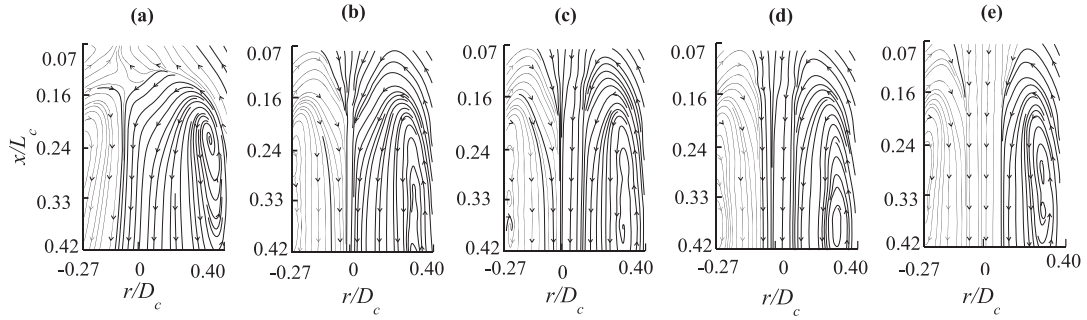

Fig. 9. Measured ensemble averaged streamlines for the experimental cases of C25-0-M-0 for (a) Blocked aperture(b) opened aperture, $V_s = 0.0$ m/s, (c) opened aperture, $V_s = 0.08$ m/s, (d) opened aperture, $V_s = 0.16$ m/s and (e) opened aperture, $V_s = 0.24$ m/s.

downstream with it open. This observation suggests that the position of the neutral pressure plane relative to ambient is not the same with the aperture opened and closed. The majority of the imaged region inside the cavity is associated with the ERZ.

Fig. 10 presents the contours of the ensemble-averaged axial velocity (V_x) normalized by the nozzle exit velocity (V_j) in the mid-plane (Z = 0) of the cavity, for different experimental configurations of C25-5-M-0, C50-0-M-0 and C50-5-M-0. The three figures on the left side correspond to the blocked aperture condition, while the middle and right side figures depict the cases for an open aperture and an external velocity of $V_s = 0.0$ m/s, and $V_s = 0.24$ m/s, respectively. Similar trends are observed for other external velocities (V_s), but are not reported for brevity. Fig. 11 presents the corresponding mean streamline patterns for the same set of conditions.

Fig. 10(a), which corresponds to $\alpha_j = 25^\circ$ and $\gamma_j = 5^\circ$, shows that the jets interact with each other on the centreline of the cavity. In contrast to Fig. 8(a), the issuing jets do not merge at the centerline of the cavity but diverge after encountering each other, consistent with previous studies of the jets with an azimuth angle [20,29]. Opening the aperture, as it is shown in Fig. 10(b), leads to a portion of the external flow being transferred into the cavity through the aperture. Therefore, the velocity on the centerline of the cavity increases over the range $0.07 < x/L_c < 0.16$. From Fig. 10(c) one can see that increasing the velocity of the external counter-flow accelerates the flow through the aperture and increases the flow velocity on the centerline of the cavity over the range $0.07 < x/L_c < 0.16$.

Fig. 10 (d) shows that jets merge at the centre of the cavity to form a combined jet at $x/L_c = 0.11$ for the jet configuration $\alpha_j = 50^\circ$ and $\gamma_j = 0^\circ$. However, the corresponding image in Fig. 11(d) shows that the flow is not truly symmetrical but exhibits some slight asymmetry. This suggests that the flow is quite sensitive to minor asymmetries in the configuration.

As it can be seen from Fig. 10(d) opening the aperture does not change the qualitative flow pattern inside the cavity significantly. Nevertheless, some quantitatively differences are evident, as is reported below in Fig. 12. Furthermore, in the open aperture case with no external flow, the resulting jet is formed slightly downstream at $x/L_c = 0.13$. A further increase in the external velocity to $V_s = 0.24$ m/s, causes the resulting jet to shift even further downstream to $x/L_c = 0.15$.

From Fig. 10(g) it is clear that the jets encounter each other at the centerline of the cavity at $x/L_c = 0.12$, for the blocked aperture of C50-5-M-0. However, the resulting jet diverges away from the centreline, consistent with previous work [29]. Fig. 10(h) and (i) show that opening the aperture does not change the qualitative flow pattern inside the cavity significantly. However, qualitatively, it does increase in the velocity at the centerline of the cavity.

From Fig. 11(a)–(c), it can be seen that the dominant feature within the imaged region in the upstream of the cavity is ERZ for C25-5-M-0. Nevertheless, a CRZ is observed from Fig. 11(a) in the region downstream from $x/L_c \geq 0.32$. The blue cross in the figure indicates the stagnation point (P_s) at $x/L_c = 0.32$. Fig. 11(b) shows that opening the aperture causes the ERZ to expand and the stagnation point to be translated further downstream to $x/L_c = 0.38$. An increase in the external velocity to $V_s = 0.24$ m/s (Fig. 11c) extends the ERZ across the entire imaged area. For this case, the stagnation point is deduced to be located downstream from the imaged region $x/L_c > 0.42$.

Fig. 11(d)–(f) show that the imaged region for C50-0-M-0 configuration is entirely dominated by the ERZ. This is consistent with the non-swirling case of C25-0-M-0. The centre of the recirculation zone for the blocked aperture case is at found $x/L_c = 0.31$. When the aperture is opened the centre of ERZ shifts further downstream to $x/L_c = 0.41$. Increasing the external velocity to $V_s = 0.24$ m/s, leads the recirculation zone to expand such that the centre of the recirculation zone shifts further downstream. Noteworthy, from Fig. 11(f) is that the centre of

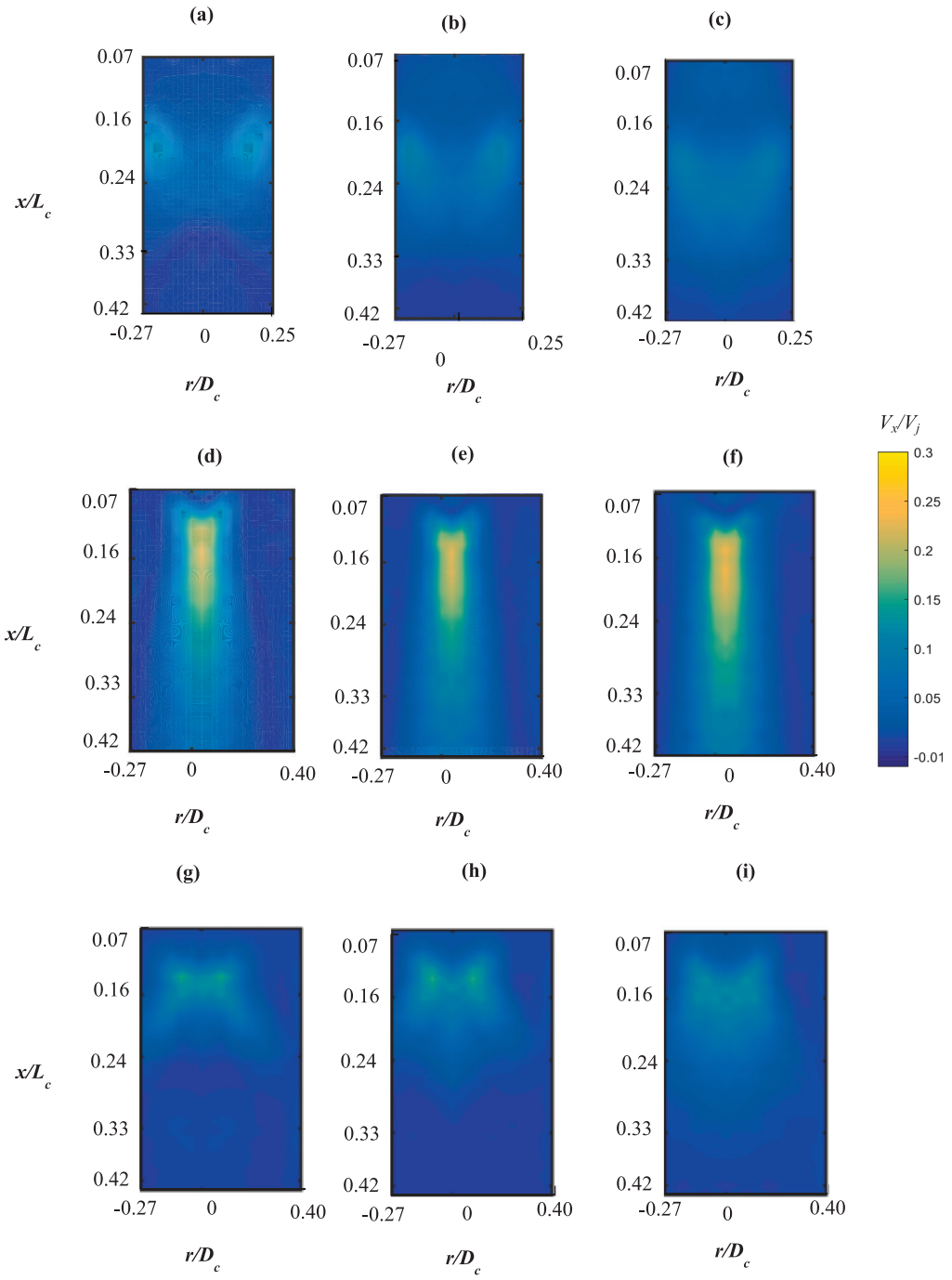

Fig. 10. Contours of the measured normalized mean axial velocity for the experimental cases of C25-5-M-0 (first row), C50-0-M-0 (second row) and C50-5-M-0 (third row), for the blocked aperture, and opened aperture with $V_s = 0.0$ m/s and $V_s = 0.24$ m/s in the left, middle and right side, respectively.

the recirculation zone is outside the imaged area and is likely to be located downstream from the imaged zone ($x/L_c > 0.42$).

From Fig. 11(g) both the ERZ and CRZ can be observed in the imaged area with a stagnation point at $x/L_c = 0.26$ for the blocked case of C50-5-M-0. Opening the aperture causes the stagnation point to shift further downstream to $x/L_c = 0.34$. Increasing the external flow velocity to $V_s = 0.24$ m/s (Fig. 11i) then translates the stagnation point further downstream to beyond the imaged area, $x/L_c > 0.42$.

The influence of the jet configuration on the flow pattern inside the cavity can be observed from Figs. 8–11. For the non-swirling flows, increasing the inclination angle from 25° to 50° causes the interaction point to move closer to the aperture, consistent with trends observed in the previous study [19]. However, the positions are different, as already noted.

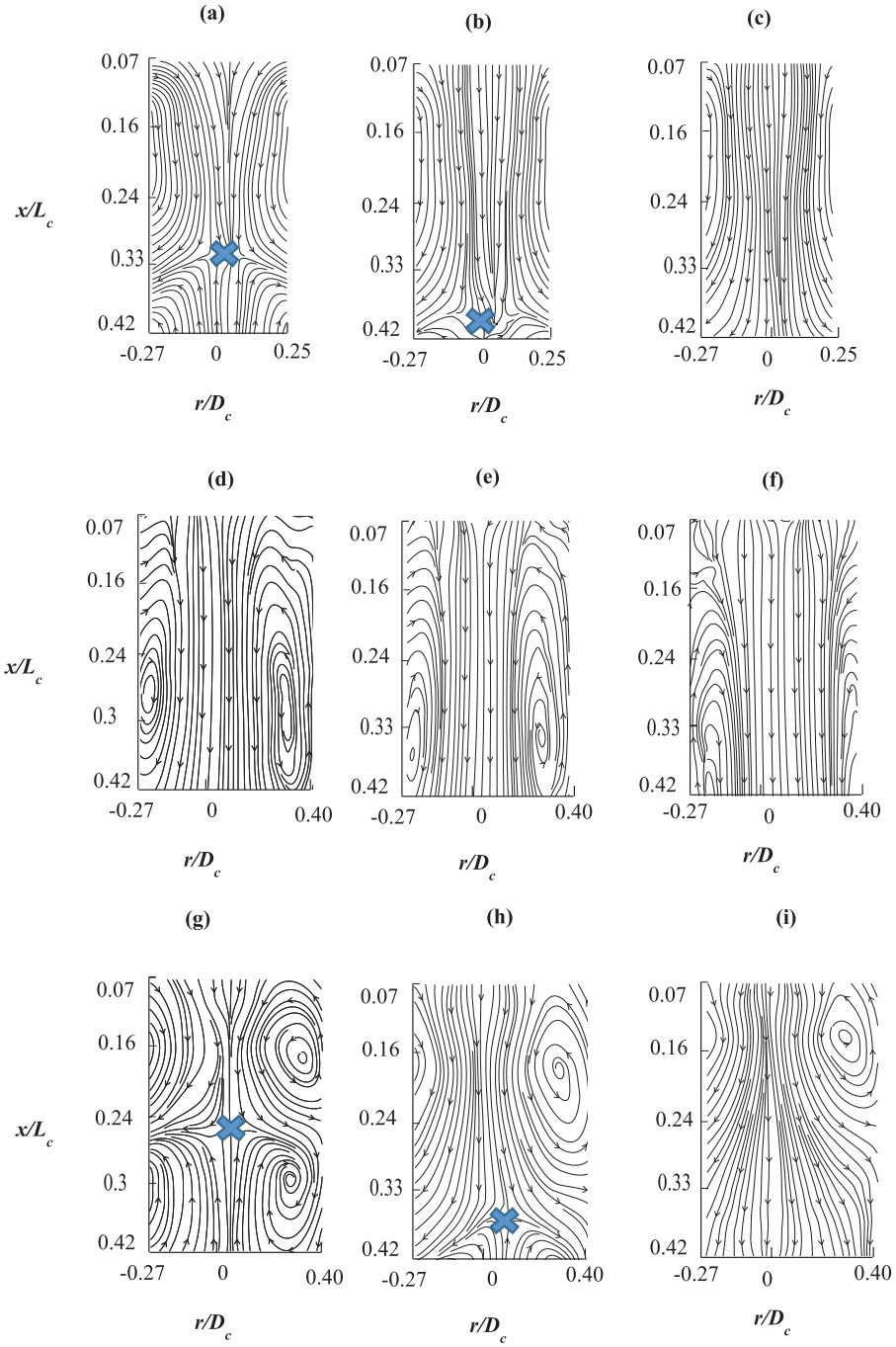

Fig. 11. Measured ensemble averaged streamlines for the experimental cases of C25-5-M-0 (first row), C50-0-M-0 (second row) and C50-5-M-0 (third row), for the blocked aperture, and opened aperture with V_s = 0.0 m/s and V_s = 0.24 m/s in the left, middle and right side, respectively.

From Figs. 9 and 11, it can be observed that the extent of the annular ERZ extends across the entire imaged area for the non-swirling jet. However, introducing a 5° swirl, generates both a CRZ and an ERZ. This observation is in good agreement with the previous studies on turbulent annular jets [20,29].

To summarise the observation from the flow contours and streamlines, it is apparent that the influences of both the jet inclination angle and jet azimuth angle on the qualitative flow patterns within the cavity are consistent with previous work. That is, opening the aperture and introducing an external flow over the range of velocities assessed here have little qualitative influence on the flow inside the cavity, except for the region in the vicinity of the aperture. This particular nozzle configuration generates an overall negative pressure in the aperture plane when it is open, inducing a strong inflow into the cavity that is

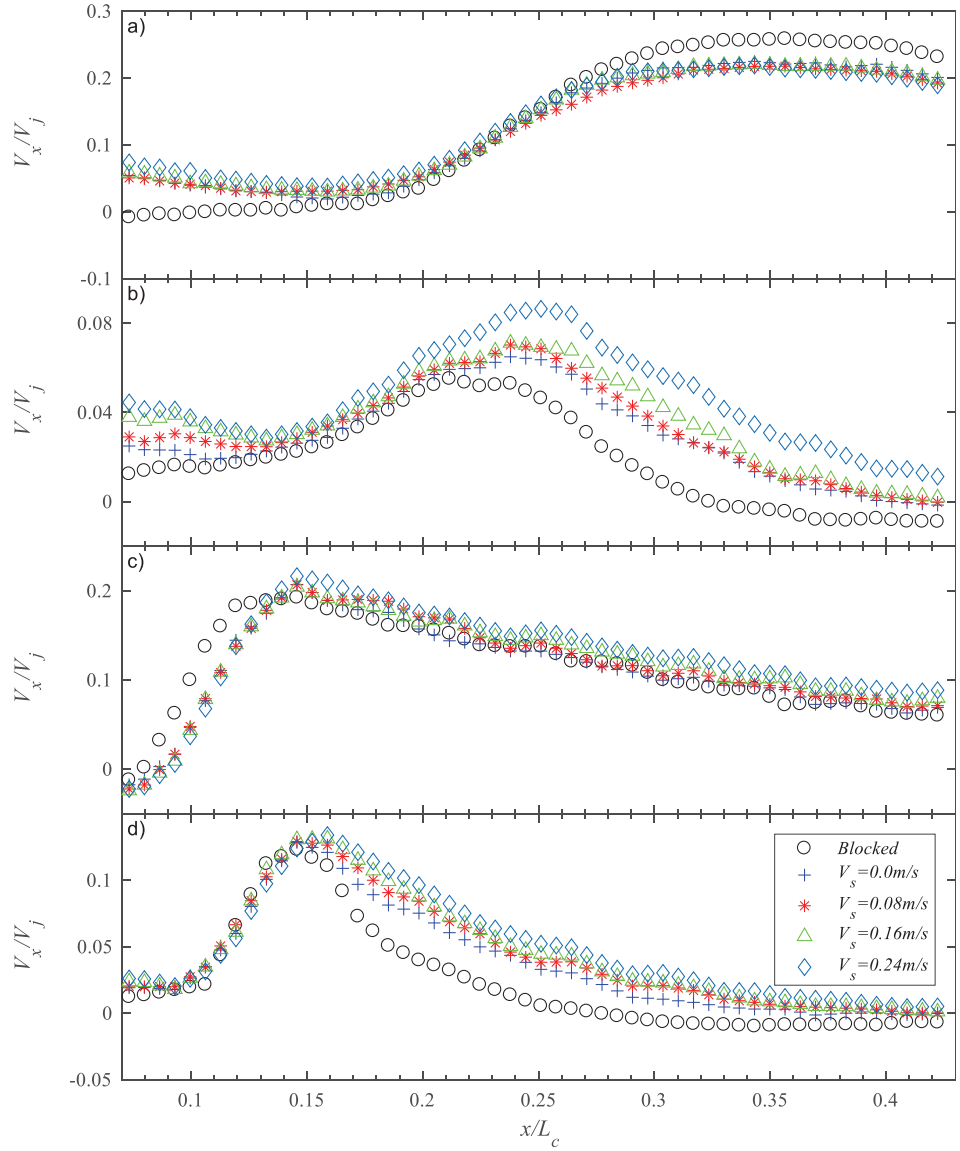

Fig. 12. Evolution of the mean axial velocity (V_x) normalized by the bulk mean jet exit velocity (V_j) along the centreline of the cavity for the different cases of (a) C25-0-M-0, (b) C25-5-M-0, (c) C50-0-M-0 and (d) C50-5-M-0 for a blocked aperture and an open aperture with stream velocities of V_s = 0.0, 0.08, 0.16 and 0.24 m/s.

augmented by the wind, since these flows are in the same direction. It further suggests that control of the back-pressure in the chamber has potential to mitigate the amount of induced flow.

3. Normalized axial velocity decay along the centreline of the chamber

Fig. 12 presents the experimental results for the time-averaged streamwise spatial variation of the normalized axial velocity along the centreline of the cavity from x/L_c = 0.07 to x/L_c = 0.42 and for the different experimental cases of C25-0-M-0, C25-0-M-0, C50-0-M-0 and C50-5-M-0. As can be seen in Fig. 12, the magnitude of the external flow does not change the general trend of the normalized velocity along the centreline of the cavity. However, for the cases with α_j = 25°, an increase in the velocity can be seen in the region close to the aperture (from x/L_c = 0.07 to x/L_c = 0.15).

The influence of the external velocity on the axial velocity profile along the centreline in the swirling experimental cases is small, as is apparent from Fig. 12. Increasing the external flow for swirling cases moves the stagnation point progressively toward the rear of the cavity.

The effect of the configuration of the jets on the mean axial velocity (V_x/V_j) profiles can also be inferred from Fig. 12. The impinging point (defined as the location of the maximum mean axial velocity along the centreline of the chamber) can be seen to occur at x/L_c = 0.38 for the blocked aperture condition with α_j = 25° and γ_j = 0° (Fig. 12a), with a magnitude of V_x/V_j = 0.16, while it is located at x/L_c = 0.21 for the case with α_j = 25° and γ_j = 5°, with a magnitude of V_x/V_j = 0.06. For the case with α_j = 50°, the stagnation point changes little from x/L_c = 0.14 to 0.13, for the different azimuth angles of 0° and 5°, respectively. However, the corresponding magnitude of the maximum normalized axial velocity decreases significantly from 0.19 to 0.12. This implies that the azimuth angle of the jet can significantly influence the strength of the "resulting jet". These results are consistent with those

presented previously [20]. It also can be seen that the position of the impingement point progresses toward the aperture from $x/L_c = 0.30$ to $x/L_c = 0.14$ as α_j increased from 25° to $\alpha_j = 50°$ without swirl, for which the magnitudes are 0.16 and 0.19, correspondingly. The position of the impinging point, changes from $x/L_c = 0.21$ to $x/L_c = 0.13$ with a magnitude of 0.06 to 0.16, for the swirling cases with $\gamma_j = 5°$, for inclination angles of $\alpha_j = 25°$ and $\alpha_j = 50°$, respectively. This shows the extent to which the strength of the resulting jet depends on the inclination angle.

The location of the impingement and minimum velocity points relative to the aperture has a direct impact on the size of the recirculation zones inside the cavity and its proximity to the aperture. This, in turn, influences the convective losses from the cavity. Fig. 13 presents the normalized location of both the jet impingement and the minimum velocity points within the imaged plane along the centreline of the cavity for experimental cases of C25-0-M-0, C25-5-M-0, C50-0-M-0 and C50-50-M-0. The impingement point is observed to be dependent on the jet configuration. As Fig. 13(a) shows for a given jet inclination angle of 25°, increasing azimuth angle from 0° to 5°, results in a 17% downstream movement of P_i. For the jet inclination angle of 50°, the change in azimuth angle results in a negligible change in the location of the impingement point. It can also be seen that, for a given azimuth angle of 0°, increasing the inclination angle from 25° to 50°, leads to a 23% upstream movement of the impinging point. Moreover, it can be seen from Fig. 13(b) that, for both $\alpha_j = 25°$ and 50°, increasing the azimuth angle from 0° to 5° shifts the location of the minimum velocity point slightly upstream.

3.2. Turbulence intensity

Figs. 14 and 15 present the evolution of normalized axial RMS (root-mean-square) velocity (V_{xrms}/V_j) and the normalized radial RMS velocity (V_{yrms}/V_j) for the case of C25-0-M-0 and C25-5-M-0, respectively, at four cross sections within plane (x,y), for a blocked aperture and an open aperture with stream velocities of $V_s = 0.0$ m/s and $V_s = 0.24$ m/s. From Fig. 14, for both the axial and radial RMS velocity, it can be seen that opening the aperture changes the RMS velocity profiles only slightly. Fig. 14(a) also shows that the axial RMS velocity has two peaks at $|r/D_c| = 0.14$ while in Fig. 14(b), the maximum axial RMS velocity occurs at $|r/D_c| = 0.19$. Furthermore, opening the aperture only changes the shear layers of the flow slightly.

In contrast, Fig. 15 shows that the magnitude of the axial RMS velocity changes significantly by opening the aperture for the swirling case with a 5° azimuth angle. For instance, at the section $x/L_c = 0.39$, the peak magnitude of the normalized axial RMS velocity is increased by 75% from 0.04 for the blocked aperture case to 0.07 for the open aperture case with $V_s = 0.0$ m/s. It is possible that this increase may be caused by greater oscillation in the flow for the open aperture, although this is yet to be assessed. The impact on the combustion process will also need to be evaluated.

3.3. Flow through the aperture

Fig. 16 presents the measured radial distribution of the mean velocity at 0.05 mm upstream of the aperture normalized by the nozzle bulk exit velocity for C25-0-M-0. It can be seen that the velocity through the aperture increases with increasing the magnitude of the external velocity in the axial direction. It is noteworthy that there is no backflow through the aperture i.e. the velocity through the aperture is always positive. This implies that the back-pressure in the cavity could be increased significantly to reduce the entrained inflow. Such an "offset" to the aperture velocity profile could be significant before any of the flow were to become "negative" (i.e. to result in part of the fluid being ejected from the edges of the aperture). The horizontal lines in the figure indicate the minimum normalized velocity through the aperture in the edges of the aperture for each external velocity. By identifying this point, it is possible to estimate how much the induced flow through the aperture could be reduced through changes to the back pressure. This approach has strong potential to greatly reduce the mass of entrained air into the cavity. The potential normalized mass flow rate reduction through the aperture ($\dot{m}_{red}$) for each case is presented in Table 3.

The fluid pressure at the outlet could be calculated by estimating the average velocity at the outlet of the cavity. The ratio of the maximum possible pressure changes to the fluid pressure at the outlet of the cavity, before inducing any back flow through the aperture ($R_p = P_{ap}/P_{outlet}$) for each external velocity, are also presented in Table 3. It can be seen that by doubling the back-pressure, the normalized mass flow rate through the aperture decreases significantly. For instance, for $V_s = 0.0$ m/s, by increasing the back-pressure by 90% the mass flow rate through the aperture could be potentially decreased by 56% to 0.11.

The mass flow rate through the aperture was calculated using a second order polynomial curves fitted to each set of the measured radial mean velocity. The curve coefficients are listed in Table 3 in the form of the mean velocity (V_{ap}) as a function of the radial distance from centre of the aperture (r), along with the corresponding R^2. Using equation (1), the mass flow rate through the aperture is calculated for each

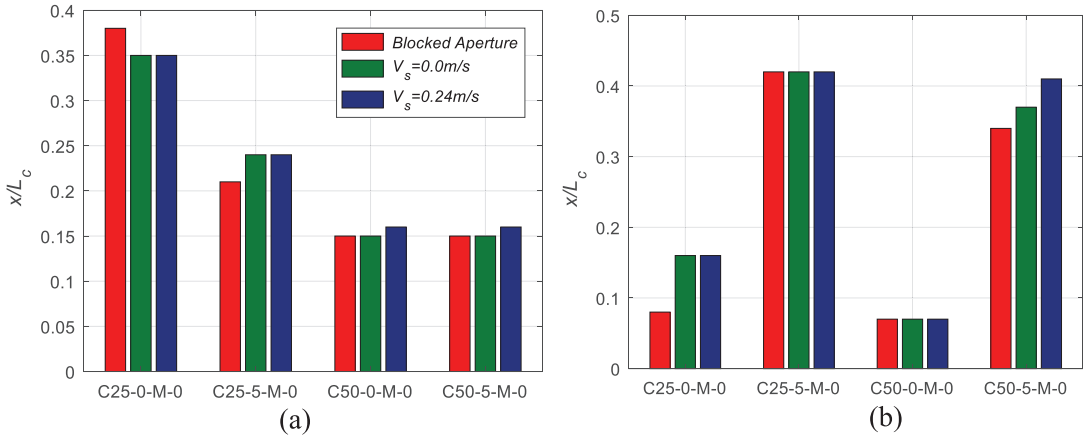

Fig. 13. Normalized location of (a) the jet impingement point (P_i), (b) the minimum velocity point (P_{min}) along the centerline of the cavity. Each figure is presented for four configuration, each with a blocked aperture and an open aperture case with a free stream velocity of $V_s = 0.0$ m/s and 0.24 m/s.

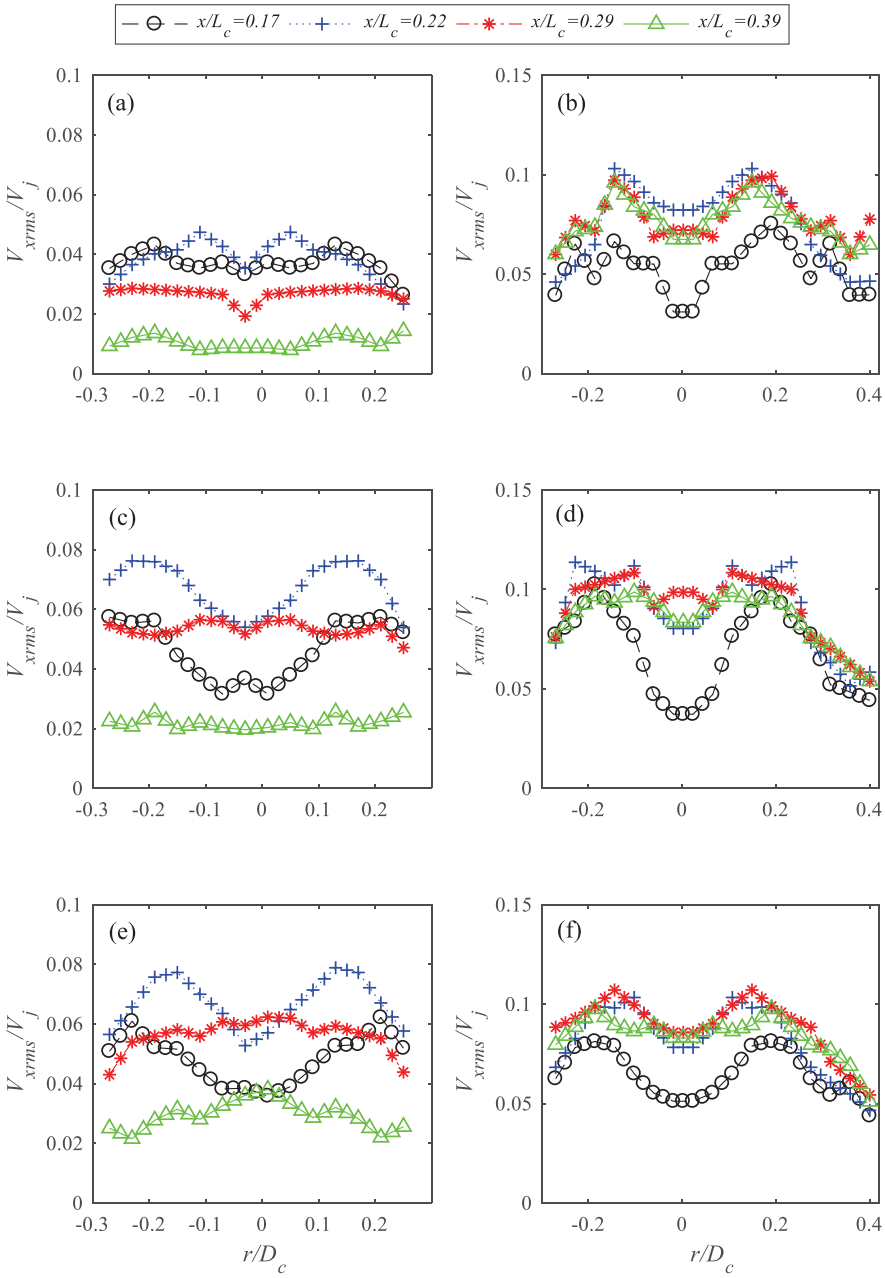

Fig. 14. Radial profiles of the normalized axial RMS velocity, V_{xrms}/V_j, and normalized radial RMS velocity V_{yrms}/V_j, at four cross-sections along the centreline of a cylindrical cavity, where $\alpha_j = 25^\circ$ and $\gamma_j = 0^\circ$, for the cases of (a) V_{xrms}/V_j, blocked aperture, (b) V_{yrms}/V_j, blocked aperture, (c) V_{xrms}/V_j, opened aperture $V_s = 0.0$ m/s (d) V_{yrms}/V_j, opened aperture $V_s = 0.0$ m/s (e) V_{xrms}/V_j, opened aperture $V_s = 0.24$ m/s, (f) V_{yrms}/V_j, opened aperture $V_s = 0.24$ m/s.

experimental case. To ensure the accuracy of the mass flow calculations, the velocity profiles in different radial sections of the aperture were measured by rotating the whole test rig. The measured velocity were within ± 2% difference from each other. Hence, the Z = 0 plane, as indicated in Fig. 2, was used for all mass flow measurements.

1. **Effect of external velocity**

Fig. 17 presents the calculated mass flow rate through the aperture of the cavity ($\dot{m}_{ap}$) normalized by the total mass flow rate through the four jets ($\dot{m}_j$) for all experimental conditions. From the figure, it can be seen that for all cases with an open aperture and an external velocity of 0.0 m/s, the normalized mass flow rate is more than 22%. This implies that the flow entrainment, even for the cases of no external flow, is significant. It can also be observed that increasing the external flow velocity leads to an increase in the mass flow entering the cavity through the aperture for all cases, although the extent of the increase depends on both angles of the nozzle. For instance, for the case of $\alpha_j = 25^\circ$, $\gamma_j = 0^\circ$, by increasing the external velocity from 0.08 m/s to 0.16 m/s, the normalized mass flow rate increases from 31% to 37%. In

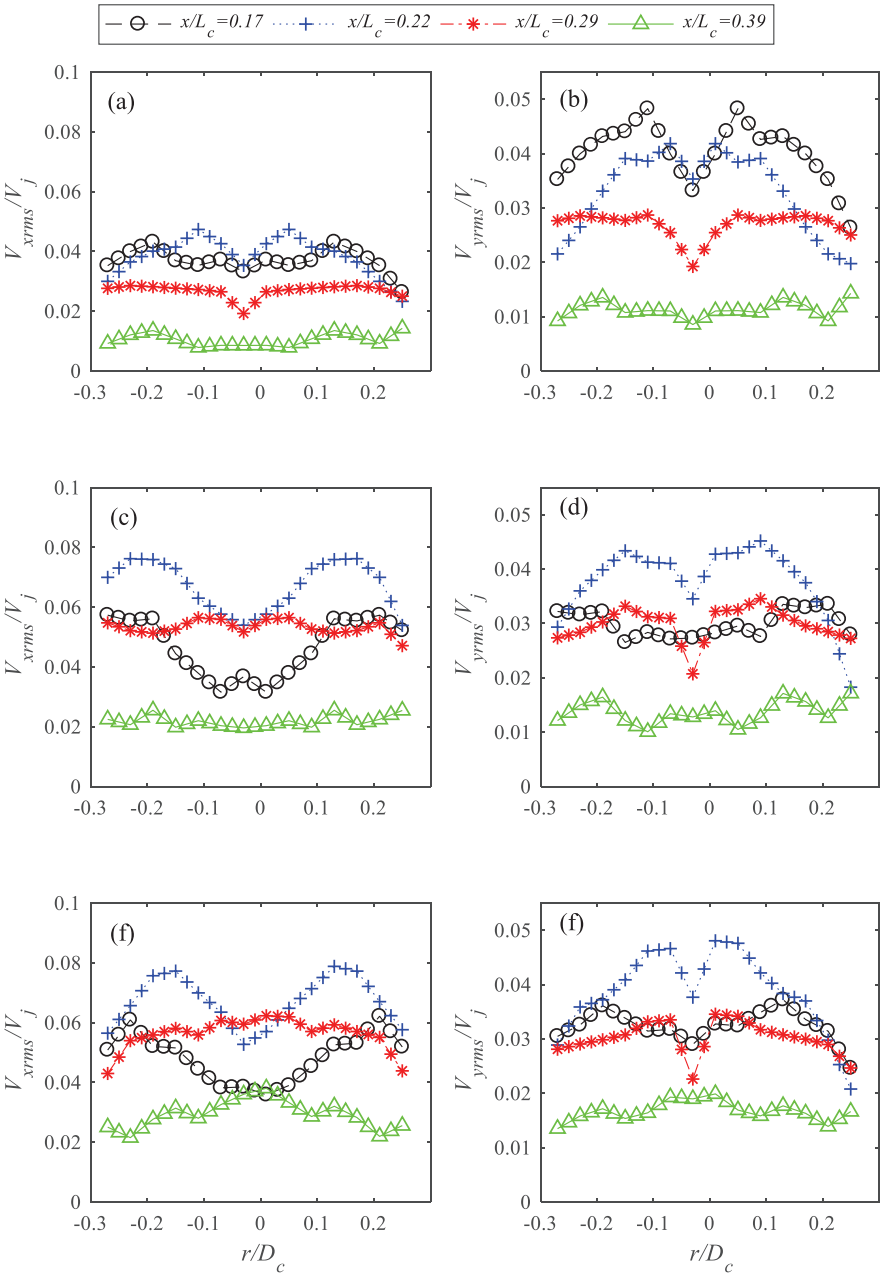

Fig. 15. Radial profiles of the normalized axial RMS velocity, V_{xrms}/V_j, and normalized radial RMS velocity V_{yrms}/V_j, at four cross-sections along the centreline of a cylindrical cavity, where $\alpha_j = 25^\circ$ and $\gamma_j = 5^\circ$, for the cases of (a) V_{xrms}/V_j, blocked aperture, (b) V_{yrms}/V_j, blocked aperture, (c) V_{xrms}/V_j, opened aperture $V_s = 0.0$ m/s (d) V_{yrms}/V_j, opened aperture $V_s = 0.0$ m/s (e) V_{xrms}/V_j, opened aperture $V_s = 0.24$ m/s, (f) V_{yrms}/V_j, opened aperture $V_s = 0.24$ m/s.

addition, the maximum mass entrainment through the aperture occurs for $\alpha_j = 25^\circ$, $\gamma_j = 5^\circ$. The reduced mass entrainment for the experimental cases with an inclination angle of 50°, can be related to the impinging point of the jets which is close to the aperture. The formation of the combined jet close to the aperture mitigates the mass flow entrainment into the cavity in the lower external velocities.

To quantify the relationship between the normalized mass flow rate and the velocity of external flow, a simple linear function is derived for each jet configuration. Table 4 presents these equations for each of the considered cases. The influence of the velocity of the external flow on the mass flow through the aperture could be estimated by using the equations.

2. Effect of the tilt angle

Fig. 18 presents the influence of the tilt angle to the external flow direction on the normalized mass flow rate through the aperture for the case of $\alpha_j = 25^\circ$, $\gamma_j = 0^\circ$ and for V_s within the range 0.08 m/s to 0.24 m/s and for θ in the range of 0° to 45°. It can be seen that increasing the velocity of external flow causes an increase in the mass flow rate

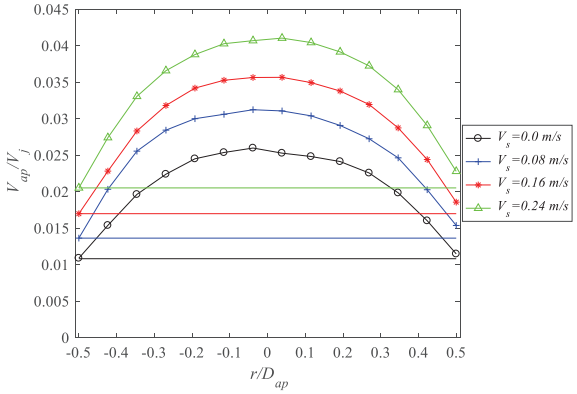

Fig. 16. Measured radial distribution of the mean velocity at 0.05 mm upstream the aperture (V_{ap}) normalized by the nozzle bulk exit velocity for C25-0-M-0 and V_s = 0.0, 0.08, 0.16 and 0.24 m/s.

Table 3
Relationship between the mean measured velocity through the aperture (V_{ap}) and the radial distance from the center of the aperture (r) for C25-0-M-0 and Vs = 0.0, 0.08, 0.16 and 0.24 m/s, corresponding R^2, R_p and $\dot{m}_{red}$.

External velocity [m/s]	Equation	R^2	R_p	$\dot{m}_{red}$
V_s = 0.0	$V_{ap} = -271.2r^2 + 0.0734$	0.99	0.90	0.15
V_s = 0.08	$V_{ap} = -306.3r^2 - 0.0893$	0.97	1.02	0.18
V_s = 0.16	$V_{ap} = -334.4r^2 + 0.102$	0.98	1.17	0.23
V_s = 0.24	$V_{ap} = -356.5r^2 + 0.116$	0.98	1.18	0.28

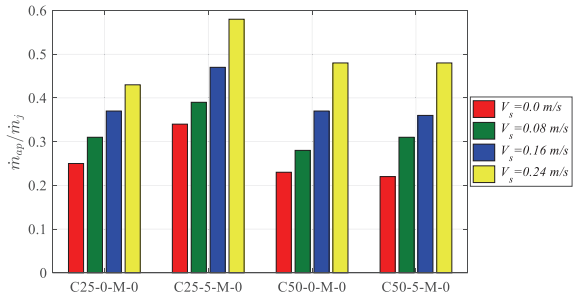

Fig. 17. Normalized mass flow rate through the aperture of the cavity.

Table 4
The relationship between the normalized mass flow rate and the velocity of the external flow.

Jet Configuration	Equation	R^2
α_j = 25°, γ_j = 0°	$\frac{\dot{m}_{ap}}{\dot{m}_j} = 0.75V_s + 0.25$	R^2 = 1.00
α_j = 25°, γ_j = 5°	$\frac{\dot{m}_{ap}}{\dot{m}_j} = 0.99V_s + 0.32$	R^2 = 0.95
α_j = 50°, γ_j = 0°	$\frac{\dot{m}_{ap}}{\dot{m}_j} = 1.06V_s + 0.21$	R^2 = 0.97
α_j = 50°, γ_j = 5°	$\frac{\dot{m}_{ap}}{\dot{m}_j} = 1.02V_s + 0.22$	R^2 = 0.97

through the aperture, for all measured tilt angles. However, for different stream velocities, the mass flow rate changes are not correlated with the variation of the tilt angle. By changing the tilt angle up to 10°, the variation in total flow, for fixed external velocity, is negligible. As the tilt angle increases, two different flow behaviours are observed. For V_s = 0.08 m/s, the amount of mass flow rate remains roughly constant and for V_s = 0.16 m/s and 0.24 m/s it increases by 8% and 15%,

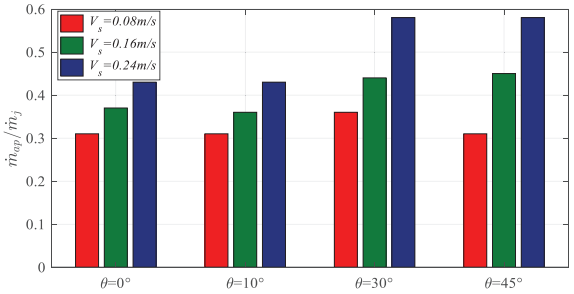

Fig. 18. Variation of the normalized mass flow rate through the aperture of the cavity as function of the tilt angle θ for experimental cases where α_j = 25°, γ_j = 0° and with V_s = 0.08, 0.16 and 0.24 m/s, for different tilt angles of the cavity where θ = 0°, 10°, 30° and 45°.

respectively. It appears that the flow is penetrating the upper corner of the aperture and changing the symmetry flow pattern inside and then penetrate into the chamber.

3. Effect of aperture diameter

Fig. 19 shows the mass flow rate through the aperture of the cavity ($\dot{m}_{ap}$) normalized by the total mass flow rate through the four jets ($\dot{m}_j$). The test were conducted for the jet configuration where α_j = 25°, γ_j = 0° and stream velocities of V_s = 0.0, 0.08, 0.16 and 0.24 m/s for different aspect ratio of the aperture to the cavity (AR), namely 0.25, 0.33, and 0.50. As the figure shows for AR = 0.25 and V_s = 0.0 m/s, the normalized mass flow rate entrainment through the aperture is 10%.

As Fig. 19 illustrates, increasing the aperture ratio leads to a significant increase in the mass flow rate through the aperture. A notable result is that for AR = 0.5, even for V_s = 0.0 m/s, the normalized mass flow rate is 0.52. That is, the need to mitigate mass entrainment through the aperture becomes increasingly significant with larger aperture ratios. Furthermore, as expected, the mass flow rate increases further by an increase in the velocity of the external flow.

4. Conclusions

The PIV technique was used in this study in order to quantify the influence of jet configuration, external flow velocity, aperture ratio and cavity tilt angle on the isothermal flow structure within a hybridized cavity emulating a hybrid solar receiver and combustor. The main findings are as follows:

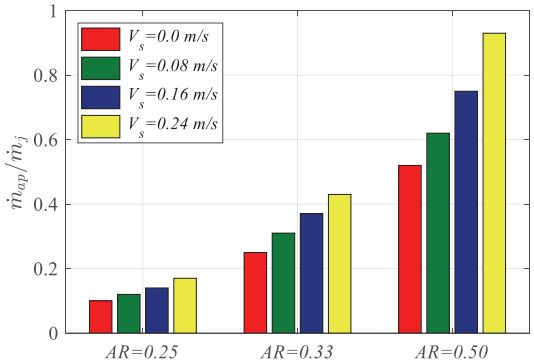

Fig. 19. The mass flow rate through the aperture of the cavity ($\dot{m}_{ap}$) normalized by the total mass flow rate through four jets ($\dot{m}_j$) for α_j = 25°, γ_j = 0° and stream velocities of V_s = 0.0, 0.08, 0.16 and 0.24 m/s for different aspect ratios of AR = 0.25, 0.33 and 0.5.

1- The flow structure within a cavity with an open aperture exhibits a stronger dependence on the jet configuration than on the external flow velocity or direction over ranges of the velocity ratios expected to be relevant to HSRC application. The entrainment of external flow through the aperture of the cavity does not change the qualitative features of the general flow within the cavity. However, it induces some quantitative changes to the positions of the "stagnation" and "impinging" points and magnitude of velocity;
2- The induced flow through the aperture is symmetrical and has a parabolic profile. Hence although the mass of induced flow through the aperture is significant for the present configuration, this could be greatly reduced by increasing the back-pressure through the chamber exit. For the open aperture case and external velocity of 0.0 m/s, the mass flow rate through the aperture normalized by the total mass flow rate through four jets is approximately 22% ($\alpha_j = 25^{\circ}$, $\gamma_j = 0^{\circ}$) and this increases to 58% ($\alpha_j = 25^{\circ}$, $\gamma_j = 5^{\circ}$) for the case of $V_s = 0.24$;
3- Minimal effect is found on the jet velocity decay as a result of the opening the aperture while a major increase of up to 75% in the turbulence intensity was recorded perhaps due to the influence of the external flow on the vortical dynamics inside the chamber.
4- An increase in the aspect ratio of the aperture to the cavity from 0.25 to 0.50, results in five times more mass entrainment through the aperture related to the total mass flow rate through four jets;
5- The mass flow rate induced through the aperture also depends both on the yaw angle of the cavity relative to the wind and the wind speed. The extent of this dependence was quantified for the isothermal case.

These results point the way toward developing a strategy to mitigate the ingress of external air into the hybridized cavity receiver. This could be done by managing the interaction of the internal and external flows through controlling the back-pressure or using a fluidic seal in the aperture. It is worth noting that due to the dominance of inertia over buoyancy forces in confined reacting flows driven by jet mixing, the findings of the current study in isothermal conditions are applicable to the real-world application of hybrid solar receiver and combustors, in which combustion happens inside the cavity.

CRediT authorship contribution statement

Elham Alipourtarzanagh: Conceptualization, Methodology, Software, Validation, Formal analysis, Investigation, Resources, Data curation, Writing - original draft, Writing - review & editing, Visualization. **Alfonso Chinnici:** Conceptualization, Methodology, Validation, Investigation, Supervision. **Zhao Feng Tian:** Conceptualization, Methodology, Supervision. **Graham J. Nathan:** Conceptualization, Methodology, Writing - review & editing, Supervision, Project administration, Funding acquisition. **Bassam B. Dally:** Conceptualization, Methodology, Validation, Writing - review & editing, Supervision, Project administration, Funding acquisition.

Declaration of Competing Interest

The authors declare that they have no known competing financial interests or personal relationships that could have appeared to influence the work reported in this paper.

Acknowledgement

The authors would like to acknowledge the support of the Australian Research Council, Australia, FCT Combustion Pty. Ltd., and Vast Solar Pty. Ltd., Australia through the ARC Linkage, Australia Grant No. LP110200060. Ms. Elham Alipour would like to acknowledge the financial support of the University of Adelaide.

References:

[1] http://www.iea-pvps.org/index.php?id=32.
[2] "Renewables 2017 Global Status Report," REN21 Secretariat, Paris.
[3] T. Faraz, Benefits of Concentrating Solar Power over Solar Photovoltaic for power generation in Bangladesh, in: 2nd International Conference on the Developments in Renewable Energy Technology (ICDRET 2012), 2012, pp. 1–5.
[4] S. Mekhilef, R. Saidur, A. Safari, A review on solar energy use in industries, Renew. Sustain. Energy Rev. 15 (4) (2011) 1777–1790.
[5] E.J. Sheu, A. Mitsos, A.A. Eter, E.M.A. Mokheimer, M.A. Habib, A. Al-Qutub, A review of hybrid solar-fossil fuel power generation systems and performance metrics, J. Sol. Energy Eng. 134 (4) (2012) pp. 041006–041006-17.
[6] G.J. Nathan, M. Jafarian, B.B. Dally, W.L. Saw, P.J. Ashman, E. Hu, A. Steinfeld, Solar thermal hybrids for combustion power plant: a growing opportunity, Prog. Energy Combust. Sci. 64 (2018) 4–28.
[7] G.J. Nathan, D.L. Battye, P.J. Ashman, Economic evaluation of a novel fuel-saver hybrid combining a solar receiver with a combustor for a solar power tower, Appl. Energy 113 (2014) 1235–1243.
[8] A. Chinnici, Z.F. Tian, J.H. Lim, G.J. Nathan, B.B. Dally, Comparison of system performance in a hybrid solar receiver combustor operating with MILD and conventional combustion. Part II: Effect of the combustion mode, Sol. Energy 147 (2017) 479–488.
[9] A. Chinnici, Z.F. Tian, J.H. Lim, G.J. Nathan, B.B. Dally, Comparison of system performance in a hybrid solar receiver combustor operating with MILD and conventional combustion. Part I: Solar-only and combustion-only employing conventional combustion, Sol. Energy 147 (2017) 489–503.
[10] J.H. Lim, G.J. Nathan, E. Hu, B.B. Dally, Analytical assessment of a novel hybrid solar tubular receiver and combustor, Appl. Energy 162 (2016) 298–307.
[11] G.J. Nathan, B. Dally, P.J. Ashman, A. Stenfeld, A hybrid receiver- combustor, 2013.
[12] A. Chinnici, G.J. Nathan, B.B. Dally, Experimental demonstration of the hybrid solar receiver combustor, Appl. Energy 224 (2018) 426–437.
[13] J. Zhu, T.H. Shih, A Numerical Study of Confined Turbulent Jets, J. Fluids Eng. 116 (4) (1994) 702–706.
[14] W.J.A. Dahm, P.E. Dimotakis, Measurements of entrainment and mixing in turbulent jets, AIAA J. 25 (9) (1987) 1216–1223.
[15] J.A. Fitzgerald, S.V. Garimella, A study of the flow field of a confined and submerged impinging jet, Int. J. Heat Mass Transf. 41 (8) (1998) 1025–1034.
[16] T. Boushaki, M.A. Mergheni, J.C. Sautet, B. Labegorre, Effects of inclined jets on turbulent oxy-flame characteristics in a triple jet burner, Exp. Therm. Fluid Sci. 32 (7) (2008) 1363–1370.
[17] S. Long, Z.F. Tian, G. Nathan, A. Chinnici, B. Dally, CFD modeling of Isothermal multiple jets in a combustor, in: presented at the Eleventh International Conference on CFD in the Minerals and Process Industries, CSIRO, Melbourne, Australia, 7-9 December, 2015.
[18] S. Long, Z. Tian, A. Chinnici, T.C.W. Lau, B.B. Dally, G.J. Nathan, Effect of Jet Inclination Angle on the Flow Field within a Hybrid Solar Receiver Combustor, in: presented at the 20th Australasian Fluid Mechanics Conference, Perth, Autralia, 5–8 December, 2016.
[19] S. Long, T.C.W. Lau, A. Chinnici, Z.F. Tian, B.B. Dally, G.J. Nathan, Experimental and numerical investigation of the iso-thermal flow characteristics within a cylindrical chamber with multiple planar-symmetric impinging jets, Phys. Fluids 29 (10) (2017) 105111.
[20] S. Long, T. Lau, A. Chinnici, Z. Tian, B. Dally, G.J. Nathan, Iso-thermal flow characteristics of rotationally symmetric jets generating a swirl within a cylindrical chamber, American Institute of Physics, 2018.
[21] S. Long, T.C.W. Lau, A. Chinnici, Z.F. Tian, B.B. Dally, G.J. Nathan, The influence of aspect ratio on the iso-thermal flow characteristics of multiple confined jets, Phys. Fluids 30 (12) (2018) 125108.
[22] A.M. Clausing, An analysis of convective losses from cavity solar central receivers, Sol. Energy 27 (4) (1981) 295–300.
[23] A.M. Clausing, Convective Losses From Cavity Solar Receivers—Comparisons Between Analytical Predictions and Experimental Results, J. Sol. Energy Eng. 105 (1) (1983) 29–33.
[24] P.L. Quere, J.A.C. Humphrey, F.S. Sherman, Numerical calculation of thermally driven two-dimensional unsteady laminar flow in cavities of rectangular cross section, Numer. Heat Transf. 4 (3) (1981) 249–283.
[25] K.L. Lee, M. Jafarian, F. Ghanadi, M. Arjomandi, G.J. Nathan, An investigation into the effect of aspect ratio on the heat loss from a solar cavity receiver, Sol. Energy 149 (2017) 20–31.
[26] L. Xiao, S.Y. Wu, Y.R. Li, Numerical study on combined free-forced convection heat loss of solar cavity receiver under wind environments, Int. J. Therm. Sci. 60 (2012) 182–194.
[27] Q. Yu, Z. Wang, E. Xu, Simulation and analysis of the central cavity receiver's performance of solar thermal power tower plant, Sol. Energy 86 (1) (2012) 164–174.
[28] M.W. Thring, M.P. Newby, Combustion length of enclosed turbulent jet flames, Symp. (Int.) Combust. 4 (1) (1953) 789–796.
[29] M. Vanierschot, E.V.D. Bulck, Influence of swirl on the initial merging zone of a turbulent annular jet, Phys. Fluids 20 (10) (2008).
[30] P.M. Gerhart, R.J. Gross, J.I. Hochstein, Fundamentals of Fluid Mechanics: Solutions Manual (no. v. 1), Addison-Wesley Publishing Company, 1992.
[31] S.R. Turns, An introduction to combustion: concepts and applications, 3rd ed., McGraw-Hill, 2012, p. 732.
[32] J. Nikuradse, Gesetzmäßigkeiten der turbulenten Strömung in glatten Rohren (Nachtrag), Forschung auf dem Gebiet des Ingenieurwesens A 4 (1) (1933) 44.

[33] W. Thielicke, E.J. Stamhuis, PIVlab – Towards User-friendly, Affordable and Accurate Digital Particle Image Velocimetry in MATLAB, J. Open Res. Soft. 2 (2014).
[34] P.M. Gerhart, R.J. Gross, Fundamentals of fluid mechanics, Addison-Wesley Pub. Co., 1985.
[35] Z. Gao, J. Han, Y. Xu, Y. Bao, Z. Li, Particle Image Velocimetry (PIV) Investigation of Flow Characteristics in Confined Impinging Jet Reactors, Ind. Eng. Chem. Res. 52 (33) (2013) 11779–11786.
[36] A. Sciacchitano, B. Wieneke, PIV uncertainty propagation, Meas. Sci. Technol. 27 (8) (2016) 084006.
[37] D.C. Cox, P. Baybutt, Methods for Uncertainty Analysis: A Comparative Survey, Risk Anal. 1 (4) (1981) 251–258.
[38] O. Lucca-Negro, T. O'Doherty, Vortex breakdown: a review, Prog. Energy Combust. Sci. 27 (4) (2001) 431–481.
[39] T. Chammem, H. Mhiri, O. Vauquelin, Experimental and computational investigation of Reynolds number effect on the longitudinal ventilation in large enclosure of twin inclined jets, Build. Environ. 67 (2013) 87–96.

Chapter 7-
Conclusions and future work

The main aim of this project is to develop innovative strategies to mitigate convective heat losses by means of adaptive air curtains, combining both blowing and suction. Both experimental and numerical methods were adopted to carry out the investigation. Further to this, the interactions of the flows inside and outside a hybrid cavity receiver have been investigated to provide an insight into the fundamentals of the air curtain design for cavities incorporating internal jets. This chapter outlines a summary of project conclusions and recommendations for future work.

7.1 **Conclusions**

The conclusions drawn from this study are categorised in the conventional cavity, hybrid cavity receivers and scalability of the results. The following sub-sections present the conclusions and outcomes for each category.

7.1.1 Conventional cavity receivers

This study experimentally demonstrated, that deployment of an air curtain can significantly reduce the convective heat losses from cylindrical solar cavity receivers with wind. The numerical study was also utilised to provide further insights into the application of the air curtains for solar cavity receivers. For a blowing air curtain cases considered here, it was found that:

- The attack angle of the air curtain is a key controlling parameter of the blowing air curtain that has a significant effect on the performance of the air curtain. The results revealed that there is a trade-off between the capability of the air curtain to restrict the interaction of the flows inside and from the surroundings, and its potential to increase the convective heat losses by mixing between the curtain and the internal flows. Therefore, it is required that the curtain be discharged with a component toward the aperture plane, especially for the high speed curtain application. As a

result, 60% reduction in convective heat losses was reported for a cavity with an aspect ratio of 1.5, with a tilt angle of 15° equipped with an air curtain with a discharge angle of 30°.

- Increasing the velocity of the air curtain increases the ability of the aerodynamic barrier to inhibit the hot gases from leaving the cavity and external cold air flowing into the cavity, thereby decreases the convective losses.
- Increasing the wind speed, which results in the transition of the heat transfer regime to forced convection ($1/Ri > 10$), reduces the effectiveness of the blowing air curtain.
- The comparison of cases with upward and downward blowing air curtains showed the better performance of the upward blowing air curtain than a downward blowing curtain for the buoyancy dominated heat transfer regime. The results show that for a horizontal cavity at a tilt angle of 0° at no wind condition, the upwards blowing air curtain was 47% more effective at reducing the convective heat losses than the downward blowing curtain. However, for the forced convection heat transfer cases, the difference between the upward and downward blowing curtains was negligible.
- The results from numerical simulation for the cases we have considered here show that for the buoyancy dominated regime and head-on wind condition, the upward blowing air curtain expands the stagnation zone inside the cavity more than the downward blowing air curtain.
- For a tilted cavity with an angle of 45°, the results provide evidence that the application of the blowing air curtain was reported to be ineffective especially at higher wind speeds (momentum dominated regime).

For a suction air curtain, our data suggests that:

- Application of low momentum of suction flow across the aperture has typically more effectiveness than blowing, in momentum dominated regime cases.
- The effectiveness of sucking air curtain, for a horizontal cavity, decreases with the inverse Richardson number, so that it can be reasonably effective in the buoyancy dominated regime, but is ineffective in the momentum dominant regime.
- For a cavity receiver tilted downward at 45° and head on wind direction, the effectiveness improves with inverse Richardson number, either by increasing the wind speed or decreasing the temperature of the cavity, so that for $1/Ri = 43.6$ a maximum effectiveness of 43% is achieved.
- For a cavity receiver tilted downward at 45°, the most effective nozzle configuration identified for either a head-on wind or no wind is one suction nozzle positioned below the aperture. These yielded effectiveness of 83% and 43% for the buoyancy and momentum dominated regimes, respectively. The application of the air suction from three sides of the aperture (both lateral and one lower sides) significantly increases the convective heat losses.
- For a horizontal cavity and head on wind condition, the trends of variation of effectiveness with nozzle configuration are similar to 45°, although the details are different.
- For a cavity receiver tilted downward at 0°, 15°, 30° and 45°, the findings of the cases investigated here show that the effectiveness for a momentum dominated heat transfer regime, increases with suction flowrate. However, for no wind condition lower extraction is needed to prevent suction of cavity air.
- For a cavity receiver tilted downward at 45° and cross wind condition, the most effective nozzle configuration identified for high inverse Richardson numbers is

one suction nozzle in the leeward position (i.e. directed across the aperture toward the wind). An effectiveness of 60% has been measured for this case.

- For a cavity tilted at 45° downward and cross wind condition at the low inverse Richardson number, the side nozzle configuration increases the convective heat losses by more than 50%.
- For the head-on wind and a cavity receiver tilted downward at 45°, the combination of blowing and suction air curtain with a variety of the fractional momentum flux of suction for $1/Ri$ = 43.6 (momentum dominated heat transfer) exhibits a 5% improvement in the effectiveness compared with suction only approach. However, for no wind condition, suction only was found to have higher effectiveness over the combined approach.

The findings show that it is imperative to design an aerodynamic barrier with variable air speed and configuration that senses the wind speed and direction and applies an effective mitigation strategy of air blowing or suction to minimize convective heat losses and maximize cavity thermal efficiency.

7.1.2 Hybrid cavity receivers

The investigation of the flow features for a cylindrical cavity incorporating internal jets with variety of jet configurations and an open aperture was performed using PIV technique. The influence of the jet configuration, external flow velocity, aperture ratio and cavity tilt angle on the isothermal flow structure within a hybridized cavity emulating a hybrid solar receiver and combustor was quantified. The analysis of the results of investigated cases here leads to the following main findings:

- For a cavity with an open aperture and internal jet flows, with a velocity relevant to hybrid solar combustor receivers, the internal flow features are more dependent on

the jet configuration than on the external flow condition. That is the entrainment of external flow through the aperture of the cavity slightly changes the quantity of some flow features such as the “stagnation” and “impinging” points and magnitude of velocity. However, the qualitative features of the flow within the cavity do not change significantly.

- The variation of jet velocity decay with the opening of the aperture displays minimal changes while a major increase of up to 75% in the turbulence intensity was recorded perhaps due to the influence of the external flow on the vortical dynamics inside the chamber.
- The mass entrainment of external flow through the open aperture compared to that from four jets is significant. So that relative mass flow for the case with external velocity of 0.0 m/s was approximately 22% ($\alpha_j = 25°$, $\gamma_j = 0°$) and this increases to 58% ($\alpha_j = 25°$, $\gamma_j = 5°$) for the case of $V_s = 0.24$. The profile of the mass flow rate through the aperture is found to be a symmetrical parabolic profile. This could be altered by changing the back pressure of the cavity through the chamber exit.
- The mass flow rate through the aperture is strongly dependent on the aspect ratio of the aperture to the cavity. So that a twofold increase of the aspect ratio from 0.25 to 0.50, results in five times more mass entrainment through the aperture related to the total mass flow rate through four jets.
- The dependence of the mass flow rate induced through the aperture on the yaw angle was quantified for the isothermal cases. It was demonstrated that for high external flow velocities, increasing the yaw angles results in higher mass flow entrainment through the aperture. So that a 15% increase in the mass flow rate was observed by increasing the yaw angle from 0° to 45°.

These results provide valuable insights that will help in developing a strategy to mitigate the ingress of external air into the hybridized cavity receiver. This could be done by managing the interaction of the internal and external flows through controlling the back-pressure or using a fluidic barrier across the aperture. It is worth noting that due to the dominance of inertia over buoyancy forces in confined reacting flows driven by jet mixing, the findings of the current study in isothermal conditions are applicable to the real-world application of hybrid solar receivers and combustors, in which combustion happens inside the cavity.

7.1.3 Scalability of the results

The experimental and numerical investigations conducted in this study were performed on a scaled down design of solar cavity receiver at a maximum temperature of 400°C. However, to apply the findings of this study to the large-scale designs of practical solar cavity receivers the approach of providing dimensionless numbers, which are most relevant to the operation of solar cavity receivers, was followed throughout the study.

The geometry of the conventional cavity was designed based on the aperture ratio of (D_{ap}/D_{cav}) of 0.1 and the aspect ratio (L_{cav}/D_{cav}) of 1.5 for a cylindrical cavity. To cover a wide range of external flow characteristic of operating cavity receivers inverse Richardson number changes from 0 to 43 corresponding to Reynolds number of 0 to 2×10^5. This range covers heat transfer regimes corresponding to buoyancy dominated, mixed natural and forced convection and momentum dominated regime. Furthermore, the external flow of laminar, transitional and turbulent regimes have also been investigated. The non dimensional numbers that are covered make it possible to generalise results to similar systems of differing scales. Finally, the deflection modulus for air curtain was adjusted between 0 to 14 to examine a wide range of air curtain operations. The momentum ratio of blowing and suction flow to wind flow

has been reported. These relative momentum and momentum flux ratios are useful measures to generalise the findings of this study for larger devices.

7.2 **Future work**

The outcomes of this study provide the baseline that can constitute guidelines for the deployment of an air curtain for solar cavity receivers. The finding from this work can be extended into additional areas of research seeking to reduce convective heat losses from solar cavity receivers by applying both active and passive methods to improve the thermal efficiency of cavity receivers. However, the findings illustrate a complex relationship between the effectiveness of an air curtain and the parameters such as the type and configuration of the air curtain, the operating conditions of the cavity receivers and the wind condition. Therefore, further investigations are required to address the challenges involved in the detailed design of air curtain to optimise a solar cavity receiver for practical applications in solar towers. Therefore, the following investigations are recommended to be undertaken to complement the research presented in this thesis.

- Further development of numerical modelling to expand the knowledge into the mechanisms of convective heat loss reduction.
- Development of the active control system of the air curtain which can activate the optimum air curtain configuration with proper flowrate based on the operating conditions such as heat transfer fluid conditions (temperature, mass flow rate), wind speed and wind direction. Active controls could utilize feedback operating conditions to dynamically alter air curtains, baffles, or other features to mitigate heat loss from the cavity. Dynamic control method with adaptive learning (AI, machine learning) is an emerging field within concentrating solar thermal applications.

- The development of passive methods of mitigating convective heat loss such as hoods and aperture coverings as a potential method of increasing the thermal efficiency of solar cavity receivers can be investigated.
- While this study has provided dimensionless numbers to generalise the findings, scaling and demonstration of these methods to actual applications and pilot-scale systems need to be performed. These pilot-scale demonstrations under "real-world" conditions with transient winds and operating conditions need to be tested and used for model validation.
- It is worth noting that the discharge angles investigated in this study were limited to 0° to 30°. Further discharge angles can be investigated either experimentally or numerically for a variety of operating conditions such as tilt angle and yaw angles.

Appendix-

Conference papers

The following is a list of the conference papers resulting from the current research:

- Alipourtarzanagh, E., Chinnici, A. Tian, Z., Nathan, G, Dally, B., **Experimental Investigation of the Flow Characteristics near the Aperture of a Model Hybrid Solar Receiver Combustor**. *21st Australasian Fluid Mechanics Conference*, Adelaide, 2018.
- Alipourtarzanagh, E., Chinnici, A. Tian, Z., Nathan, G, Dally, B., **Experimental Investigation of the Interaction of the Flow Inside and Outside a Cavity Receiver**. *Asia-Pacific Solar Research Conference*, Sydney, 2018.
- Alipourtarzanagh, E., Chinnici, A., Nathan, G.J., Dally, B.B., **Experimental Investigation on the Influence of an Air Curtain on the Convective Heat Losses from Solar Cavity Receivers under Windy Condition**, *SolarPaces*. Daegu, South Korea, 2019.
- Alipourtarzanagh, E., Chinnici, A. Tian, Z., Nathan, G, Dally, B., **Impact of Yaw angle on the Effectiveness of an Air Curtain for Solar Cavity Receivers**. *22nd Australasian Fluid Mechanics Conference*, Brisbane, Australia, 2020;

21st Australasian Fluid Mechanics Conference
Adelaide, Australia
10-13 December 2018

Experimental Investigation of the Flow Characteristics Near the Aperture of a Model Hybrid Solar Receiver Combustor

E. Alipourtarzanagh, A. Chinnici, Z. Tian, G. Nathan, B. Dally

Centre for Energy Technology, School of Mechanical Engineering
The University of Adelaide, South Australia 5005, Australia

Abstract

Presented in this paper is an experimental investigation of the flow structure near the aperture of a scaled down laboratory model of a Hybrid Solar Receiver Combustor (HSRC). The aim of the work is to evaluate the flow characteristics in the vicinity of the cavity aperture as function of the external flow velocity, simulating wind, and the flow patterns within the cavity induced by four jets simulating the burners. This interaction is expected under the mixed mode of utilizing both solar and combustion energy. Under this mode, ingress/egress into and from the solar cavity receiver due to the pressure difference between the inside of the cavity and the ambient, leads to convection losses, particularly under high wind velocities. In the current study, a simplified and scaled down HSRC geometry is used. It includes a cylindrical cavity of diameter 74 mm and length 225 mm. The configuration includes four jets with a diameter of 3.5 mm to model burners with different inclination angles of α_{jet}=25° and 50° and different azimuth angles of γ_{jet}=0°, 5°and 15°. The tests were conducted in the water channel using Particle Image Velocimetry (PIV) technique to measure the flow field. The conducted experiments aimed to investigate the influence of jet inclination and azimuth angle on the flow patterns through the aperture of the cavity. Furthermore, the influence of external flow changes on the flow pattern inside the cavity is investigated by adjusting the water channel stream velocity to 0.0, 0.08, 0.16 and 0.24 m/s. The results show that the flow behavior through the aperture strongly depends on two main factors. Firstly the flow fields induced by the variation of the inclination angle of the jets and secondly the external stream velocity. These results point to a complex interaction of the external and internal flows and highlight the need for the development of a fluidic barrier to de-couple them.

Introduction

Renewable energy is being deployed in order to mitigate climate change, cater for the increase in energy demand and as a clean energy source to support the de-carbonization of industrial processes. Solar energy, as a form of renewable energy, has been utilized for electricity generation using Photovoltaic (PV) and thermal energy using Concentrating Solar Thermal (CST) technologies [1]. However, due to the intermittent nature of the solar resource new approaches are being developed to increase solar share and guarantee firm supply. CST systems can greatly benefit from hybridisation and thermal storage as methods to overcome the problems with the intermittency of solar energy [2, 3]. To address the intermittent nature of CST, backup system where an auxiliary fossil based energy device is maintained for the time when solar energy is not enough is being used. Hybrid concepts such as solar with combustion of biomass or fossil fuels and wind energy are some of the proposed combination and it is believed to be a promising combination. Integration of CST into a conventional fossil fuel power plant has been suggested to solve the problems of the continuous dispatch of power or thermal energy [2]. The newly developed, hybrid solar receiver combustor (HSRC) concept provides a unique and cost effective solution for the aforementioned problem by providing a firm supply and reduced infrastructure costs as compared to stand alone systems [4, 5]. The distinctive geometry of HSRC features a single cavity which acts both as a combustion chamber and a solar receiver, where multiple burners and a heat exchanger are found within the cavity (Figure 1). The integrated combustion energy source into the cavity receiver opens the way for a mixed mode of operation, combustion and CST. This system avoids start-up and shut-down losses related to application of conventional hybrid systems [6].

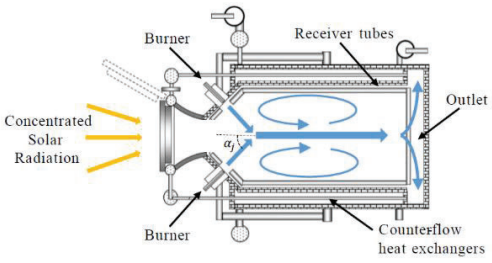

Figure 1- Schematic diagram of Hybrid Solar Receiver Combustor

The unique configuration of HSRC makes it necessary to study the flow field inside the cavity in order to optimize the flow behavior induced by the multiple jets inside a confined cavity and its interaction with the outside flow through the aperture.

Many studies in the literature have targeted the investigation of the flow field induced by multiple jets including parallel jets, opposed jets and inclined jets. Gao et al. [7] investigated the flow characteristics in confined impinging jet reactors by using PIV. They studied the effect of various geometric parameters and operating condition on the normalized mean velocity, turbulent kinetic energy and stagnation point offset from the center of the cavity. They found that in Reynolds number range of 10,620 to 21,210, the effect of Reynolds number on the normalized velocity is negligible. The normalized stagnation point is very sensitive to the jet velocity ratio. They emphasized that an equal volumetric ratio of the jets

is essential to locate the stagnation point in the center of the cavity. Long et al. [8] used numerical modelling to investigate the effect of the jet inclination angle (α_{jet}) in a cylindrical cavity, similar to the HSRC configuration, equipped with four jets and using water as working fluid. They studied the configuration with a closed aperture and a throat, using CFD code ANSYS CFX in their modelling. Their work has identified four flow regimes within the cavity. The regimes have a strong inward annular recirculation for $0\ ^\circ \leq \alpha_{jet} < 10^\circ$, outward recirculation dominant flow for $10\ ^\circ \leq \alpha_{jet} < 40^\circ$, outward recirculation with back flow for $40\ ^\circ \leq \alpha_{jet} < 60^\circ$ and jet impinging flow $60\ ^\circ \leq \alpha_{jet} < 90^\circ$. The results show that configuration of the jets not only changes the flow pattern inside the cavity but it also affects the backflow through the throat. Long et al. [9] have also investigated flow structure within a cylindrical chamber generated by planar-symmetric isothermal jets using water as the working fluid. In their joint systematic experimental and numerical study, they evaluated the cases with two and four jets for the inclination angles (α_{jet}) over the range of 0 to 90. Their results show that the mean flow field strongly depends on the inclination angle and the number of the jets. Their research reveals that, the extent of the backflow inside the cavity through the throat, the turbulent intensity, the flow stability and the dominant recirculation zone depend on the inclination angle of the jets, as expected. However, the number of jets has a secondary influence on the turbulence intensity, the flow stability and the transition between different flow regimes.

To the best of the authors' knowledge, the interactions of the flows inside and outside a cavity with injected jets has not been investigated in the literature and requires further research. In this paper, we investigate the flow behaviour through the aperture induced by the jets inside the cavity and the external flows. To characterise the flow behaviour and identify the effect of the key controlling parameters on the velocity field, extensive experimental investigations were conducted in the University of Adelaide water channel. The findings and interpretations are presented in this paper.

Methodology

To determine the effect of internal flow pattern change on the flow through the aperture, several prototype models of a cylindrical cavity, with an open aperture, were designed and built. These prototypes aremade of Acrylic material and include different internal jet configurations. The transparent prototypes have a similar refractive index as water which allows it to be used with water as the working fluid and lend itself to the application of laser-based techniques such as PIV.

Figure 2 and Table 1 illustrate the key geometric features of the experimental configurations. The experimental setup is designed so that the different jet configurations, as shown in Table 2, can be investigated while using the same cavity. The cylindrical model has 74mm of internal diameter and is 225mm in length with an annular gap as the outlet of the cavity. The cavity inlet is configured with a straight desk which has an aperture of 24.6mm diameter. Four equi-spaced jets are included on the aperture side to model the combustion burners. Previous investigation, using similar geometries [9], has shown that the mass flow rates through the aperture will increase significantly when the flow pattern within the cavity changes due to the change in the inclination angle of the jets. The two configurations considered give a flow pattern which is classified as 'outward recirculation' when the inclination angle of 25° (α_j =25°) or 'outward recirculation with back flow' when the inclination angle is 50° (α_j =50°). Therefore, these two inclination angles of jets are considered for the current project. The cases of the jets with 50° inclination angle has three different azimuth angles of γ_{jet}=0°, 5°and 15° while the case with 25° inclination angle has azimuth angle of 15°.

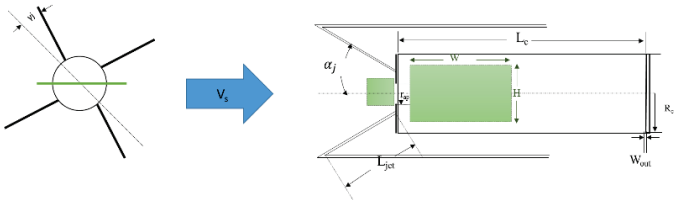

Figure 2- Schematic of the experimental model showing key geometric features of the configuration

Table 1- Values of the geometric parameters of the experimental configuration

Geometric Parameter	Value	Description	Geometric Parameter	Value	Description
L_c	225 mm	The length of the cylinder	D_{jet}	3.35 mm	The diameter of the nozzle
R_c	37 mm	The Radius of the cylinder	R_{ap}	24.6 mm	The radius of the aperture
L_{jet}	150 mm	The length of the jet supply pipe	α_j	50°, 25°	Jet inclination angle
W_{out}	3 mm	The width of the outlet for the exhaust	γ_j	0°,5°, 15°	Jet azimuthal angle

The tests were conducted in a recirculating water channel with a maximum speed of 0.3 m/s. The rectangular test section is 2.0 m long with a cross-section of 0.5m × 0.5 m. The device is submerged in the water and held there using a specially designed holder. The blockage ratio of the test section is 7.2% which is small enough to prevent wall effects. The volume flow rate of the jets were set at 1.4 l/min, resulting in a jet inlet velocity of 2.8 m/s and a Reynolds number of 10,500.

Table 2- Cases notation for the configurations investigated experimentally in the present study

Cases	Jet inclination angle, α_j	Jet azimuthal angle, γ_j	Stream velocity of the water channel (m/s)
25-15-(B-0-0.08-0.16-0.24)	25°	15°	Blocked aperture, 0.0, 0.08,0.16,0.24
50-15-(B-0-0.08-0.16-0.24)	50°	15°	Blocked aperture, 0.0, 0.08,0.16,0.24
50-5-(B-0-0.08-0.16-0.24)	50°	5°	Blocked aperture, 0.0, 0.08,0.16,0.24
50-0-(B-0-0.08-0.16-0.24)	50°	0°	Blocked aperture, 0.0, 0.08,0.16,0.24

The PIV technique was used to measure the instantaneous velocity field in the vicinity of cavity aperture and inside the cavity. The flow is seeded with polyamide seeding particles with a mean diameter of 50 µm and the density of 1.03 g/cm^3. The water within the channel is circulated back into a reservoir creating a closed loop operation. Seeds are added to the reservoir at the start of the test campaign, in order to provide a continuous seeding of the flow. The seeded particles were illuminated using an Nd-YAG double-Pulsed laser (Quantel Evergreen 200-200 mJ) operating on the second harmonic mode, giving two laser pulses at 532nm. The pulses were formed, using suitable optical components, to give horizontal laser sheets with a thickness of ~2 mm. PIV images are recorded by the sCMOS camera (Andor Zyla 5.5) with 5.5 megapixel resolution, capturing a region of interest with 2000×2000 pixels. The Andor SOLIS image capturing software is used for image collection. The laser and camera are connected to a pulse generator (Berkeley Nucleonics, Model 565) and a timer box to synchronize the data collection. Images were recorded from the bottom view of the cavity.

The images were acquired at a rate of 15 Hz with delay time of 4ms and 0.15ms for outside and inside measurement, respectively. A total of 500 image pairs were captured for each case. The post processing of the captured images was conducted using the PIVlab toolbox of MATLAB. The instantaneous velocity vectors were measured for an area of 24.6×24.6 mm^2 upstream region of the aperture inlet and 50×90 mm^2 inside the cavity. The images were processed using an interrogation window size of 64×64 pixels with an overlap of 50%.

Results and discussions

Figure 3 depicts the measured streamline patterns and the velocity contours within the cavity for the case with inclination angle of 50° and azimuth angle of 15° for the blocked aperture, stream velocity of 0.0 m/s, 0.08 m/s, 0.16 m/s and 0.24 m/s.

As could be seen, opening the aperture changes the flow pattern inside the cavity and expands the recirculation zones further downstream inside the cavity. Such changes show that the external flow changes the flow characteristics inside the cavity. Figure 4 shows the evolution of the mean axial velocity along the centreline of the cavity normalized by the jet inlet velocity.

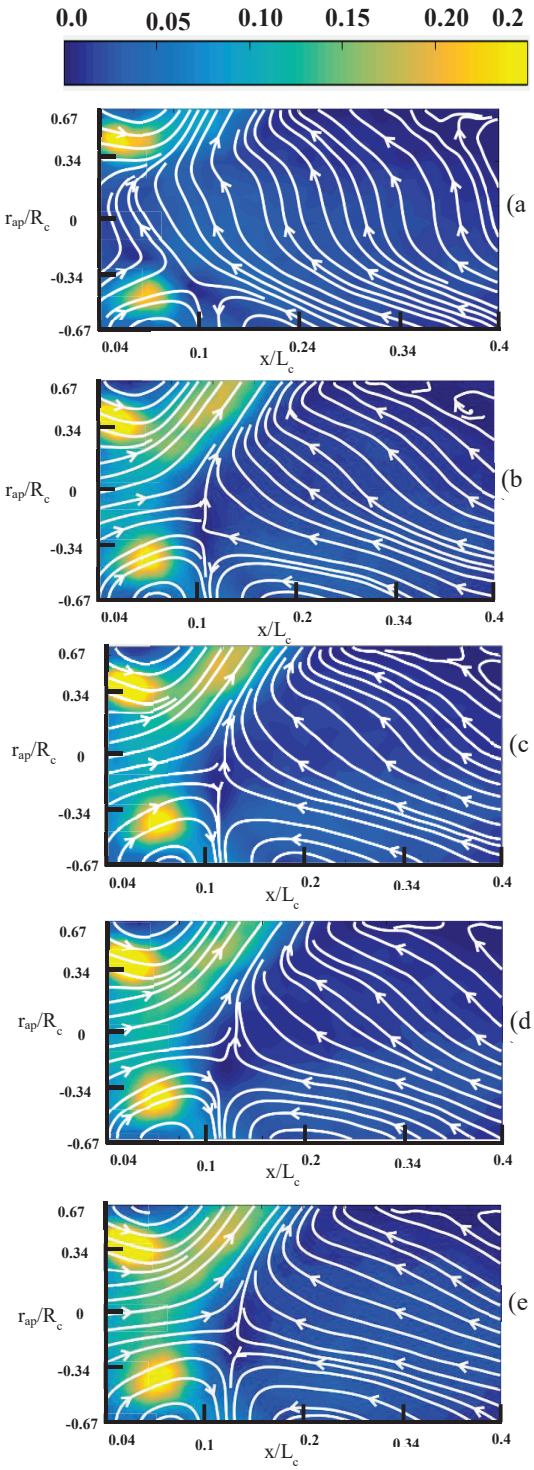

Figure 3- Velocity contour and streamlines inside the cavity for the case with α_j = 50° and γ_j=15°, a) Blocked aperture (50-15-B), b) V_s=0.0 m/s (50-15-0), c) V_s= of 0.08m/s (50-15-0.08), c) V_s= 0.16m/s (50-15-0.16), and d) V_s=0.24m/s (50-15-0.24).

As can be seen for the all cases the stagnation point, (the point that axial component of the velocity (V_x) to the velocity of the jet (V_{jet}) equals to 0.0) is located on the axis. The stagnation point transfers from x/L_c=0.15 to x/L_c=0.18 by changing the external velocity which shows expansion of the vortices in the vicinity of the aperture. Furthermore, opening the aperture affects the flow field in the vicinity of the aperture, and moves the highest velocity zone further downstream.

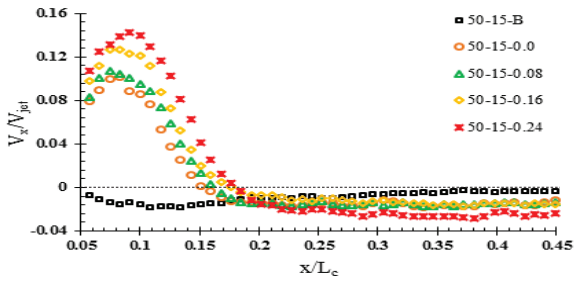

Figure 4- Spatial variation of the mean axial velocity (V_x/V_{jet}) along the centerline of the cylindrical chamber normalized by the inlet velocity as function of chamber length for α_j = 50° and γ_j=15°. Cases plotted are Blocked aperture (50-15-B), V_s=0.0 m/s (50-15-0), V_s= 0.08m/s (50-15-0.08), V_s=0.16m/s (50-15-0.16), and V_s=0.24m/s (50-15-0.24).

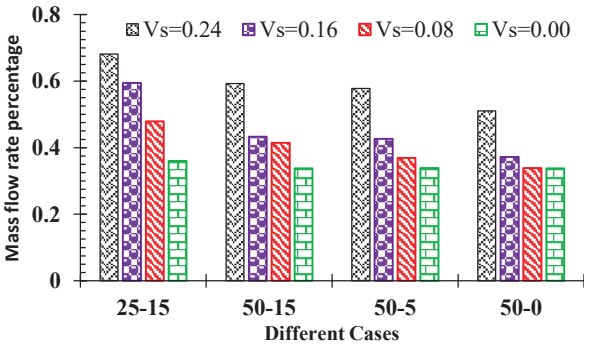

Figure 5-Percentage of the mass flow through the aperture to total mas flow from the jets, for different cases with inclination angles of 25° and 50° and azimuth angles of 15° ,5° and 0° in different stream velocities of 0.24, 0.16, 0.08 and 0.0 m/s.

Figure 5 shows the effects of the jets configuration and external stream velocity on the percentage of normalized mass flow rate through the aperture. As can be seen even for the stream velocity of 0.0 m/s, the ratio of mass flow through the aperture to the mass flow through four jets is 30% which shows that opening the aperture even in no wind condition causes a significant air ingress to the cavity. In addition, the measured normalized mass flow rates show that increasing the inclination angle from 25° to 50°, decreases mass flow rate by 10% for the stream velocity of 0.24 m/s while for cases with zero velocity of water channel stream, changing the inclination angle from 25° to 50° makes only 2% changes in normalized mass flow rate. This result is reasonable when observing the different flow patterns induced by the inclination angles of 25° and 50°. For the inclination angle of the 25°, the recirculation zones are closer to the centerline creating negative pressure that induce more flow through the aperture. While for the inclination angle of 50° the center of the recirculation zones are closer to the wall and have less effect on the flow behavior through the aperture. Furthermore, for the same inclination angle of 50°, by decreasing the jet azimuth angle from 15° to 0°, the mass flow rate through the aperture decreases markedly. It is quite clear that in higher stream velocities (V_s=0.24 m/s), the inclination angle has more effect on the variations of mass flow rate through the aperture than the azimuth angle of the jets.

Conclusions

A combined experimental study was conducted to investigate the flow field inside and in the inlet of a cylindrical cavity with four jets inclined at two different angles of 25° and 50° and for different azimuth angles of 0°, 5° and 15° degrees. It was found that there is strong interaction of the flow field inside the cavity and the flow behavior through the aperture. Opening the aperture of the cavity for operation in mixed mode, causes more than 30% of dimensionless mass flow rate into the cavity even for no wind condition. These results point to a complex interaction of the external and internal flows and highlight the need for the development of a fluidic barrier to de-couple these two flows.

References

[1] Sarbu, I. and C. Sebarchievici, Chapter 3 - *Solar Collectors, in Solar Heating and Cooling Systems*. 2017, Academic Press. p. 29-97.

[2] Sheu, E.J., et al., *A Review of Hybrid Solar–Fossil Fuel Power Generation Systems and Performance Metrics*. Journal of Solar Energy Engineering, 2012. 134(4): p. 041006-041006-17.

[3] Lovegrove, K. and J. Pye, 2 - *Fundamental principles of concentrating solar power (CSP) systems, in Concentrating Solar Power Technology.* 2012, Woodhead Publishing. p. 16-67.

[4] Nathan, G.J., D.L. Battye, and P.J. Ashman, *Economic evaluation of a novel fuel-saver hybrid combining a solar receiver with a combustor for a solar power tower*. Applied Energy, 2014. 113: p. 1235-1243.

[5] Lim, J.H., et al., *Analytical assessment of a novel hybrid solar tubular receiver and combustor.* Applied Energy, 2016. 162: p. 298-307.

[6] Lim, J.H., E. Hu, and G.J. Nathan, *Impact of start-up and shut-down losses on the economic benefit of an integrated hybrid solar cavity receiver and combustor.* Applied Energy, 2016. 164: p. 10-20.

[7] Gao, Z., et al., *Particle Image Velocimetry (PIV) Investigation of Flow Characteristics in Confined Impinging Jet Reactors*. Industrial & Engineering Chemistry Research, 2013. 52(33): p. 11779-11786.

[8] Long, S., et al., *Effect of Jet Inclination Angle on the Flow Field within a Hybrid Solar Receiver Combustor, in 20th Australasian Fluid Mechanics Conference*. 2016: Perth, Autralia.

[9] Long, S., et al., *Experimental and numerical investigation of the iso-thermal flow characteristics within a cylindrical chamber with multiple planar-symmetric impinging jets*. Physics of Fluids, 2017. 29(10): p. 105111.

ASIA-PACIFIC
SOLAR RESEARCH
CONFERENCE

Elham Alipour

Experimental Investigation of the Interaction of the Flow Inside and Outside a Cavity Receiver

E.Alipourtarzanagh, A. Chinnici, Z. Tian, G.Nathan and B. Dally

[1]*Centre for Energy Technology, School of Mechanical Engineering*
The University of Adelaide, South Australia 5005, Australia
E-mail: elham.alipour@adelaide.edu.au

Abstract

A qualitative and quantitative flow field study using an experimental method has been carried out to investigate the flow behaviour inside and outside a cylindrical cavity receiver. The cavity is a simplified scaled down geometry of a Hybrid Solar Receiver Combustor (HSRC), which operates in three different modes of solar only, combustion only and mixed mode. In the mixed mode, some ingress of air and egress of chamber gases into and out from the solar cavity receiver will occur, due to the pressure difference between the inside of the cavity and the ambient. This leads to convection losses, particularly under high wind velocities. To determine the interaction of the internal and external flow patterns under simplified, isothermal conditions, a cylindrical cavity model was constructed of acrylic. Four equi-spaced jets of 3.35 mm internal diameter, were included on the aperture side to model the combustion burners. The jets in this model were inclined α_j=25° and had an azimuth angle of γ_j=5°. The model was placed in the water channel, under isothermal conditions and velocity of water in the channel aimed to emulate the wind conditions to the cavity. Water was also used for the jets in the model cavity. The systematic investigations include both closed and opened aperture with free stream velocities of 0.0 and 0.24 m/s. The flow velocity of the jets inside the cavity was fixed at 2.8 m/s to achieve the aerodynamics similarity between the speeds of the jets and wind and to ensure that the jet flow is in the fully turbulent regime (Re=10,500). The cavity is made of acrylic material that makes it possible to visualise flow behaviour using the Particle Image Velocimetry (PIV) technique. The results show that the flow behaviour through the aperture depends on external flow condition. Opening the aperture and introducing the external velocity induces a mass flow rate through the aperture of up to 58 percent of the total mass flow rate through four jets. These measurements reveal a complex interaction between the external and internal flows within the cavity receiver.

1. Introduction

Renewable energy has been proposed as a reliable and clean energy source to replace fossil-based energy generation which helps support the industrialization of the major economies of the world and cater for population growth. Such growth in demand for energy usage (Stulz, Tanner & Sigg 2011), has motivated the search for alternative sources of energy since fossil fuels are a finite resource and its use is contributing to global warming and environmental and economic impacts. Solar energy, as one of the most abundant renewable energy sources, opened

the door for sustainable and clean energy provision. Concentrating Solar Thermal (CST) systems, concentrate the solar radiation using reflective surfaces to generate thermal energy. Due to the intermittent nature of the solar resource new approaches are being developed to increase solar share and guarantee firm supply. CST systems can greatly benefit from hybridisation and thermal storage as methods to overcome this problem (Lovegrove & Pye 2012; Sheu et al. 2012). One solution, to address the intermittent nature of CST, is the use of a backup system where an auxiliary fossil-based energy device is maintained for the time when solar energy resource is not enough. Hybrid concepts such as solar with the combustion of renewable or fossil fuels and wind energy are some of the proposed combinations and it is believed to be a promising combination. Integration of CST into a conventional fossil-fuel-powered plant has been suggested to overcome the problems of the continuous dispatch of power or thermal energy (Sheu et al. 2012). The newly developed, hybrid solar receiver combustor (HSRC) concept provides a unique, cost-effective solution for the aforementioned problem. Integrating the combustion energy source into the cavity receiver opens the way for a mixed mode of operation, combustion and CST. For the mixed mode, a strategy is needed to fluidically seal the aperture to prevent hot gases escaping from the cavity and cold air entering from the outside (due to the wind and the internal flow pattern), in order to minimize losses and ensure efficient operation. However, to the best of the authors' knowledge, there are no known fluidic seals for the mixed-mode solar hybrid application. To design hydrodynamic sealing strategies for cavity receivers, investigation of the fluid flow behaviour of the hybrid solar cavity receivers is essential.

Therefore, the aim of the current study is to investigate the flow behaviour inside a cavity equipped with lateral jets with an outlet, and open aperture interacting with the flow outside the cavity. In the literature, many studies have been carried out to investigate the physics of turbulent jets (Dahm & Dimotakis 1987; Zhu & Shih 1994). From another point of view, some studies have been conducted to present the behaviour of flow induced by multi jets (Gao et al. 2013; Long, S. et al. 2018; Thong et al. 2015). The iso-thermal flow characteristics within a cylindrical chamber including multiple planar symmetric jets have also been investigated in a joint experimental and numerical study by Long et al. (Long, Shen et al. 2017). The results show the great dependence of the flow field on the inclination angle of the jets and the number of the jets. In another study, Long et al. (Long, S. et al. 2018) investigated the interaction between four rotationally symmetric jets within a cylindrical cavity. They found that the mean and root-mean-squared- fields are significantly depended on the azimuthal angle and inclination angle of the jets. Based on their findings three different flow regimes within the cavity were identified for different jets configurations. However,(Long et al.2017) have not assessed the flow regimes within a cavity with an open aperture. Furthermore, the interaction of internal and external flows has not been investigated yet.

In this paper, the flow behaviour of a cavity with an open aperture is investigated both inside the cavity and in the vicinity of the aperture. In order to characterise the flow behaviour and identify the key controlling parameters on the velocity field, extensive experimental investigations were conducted. The effect of the external flow on flow exchange through a solar cavity receiver aperture is investigated.

2. Experimental Setup

The measurements described here have been carried out in the water channel of the University of Adelaide. The water channel can be operated at speeds of up to V_s= 0.3 m/s. The rectangular test section is 2.0 m long with a cross-section of 0.5 m × 0.5 m.

A scaled down model of the cavity receiver has been designed and built as illustrated in Figure1 and Table1. The device consisted of a cylindrical chamber and 4 planar pipes, with an inner diameter of 3.35 mm, injecting external fluids into the 'cavity model' simulating fuel and air injection jets. The cylindrical part of the device was made of acrylic and had a similar refractive index as water which allowed it to be used with water as the working fluid and the application of laser-based techniques such as PIV. The green squares show the regions of interest for visualizing the flow. The arrangements of the jets were produced utilizing 3-D printing technique and were installed on the same cavity. The internal diameter of the cavity was 74 mm with a 3 mm wall thickness and 225mm long. The outlet of the cavity was an annular gap with 3 mm width. The inlet to the cavity was partially covered with a straight desk which had an aperture of 24.6 mm diameter. The device was submerged in the water held by a specially designed holder. To prevent the wall effects, the blockage ratio of the test section was kept small enough at below 7.2%.

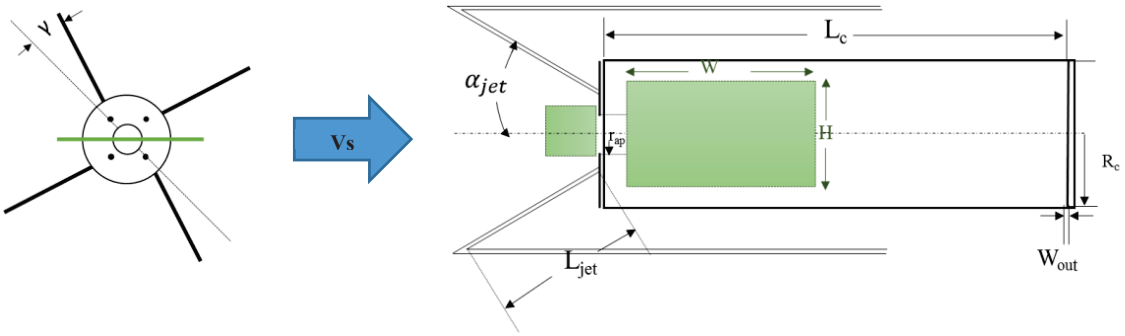

Figure 1. Schematic diagram of the experimental model showing key geometric features of the configuration

Table 1. Values of the geometric parameters of the experimental configuration

Geometric Parameter	value	Description	Geometric Parameter	value	Description
L_c	225 mm	The length of the cavity	D_{jet}	3.35 mm	The diameter of the nozzle
R_c	37 mm	The radius of the cavity	R_{ap}	12.3 mm	The radius of the aperture
L_{jet}	150 mm	The length of the jet supply pipe	α_j	25°	Jet inclination angle
W_{out}	3 mm	The width of the outlet for the exhaust	γ_j	5°	Jet azimuthal angle

Four lateral jets with an inclination angle of 25° and two different azimuth angle of 5° injected the water with jet outlet velocity (V_j) of 2.8 m/s resulting in a volume flow rate of 1.41 L/min for each jet and the Reynolds number of 10,500. Seeded water was pumped from the water channel tank to the jets through two flowmeters. Each flowmeter supplied two of the jets in order to reach equal flow rates through four jets. To ensure the equal flow rate from each jet, the outlet flow rate of each jet were measured. Figure 2 schematically illustrates the PIV setup that was used to measure the instantaneous velocity field in the entrance of the cavity and inside the cavity. The water was seeded with polyamide seeding particles with a mean diameter of 50 µm and the density of 1.03 g/cm^3. It is worth noting that the water within the channel is circulated back into a reservoir creating a closed loop operation. The stream velocity was set to 0.0 m/s and 0.24 m/s for different experimental cases. The seeds are added to the reservoir at the start of the test campaign, in order to provide a continuous seeding of the flow.

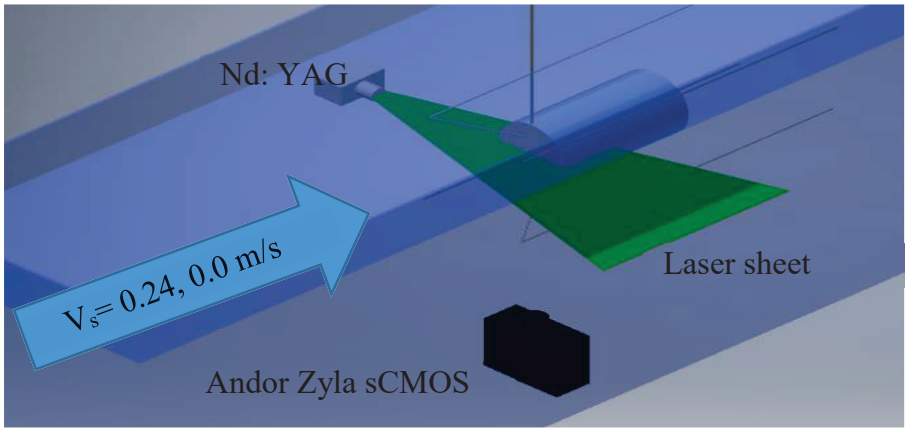

Figure 2. Schematic diagram of PIV setup

The flow field was illuminated with a laser sheet from a double-pulsed Nd: YAG laser source (Quantel Evergreen 200-200 mJ) at 532 nm wavelength. The sheet was located parallel to the bottom surface of the channel at a height of 200 mm and coincide with mid-plane of the cylinder. The two successive laser beams were formed using suitable optical components to give horizontal laser sheets with a thickness of ~2 mm. The images were acquired at a rate of 15 Hz for all measurements and the time between laser pulses was set to 4ms and 0.15 ms for outside and inside measurement, respectively. The images were recorded by the sCMOS camera (Andor Zyla 5.5) with 5.5-megapixel resolution, capturing images through the Andor SOLIS image capturing software. The camera was installed in the side view of the water channel recording the images from the bottom side of the water channel using a mirror located at 45-degree angle in the bottom side of the channel. In order to synchronize the data acquisition, the laser and the camera were connected to a pulse generator (Berkeley Nucleonics, Model 565). For each measurement case, 500 successive image pairs were captured. The PIV images of the test section occupy an area of 1850 × 950 pixels and 500× 500 pixels for the measurements of inside and outside of the cavity, respectively. The image processing was carried out using the PIVlab toolbox of MATLAB (Thielicke & Stamhuis 2014). 2-D velocity vectors were obtained using an interrogation window size of 64×64 pixels with an overlap of 50%.

The measurements of the experiments are subject to some uncertainties come from both measuring instruments and manufacturing process. The measurement uncertainty arises from flowmeters estimated to be around 1%. The measurement error of the stream velocity of the water channel found to be 0.8%. A grid plate was used for the calibration process required for image processing. The error caused by inaccuracy of the spatial resolution is 1.25%. Particle image processing is companied by an error of around 1/10 of the seed particle diameter. Therefore the experimental error caused by the particle size is 1%. Therefore, the overall uncertainty of the measured mean velocities for the present study is estimated to be less than ±5%.

3. Results and discussions

Figure 3 shows the measured time-averaged normalized velocity contours inside the cavity, for the cases a) $\alpha_j = 25°, \gamma_j = 5°$, blocked aperture b) $\alpha_j = 25°, \gamma_j = 5°$, V_s=0.0 m/s c) $\alpha_j = 25°, \gamma_j = 5°$, V_s=0.24 m/s. The velocity vector is equal to $V = \overrightarrow{V_x} + \overrightarrow{V_y}$, where V_x and V_y are the velocity components of the section and are normalized by the outlet velocity of the jet (V_j). The figure also shows the vectors of the normalized axial velocity vectors in the measured region. It can be seen that by opening the aperture the velocity in the vicinity of the aperture inside the cavity increases. Moreover, introducing the external velocity into the cavity is followed by a slight movement of the higher axial velocity regions towards the downstream.

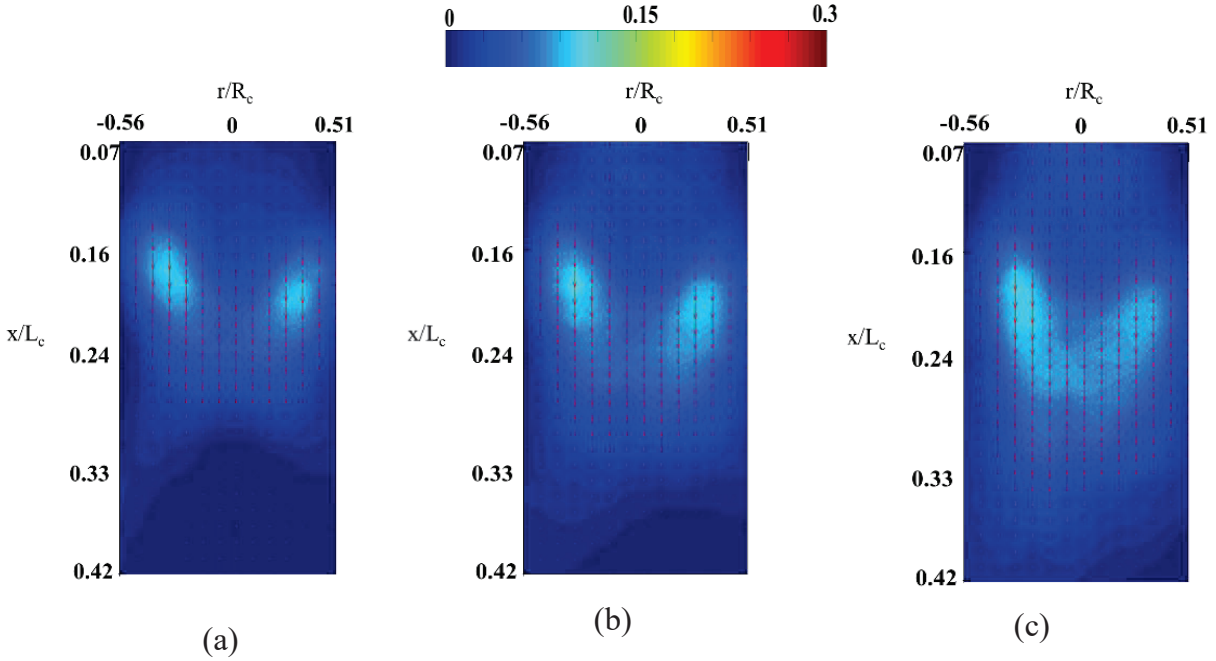

Figure 3. Measured time-averaged and normalized velocity contours inside the cavity, for the case of $\alpha_j = 25°, \gamma_j = 5°$,a)blocked aperture, b) V_s=0.0 m/s and c) V_s=0.24 m/s.

Figure 4 presents the streamlines of the experimental cases marked by the arrows on the lines showing the flow direction. It can be seen that by opening the aperture the flow structure inside the cavity changes and the length of the recirculation zones expand. The induced external flow also pushes the recirculation zones away from the centerline of the cavity.

Figure 5 shows the spatial variation of the normalized axial velocity along the centerline of the cavity from $\frac{x}{L_c} = 0.05$ to $\frac{x}{L_c} = 0.45$ for different the experiments. It can be seen that for the case with the blocked aperture the peak occurs in the distance equal to $\frac{x}{L_c} = 0.22$. By opening the aperture the velocity in the vicinity of the aperture increases. It also shows that even by opening the aperture with no external velocity conditions, the flow is 'sucked' into the cavity due to the negative pressure induced by the internal flow close to the aperture. By increasing the external velocity to 0.24 m/s, the velocity along the centerline increases. It is worth noting that the peak value occurs at distances further downstream. However, for all three cases, the axial velocity follows a similar trend. Another visible feature is the increase in maximum normalized velocity along the centerline of the cavity from 0.055 to 0.086 for the case with blocked aperture and open aperture with an external velocity of 0.24 m/s.

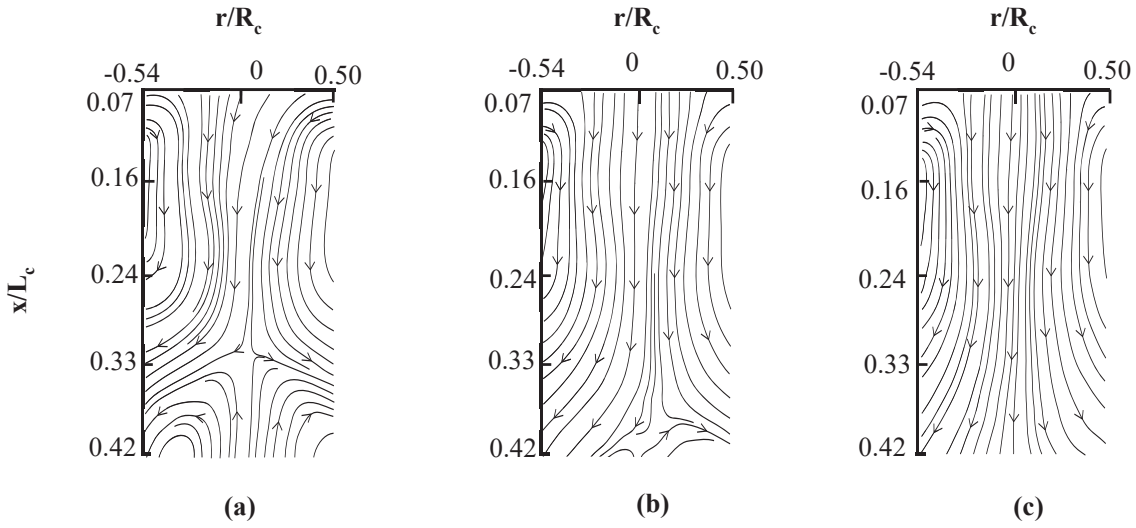

Figure 4. Measured time averaged streamline for the case of α_j = 25°,γ_j = 5° (a) blocked aperture b) V_s=0.0 m/s c) V_s=0.24 m/s.

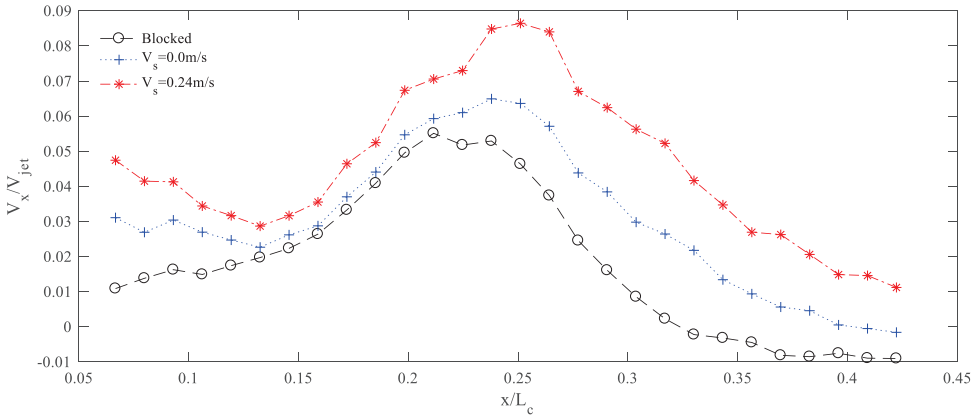

Figure 5. Evolution of normalized mean axial velocity (V_x) by the mean jet outlet velocity (V_j) along the centreline of the cavity for the different cases of α_j = 25°, γ_j = 5° (blocked aperture / V_s=0.0 m/s / V_s=0.24 m/s).

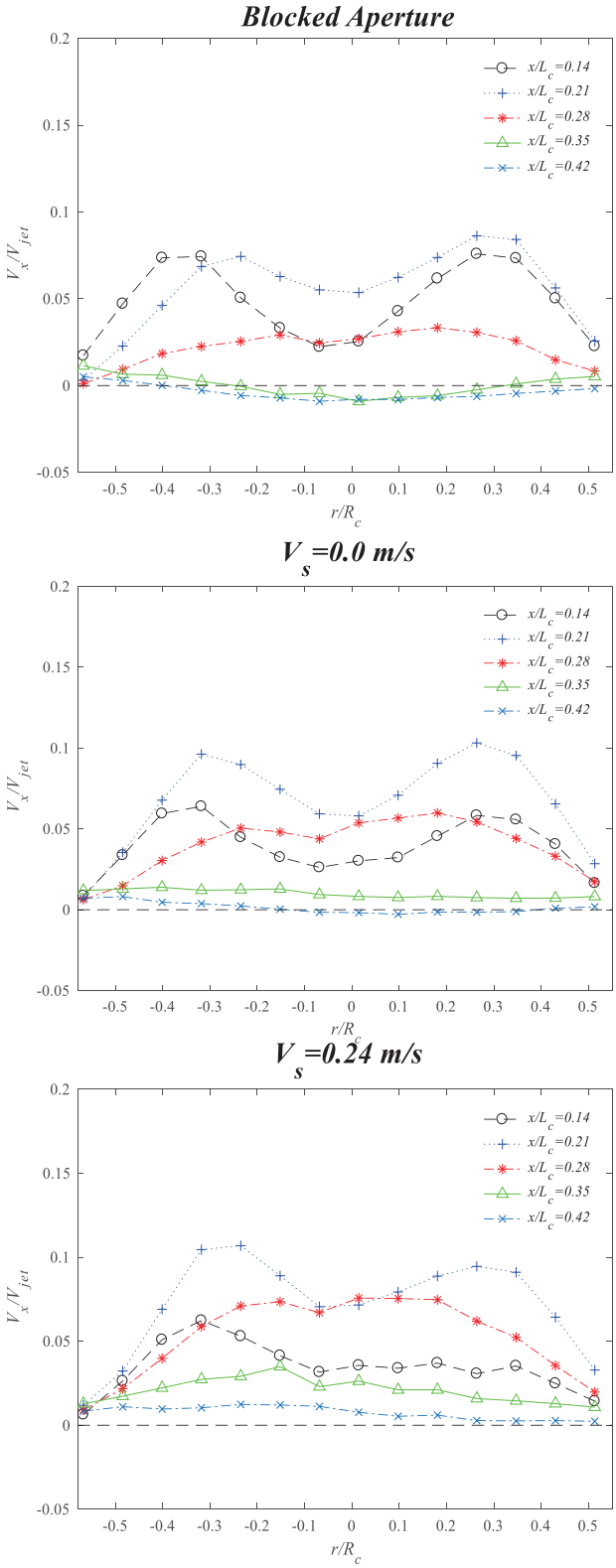

Figure 6. The radial profile of mean axial velocities (V_x) normalized by the mean jet velocity (V_j), in five different sections along the cavity (x/L_c =0.14, x/L_c =0.21, x/L_c =0.28, x/L_c =0.35, x/L_c =0.42)

Figure 6 presents the radial profile of axial velocities (V_x) normalized by the mean jet velocity (V_j), in five different locations along the cavity (x/L_c =0.14, x/L_c =0.21, x/L_c =0.28, x/L_c =0.35, x/L_c =0.42). The results presented here are consistent with the results shown by Long et al. (Long, S. et al. 2018) for the blocked aperture and shows a bifurcate profile of normalized axial velocity at x/L_c =0.14 and x/L_c =0.21. As seen in the figure, similar trends are observed for all cases including blocked aperture, no external velocity and stream velocity of 0.24 m/s. It shows that although opening the aperture causes some minor changes in peak velocity and flow behaviour, it does not change the velocity fields significantly. The calculation of the mass flow rate through the aperture for the cases with Vs=0 m/s and Vs= 0.24 m/s shows that opening the aperture causes an external flow rate equal to 35% and 58% of total mass flow rate from the four jets, respectively.

4. Conclusions

An experimental investigation was carried out to reveal the interaction of the internal and external flows within a scaled down model of a Hybrid Solar Receiver Combustor (HSRC) equipped with four jets, jet inclination angle of 25° and azimuth angles of 5°. The PIV technique was used in the water channel with stream velocity of 0.0 m/s and 0.24 m/s. It is revealed that although the general flow field does not change by opening the aperture, the position of the recirculation zones inside the cavity changes. In addition, increasing the external velocity leads to changes in the flow patterns and the structure of recirculation zones. The results show that the present nozzle configuration with an open aperture causes a significant mass flow into the cavity through the aperture. This implies that the optimal configuration for the device is different for the cases with and without an open aperture. It is also found that by increasing the stream velocity from 0.0 m/s to 0.24 m/s, the normalized mass flow rate through the aperture increases by 60%. In addition, these results highlight the need for developing a fluidic seal that can prevent or minimize the ingress of external air into the cavity receiver, especially those with an internally induced flow like the HSRC.

References

Dahm, WJA & Dimotakis, PE 1987, 'Measurements of entrainment and mixing in turbulent jets', *AIAA Journal*, vol. 25, no. 9, 1987/09/01, pp. 1216-1223.

Gao, Z, Han, J, Xu, Y, Bao, Y & Li, Z 2013, 'Particle Image Velocimetry (PIV) Investigation of Flow Characteristics in Confined Impinging Jet Reactors', *Industrial & Engineering Chemistry Research*, vol. 52, no. 33, 2013/08/21, pp. 11779-11786.

Long, S, Lau, T, Chinnici, A, Tian, Z, Dally, B & Nathan, GJ 2018, 'Iso-thermal flow characteristics of rotationally symmetric jets generating a swirl within a cylindrical chamber', American Institute of Physics, *Physics of Fluids,* vol. 30,p 055110.

Long, S, Lau, TCW, Chinnici, A, Tian, ZF, Dally, BB & Nathan, GJ 2017, 'Experimental and numerical investigation of the iso-thermal flow characteristics within a cylindrical chamber with multiple planar-symmetric impinging jets', *Physics of Fluids*, vol. 29, no. 10, p. 105111.

Lovegrove, K & Pye, J 2012, '2 - Fundamental principles of concentrating solar power (CSP) systems', *Concentrating Solar Power Technology*, Woodhead Publishing, pp. 16-67.

Sheu, EJ, Mitsos, A, Eter, AA, Mokheimer, EMA, Habib, MA & Al-Qutub, A 2012, 'A Review of Hybrid Solar–Fossil Fuel Power Generation Systems and Performance Metrics', *Journal of Solar Energy Engineering*, vol. 134, no. 4, pp. 041006-041006-041017.

Stulz, R, Tanner, S & Sigg, R 2011, 'Chapter 16 - Swiss 2000-Watt Society: A Sustainable Energy Vision for the Future', in FP Sioshansi (ed.), Energy, *Sustainability and the Environment,* Butterworth-Heinemann, Boston, pp. 477-496.

Thielicke, W & Stamhuis, EJ 2014, 'PIVlab – Towards User-friendly, Affordable and Accurate Digital Particle Image Velocimetry in MATLAB', *Journal of Open Research Software*, vol. 2.

Thong, CX, Kalt, PAM, Dally, BB & Birzer, CH 2015, 'Flow dynamics of multi-lateral jets injection into a round pipe flow', *Experiments in Fluids*, vol. 56, no. 1.

Zhu, J & Shih, TH 1994, 'A Numerical Study of Confined Turbulent Jets', *Journal of Fluids Engineering,* vol. 116, no. 4, pp. 702-706.

Experimental Investigation on the Influence of an Air Curtain on the Convective Heat Losses from Solar Cavity Receivers under Windy Condition

Elham Alipourtarzanagh[1], Alfonso Chinnici, Graham J. Nathan and Bassam B. Dally

[1] School of Mechanical Engineering, Centre for Energy Technology, The University of Adelaide, SA 5005, Australia.

[a)]Corresponding author: elham.alipour@adelaide.edu.eu

Abstract. An experimental study is performed to measure the convective heat losses from a heated solar cavity receiver with an air curtain. The air curtain is a plane jet blowing downward across the aperture to mitigate the convective heat losses. The cavity is placed in an open section of a wind tunnel to provide a controlled environment for measurement of the influence of winds speed of 0 m/s, 6 m/s and 9 m/s on the performance of the air curtain. The velocity of the air curtain was varied from 9 m/s to 18 m/s with two different discharge angles of 0° and 30°. The results show that for a head-on wind condition, the air curtain with a discharge angle of 30° has a better performance than that with a discharge angle of 0°. The use of curtain was found to reduce the natural and mixed convective heat losses between 40% and 66% relative to the case without an air curtain. The heat losses distribution on the surface of the cavity was also measured, which revealed that heat losses are greatest from the lower part of the cavity.

INTRODUCTION

In recent years, interest in solar thermal cavity receivers is growing as the cavity receivers achieve temperatures from 800° C to well over 1000° C. The solar energy absorbed by cavity receivers can be used for different downstream applications such as electricity generation or thermal storage by use of storage mediums [1]. Convective heat losses from solar cavity receivers are a significant part of heat losses that affect the thermal efficiency. Many studies have been conducted to quantify the effect of different parameters on the convective heat losses from cavity receivers. Some research has been conducted to investigate the effect of operating conditions such as wind speed and direction, the tilt angle of the cavity and the internal thermal distribution on convective heat losses [2-5]. While others investigated the effect of geometrical parameters of the cavity such as the design of the cavity [6], aspect ratio [5] and aperture ratio [7] of the cavity on convective heat losses. In the literature, several solutions are suggested to mitigate the convective heat losses. For instance, the geometrical parameters are suggested to be chosen as per the findings of the literature [8]. Moreover, covering the cavity opening with a transparent window, partially covering the aperture [9] and the use of air curtains or aerowindow across the cavity [10] opening are suggested to increase the efficiency of the solar cavity receivers. Air curtains have been applied to buildings and industrial processes in the past to suppress convective heat losses through the main doors or opening [11]. However, there are significant differences between the shape and orientation of a cavity receiver relative to a building, so that these previous results are not directly applicable. Also, many possible configurations of air curtain are possible and no direct measurements of the effectiveness of any of these are available for a solar cavity receiver.

The application of air curtain in solar cavity receivers has also been investigated through numerical and analytical studies and is found to be economically viable [12, 13]. The aim of employing air curtains to the aperture of the solar

receivers is to inhibit the hot air from leaving the cavity and prevent the cold air entering cavity. Numerical analysis of applying active airflow in the vicinity of a cavity receiver [14] showed that convective heat losses could be reduced by 50% in a solar cavity receiver and the importance of applying air curtain with optimum jet speed and direction is highlighted. However, there is a lack of experimental evidence in the literature to show the effect of variation of the velocity and inclination angle of air curtain on convective heat losses from solar cavity receivers.

In summary, to the best of our knowledge, no previous experimental data are available investigating the influence of an aerodynamic curtain on the convective heat losses from a solar cavity receiver. Therefore the aim of the present investigation is to meet this need.

METHODOLOGY

An experimental campaign is conducted on an electrically heated cavity receiver in an open section of the large wind tunnel of the University of Adelaide with a cross-section of 2.75 m × 2.19 m. The average wind speeds used in the experiments are 0 m/s, 3 m/s, 6 m/s and 9 m/s. The cavity has a length of 0.45 m, a diameter of 0.3 m and an aperture of 0.10 m. The details of the experimental heated cavity used in the current study have been published previously by Lee et al [3]. Figure 1 illustrates a schematic diagram of the cavity and air curtain (AC) used in the current study

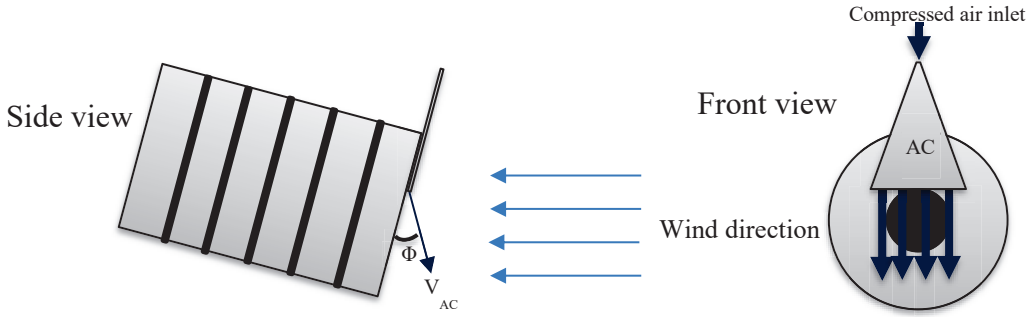

FIGURE 1. Schematic diagram of the experimental setup.

The tilt (θ) and yaw (α) angle of the cavity are set to 15° and 0°, respectively for all experimental cases investigated in the current study. The projected area of the cavity to the open section of the wind tunnel is about 4.1% which is small enough to avoid blockage effect. The internal walls of the cavity are consist of copper plates which are heated with 16 electric strip heaters. Each heater is maintained at a constant uniform temperature of 300°C by using a feedback controller system which records the supplied power to each heater. A set of 16 K-type thermocouples are attached to the heaters to measure the temperature. The temperature of each heater is recorded by Datataker DT85 and is used for the temperature feedback control system using MATLAB and Simulink. A specially designed air curtain is attached at a position above the aperture. The air curtain has an outlet gap of 2 mm width and a length of 165 mm. The resulting air flow is reasonably uniform with the outlet velocity of 20±0.4 m/s. A Kaeser rotary screw compressor SM 9 is used to provide the compressed air through the air curtain.

The minimum deflection modulus method proposed initially by Hayes and Stoecker [15, 16] and modified by Zhang et al. [17] is used to define the required minimum velocity of the air curtain to form a stable aerodynamic barrier across the aperture. It is found that a minimum velocity of 18 m/s at a wind speed of 9 m/s is required to reach a stable virtual wall. Therefore, the air jet velocities of 9 m/s and 18 m/s are applied for different experimental cases to investigate the effect of discharge velocity of the air curtain. The volumetric air flow rate is controlled using Alicat Scientific MCR-1000SLPM to 160 SLPM and 320 SLPM corresponding to the air velocity of 9 m/s and 18 m/s, respectively.

The total heat losses from the cavity are a combination of the conduction, convection and radiation heat losses. By closing the aperture under the same experimental conditions, conduction heat losses are measured. The radiation heat losses are calculated as a fourth-order dependence on temperature. The convection heat losses then are determined by

subtraction of conduction and radiation heat losses from total heat losses.

$$Q_{conv} = Q_{total} - (Q_{cond} + Q_{rad})$$

RESULTS AND DISCUSSIONS

Figure 2 presents the measured absolute convective heat losses (W) from a cavity receiver with and without an air curtain. Two jet discharge angles of a) $\Phi = 30°$ and b) $\Phi = 0°$ and different wind speeds of 0 m/s, 6 m/s and 9 m/s are tested for the air curtain velocity of 9 m/s and 18 m/s.

It is apparent from the figure that the convective heat losses for a discharge angle of 30° are less than those for a discharge angle of 0° under all experimental conditions. Moreover, results show that at a discharge angle of 30°, an increase in the velocity of the air curtain for all wind speeds results in a reduction in the convective heat losses. This can be justified by the effect of air curtain as an aerodynamic barrier in the vicinity of the aperture which mitigates the transfer of hot air to the surrounding of the cavity from the upper part of the aperture. It increases the stagnation zone inside the cavity by trapping the hot air inside and as a result, the convective heat losses reduce. Nevertheless, for Φ=0°, increasing the velocity of the air curtain results in a growth in convective heat losses. For example for the wind speed of 0 m/s, employing an air curtain at V_{ac} = 18 m/s increases the convective heat losses from 262 W for no air curtain case to 375 W. The reason is that at a discharge angle of 0° and under high velocity as the jet spreads downstream a great amount of cold air from the air curtain is mixed with the hot air from the interior section of the cavity and this is followed by a drop in the performance of the air curtain.

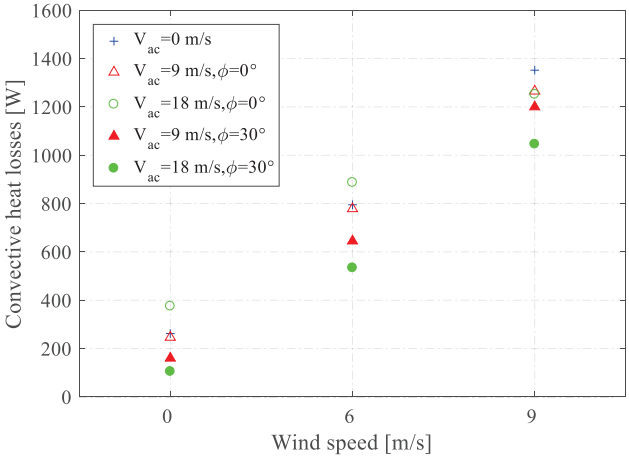

FIGURE 2. Measured convective heat losses from a cavity with and without air curtain at wind speeds of 0 m/s, 6 m/s and 9 m/s. at $\Phi = 0°$ and 30°. Test conditions: $\alpha = 0°$, T = 300° C, $\theta = 15°$.

To get a better insight of the convective losses from different parts of the cavity, the heaters on the inner side of the cavity are divided into five different sections including upper rear, upper front, lower rear, lower front and back plate. Figure 3a presents the relative natural convective heat losses from different sections of the cavity at V_{ac}= 0 m/s (no air curtain), 9 m/s and 18 m/s to the natural convective heat losses of no air curtain. The total natural convective heat losses from the cavity are also presented in Figure 3b. As it is mentioned above, the air curtain has a better performance at a discharge angle of 30°, therefore the results for $\Phi = 30°$ are presented here. Figure 3a shows that as the velocity of the air curtain increases the convective heat losses from all sections of the cavity except the back plate decrease constantly. As it is shown in Figure 3b, by employing an air curtain with a velocity of 18 m/s the total convective heat losses decrease by 157 W. A significant part of this decrease occurs at the lower front section which is more than 60% of total convection losses reduction. The relative convective heat losses from each section of the cavity to the total convective heat losses for each experimental case are presented in Table 1. As can be seen from the table, the lower front part of the cavity contributes the most to the convective heat losses within the cavity for all experimental cases.

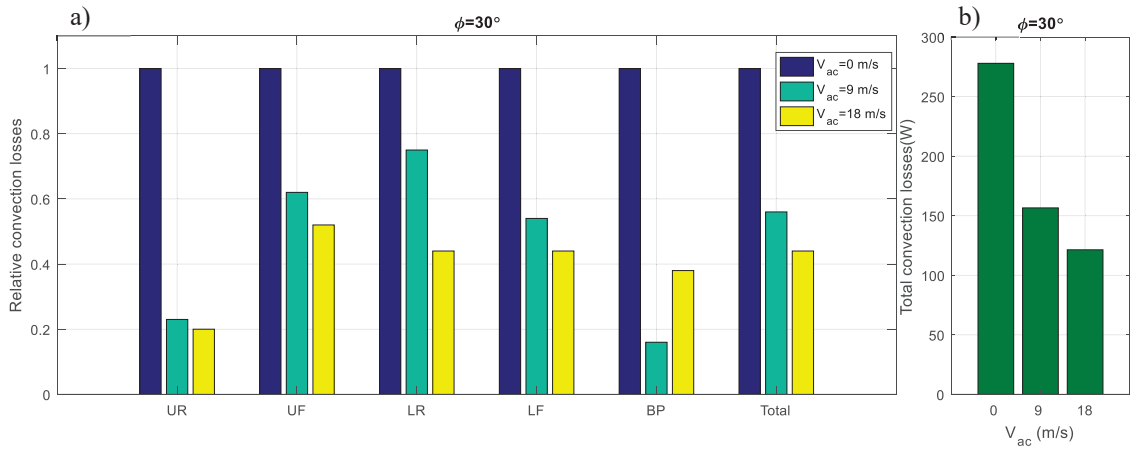

FIGURE 3. a) The relative partial and total natural convective heat losses at V_{ac}= 0 m/s, 9 m/s and 18 m/s to those at no air curtain condition, b) Absolute natural convective heat losses from cavity at different velocity of air curtain of 0 m/s, 9 m/s and 18 m/s at discharge angle of 30°. (UR: Upper Rear, UF: Upper Front, LR: Lower Rear, LF: Lower Front, BP: Back Plate).

TABLE 1. Percentage of natural convective heat losses from each section of the cavity for the different experimental cases with V_{ac}=0 m/s, 9 m/s and 18 m/s at Φ=30°.

V_{ac}	Upper Rear	Upper Front	Lower Rear	Lower Front	Back Plate
0 m/s	3	7	22	63	5
9 m/s	1	8	29	60	1
18 m/s	1	8	22	64	4

The variation of the convection losses from different sections of the internal surface of the cavity at V_{ac}= 18 m/s for both discharge angles of Φ=0° and 30° are illustrated in Figure 4a. As the figure presents, as the discharge angle increases from 0° to 30°, the total convective heat losses decrease by 70%. The main reduction occurs at the lower sections of the cavity which are mainly involved with the turbulence of the flow from the air curtain at a discharge angle of 0°. This highlights the importance of use an air curtain at a proper discharge angle to mitigate the convective heat losses.

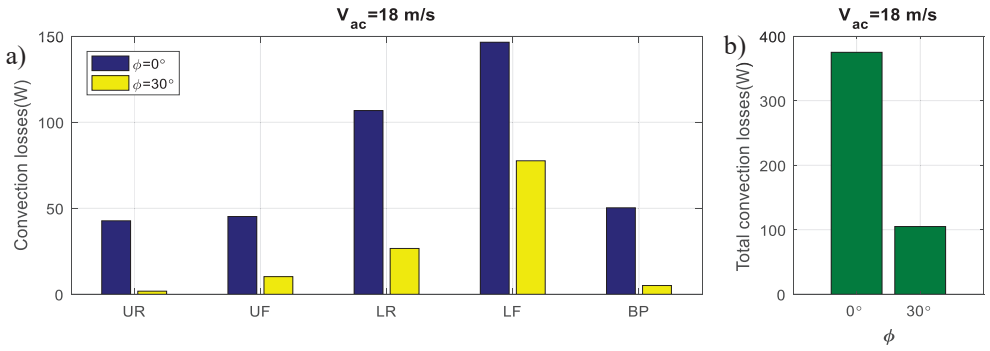

FIGURE 4. The variation of natural convective heat losses from a) different sections of a cavity and b) total cavity surface at V_{ac}=18 m/s for two different discharge angles of 0° and 30°. (UR: Upper Rear, UF: Upper Front, LR: Lower Rear, LF: Lower Front, BP: Back Plate).

The measured distribution of relative heat losses from different sections of the cavity to total convective heat losses with and without an air curtain at a wind speed of 9 m/s where the forced convective heat losses are dominant are presented in Figure 5a. As the figure illustrates, in general, by applying an air curtain the convective heat losses from all different sections of the cavity reduce. As the velocity of the air curtain increases the convective heat losses decline gradually. However, the current study examined a limited increase in the velocity of the air curtain and the effect of a further increase of the air curtain on convective heat losses needs to be investigated.

Table 2 presents the percentage of the convective heat losses from different sections of the cavity for each experimental case. As the table depicts, consistent with no wind condition, the maximum convective heat losses are from the lower front part of the cavity. This highlights the importance of developing a strategy which mitigates the convective heat losses from the lower part of the cavity. For instance, using an air curtain, blowing from the lower side of the aperture upward has the potential to reduce the convective heat losses [10] and it can lessen the convective heat losses from the lower part by preventing the cold air entrainment into the cavity from the lower part.

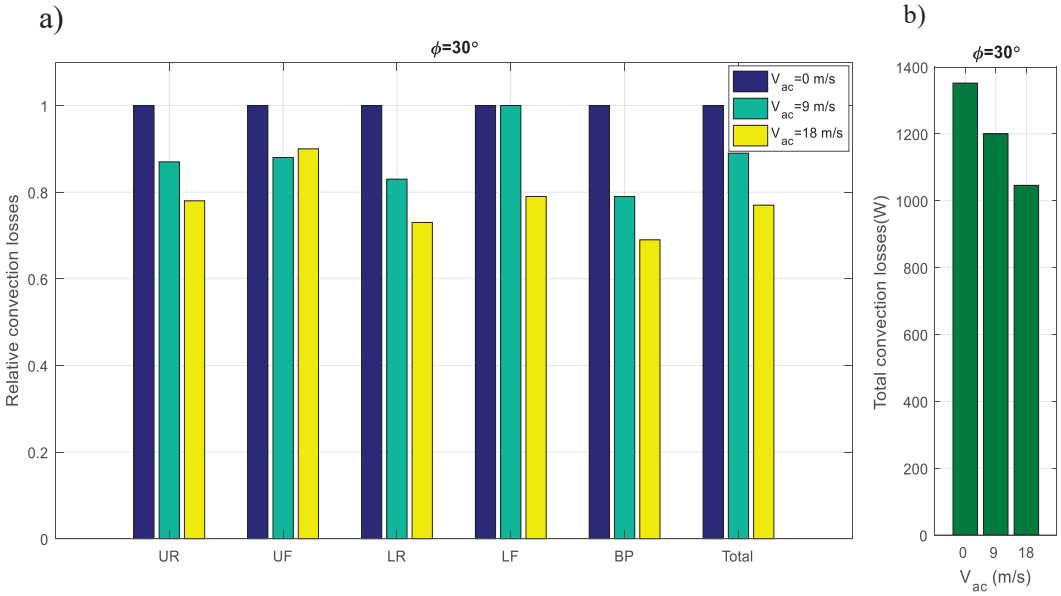

FIGURE 5. a) The relative partial and total convective heat losses at V_{ac}= 0 m/s, 9 m/s and 18 m/s to those at no air curtain condition, b) Absolute convective heat losses form the cavity at different velocity of air curtain of 0 m/s, 9 m/s and 18 m/s at discharge angle of 30° and wind speed of 9 m/s. (UR: Upper Rear, UF: Upper Front, LR: Lower Rear, LF: Lower Front, BP: Back Plate)

TABLE 2. Percentage of convective heat losses from each section of the cavity for the experimental cases with V_{ac}=0 m/s, 9 m/s and 18 m/s at Φ = 30° and wind speed of 9 m/s.

V_{ac}	Upper Rear	Upper Front	Lower Rear	Lower Front	Back Plate
0 m/s	18	16	27	28	13
9 m/s	17	16	25	32	11
18 m/s	18	18	25	28	12

The variation of the convective heat losses from different sections within the cavity by use an air curtain at a velocity of 18 m/s and two different discharge angles of 0° and 30° is illustrated in Figure 6a. The total convective heat losses from the cavity corresponding to the cases presented in Figure 6a are presents in Figure 6b. As the figure presents by varying the discharge angle of the air curtain, the convection losses from all sections of the cavity decrease. However, the total convective heat losses reduce by 16% which is significantly less than that for no wind condition. This shows that the improvement in the performance of the air curtain through the variation of the discharge angle at higher wind speeds decreases.

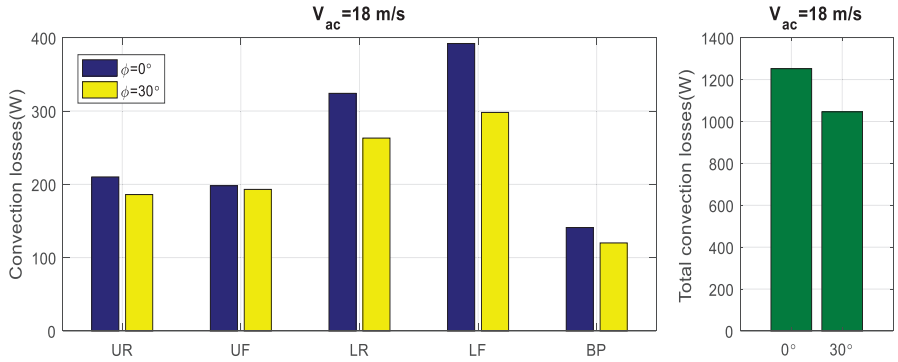

FIGURE 6. a) Absolut convective heat losses (w) from different sections of a cavity b) Total absolute convective heat losses (W) at wind speed of 9 m/s for the velocity of air curtain of 18 m/s and two discharge angles of 0° and 30°. (UR: Upper Rear, UF: Upper Front, LR: Lower Rear, LF: Lower Front, BP: Back Plate).

CONCLUSIONS

In conclusion, the use of an air curtain has found to generate a complex influence on convective heat losses, which vary with the wind speed, velocity and angle of the air curtain. It is found that using an air curtain with an angle of 30° outward the aperture yields better performance than one aligned parallel to the face of the receiver. However, for high external wind speeds the effect of the discharge angle is less than the low wind speed cases. In the best case of the configuration investigated here, the natural convective heat losses were lowered by 60% and the mixed heat losses were reduced by 32 %. The distribution of heat losses from different sections of the cavity reveals that the lower front part of the cavity is the most critical section as it has the highest convective heat losses even after the application of a downward-blowing an air curtain. It is investigated that the greatest reduction of convective heat losses by use of an air curtain occurs at the lower section of the cavity.

REFERENCES

1. H. M.-S. FREng and F. Trieb, "Concentrating solar power: A review of the technology," Ingenia Inform QR Acad Eng, vol. 18, pp. 43-50, 2004.
2. A. M. Clausing, "An analysis of convective losses from cavity solar central receivers," Solar Energy, vol. 27, pp. 295-300, 1981.
3. K. L. Lee, A. Chinnici, M. Jafarian, M. Arjomandi, B. Dally, and G. Nathan, "Experimental investigation of the effects of wind speed and yaw angle on heat losses from a heated cavity," Solar Energy, vol. 165, pp. 178-188, 2018.
4. K. L. Lee, A. Chinnici, M. Jafarian, M. Arjomandi, B. Dally, and G. Nathan, "The influence of wall temperature distribution on the mixed convective losses from a heated cavity," Applied Thermal Engineering, vol. 155, pp. 157-165, 2019/06/05/ 2019.

5. K. L. Lee, A. Chinnici, M. Jafarian, M. Arjomandi, B. Dally, and G. Nathan, "The influence of wind speed, aperture ratio and tilt angle on the heat losses from a finely controlled heated cavity for a solar receiver," Renewable Energy, vol. 143, pp. 1544-1553, 2019.
6. R. D. Jilte, S. B. Kedare, and J. K. Nayak, "Investigation on Convective Heat Losses from Solar Cavities under Wind Conditions," Energy Procedia, vol. 57, pp. 437-446, 2014.
7. K. L. Lee, M. Jafarian, F. Ghanadi, M. Arjomandi, and G. J. Nathan, "An investigation into the effect of aspect ratio on the heat loss from a solar cavity receiver," Solar Energy, vol. 149, pp. 20-31, 2017.
8. S.-Y. Wu, L. Xiao, Y. Cao, and Y.-R. Li, "Convection heat loss from cavity receiver in parabolic dish solar thermal power system: A review," Solar Energy, vol. 84, pp. 1342-1355, 2010.
9. R. Uhlig, R. Flesch, B. Gobereit, S. Giuliano, and P. Liedke, "Strategies Enhancing Efficiency of Cavity Receivers," Energy Procedia, vol. 49, pp. 538-550, 2014.
10. S. Yang, J. Wang, P. D. Lund, S. Wang, and C. Jiang, "Reducing convective heat losses in solar dish cavity receivers through a modified air-curtain system," Solar Energy, vol. 166, pp. 50-58, 2018.
11. S. Goubran, D. Qi, W. F. Saleh, L. Wang, and R. Zmeureanu, "Experimental study on the flow characteristics of air curtains at building entrances," Building and Environment, vol. 105, pp. 225-235, 2016.
12. R. T. Taussig, "Aerowindows for central solar receivers," American Society of Mechanical Engineers, Winter Annual Meeting, New Orleans, LA, , p. 12, Dec. 9-14, 1984 1984.
13. J. J. Zhang, J. D. Pye, and G. O. Hughes, "Active Air Flow Control to Reduce Cavity Receiver Heat Loss," p. V001T05A023, 2015.
14. J. P. Graham Hughes, Martin Kaufer, Ehsan Abbasi- Shavazi, Jack Zhang, Adam McIntosh, Tim Lindley, "Reduction of convective losses in solar cavity receivers," presented at the SolarPACES 2015, Cape Town, South Africa, 2015.
15. F. C Hayes and W. F. Stoecker, "Heat transfer characteristics of the air curtain," vol. 2120, ed. ASHRAE Trans., 1969.
16. F. C Hayes and W. F. Stoecker, "Design data for air curtains," vol. 2121, ed: ASHRAE Trans, 1969.
17. L. Zhang, Z.-z. Yan, Z.-h. Li, X.-m. Wang, X.-f. Han, and J.-c. Jiang, "Study on the Effect of the Jet Speed of Air Curtain on Smoke Control in Tunnel," Procedia Engineering, vol. 211, pp. 1026-1033, 2018.

22nd Australasian Fluid Mechanics Conference AFMC2020
Brisbane, Australia, 7-10 December 2020
https://doi.org/10.14264/43dd30b

Impact of Yaw angle on the Effectiveness of an Air Curtain for Solar Cavity Receivers

E. Alipourtarzanagh[1], A. Chinnici[1], Z. Tian[1], G. Nathan[1] and B. Dally[1]

[1]Centre for Energy Technology, School of Mechanical Engineering

The University of Adelaide, South Australia 5005, Australia

Abstract

An experimental study was performed to quantify the effectiveness of an air curtain through the direct measurement of the convective heat losses from a scaled-down heated cavity receiver (0.3 m ID, 0.45 m length and 0.1 m aperture) in a large wind tunnel. The tilt angle of the cavity was kept constant at 15° while the yaw angle changed from 0° to 45° and 90° for wind speeds of 0, 3, 6 and 9 m/s. A blowdown purpose-designed air curtain was used to establish an aerodynamic barrier across the aperture of the cavity. The velocity of the air curtain flow was changed from 4.5 to 9 and 18 m/s with two different discharge angles of 0° and 30°. The results show that a low velocity side-wind decreases the convective heat losses. It is also found that the application of the blowdown air curtain with a side wind (yaw angles of 45° and 90°) increases the convective heat losses by 2.7 times over the no air curtain case for these conditions.

Keywords

Aerodynamics; convection; solar cavity receiver; air curtain; heat losses, thermal efficiency.

Introduction

The installation of Concentrated Solar Thermal energy (CST) technology, as an alternative to fossil based energy generation, has been growing steadily over the years to a worldwide installed capacity of 6.3 GW in 2019 [1]. Such a development is accompanied by the growth in the deployment of solar towers as a cost-effective way to achieve high temperatures at scales of order 100 MW. Solar tower systems include the three main components of a tower, a heliostat field and a central receiver. There are two main types of the solar tower central receiver, namely externally radiated and cavity receivers. The cavity type central receivers have the potential to provide an energy source for temperatures of up to ~1200℃ [2]. However, the losses from cavity receivers, comprising convection, conduction and radiation, reduce their thermal efficiency markedly [3]. The reduction of these losses, including convection losses as the most complex one, is driving technology development toward higher thermal efficiency and to secure cost reduction of the whole power plant. In this context, the application of fluidic barrier that can establish a transparent shield across the aperture in order to reduce convection heat losses, while permitting the solar radiation into the cavity, is being investigated [4].

The deployment of an air curtain as an aerodynamic barrier in the vicinity of the aperture of the solar cavity has been studied both experimentally and numerically [5-10]. It has been found that the velocity, the discharge angle, the orientation and the momentum of the curtain flow are parameters that influence the effectiveness of the air curtain. The operating conditions of the cavity are also found to affect the performance of the air curtain including the wind speed and tilt angle of the cavity. In our previous experimental study [7], it is found that the application of a downward blowing air curtain for the heated cylindrical cavity at a tilt angle of 15° and head-on wind conditions, reduces the natural convective heat losses by 60%. For the momentum dominated heat transfer regime reduction of 7% has been reported. However, the effect of wind direction on the performance of the air curtain was yet to be investigated.

Considering the practical operating conditions of the solar cavity receivers under the varying wind direction, this study aims to investigate the effect of wind direction on the effectiveness of a downward blowing air curtain.

Methodology

The current experiments were carried out in the open section of the large wind tunnel of the University of Adelaide using the experimental setup that was primarily composed of an electrically heated cavity receiver, power control system and an air curtain. The test section of the wind tunnel (3 m × 3 m) was used to provide air with a mean velocity of 0, 3, 6 and 9 m/s. A scale-down model of cylindrical solar cavity receiver (ID = 0.3 m, L = 0.45 m) was designed and built using 16 electrically heaters. An aperture with a diameter of 0.1 m was fitted on the front plane of the cavity. The details of the cavity have been previously provided by Lee *et al.* [11]. Hence, and for brevity, only an overview of the experimental apparatus is presented here. The internal surfaces of the cavity are composed of copper plates attached to the band heaters providing reasonably uniform temperature across each section of the internal surface. The power required to maintain the internal surface of the cavity at 300°C was measured and recorded for the steady-state of 300 s as it is defined in our previous work [7]. The external surfaces of the cavity were covered with insulating material to minimize the conductive heat losses. The cavity was manufactured on a standing frame so that the tilt angle of the cavity can be varied according to the experimental plan. The tilt angle of the cavity was fixed for all experimental cases investigated here at θ = 15°. The yaw angle of the cavity defined as the horizontal angle between the normal direction of the aperture plane and wind direction (α) varied between 0° to 90° by variation of the cavity position in the open test section of the wind tunnel (Figure 1).

An air curtain was engineered to provide airflow across a rectangular slit of 2 mm×165 mm with a mean outlet velocity of u_0 = 0, 4.5, 9 and 18 m/s consistent with our previous study [7]. A rotary screw compressor (Kaeser -SM9) was used to supply air into the inlet section of the air curtain. A flowmeter (Alicat Scientific MCR-1000 SLPM) was used to measure the volumetric airflow rates. The discharge angle of the air curtain (φ) was changed between 0° to 30° by rotating the air curtain around the pivot points on the upper side of the aperture.

The power control system measured the total power of each experimental case using K-type thermocouples, data logger, MATLAB and Simulink programs installed on a computer, Arduino and DMX (lighting boxes). The temperature of each internal surface of the cavity was measured using K-type thermocouples and was recorded by the data logger. These temperatures were used for the feedback control system which uses installed software on the computer. The output power

signal from the computer was controlled by Arduino and DMX lightning box.

The total power comprises the convective, conductive and radiative losses. Providing the equivalent experimental conditions for two cases with a closed aperture and open aperture, conductive heat losses could be obtained. The radiation losses could be calculated with high accuracy using the fourth power of the cavity temperature. By deduction of conductive and radiative losses, the convective losses of each experimental case were obtained (Equation1).

$$Q_{conv} = Q_{total} - (Q_{cond} + Q_{rad}). \quad (1)$$

The effectiveness (ε) of the air curtain is defined as the difference of the Q_{conv} of the cases with and without an air curtain relative to those of the equivalent case without an air curtain as the reference case:

$$\varepsilon = \frac{Q_{conv,ref} - Q_{conv,0}}{Q_{conv,ref}} \quad (2)$$

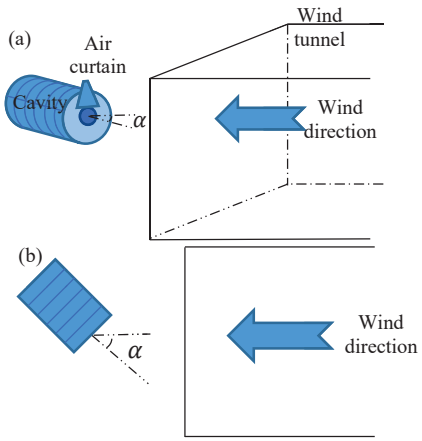

Figure 1. Schematic of the cavity at the wind tunnel a) isometric b) top view.

The dimensionless inverse Richardson number (the ratio of the Grashof number to the square of the Reynolds number) is used to characterise the heat transfer regime within the cavity, as defined in equation 3. The low values of inverse Richardson number designate the buoyancy dominated convection regime whereas the high values (i.e $1/Ri$ >10) indicate the dominance of momentum in the heat transfer process.

$$Ri = \frac{Gr}{Re^2} = \frac{g\beta(T_{wall} - T_\infty)D_{cav}}{u_w^2}, \quad (3)$$

where g is the gravitational acceleration, β is thermal expansion coefficient, T_{wall} is the temperature of the internal surfaces of the cavity, T_∞ is the temperature of the ambient, D_{cav} is the internal diameter of the cavity and u_w is the wind speed.

Uncertainty

The experimental apparatus and wind tunnel used in this study are similar to our previous work [7], hence the uncertainty of the mean wind speed, heat loss measurements and velocity of blown air curtain are as stated in the previous work.

The following table provides the accuracy of the measurement tools.

Parameter	Accuracy
Yaw angle	0.01°
Tilt angle	0.01°
Volumetric flow	0.8% Of reading
Temperature	0.01℃
Wind velocity	0.01 m/s

Table 1. Accuracy of the measurement devices.

Results and discussion

Figure 2 presents the absolute values of convective heat losses from the cavity without an air curtain at three yaw angles of 0°, 45° and 90° for wind speeds of 0, 3, 6 and 9 m/s. As the figure shows increasing the yaw angle significantly decreases the convective heat losses. So that at a wind speed of 9 m/s, 62% and 75% reduction in convective heat losses are reported for yaw angle of 45° and 90°, respectively compared to head-on wind condition. This is mainly because of the protecting role of the cavity as an enclosure which results in less external cold flow into the cavity.

In general, it is expected that increasing the wind speed causes more convective heat losses due to the higher velocity of the flow inside the cavity that shrinks the stagnant zone and results in more exchange of the cold air outside the cavity with hot air inside the cavity. However, an exception for this is the low side wind condition for which the convective heat losses reduce compared to no wind condition. As it can be seen in Figure 2 by increasing the wind speed from 0 to 3 m/s, for both yaw angles of 45° and 90°, the Q_{conv} decreases by 33% and 63%, respectively. Furthermore, at yaw angle of 90° even at a wind speed of 6 m/s there is a 2% reduction in convective heat losses compared with no wind case. This implies that airflow with appropriate direction and velocity has the potential to act as an aerodynamic shield across the aperture. The aerodynamic barrier restricts the interaction of the external flows and hot air inside the cavity and consequently the convective heat losses decreases.

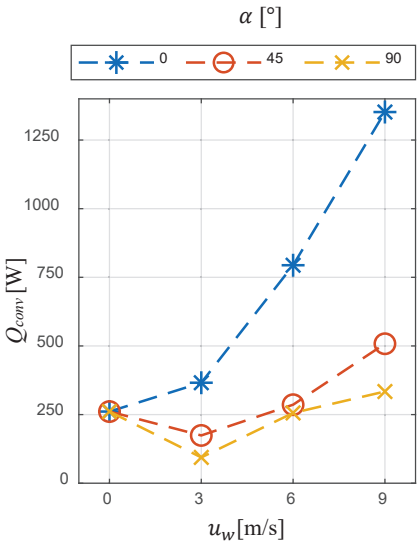

Figure 2. Absolute values of convective heat losses for a variety of yaw angles at u_w= 0, 3, 6 and 9 m/s, for the cases without an air curtain. Test conditions: T = 300℃, θ = 15°.

Figure 3 presents the effectiveness of the air curtain of the experimental cases with a wind speed of a) 3, b) 6 and c) 9 m/s and curtain velocity of 4.5, 9 and 18 m/s for two discharge angles of 0° and 30°. From Figure 3.a, which corresponds to a wind speed of 3 m/s, it is clear that the application of air curtain at yaw angles of 45° and 90° increases the convective heat

losses significantly so that they are about 2.7 times compared with the case with no air curtain. The results indicate that for a wind speed of 3 m/s where the inverse Richardson number is 4.8 (mixed convective heat losses), the application of air curtain at either discharge angles is not beneficial. The results for a wind speed of 6 m/s at Figure 2.c, corresponding to inverse Richardson number of 19 (momentum dominated regime) also show that the application of the air curtain failed to decrease the convective heat losses at a yaw angle of 45°. However, at a yaw angle of 90°, the low-speed curtain with a discharge angle of 30° has an effectiveness of 35%. At a wind speed of 9 m/s, corresponding to an inverse Richardson number of 43 (momentum dominated regime), as presented in Figure 2.c the low-speed curtain at a yaw angle of 45°, reduces the convective heat losses by 19% compared to no curtain case. For a yaw angle of 90°, the effectiveness of an order of 10% is reported for both low and high curtain velocities.

The results revealed that for a yaw angle of 0° (head on wind condition), as it is discussed in our previous paper [7], the discharge angle of the air curtain is an important metrics that affect effectiveness of the air curtain. An air curtain pointed downward with a 30° angle relative to the aperture plane establishes an aerodynamic barrier that partially inhibits the hot air egress from cavity and external cold air ingress into the cavity. Although, the air curtain flow parallel to the aperture plane establishes the aerodynamic shield across the aperture, the expansion of the air flow downstream the curtain outlet increases the mixture of the cold air with the hot air from cavity. This results in an increase in the convective heat losses compared to no air curtain case.

For the yaw angle of 45° and a discharge angle of 30°, the wind is flowing with a horizontal angle of 45° toward the normal direction of the aperture while the inclination angle of the air curtain toward the aperture plane permits the wind flow enters the cavity. On the other hand, the wind flow redirects the curtain flow, which is expanded downstream, into the cavity. The additional flow from the air curtain causes more convective heat losses compared with no air curtain cases. At a discharge angle of 0°, due to the expansion of the curtain flow downstream the curtain outlet, airflow enters the cavity and causes more convective heat losses compared to no curtain case. For side on wind condition, the wind flow encounters the side of the curtain flow. The expanded air jet flow from the air curtain is not preventing the forced convective heat losses and increases the losses due to the mixing of the flows in the vicinity of the aperture.

Figure 4 presents the distribution of the convection losses from different sections of the cavity at a yaw angle of 45° and wind speed of 9 m/s for the cases with u_0 = 4.5 and 18 m/s and both discharge angles of 0° and 30°. As can be seen from the figure the application of an air curtain with low velocity of 4.5 m/s reduces the convective losses from all sections of the cavity for both discharge angles. This implies that curtain flow establishes a partial shield at upper side of the aperture that inhibits hot air from leaving the cavity and as a result the stagnant zone inside the cavity, that contains hot air, expands and the convective heat losses reduces.

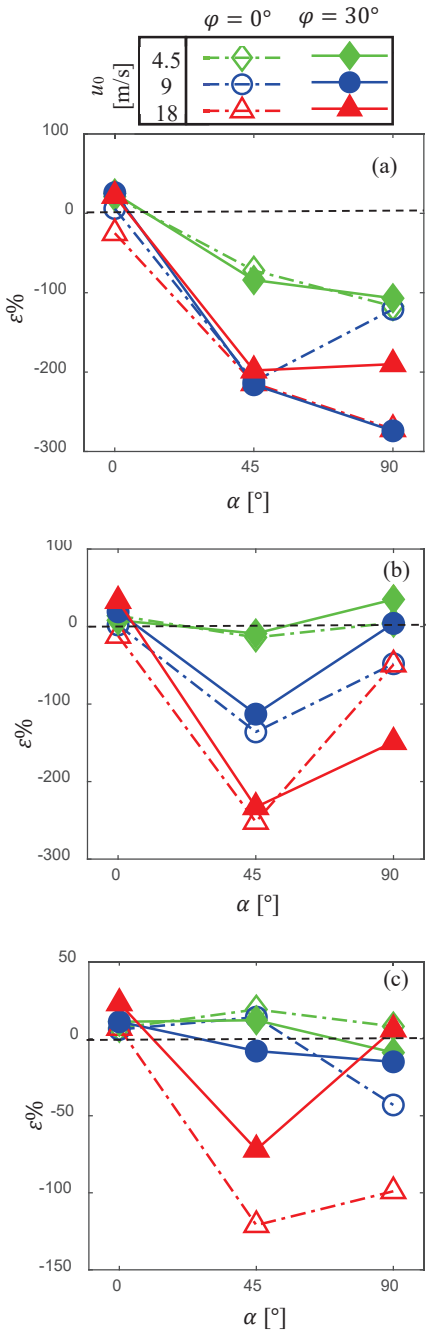

Figure 3. Effectiveness of the air curtain at verity of velocities (u_0 = 4.5, 9 and 18 m/s) as a function of yaw angle of the cavity (α = 0°, 45° and 90°) for wind speeds of (a) 3 m/s, (b) 6 m/s and (c) 9 m/s. Test conditions: T = 300°C, θ = 15°.

As the figure shows increasing the velocity of the air curtain results in an increase in the losses from the lower front section of the cavity. For the air curtain with u_0 =18 m/s and φ = 0°, there is a significant increase in losses from the lower front section of the cavity. That is, this configuration of air curtain, induces additional cold air into the cavity to increase convective heat losses from the internal section in the proximity of the lower aperture. The figure also shows that for high speed curtain configuration the convective heat losses from all sections of the cavity increases. The egress of cold air into the

cavity generates a large eddy circulation inside the cavity [7] and expands the convection zone.

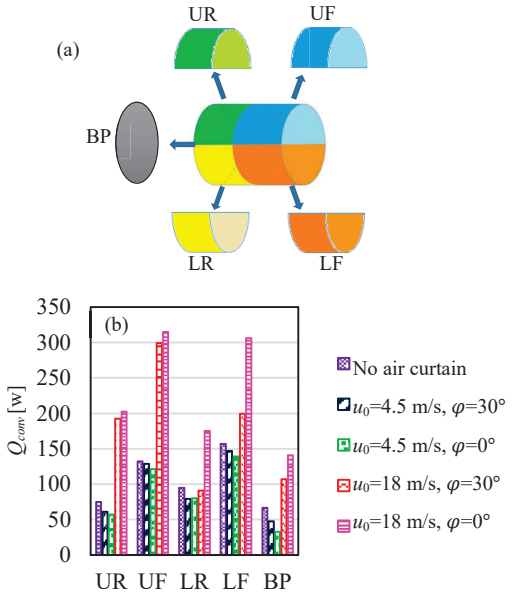

Figure 4. a) Schematic diagram of different sections of the cavity (UR: Upper rear, UF: Upper front, LR: Lower rear, LF: Lower front, BP: Back plate), b) convective heat losses from different sections of the cavity for u_w= 9 m/s, α = 45° for the cases without air curtain, u_0= 4.5 m/s (φ = 0° and 30°) and u_0= 18 m/s (φ = 0° and 30°). Test conditions: T = 300℃, θ = 15°, φ = 30°.

Conclusions

Reported in this experimental study is the effectiveness of a downward blowing air curtain to reduce convective heat losses from a laboratory-scale cylindrical heated cavity receiver. The results provide insights into the design of fluidic barriers of tower type solar cavity receivers aiming to mitigate the convective heat losses to achieve higher thermal efficiency of solar plants. The absolute values of convective heat losses measured at a variety of wind speeds and yaw angles of the cavity demonstrated that the external lateral airflow has the potential to reduce the convective heat losses. So that a side on wind speed of 3 and 6 m/s reduced the convective heat losses 63% and 2%, respectively compared with no wind conditions.

It is also found that while a low-velocity air curtain, at yaw angles of 45° and 90°, reduces the convective heat losses slightly, in most cases the deployment of the downward blowing air curtain increases the losses. In particular, a high velocity curtain flow was found to increase the convective heat increased by up to 2.7 times. Our other investigations, currently under review elsewhere, report the application of a side suction curtain as a more effective strategy to mitigate heat losses.

Acknowledgments

The authors would like to acknowledge the support of the Australian Research Council, Australia, FCT Combustion Pty. Ltd., and Vast Solar Pty. Ltd., Australia through the ARC Linkage, Australia Grant No. LP110200060.

References

[1] EIA, International Energy Outlook 2019. 2019.

[2] Nathan GJ, Jafarian M, Dally BB, Saw WL, Ashman PJ, Hu E, et al. Solar thermal hybrids for combustion power plant: A growing opportunity. Progress in Energy and Combustion Science. 2018; 64:4-28.

[3] Loni R, Askari Asli-Ardeh E, Ghobadian B, Kasaeian AB, Gorjian S. Numerical and experimental investigation of wind effect on a hemispherical cavity receiver. Applied Thermal Engineering. 2017; 126:179-93.

[4] Taussig RT. Aerowindows for central solar receivers. American Society of Mechanical Engineers, Winter Annual Meeting, New Orleans, LA, 1984:12.

[5] McIntash A, Hughes G, Pye J. Use of an Air Curtain to Reduce Heat Loss from an Inclined Open-Ended Cavity. 19th Australasian Fluid Mechanics Conference; 8-11 December 2014; Melbourne, Australia2014.

[6] Alipourtarzanagh E, Chinnici A, Nathan GJ, Dally BB. Experimental Investigation on the Influence of an Air Curtain on the Convective Heat Losses from Solar Cavity Receivers under Windy Condition, SolarPACES 2019; Daegu, South Korea2019.

[7] Alipourtarzanagh E, Chinnici A, Nathan GJ, Dally BB. Experimental insights into the mechanism of heat losses from a cylindrical solar cavity receiver equipped with an air curtain. Solar Energy. 2020; 201:314-22.

[8] Fang J, Tu N, Torres JF, Wei J, Pye J.D. Numerical investigation of the natural convective heat loss of a solar central cavity receiver with air curtain. Applied Thermal Engineering. 2019;152:147-59.

[9] Yang S, Wang J, Lund PD, Wang S, Jiang C. Reducing convective heat losses in solar dish cavity receivers through a modified air-curtain system. Solar Energy. 2018; 166:50-8.

[10] Zhang J.J., Pye J.D., Hughes G.O. Active Air Flow Control to Reduce Cavity Receiver Heat Loss. 2015:V001T05A23.

[11] Lee KL, Chinnici A, Jafarian M, Arjomandi M, Dally B, Nathan G. Experimental investigation of the effects of wind speed and yaw angle on heat losses from a heated cavity. Solar Energy. 2018; 165: 178-88.